US Army Corps of Engineers

AD-A197 363
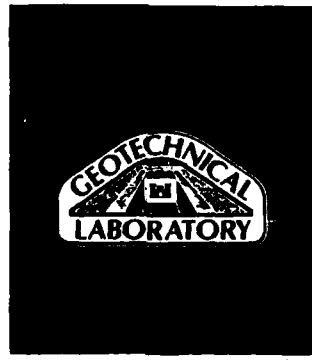
LATERAL PILE-GROUP INTERACTION FACTORS FOR FREE-HEADED PILE GROUPS IN SAND FROM FULL-SCALE EXPERIMENTS

by

Mauricio Ochoa, Michael W. O'Neill

Department of Civil Engineering
University of Houston-University Park
Houston, Texas 77004

DTIC
ELECTE
JUL 1 1 1988
S D
H

June 1988
Final Report

GEOTECHNICAL LABORATORY

88 7

ADA197363

REPORT DOCUMENTATION PAGE

1a. REPORT SECURITY CLASSIFICATION Unclassified		1b. RESTRICTIVE MARKINGS			
2a. SECURITY CLASSIFICATION AUTHORITY		3. DISTRIBUTION / AVAILABILITY OF REPORT Approved for public release; distribution unlimited			
2b. DECLASSIFICATION / DOWNGRADING SCHEDULE					
4. PERFORMING ORGANIZATION REPORT NUMBER(S) Report No. UHCE86-12		5. MONITORING ORGANIZATION REPORT NUMBER(S) Miscellaneous Paper GL-88-12			
6a. NAME OF PERFORMING ORGANIZATION Department of Civil Engineering University of Houston	6b. OFFICE SYMBOL (If applicable)	7a. NAME OF MONITORING ORGANIZATION USAEWES Geotechnical Laboratory			
6c. ADDRESS (City, State, and ZIP Code) University Park Houston, TX 77004		7b. ADDRESS (City, State, and ZIP Code) PO Box 631 Vicksburg, MS 39180-0631			
8a. NAME OF FUNDING / SPONSORING ORGANIZATION See reverse	8b. OFFICE SYMBOL (If applicable)	9. PROCUREMENT INSTRUMENT IDENTIFICATION NUMBER DACW39-85-M-1540			
8c. ADDRESS (City, State, and ZIP Code) See reverse		10. SOURCE OF FUNDING NUMBERS			

10. SOURCE OF FUNDING NUMBERS			
PROGRAM ELEMENT NO.	PROJECT NO	TASK NO.	WORK UNIT ACCESSION NO

11. TITLE (Include Security Classification)
Lateral Pile-Group Interaction Factors for Free-Headed Pile Groups in Sand from Full-Scale Experiments

12 PERSONAL AUTHOR(S)
Ochoa, Mauricio; O'Neill, Michael W.

13a. TYPE OF REPORT Final report	13b. TIME COVERED FROM _____ TO _____	14 DATE OF REPORT (Year, Month, Day) June 1988	15. PAGE COUNT 215

16. SUPPLEMENTARY NOTATION
Available from National Technical Information Service, 5852 Port Royal Road, Springfield, VA 22161

17. COSATI CODES			18. SUBJECT TERMS (Continue on reverse if necessary and identify by block number)
FIELD	GROUP	SUB-GROUP	Cohesionless soils Interaction factors Cyclic lateral loading Pile groups

19. ABSTRACT (Continue on reverse if necessary and identify by block number)

To analyze foundations supported by groups of vertical, pin-headed, laterally loaded piles, it is necessary to include in some rational way the effect of pile-soil-pile interaction, or the increase in pile-head flexibility that occurs in each pile in a group in comparison with an isolated pile. This study was undertaken to measure experimentally pile-head flexibility reduction (interaction) factors for the pile group in sand. Tests were made cyclically at varying magnitudes of applied groundline shear on single piles and two-pile and three-pile subgroups, and the response of unloaded piles in the group was measured. A consistent set of interaction factors was developed from the experiments.

20. DISTRIBUTION / AVAILABILITY OF ABSTRACT ☒ UNCLASSIFIED/UNLIMITED ☐ SAME AS RPT ☐ DTIC USERS	21 ABSTRACT SECURITY CLASSIFICATION Unclassified	
22a. NAME OF RESPONSIBLE INDIVIDUAL	22b TELEPHONE (Include Area Code)	22c OFFICE SYMBOL

DD FORM 1473, 84 MAR   83 APR edition may be used until exhausted
All other editions are obsolete

8a. & 8c.   NAME AND ADDRESS OF FUNDING/SPONSORING ORGANIZATION

Minerals Management Service
US Department of Interior
Reston, VA   22090

Department of Research
Federal Highway Administration
Washington, DC   20590

US Army Engineer Division, Lower Mississippi Valley
PO Box 80
Vicksburg, MS   39180-0080

PREFACE

This study was performed by the Department of Civil Engineering, University of Houston - University Park, under contract to the US Army Engineer Waterways Experiment Station (WES), Vicksburg, Mississippi, for the Minerals Management Service, US Department of Interior; the Department of Research, Federal Highway Administration; and the US Army Engineer Division, Lower Mississippi Valley. The report was prepared under Contract No. DACW39-85-M-1540.

This report was prepared by Mr. Mauricio Ochoa and Dr. Michael W. O'Neill, University of Houston, and was reviewed by Mr. G. Britt Mitchell, Chief, Engineering Group, Soil Mechanics Division (SMD), Geotechnical Laboratory (GL), WES. General supervision was provided by Mr. Clifford L. McAnear, Chief, SMD, and Dr. William F. Marcuson III, Chief, GL.

COL Dwayne G. Lee, CE, is Commander and Director of WES. Dr. Robert W. Whalin is Technical Director.

DTIC
COPY
INSPECTED
6

Accession For		
NTIS GRA&I	☑	
DTIC TAB	☐	
Unannounced	☐	
Justification		
By		
Distribution/		
Availability Codes		
	Avail and/or	
Dist	Special	
A-1		

i

ACKNOWLEDGMENTS

BACKGROUND

In order to analyze foundations supported by groups of vertical, pin-headed, laterally loaded piles, it is necessary to include in some rational way the effect of pile-soil-pile interaction, or the increase in pile-head flexibility that occurs in each pile in a group in comparison with an isolated pile. Flexibility reduction factors have been computed by others from elastic boundary integral models and from finite element solutions. Those solutions, however, fail to consider the effects of pile shadowing and of nonlinearity and cyclic behavior in frictional soils. Consequently, a study was undertaken to measure experimentally pile-head flexibility reduction ("interaction") factors in a full-scale pile group in sand. The measurements were accomplished by testing individual piles within a pile group of nine piles cyclically at varying magnitudes of applied ground line shear, two-pile subgroups and three-pile subgroups. The response of certain unloaded piles was also monitored during these individual-pile and small-group tests. Analysis of the results indicated a significant effect of position on flexibility reduction in a two-pile group (leading or trailing) for piles spaced 3 diameters on center and loaded in line and a lesser effect for piles loaded side-by-side.

Cont'd

iii
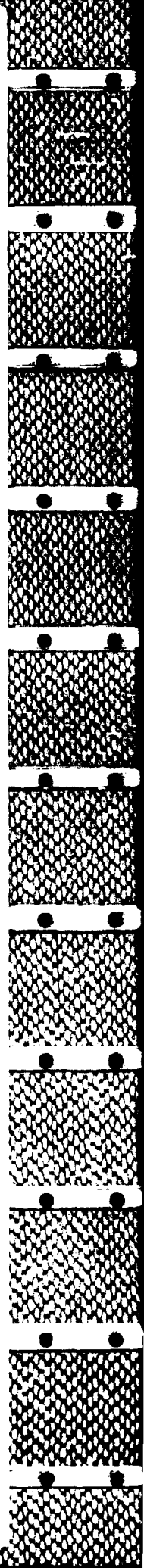
A consistent set of interaction factors was developed
from the experiments and applied to the analysis of de-
flection and shear load distribution in the full nine-pile
group, which had been tested earlier on the same test site,
through the use of simple matrix techniques. Generally good
agreement was obtained between the measured behavior of the
large group and the predictions made with the experimentally
developed interaction factors. Similar factors developed
from elastic boundary integral solutions also provided
generally accurate predictions of group deflections but
failed to predict the correct patterns of shear load distri-
bution.

TABLE OF CONTENTS

TABLE OF CONTENTS (Cont'd)

LIST OF TABLES

LIST OF FIGURES

CHAPTER I

INTRODUCTION

For many years, pile groups have been extensively used for the support of structures such as higway bridges, locks, dams, and waterfront structures. During the past two decades, grouped-pile foundations have also been applied to offshore platforms. Such structures often are subjected to significant lateral forces and movements that require clear identification of the factors affecting the behavior of pile foundations. Unconservative analysis can result in excessive pile-head deflections and rotations, distressing the superstructure. Overconservative analysis can lead to uneconomical foundations.

The geometric constraints in foundations subjected to high lateral loads often require the piles to be driven closely-spaced in a group. The stiffness of each pile in the group is therefore affected by loads on neighboring piles. This phenomenon occurs because such loads produce reactions in the soil, which in turn induce deformations in the soil surrounding the other piles, which reduces (usually) the load required to produce a given deformation in the pile being affected. Computationally, such an effect may be treated by describing the altered stiffness through the use

1

of an interaction factor, known as α, defined for a specific mode in Eq. 1.1 and displayed graphically in Fig. 1.1.

$$^{UP}\alpha_{12} = \delta_1 / \delta_2 , \qquad (1.1)$$

in which,

$^{UP}\alpha_{12}$ = Interaction factor for lateral head deflection between free-headed Piles 1 and 2 in the direction of loading, U.

δ_2 = Pile-head deflection for Pile 2 loaded with a head shear of magnitude P.

δ_1 = Corresponding Pile-head deflection for unloaded Pile 1.

Poulos (1971) computed interaction factors from elastic solutions for a pair of identical equally loaded piles embedded in an elastic half space. The computations were carried out by the use of Mindlin's equations for soil deformations. Poulos and Davis (1980) published charts showing lateral interaction factors for various conditions of loading and head fixity as a function of the departure angle β (defined in Fig. 1.2), pile flexibility K_r, and geometry. Free-head α values for displacement of a pile at the ground surface for values of L/D (length/diameter) of 10, 25 and 100, and pile flexibility of 10^{-1} (relatively stiff pile) are shown in Fig. 1.2. In an elastic medium, $\alpha_{\rho H}$ would be identical to $^{UP}\alpha_{12}$. Pile group interaction factors for free-head piles $^V\alpha$ (for vertical loads), $^{UP}\alpha$ (for head displacements), $^{\theta M}\alpha$ (for head rotations), $^{\theta P}\alpha$ (for cross-coupling

2
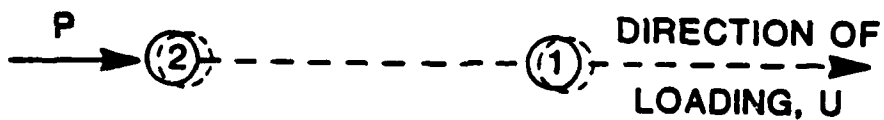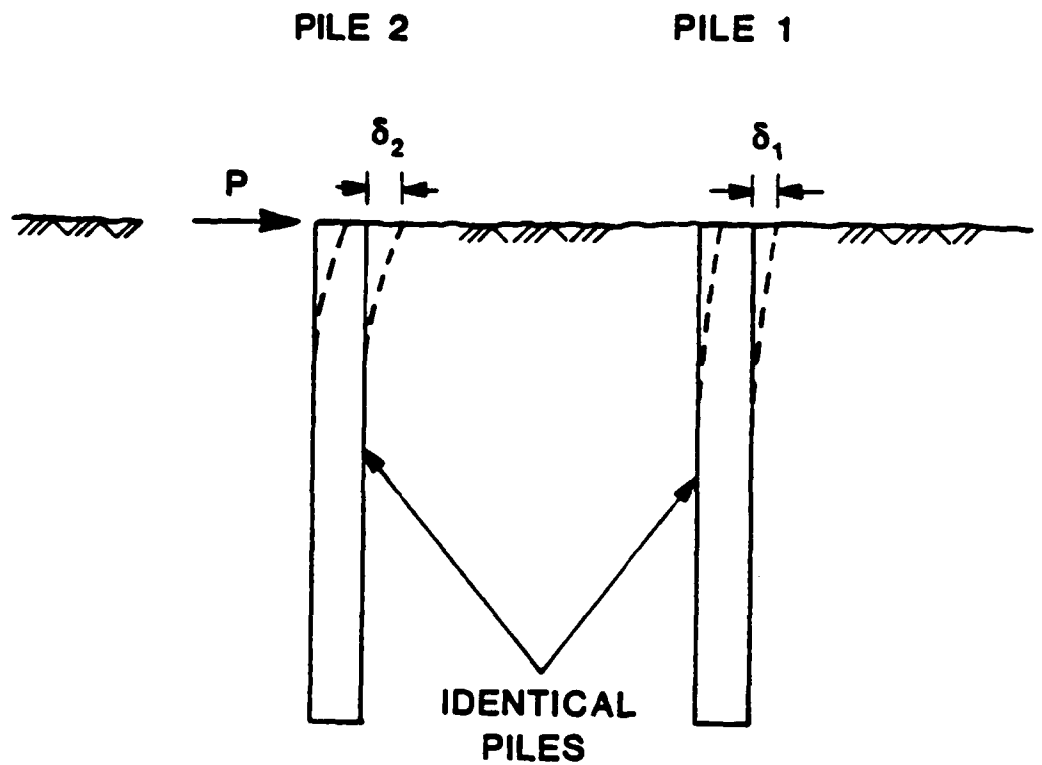
PILE 2   PILE 1

$$^{UP}\alpha_{12} = \frac{\delta_1}{\delta_2}$$

$^{UP}\alpha_{12}$ = INTERACTION FACTOR BETWEEN PILES 1 AND 2
IN THE DIRECTION OF LOADING, U

δ_2 = PILE-HEAD DEFLECTION FOR PILE 2 LOADED
WITH A GROUNDLINE SHEAR, P

δ_1 = PILE-HEAD DEFLECTION FOR UNLOADED PILE 1

Fig. 1.1. Definition of α.

3
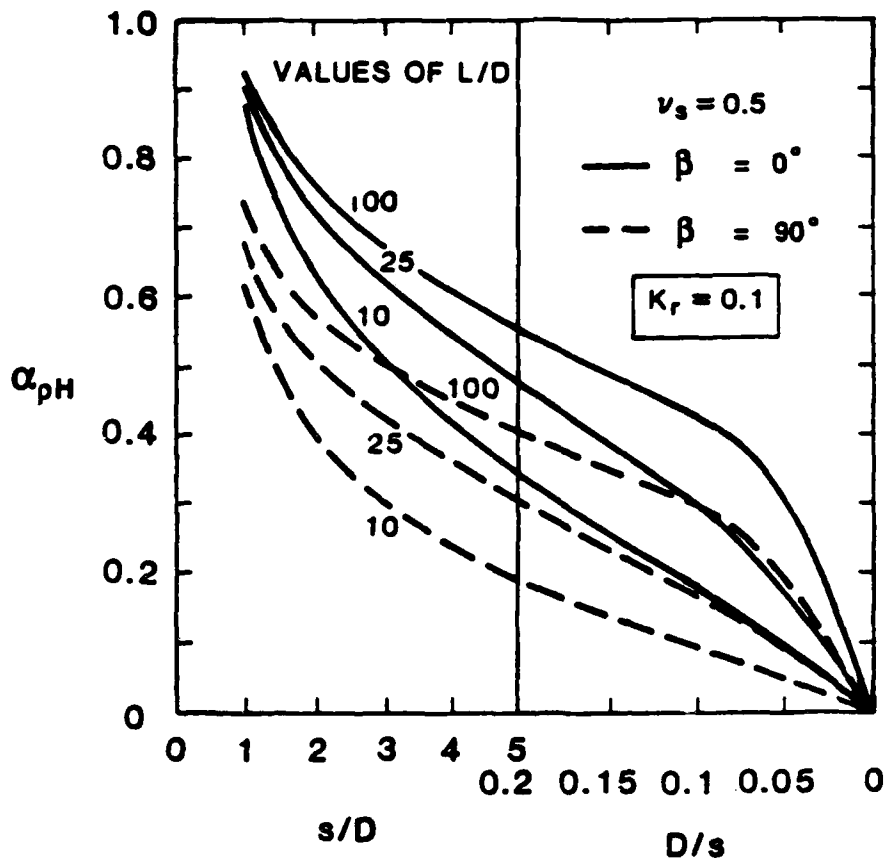
$\alpha_{\rho H}$ = FREE-HEAD INTERACTION FACTOR (DISPLACEMENT)

$$K_r = \frac{(EI)_{PILE}}{E_{SOIL} L^4}$$

E = YOUNG'S MODULUS

I = MOMENT OF INERTIA

L = PILE LENGTH

β = DEPARTURE ANGLE

ν_s = POISSON'S RATIO

s = SPACING BETWEEN PILES

D = PILE DIAMETER
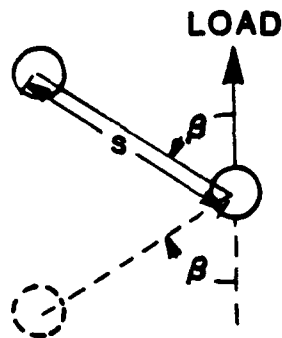
Fig. 1.2.   Free-Head α Factors for Displacement vs. S/D,
$K_r = 10^{-1}$ (After Poulos and Davis, 1980).

4

between head rotations and shears), $^{UM}\alpha$ (for cross-coupling between head deflections and moments), in addition to another factor $^{UF}\alpha$ (for fixed-head conditions, not specifically considered here), from finite element analyses of elastic media by Randolph and Poulos (1982) are presented in Fig. 1.3, in which the critical depth (L_c) is the depth below which the pile does not deform appreciably under lateral loading. Butterfield and Douglas (1981) also presented elastic flexibility coefficients for the design of piles and pile groups from a parametric study using computer program PGROUP. Two features from these elastic solutions are of significance: (1) The factors for lateral interaction are identical for departure angles $\beta = \beta + \pi$ (radians), and (2) the interaction factors $^{\Theta M}\alpha$, $^{UM}\alpha$, and $^{\Theta P}\alpha$ are expressible in terms of $^{UP}\alpha$ and are independent of load magnitude.

Figure 1.4 describes how interaction factors $(^{UP}\alpha)$ can be used to form flexibility matrices for solving for deflection and load distribution in simple free-head groups (O'Neill, 1983) under the assumption that lateral flexibilities for the individual piles are known from experiments or from mathematical synthesis. In Fig. 1.4, the piles are pinned to the cap so that only one interaction factor is needed to define the effect of group action.

Interaction factors computed from Eq. 1.1 and Figs. 1.2 and 1.3 are only valid if pile response is linear and elastic and if conditions of reciprocity hold. As a consequence,

5

MODE OF INTERACTION	EQUATION
VERTICAL ($^V\alpha$)	$^V\alpha = [\, 0.5 \ln (\frac{L}{S})\,] / \ln (\frac{L}{D\rho})$ ($\lambda = 500$)
LATERAL DEFLECTION, FIXED HEAD ($^{UF}\alpha$)	$^{UF}\alpha = 0.6\, \rho_c (\frac{E_p^*}{G_c})^{0.143} (\frac{R}{S})(1 + \cos^2\beta) \le 0.33$ $= 1 - 2 / [27\ ^{UF}\alpha\ \text{(above)}]^{0.5} \ge 0.33$
LATERAL DEFLECTION DUE TO SHEAR, FREE HEAD ($^{UP}\alpha$)	$^{UP}\alpha = 0.7\ ^{UF}\alpha$
ROTATION DUE TO MOMENT ($^{\theta M}\alpha$)	$^{\theta M}\alpha = {}^{UP}\alpha^3$
LATERAL DEFLECTION DUE TO MOMENT OR ROTATION DUE TO SHEAR ($^{UM}\alpha = {}^{\theta P}\alpha$)	$^{UM}\alpha = {}^{\theta P}\alpha = {}^{UP}\alpha^2$ NOTE : PRESUPERSCRIPTS ARE INDICES. POSTSUPERSCRIPTS ARE EXPONENTS

$$L_c = 2R (\frac{E_p^*}{G_c})^{0.286}$$

YOUNG'S MODULUS $= E_p$

DIRECTION OF LOAD
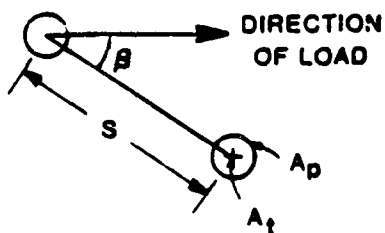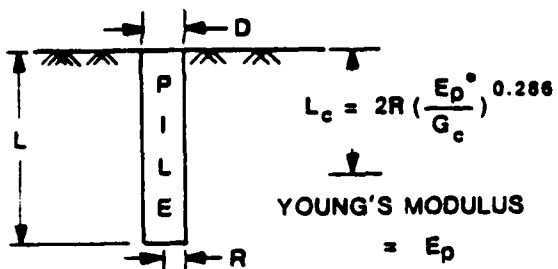
$$\rho = \frac{G(\text{avg. over } L)}{G(\text{at depth} = L)}$$

$$G_c = G(\text{avg. over } L_c)$$

$$\rho_c = \frac{G(\text{at depth} = L_c / 4)}{G(\text{at depth } L_c)}$$

E_p = YOUNG'S MODULUS OF PILE

G = SOIL SHEAR MODULUS x 1.375

$$\lambda = \frac{E_p(A_p/A_t)}{G(\text{depth} = L_c)}$$

$E_p^* = (E_p I_p)/(\pi\, r_o^2 / 4)$
(LATERAL FACTORS ARE FOR RELATIVELY FLEXIBLE PILES, $L \ge 20R$)

Fig. 1.3. Pile Group Interaction Factors for Fixed and Free Heads from Finite Element Analysis of Elastic Media (After Randolph and Poulos, 1982).

6

3-PILE, VERTICAL GROUP (FREE-HEADED)
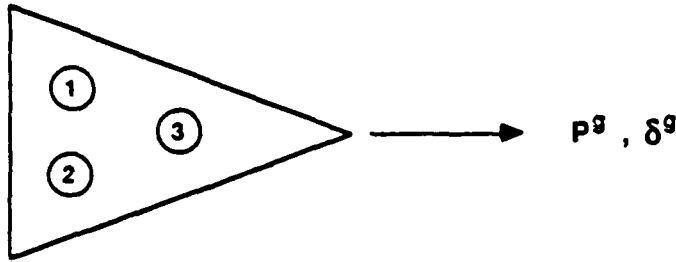
HORIZONTAL INTERACTION FLEXIBILITY EQUATION :
(IN DIRECTION OF LOADING)

$$
\begin{bmatrix}
1 & {}^{UP}\alpha_{12} & {}^{UP}\alpha_{13} & -1 \\
{}^{UP}\alpha_{21} & 1 & {}^{UP}\alpha_{23} & -1 \\
{}^{UP}\alpha_{31} & {}^{UP}\alpha_{32} & 1 & -1 \\
1 & 1 & 1 & 0
\end{bmatrix}
\begin{bmatrix}
P_1 \\
P_2 \\
P_3 \\
\delta^g/f_H^1
\end{bmatrix}
=
\begin{bmatrix}
0 \\
0 \\
0 \\
P^g
\end{bmatrix}
$$

- P_1, P_2, P_3 = PILE LOAD

- P^g = GROUP LOAD

- δ^g = GROUP DEFLECTION

- f_H^1 = HORIZONTAL DEFLECTION OF SINGLE PILE UNDER UNIT LOAD

- ${}^{UP}\alpha_{12}$, $\cdots$, ${}^{UP}\alpha_{32}$ = INTERACTION FACTORS BETWEEN SUBSCRIPTED PILES

  (U = HORIZONTAL DEFLECTION; P = HORIZONTAL LOAD)

- LATERAL LOADING IS AT GROUND LINE

Fig. 1.4. Mathematical Procedure for Predicting Pile Group Deflection and Load Distribution on Individual Piles; Free-Headed Piles (After O'Neill, 1983).

7

the shadowing effect of a leading pile on a trailing pile (and vice versa) can not be evaluated. In addition, lateral soil response is highly nonlinear, making the use of such interaction factors problematical, especially in granular soil. It is intented in this study to develop nonlinear interaction factors experimentally for laterally loaded pile groups embedded in sand for free-head conditions that model the shadowing effect, as a function of the following:

1. Departure angle,

2. Spacing between piles,

3. Magnitude of groundline shear, and

4. Number of cycles of applied load.

The physical approach for making the necessary measurements could proceed in two ways:

A. Load any pile in a group, measure the deflection of the loaded pile and any other unloaded pile, and determine the interaction factor directly from Eq.(1.1).

B. Load one pile, then load that pile along with a second pile at the same load per pile, and define the interaction factor by describing the difference in flexibility in the first pile for the two loading conditions.

Method A would be appropriate in a linearly elastic system; however, Method B is preferable in a nonlinear, inelastic soil. Furthermore, to avoid errors in scaling the phenomena, Method B should be applied at essentially full scale. This approach was taken in the study described here.

The new definition of the interaction factor is given in Eq. (1.2),

$$^{UP}\alpha_{12} = \delta_{12} / \delta_1 , \qquad (1.2)$$

where

$^{UP}\alpha_{12}$ = Interaction factor between Piles 1 and 2, in the direction of loading,

δ_1 = Pile-head deflection for single pile (Pile 1) loaded with a head shear of magnitude P.

δ_{12} = Additional pile-head deflection of the two piles (Piles 1 and 2) loaded simultaneously with the same load P.

This introduction is followed by a description in Chapter II of the geotechnical conditions at the site at which the full-scale tests were conducted. Chapter III describes the testing program that includes pile properties and layout, loading and data acquisition systems and test procedures. Evaluations of the experimental interaction factors between any two piles in the test group for different spacings, departure angles, number of cycles and loading levels, as well as preliminary design charts are described in Chapter IV. The validity of experimental interaction factors is investigated in Chapter V. That is done by comparing load distribution and group deflection computed using the experimental α factors and those from an elastic

9

(Poulos-Randolph) analysis with measurements obtained by Morrison (1986) from an earlier test on a nine-pile group at the same test site. Also included in Chapter V is a preliminary design procedure, as well as a preliminary evaluation of the general effects of group action on bending moments. A summary, conclusions and recommendations for additional research are presented in Chapter VI.

CHAPTER II

GEOTECHNICAL EVALUATION

2.1. Site Location

The specific site on which the experiment was conducted is located as shown on Fig. 2.1, at the University of Houston Foundation Test Facility, east of the University Park campus building designated as the "Band Annex."

2.2. Geotechnical Conditions at Test Site

The geology at the site has been extensively investigated in relation to earlier studies (Mahar and O'Neill, 1983; O'Neill, Hawkins, and Audibert, 1982; O'Neill and Dunnavant, 1984). The soils to a depth exceeding 250 ft are unconsolidated deltaic sediments (in a geologic sense).

The natural soil to a depth of 24 ft consists primarily of stiff to very stiff overconsolidated red and gray fissured clays of the Pleistocene-aged Beaumont formation. The older Pleistocene-aged Montgomery formation is encountered below 24 ft. This formation consists of very stiff overconsolidated sandy clays, with thin sand layers between depths of 37 and 55 ft.

Following a lateral group load test on a group of nine pipe piles in clay (Brown and Reese, 1985), the near-surface natural soil was excavated around that group and replaced by

11
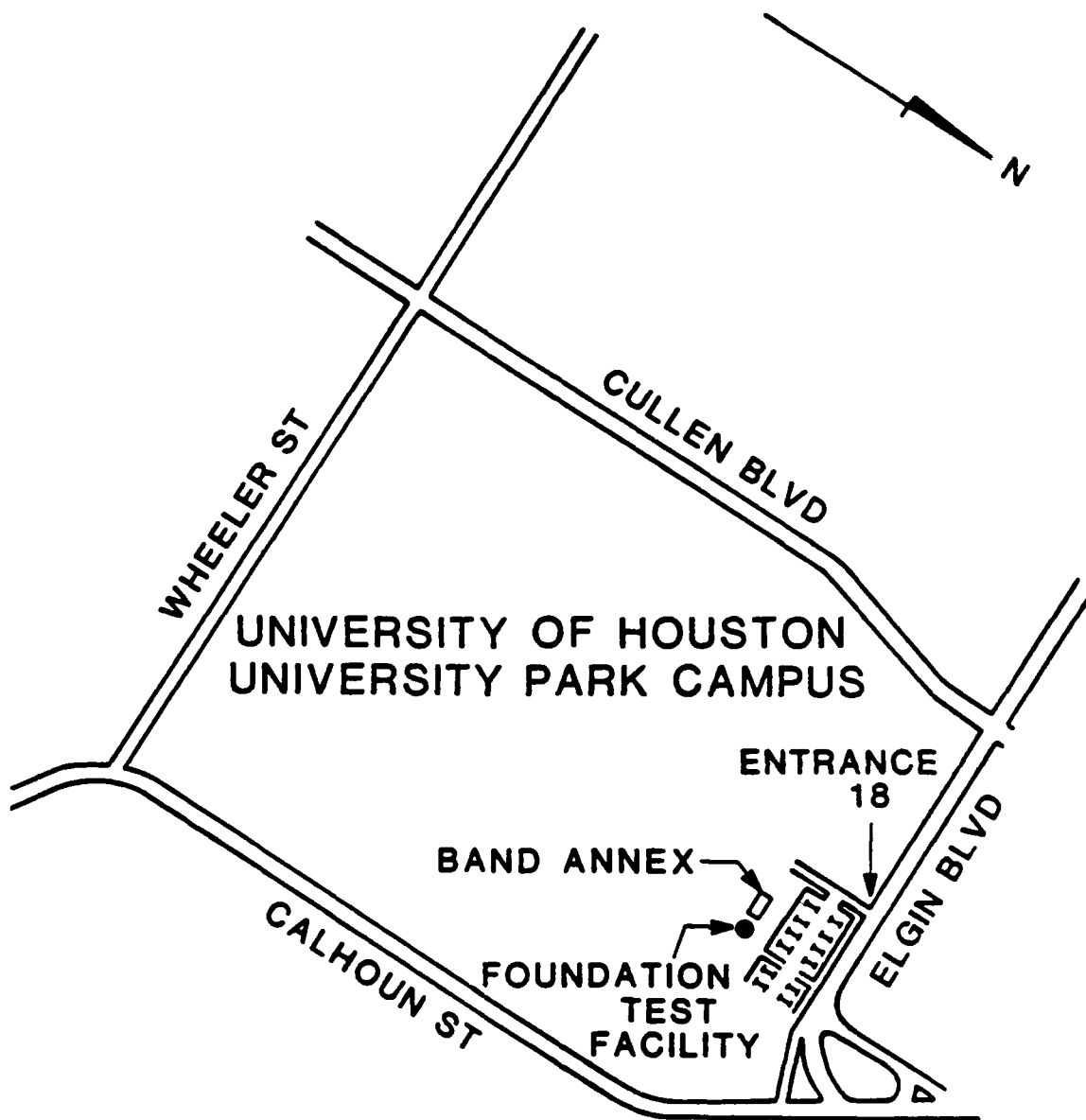
Fig. 2.1. Test Site Location.

medium-graded clean sand that was hand compacted in thin layers to a relative density of about 50% to within 2 ft below natural (clay) grade, so as to form a pit. Dewatering was not required during this operation. The resulting general site stratigraphy for the current study is shown on Fig. 2.2. The sand was subsequently densified when the entire pile group was tested cyclically to large displacements as a unit of pinned-(free-) headed piles (Morrison, 1986). Fig. 2.3 shows the variation of the total unit weight with depth based on tests of undisturbed clay samples and surface nuclear density measurements made in the sand fill at the time of placement. Figs. 2.4 and 2.5 provide profiles of the undrained shear strength vs. depth and ε_{50} (axial strain in UU triaxial test at which one-half of the maximum principal stress difference is developed) vs. depth for the clay strata.

The natural water table at the site is located about 3 ft below the test surface. In order to simulate river-bottom or offshore conditions during the testing, the water level was kept 1 ft above the test surface by flooding the test pit.

2.3. Geotechnical Test Results

Testing for evaluation of the angle of internal friction ϕ for the fill consisted of standard penetration and quasi-static cone penetration tests. These tests were conducted on the saturated sand down to a depth of 10 ft below the test surface. Sieve analyses were also performed on

13
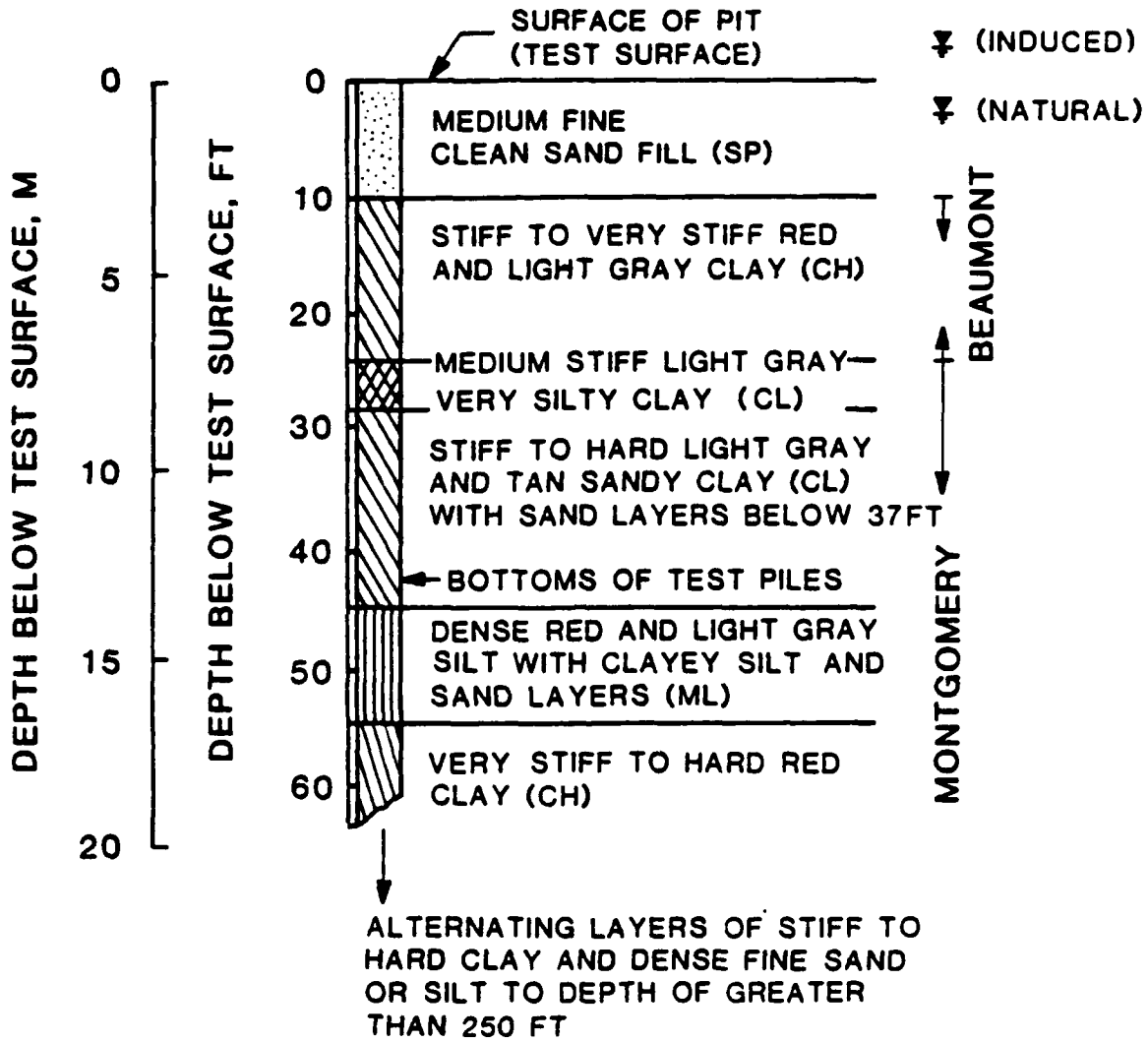
Fig. 2.2. Site Stratigraphy (After O'Neill and Dunnavant, 1984).

14
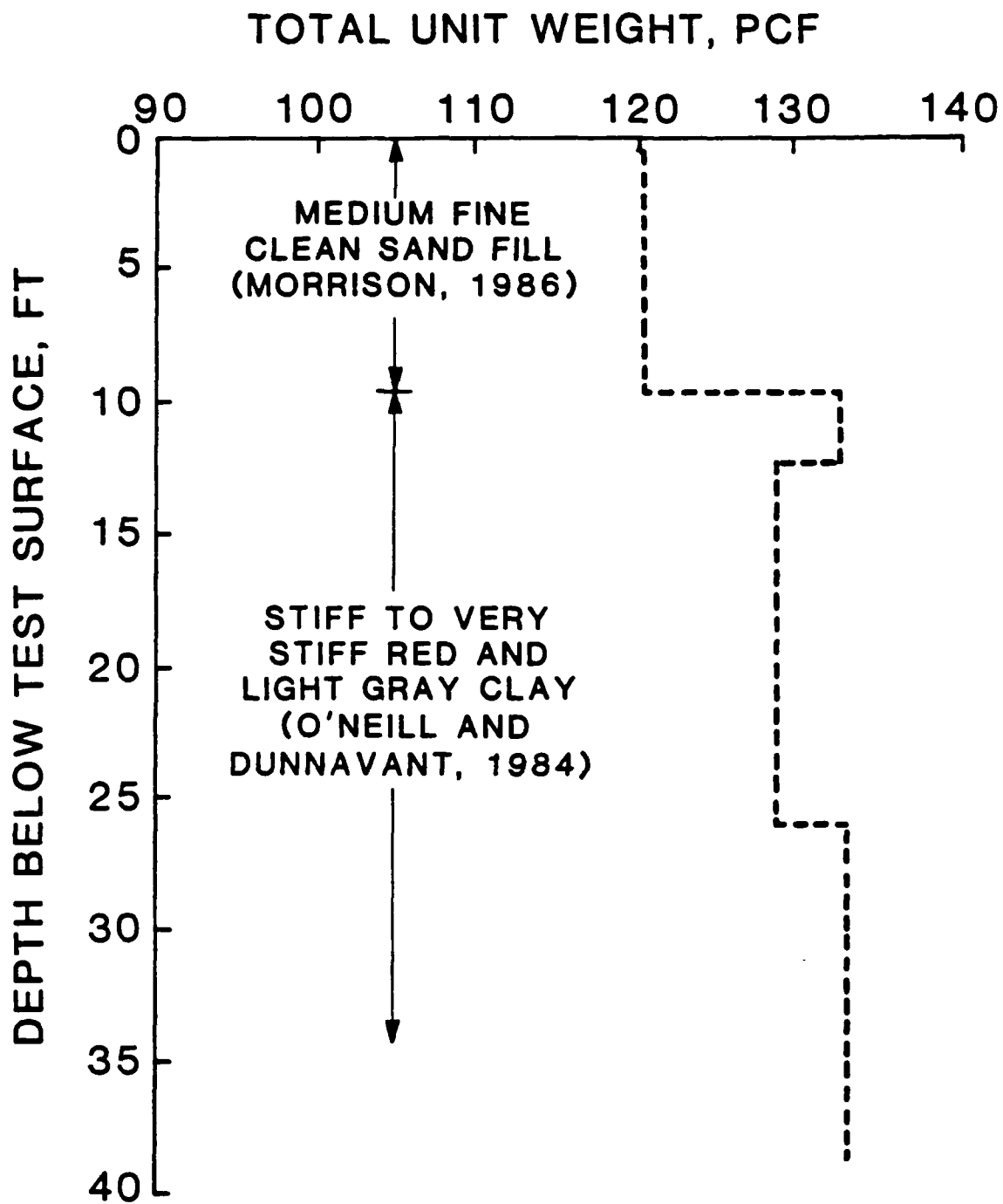
Fig. 2.3.   Total Unit Weight vs. Depth.

15
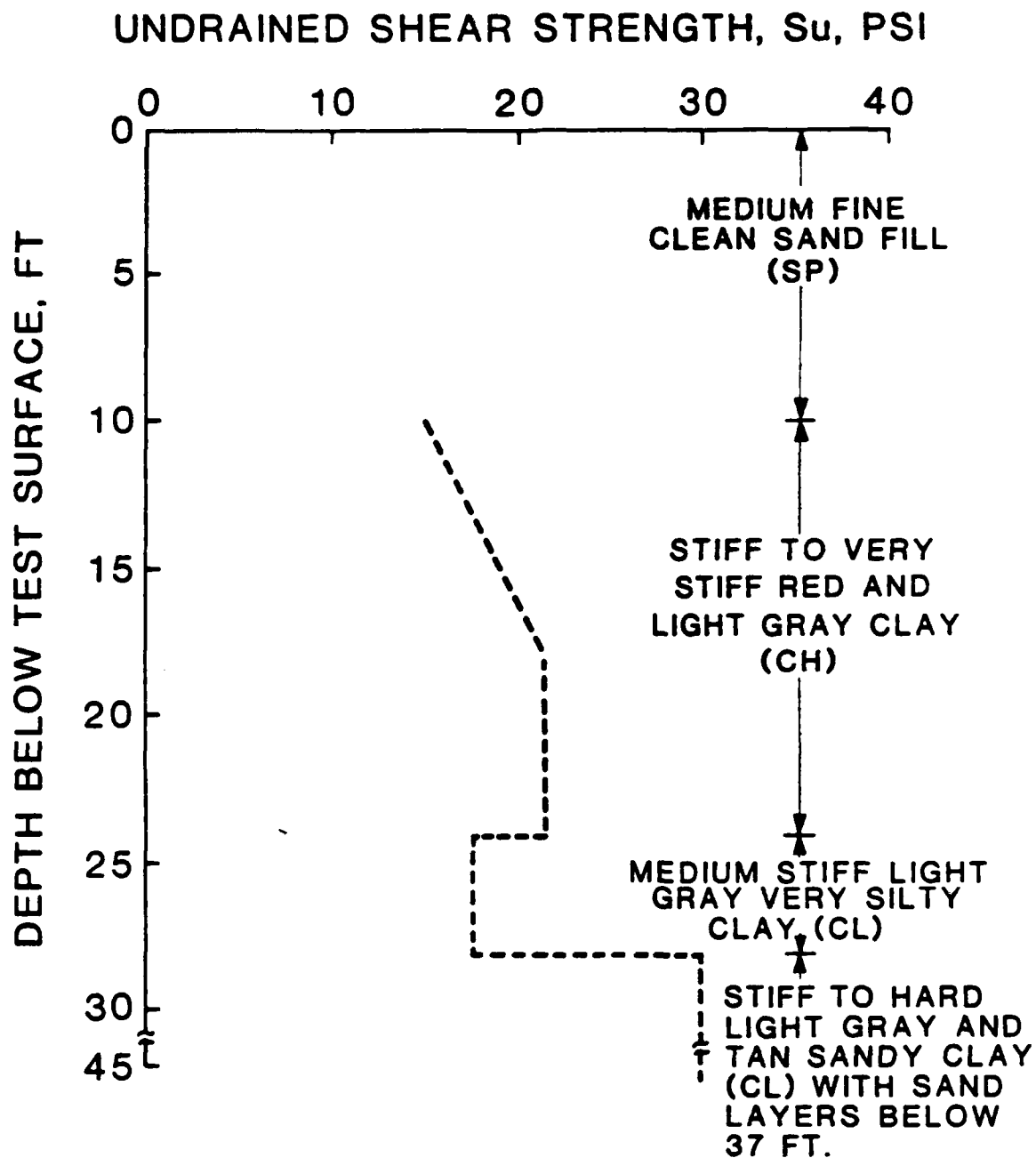
Fig. 2.4.   Undrained Shear Strength vs. Depth
(After O'Neill and Dunnavant, 1984).

16
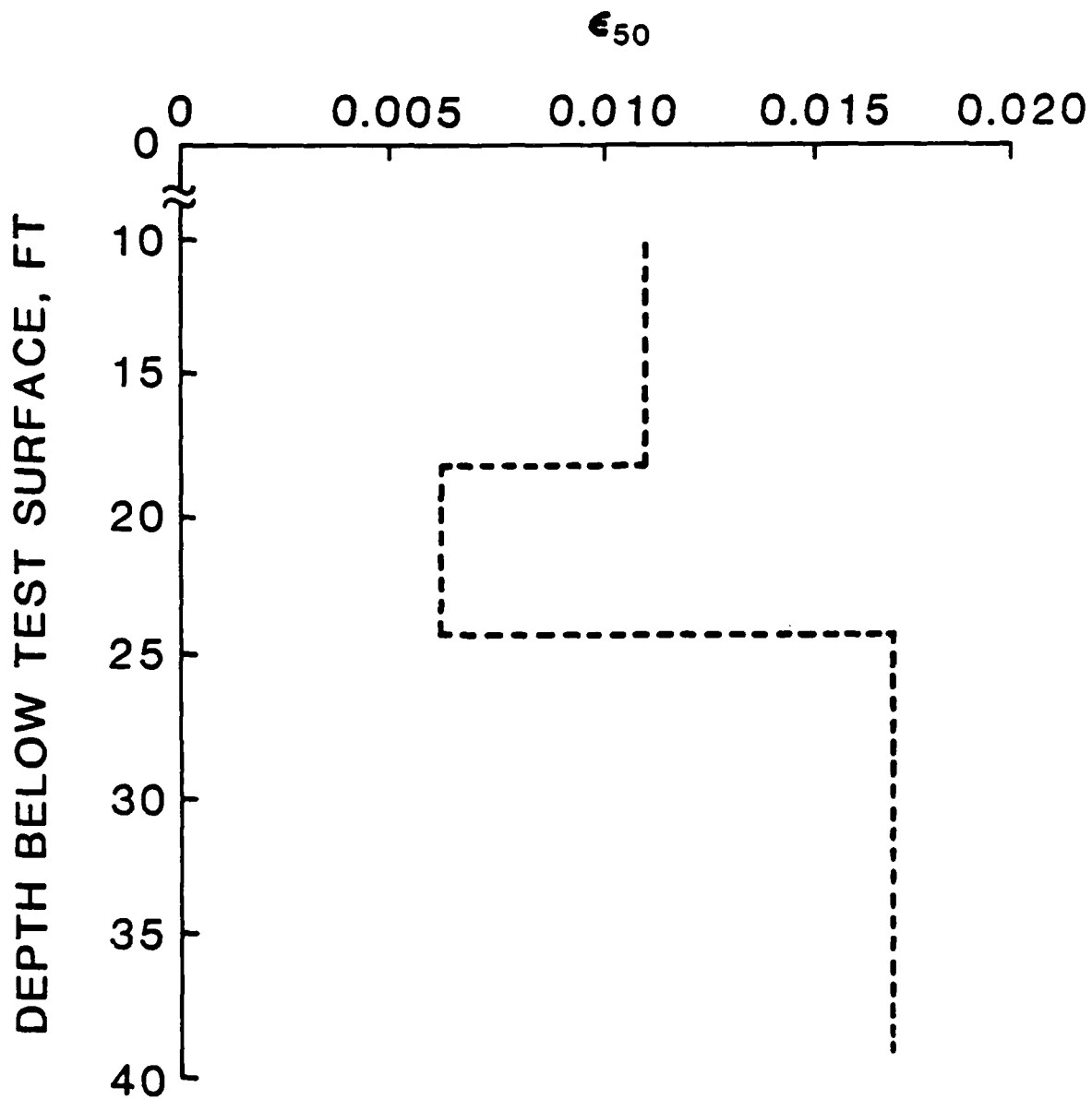
Fig. 2.5. ε_{50} vs. Depth (After O'Neill and Dunnavant, 1984).

split spoon samples taken from SPT tests at two different levels.

2.3.1. Standard Penetration Tests (SPT)

Two SPT tests were conducted in May, 1985, after all pile testing was completed, by using a truck mounted-drilling rig. Two locations were selected for such tests, governed by the limitations that the drill had to be positioned close to the pile group but far enough from the edge of the pit to avoid boundary effects arising from the presence of the clay surrounding the sand pit. Test locations for the SPT borings are shown on Fig. 2.6.

A standard 2-in.-diameter split-spoon sampler was driven at different depths using a 140-lb driving mass falling free from a height of 30 in. The SPT blowcount profiles for both tests are shown on Fig. 2.7. The blowcount profile for the soil below 10 ft (stiff to very stiff clay) developed from a previous study is also presented on Fig. 2.7 in order to provide an idea of the clay consistency.

Relationships between the number of blows per foot, N, and the angle of internal friction, ϕ, displayed on Fig. 2.7 are based on correlations presented graphically by Peck, Hanson, and Thornburn (1974).

2.3.2. Quasi-Static Cone Penetration Tests (CPT)

Three CPT tests were performed following the SPT tests using a 10 ton-capacity Fugro-type electronic penetrometer, model Mark II, manufactured by Terrametrics-SINCO, and a 30

18
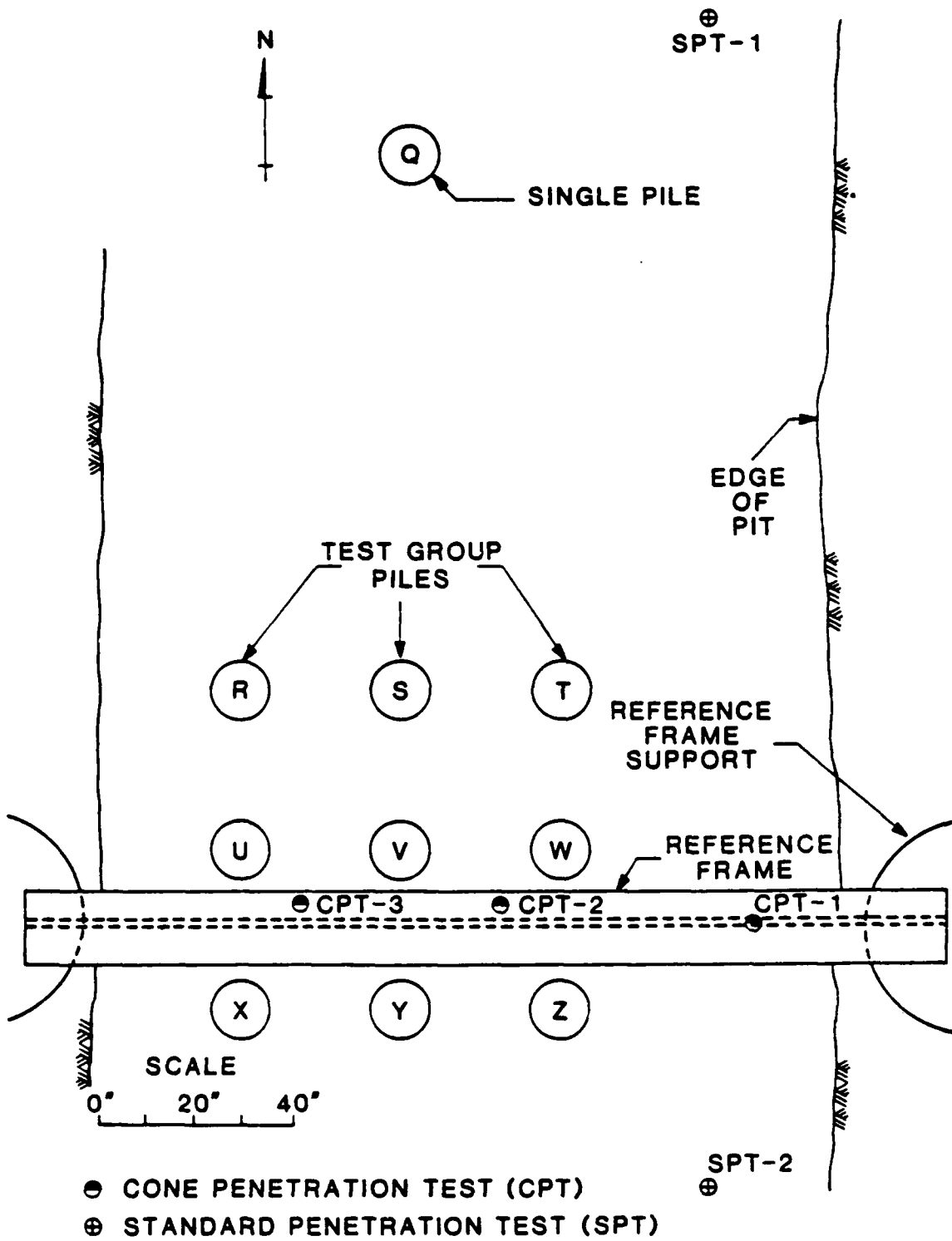
Fig. 2.6.   SPT and CPT Test Locations.

19
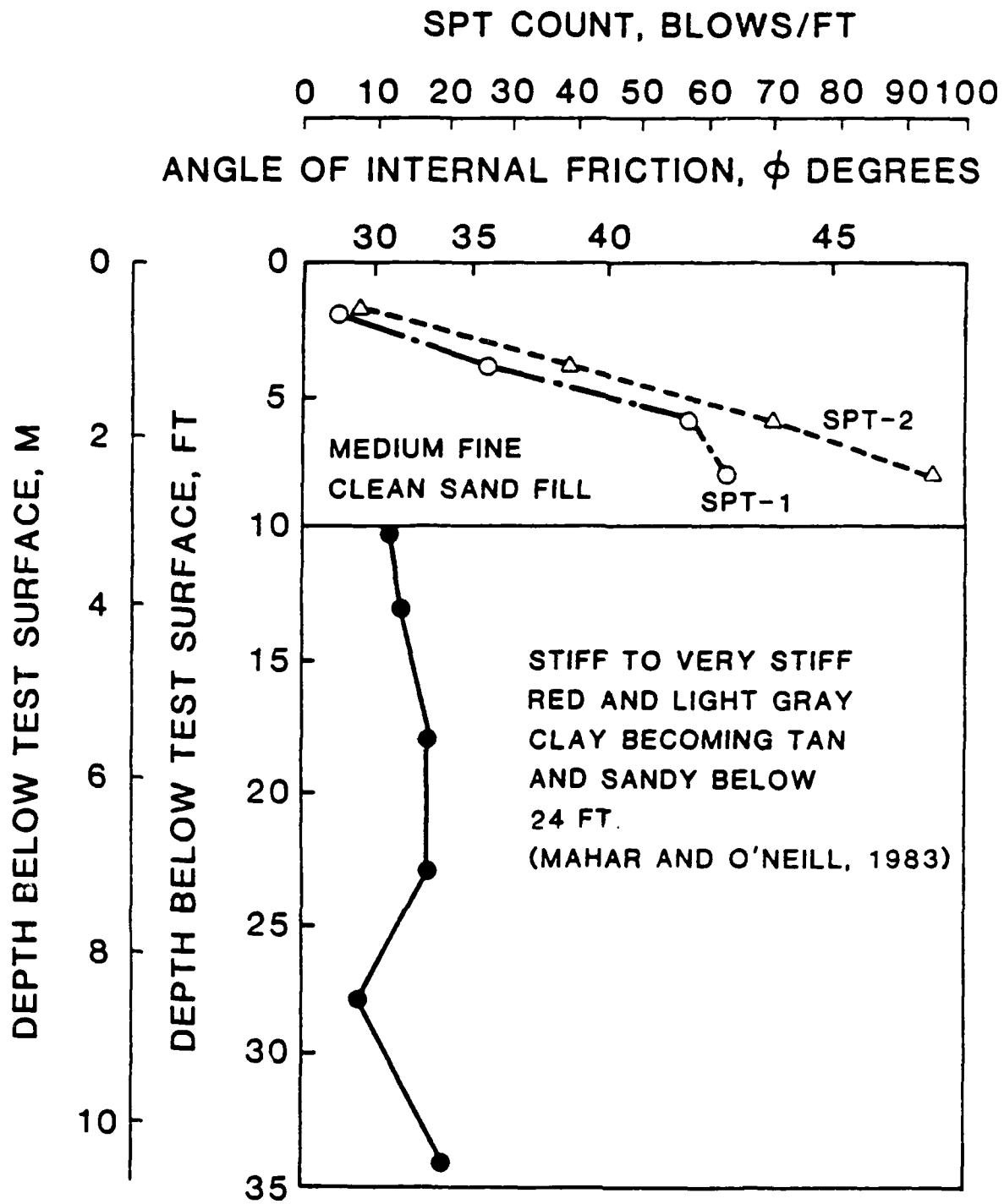
Fig. 2.7. SPT Blowcount vs. Depth.

ton-capacity hydraulic jack activated by a portable electric pump. An existing steel beam (W14 X 90), utilized to support the reference system for the pile tests, was used as a reaction. The data acquisition system consisted of a 10-volt AC power supply, a Hewlett-Packard 3497A data acquisition/control unit, and a Hewlett-Packard 85 microcomputer.

Fig. 2.6 shows the locations at which CPT tests were performed. Points CPT-2 and CPT-3 were not located exactly below the web of the reaction beam due to the presence of the loading frame around the pile group. Tests CPT-2 and CPT-3 were terminated at about 4 feet below the test surface when the load applied to the reaction beam by the cone was high enough to cause visible rotation of the reaction beam.

Relationships between tip resistance q_c (kg/sq cm) and the angle of internal friction ϕ depicted on Figs. 2.8 and 2.9 have been estimated by assuming a K_o (coefficient of earth pressure at rest) value of 0.6 for a dense sand (Prakash, 1981), an OCR (overconsolidation ratio) value of 2 (Brooker and Ireland, 1965), and following the approach developed by Schmertmann (1975).

Since tests SPT-1, SPT-2 and CPT-1 were conducted some distance away from the test piles, they may reflect initial soil conditions (medium to dense) when the fill was placed prior to the first lateral pile group test in sand. Tests CPT-2 and CPT-3, conducted within the group, suggest that earlier cyclic loading of the group produced a high degree of densification (dense to very dense) in the sand immedi-
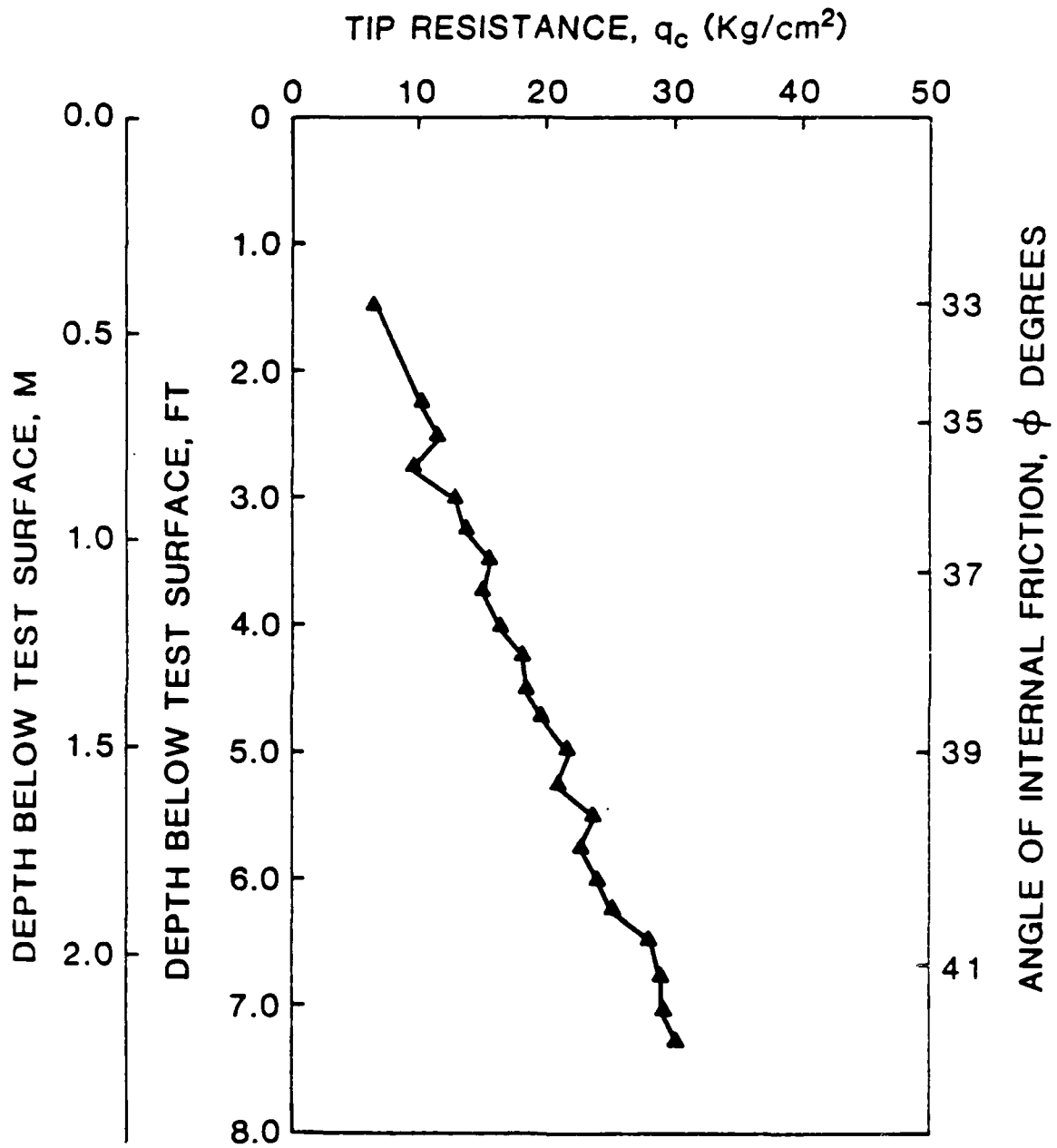
Fig. 2.8.   Angle of Internal Friction vs. Depth Based
            on CPT-1.

22
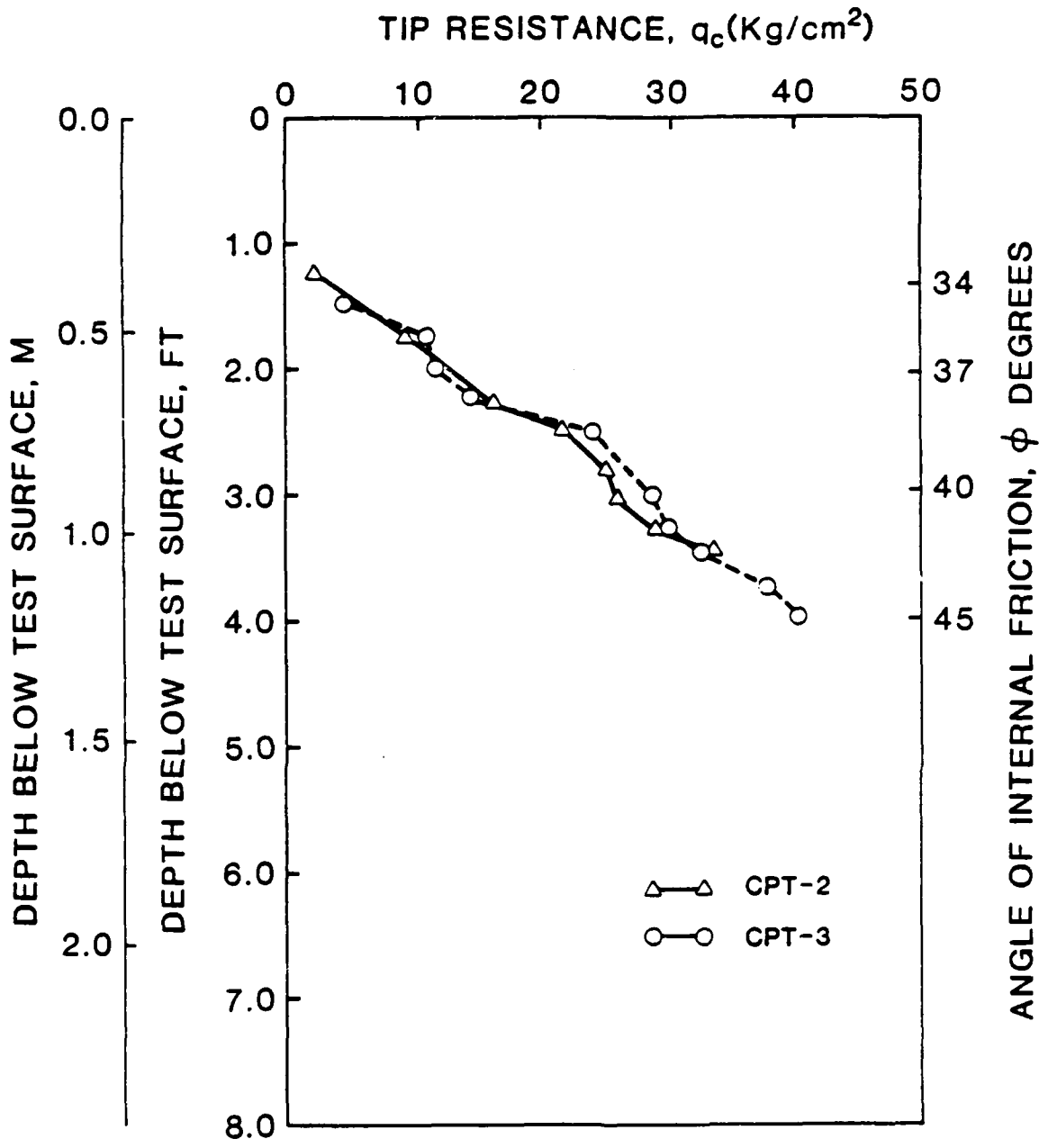
Fig. 2.9. Angle of Internal Friction vs. Depth Based
on CPT-2 and CPT-3.

23

ately surrounding the piles.

2.3.3. Sieve Analyses

Two samples of about 900 g each were obtained from the sand fill at penetrations of 3.5 and 7 ft below the test surface from SPT-2. Oven dry samples were passed through a set of sieves consisting of Nos. 4, 10, 20, 40, 80, 100, 200 U. S. standard sieves. The results of the tests are given in Table 2.1 and displayed graphically on Fig. 2.10.

The average effective grain size, D_{10}, for the samples is 0.24 mm, while the average coefficient of uniformity, D_{60}/D_{10}, is 2.17. The sand is consequently classified as a poorly graded fine sand, or "SP," according to the Unified Soil Classification System.

Table 2.1. Grain Size Distribution of Test Pit Sand

SIEVE SIZE	PERCENT PASSING, BY WEIGHT	
	SAMPLE 1 (3.5 FT)	SAMPLE 2 (7.0 FT)
4	100	100
10	99	98
20	94	90
40	39	31
80	5	3
100	3	2
200	1	1
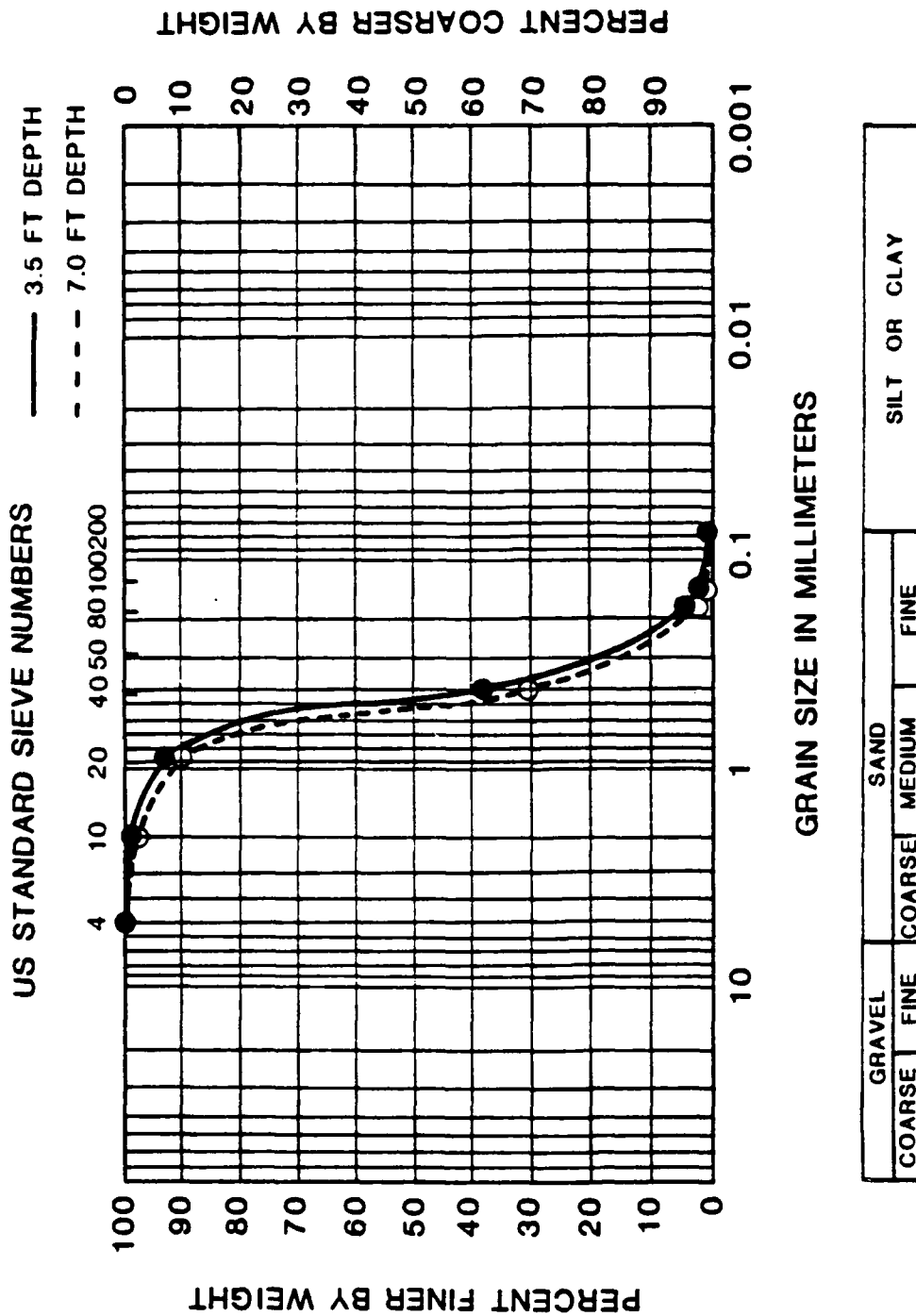
Fig. 2.10. Grain-Size Distribution of Test Pit Sand.

CHAPTER III

TESTING PROGRAM

3.1. Pile Properties and Layout

The piles used in the current study consisted of 10 instrumented steel pipes with an outside diameter of 10.75 in. and wall thickness of 0.365 in. The piles were driven in 1979 (into clay) closed-ended at a center-to-center spacing of three diameters, to a depth of 43 ft (O'Neill, Hawkins and Audibert, 1982). During 1979-81 the piles were subjected to vertical load tests to failure (O'Neill and Hawkins, 1982) and to low-amplitude vertical and lateral vibratory tests (Blaney, 1983). In the fall of 1983, the piles were reconditioned in place for research projects concerning an investigation of the lateral behavior of pile groups in clay (Brown and Reese, 1985), and in sand (Morrison, 1986) several months later. A six-inch-diameter steel pipe, with 0.310-in. wall thickness, 21 ft long, was inserted into each of the 9 group piles and then grouted, to act as a unit with the outer pile. These insert pipes were instrumented with strain gages. The single pile (Pile Q, Fig 2.6) was instrumented by placing strain gages on its outer surface when the clay surrounding the piles was excavated to prepare for placement of sand. The purpose of the strain gage instrumen-

27

tation was to permit measurements to be made of bending moments in each of the closely-spaced group piles and in the "far-field" single pile.

A plan view and cross sections A-A and B-B of the test site are shown on Figs. 3.1, 3.2 and 3.3, respectively. A larger-scale plan view of the pile group geometry showing spacing between piles and the labelling scheme for the test conducted in this study is shown on Fig. 3.4. Schematic sections of the 10.75-in.-O.D. group and single piles, the 6-in.-O.D. insert pipe, and locations of strain gages and linear potentiometers used to measure pile-head deformations are shown on Figs. 3.5.a and 3.5.b.

The piles were calibrated as free-standing cantilivers to determine the relation between bending moment, gauge output, pile deflection and, indirectly, pile flexural stiffness after the lateral load test of the pile group in clay (Brown and Reese, 1985). The piles were prepared for calibration by excavating around around the piles to a depth of 9.5 ft. A known shear was applied individually to the head of each pile. Calibration constants (moment/gage output) were thus obtained that produced an accuracy of ± 10% in measured bending moment values over the full range of loads (Brown and Reese, 1985). EI values were estimated by back-analysis of the piles acting as cantilivers supported by the clay (Brown and Reese, 1985). The variations of the estimated EI values with depth for the piles in the group and the single pile are shown in Fig. 3.6.
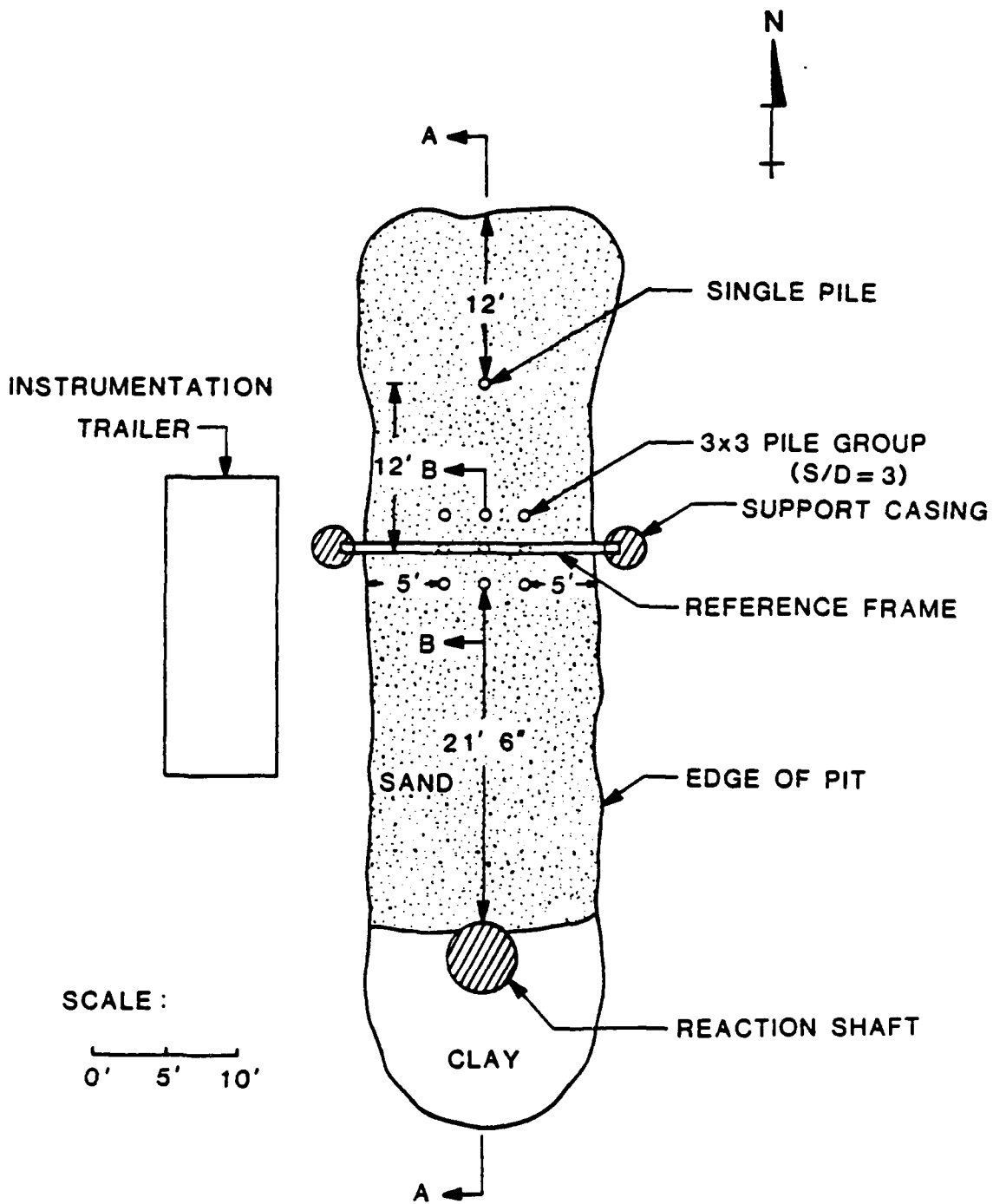
Fig. 3.1. Plan View of Test Site.

29
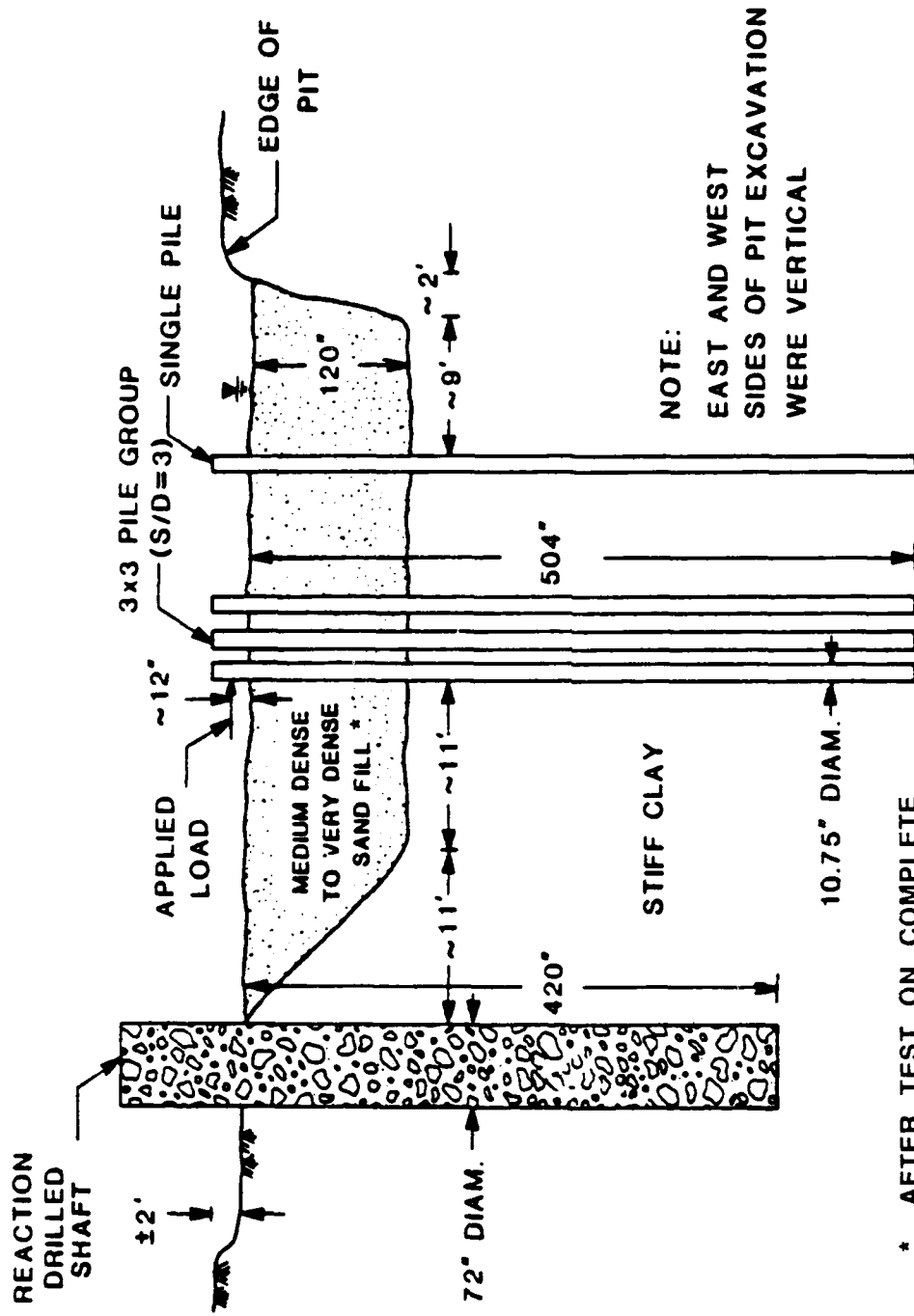
Fig. 3.2. Test Site - Cross Section A-A.

30
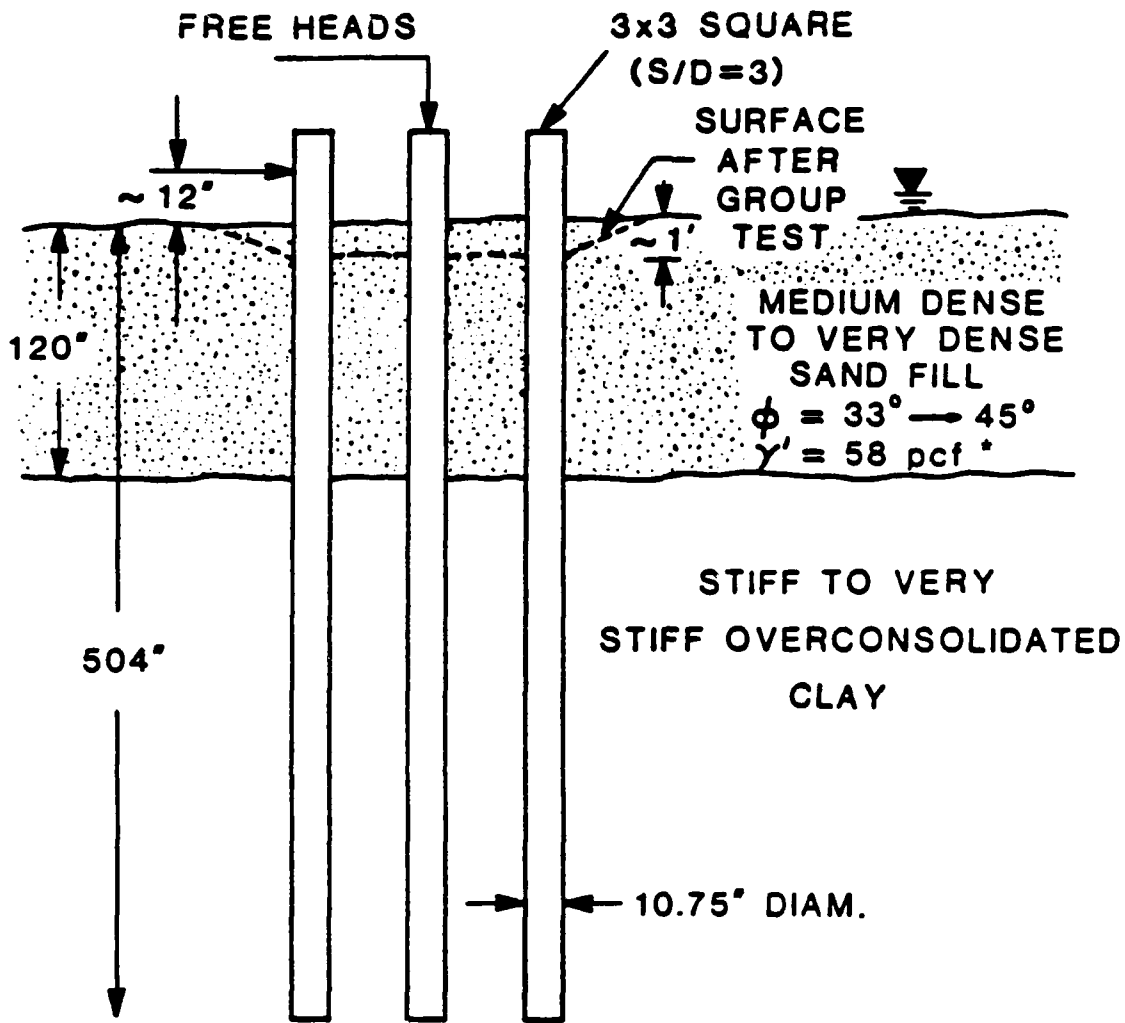
Fig. 3.3.   Test Site - Cross Section B-B.

31

N

Q

2-WAY
CYCLING

12'

R   S   T

S/D = 3

U   V   W

S/D = 3

X   Y   Z

D = 10.75″
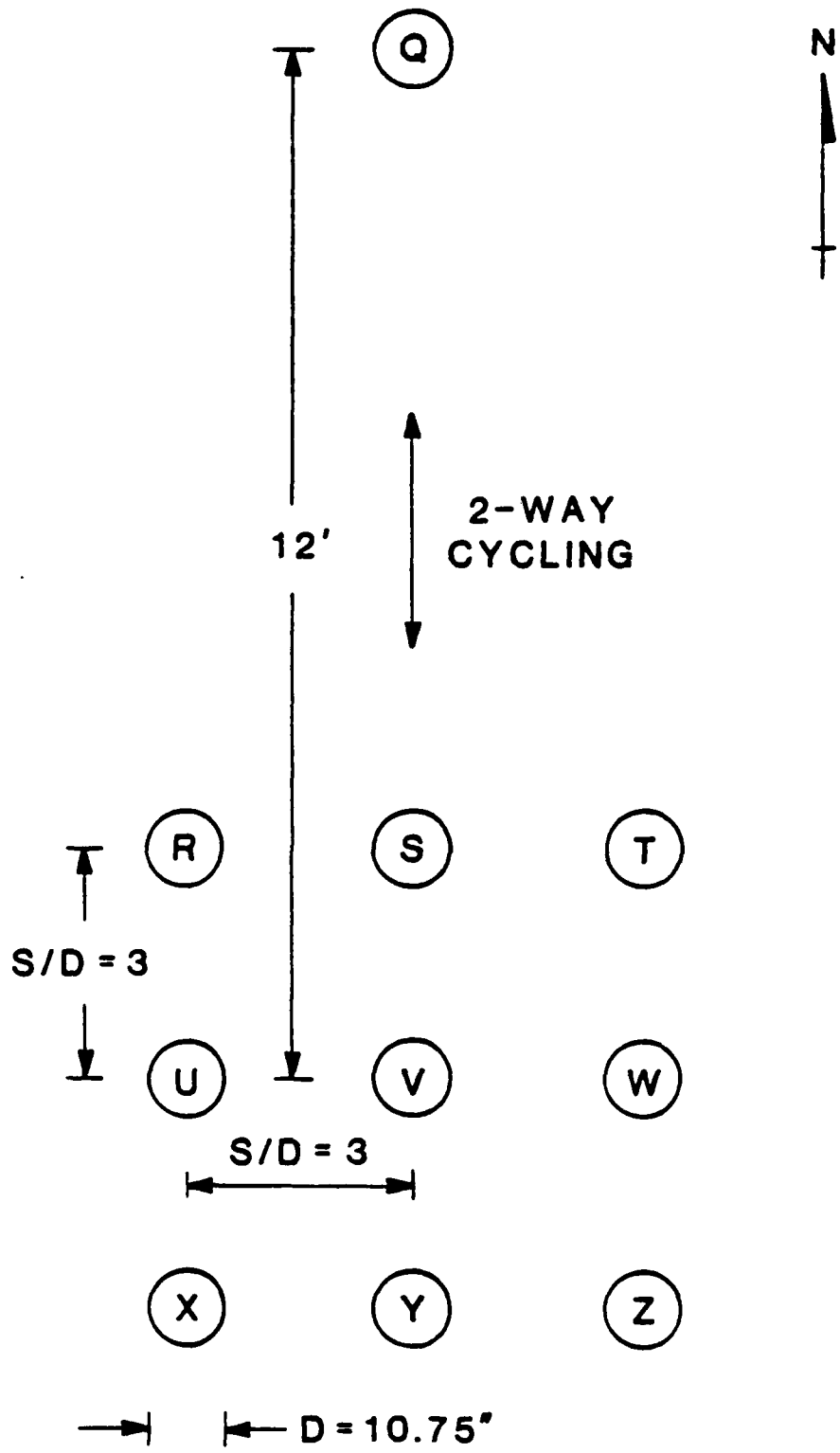
Fig. 3.4.   Pile Labelling Scheme.
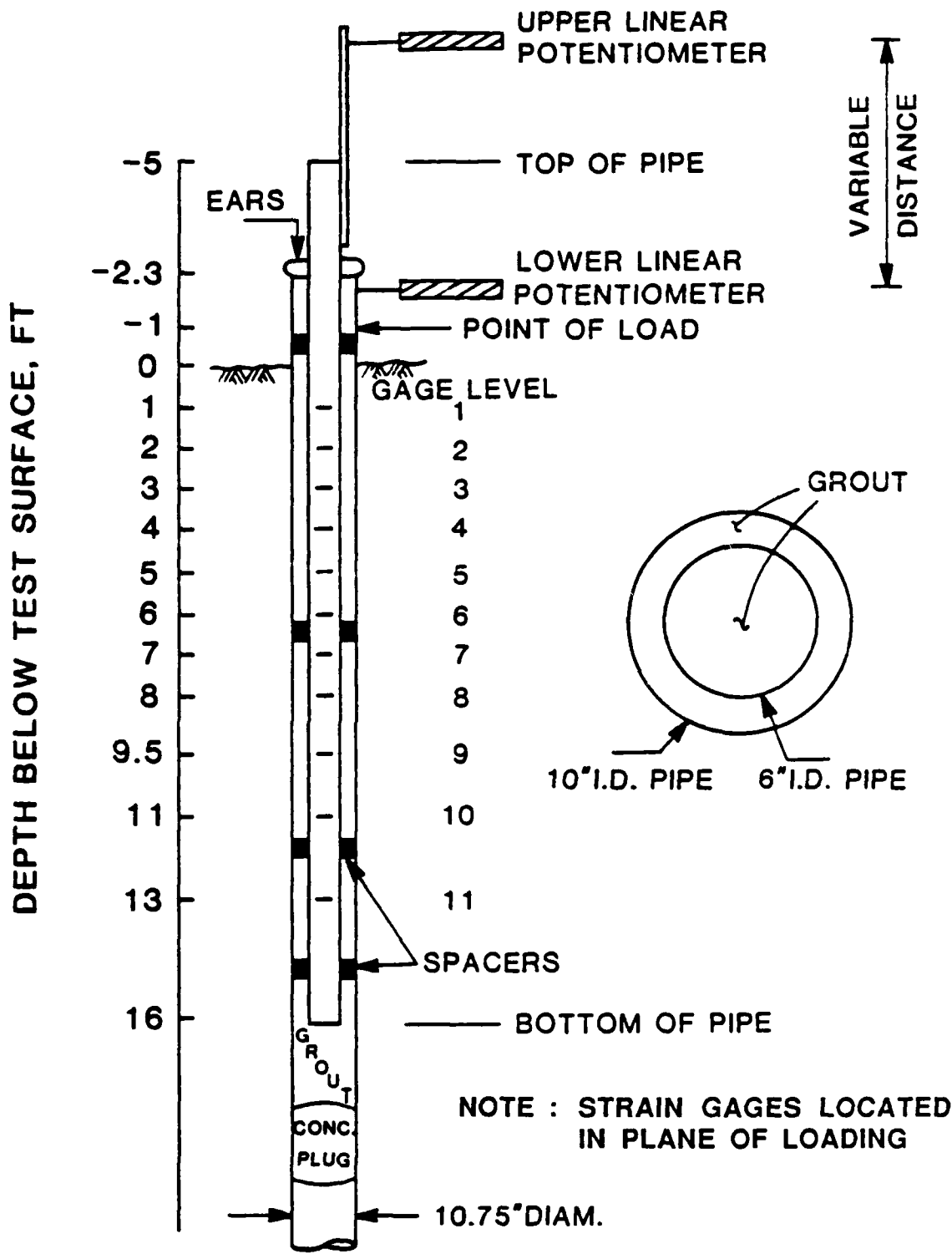
Fig. 3.5.a.   Schematic Section of an Instrumented Group
Pile (After Brown and Reese, 1985).

33
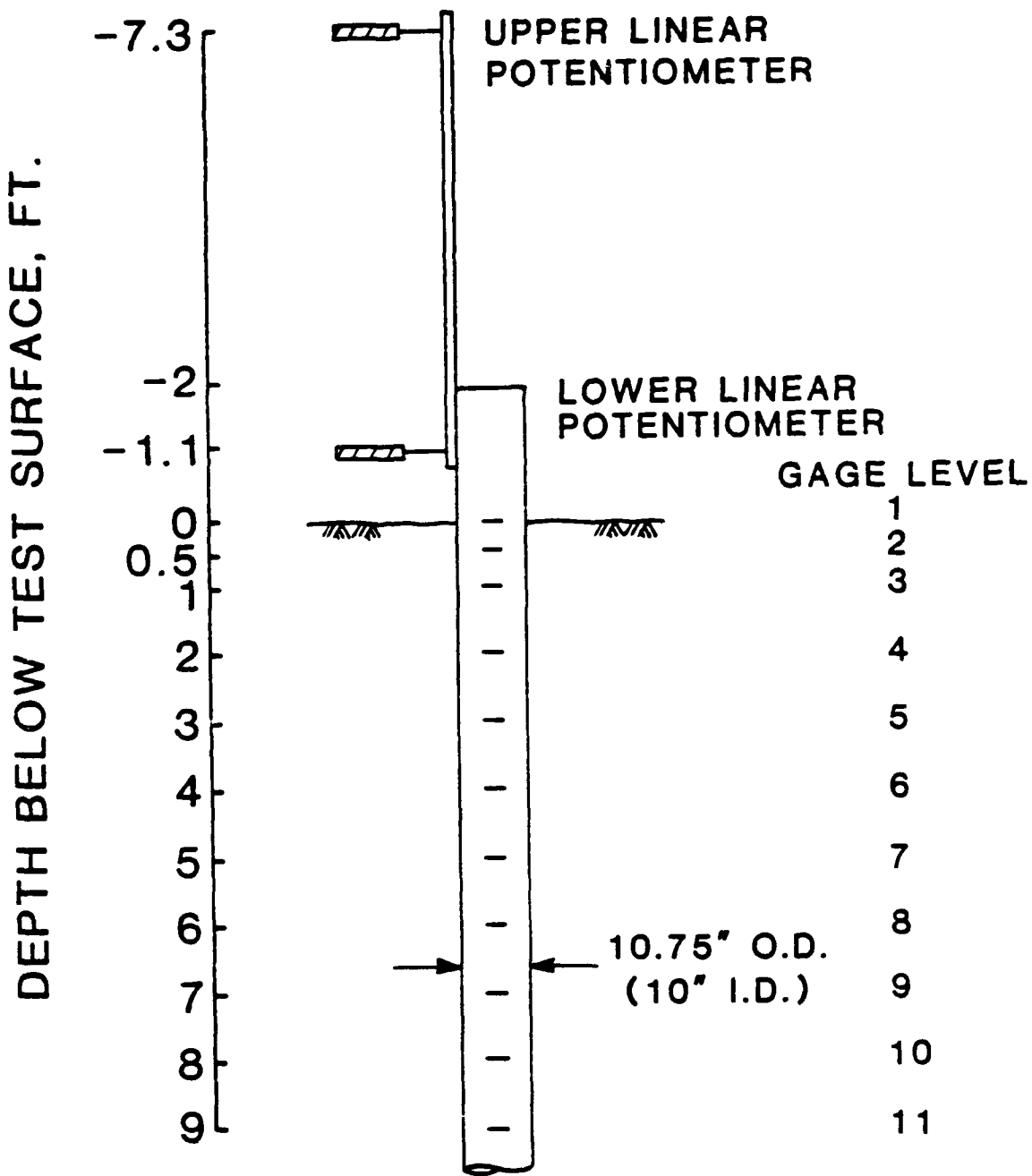
NOTE : STRAIN GAGES LOCATED IN
PLANE OF LOADING

Fig. 3.5.b.   Schematic Section of the Intrumented "Far
Field" Pile.

34
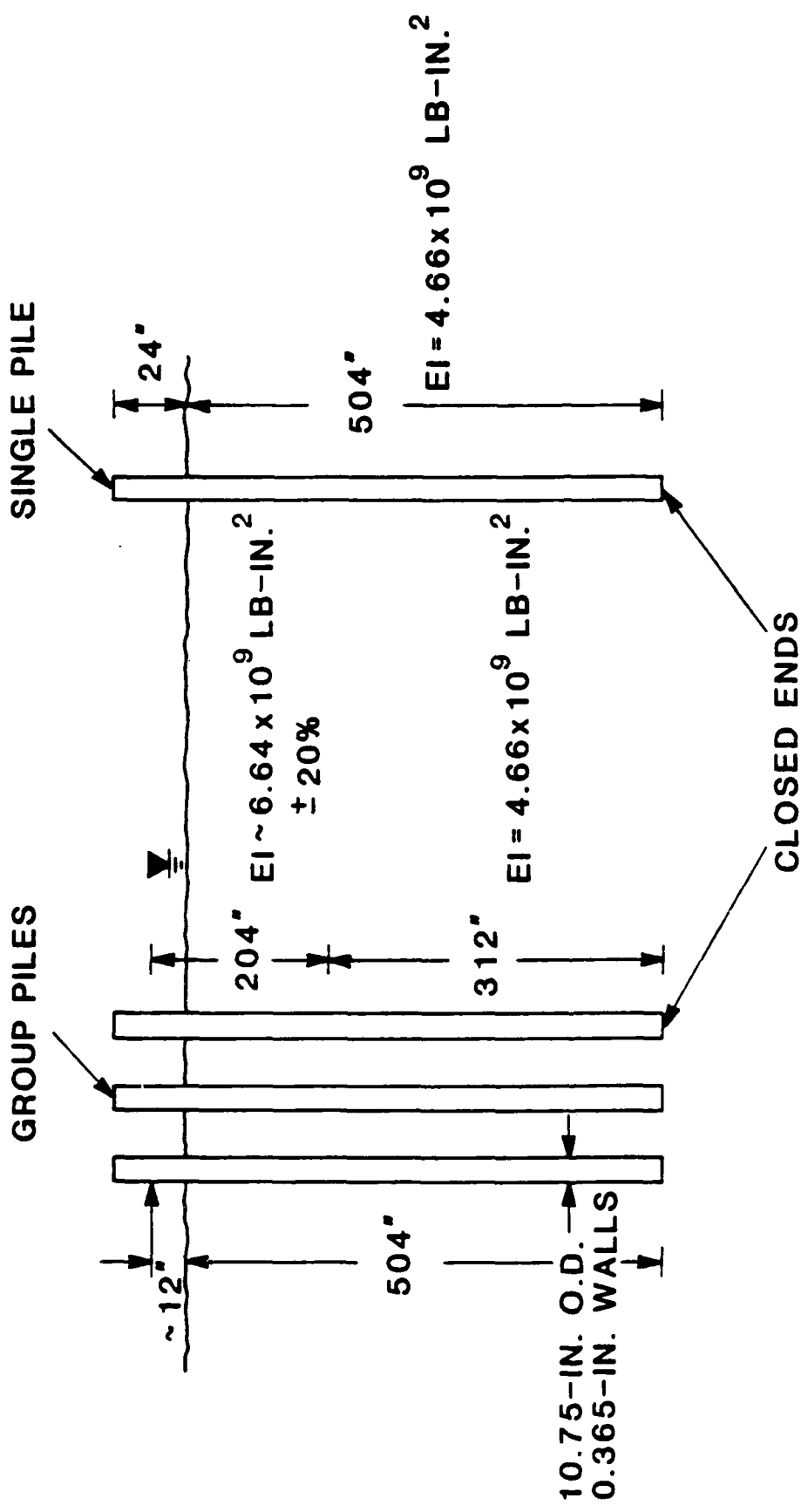
Fig. 3.6. Estimated Values of EI with Depth (After Brown and Reese, 1985).

SINGLE PILE

24"

504"

$EI = 4.66 \times 10^9$ LB-IN.^{2}

GROUP PILES

CLOSED ENDS

204"

$EI \approx 6.64 \times 10^9$ LB-IN.^{2} $\pm 20\%$

312"

$EI = 4.66 \times 10^9$ LB-IN.^{2}

~12"

504"

10.75-IN. O.D. 0.365-IN. WALLS

Due to the densification that took place during the testing of the complete group in sand, which preceded the test in the present study, the test surface settled about one ft in the vicinity of all group piles. (See dashed line on Fig. 3.3.) The site was then refilled to original grade in order to raise the test surface to its previous level. The soil was then "exercised" by drawing down the water level through an underdrain system installed at the time the sand fill was placed and reflooding three times. This was done in an attempt to ensure uniformity in the density of of the sand fill placed to relevel the surface of the pit.

3.2. Testing Procedure

The primary purpose of the test program described here was to develop 2-pile interaction factors for displacement of a free-head (or pinned-head) pile group. As mentioned in Chapter I, two approaches are possible for making the necessary measurements: (A) load a pile in the group, measuring its pile-head deflection, and measuring the deflection of neighboring unloaded piles; such an approach is expressed in Eq. 1.1 and is only valid for elastic conditions; and (B) load one pile, measuring its pile-head deflection; then load any two piles to the same load per pile and measure the deflection of the 2-pile group, as expressed in Eq. 1.2. Method B was selected over Method A since it allows for consideration of strong nonlinear effects such as the computation of the resistance reduction in the trailing pile due to the motion of the leading pile and vice versa when the piles in

36

the group are loaded simultaneously. Calculations of α are based on considerations of relative flexibilities, as described in Chapter IV. Based on this approach, the general sequence for the pile testing was therefore as follows. (See Fig. 3.4.)

(1) Load Pile V   ----> CONFIGURATION 1

(2) Load Pile Y   ----> CONFIGURATION 2

(3) Load Piles V and Y   ----> CONFIGURATION 3

(4) Load Piles S, V, and Y   ----> CONFIGURATION 4

(5) Load Piles X, Y, and Z   ----> CONFIGURATION 5

The logic behind this sequence is explained below.

- Loading of Pile V (CONF. 1) gives the single-pile flexibility for Pile V.

- Loading of Pile Y (CONF. 2) gives the single-pile flexibility for Pile Y and an independent check on single pile flexibility in general when flexibilities of Piles V and Y are compared.

- Loading of Piles V and Y (CONF. 3) gives the additional flexibility in Pile V due to load on Pile Y, and vice versa. Therefore, α factors can be computed for a spacing of 3 diameters as a function of: departure angle ($\xi = 0°$ and $180°$, where ξ is defined in Fig. 3.7); number of cycles of load; and load magnitude.

- Loading on Piles S, V, and Y (CONF. 4) gives the additional flexibility in Pile S due to loads on Pile

37
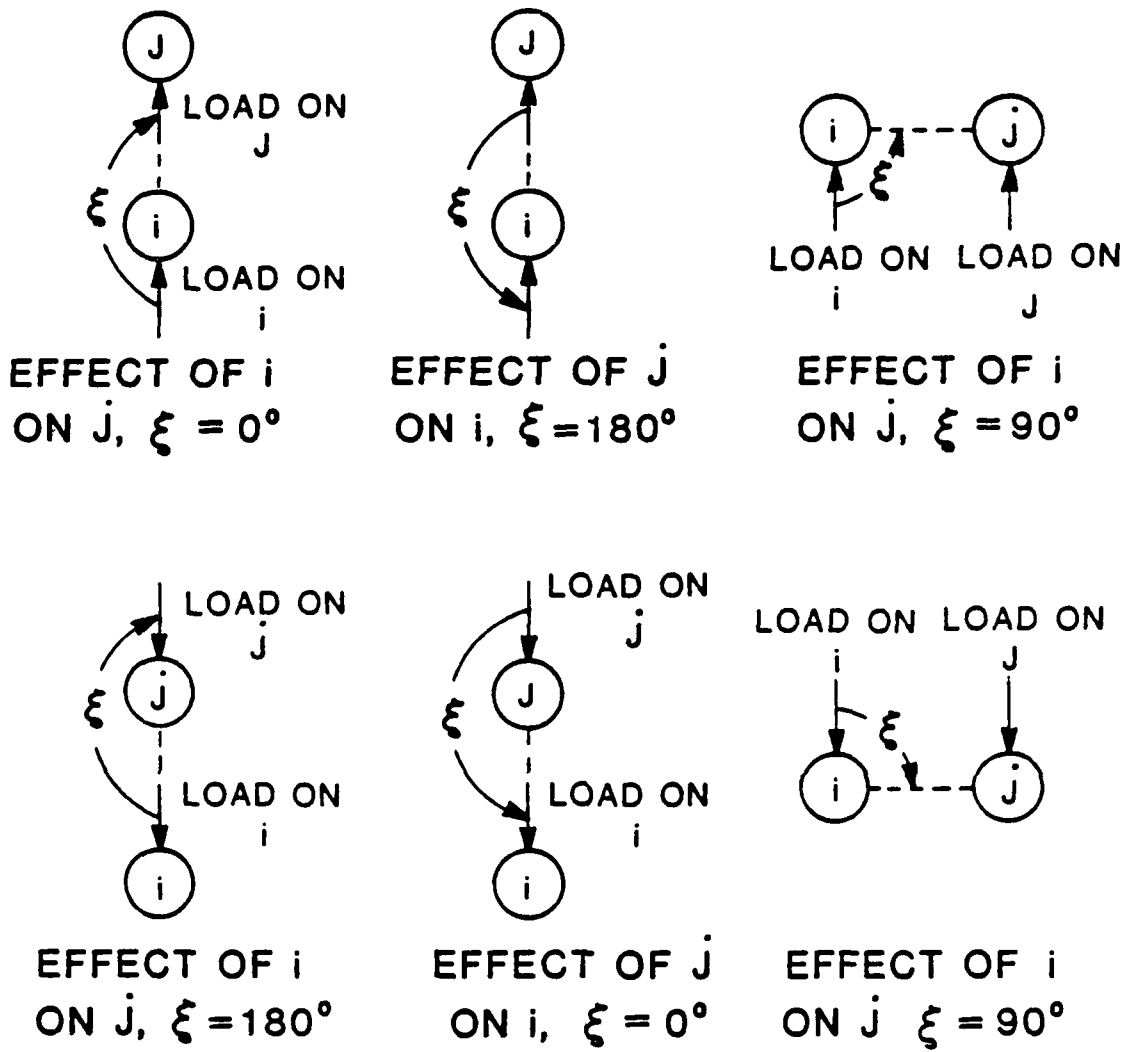
Fig. 3.7. Definition of ξ.

Y, and vice versa. The effect on Pile S due to Pile Y is obtained indirectly by calculating the additional flexibility on Pile S due to Piles V and Y, and substracting the influence of Pile V on Pile S, obtained from the 2-pile group analysis (CONF. 3). Similarly, the effect on Pile Y due to S is obtained by calculating the additional flexibility on Pile Y due to Piles S and V, and substracting the influence of Pile V on Pile Y. α factors can thus be calculated for a spacing of 6 diameters as a function of: departure angle ($\xi = 0°$ and $180°$); number of cycles of load; and load magnitude.

- Loading on Piles X, Y, and Z (CONF. 5) gives the additional flexibility in Pile Y due to loads on Piles X or Z. It is assumed that the influence of Pile X on Pile Y and the influence of Pile Z on Pile Y are the same, since no test for a 2-pile group, loaded side by side, was feasible with the available test arrangement. α factors can be calculated for a spacing of 3 diameters as a function of: departure angle ($\xi = 90°$); number of cycles of load; and load magnitude.

- In addition, observation of deflections of unloaded "far field" piles (> 6 diameters away from a loaded pile, where Method A (Chapter I) is assumed to be valid; e.g., Pile Q) yielded approximations of α factors at distances exceeding the distances between the loaded piles. This "far field" effect is assumed not

39

to be influenced by the shadowing effect. Table 3.1 provides a chronology of the testing program and comments on anomalies during testing.

Loading and data acquisition protocol for each of the five configurations consisted of: (1) applying the first cycle of load (or virgin cycling) for a load of $\pm$ 4 kips per pile; (2) cycling (100 cycles) at deflections equal to those attained for the first cycle; and (3) repeating the procedure for nominal loads of 12 and 20 kips per pile. After the first cycle was achieved, cycled loading was by controlled deflection. During cycling, load was applied to the loaded piles through a hydraulically powered actuator. Table 3.2 summarizes the loading levels and reading procedure within each loading set. One set of readings consisted of shears, deflections, head rotations, and moments at each gage level on all piles.

The loading frame used to apply load to the piles in all tests consisted of a main loading beam (W21 X 62), 4 loading columns (W8 X 31) and 9 channel cross members (C6 X 8.2). A schematic plan view of the loading frame is shown on Fig. 3.8. The specific pile(s) to be loaded were controlled by connecting the appropriate pile(s) to the frame by load cells.

Since the loading frame was structurally unstable for Configurations 1 and 2, with initial support only at the load cell connection, additional supports (2 on each side) were installed to prevent instability of the loading frame

40

Table 3.1. Chronology of the Testing Program

TEST	DATE	OBSERVATIONS
Config. 1	Dec 17, 1984	Load cells on Piles U and V switched due to malfunction of load cell on Pile V at the first load level (4 kips).
Config. 2	Dec 18, 1984	–
Config. 3	Dec 18, 1984	Load cell on Pile U placed on Pile V for all load levels.
Config. 4	Dec 19, 1984	Load cell on Pile U placed on Pile V for all load levels.
Config. 5	Dec 19, 1984	–

Note: Rate of loading was set to 4 cycles per minute

Table 3.2. Loading Level and Reading Procedure

First Cycle Loading Level	Readings (Cycle Number and Load Directions)
	*
± 4 kips	1(N,S), 5(N,S), 10(N,S) 20(N,S), 100(N,S)
± 12 kips	1(N,S), 5(N,S), 10(N,S) 20(N,S), 100(N,S)
± 20 kips	1(N,S), 5(N,S), 10(N,S) 20(N,S), 100(N,S)

* N indicates piles translated to the north
  S indicates piles translated to the south
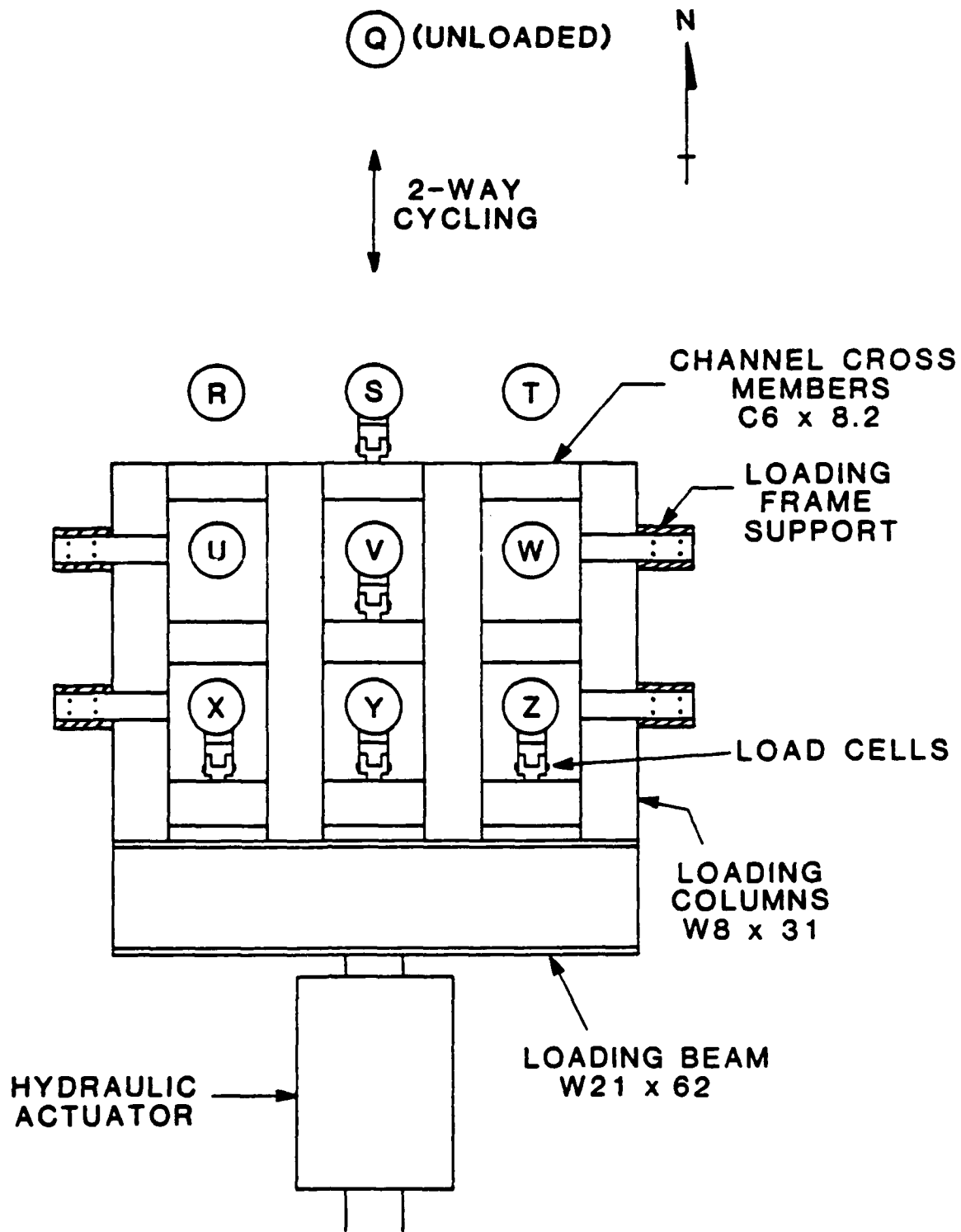
Fig. 3.8. Loading Frame.

during testing. Fig. 3.9 shows a cross section of a typical support. The purpose of the teflon and the grease was to minimize the friction between the loading frame and the steel support. A mixture of sand and cement was prepared and placed around 3 sides of each support (away from the test piles) to increase its stability.

As stated previously, removable load cells were placed between the cross channels and the loaded piles for a particular configuration. Each load-cell assembly consisted of a hinge bracket, a pile mounting plate (welded to the pile), a rod clevis, a load cell and a load-cell mounting plate (welded to the cross channels). A load-cell assembly is illustrated on Fig. 3.10.

The load was applied by a double-acting sinusoidally controlled hydraulic actuator with a 12-in.-diameter bore, situated between the loading frame and a reaction frame attached to the reaction shaft. The actuator also served to "balance" the load frame by carrying a small component of its dead weight. An existing 72-in. diameter, 37-ft long reinforced concrete drilled shaft (Fig. 3.2) was used as the reaction for the system. A 21-gallon-per-minute capacity hydraulic pump, operating at 3000 psi pressure, supplied hydraulic pressure to the actuator.

3.3. Data Acquisition System

Loads, deflections and strain gage output were monitored during the test with electronic data acquisition

44
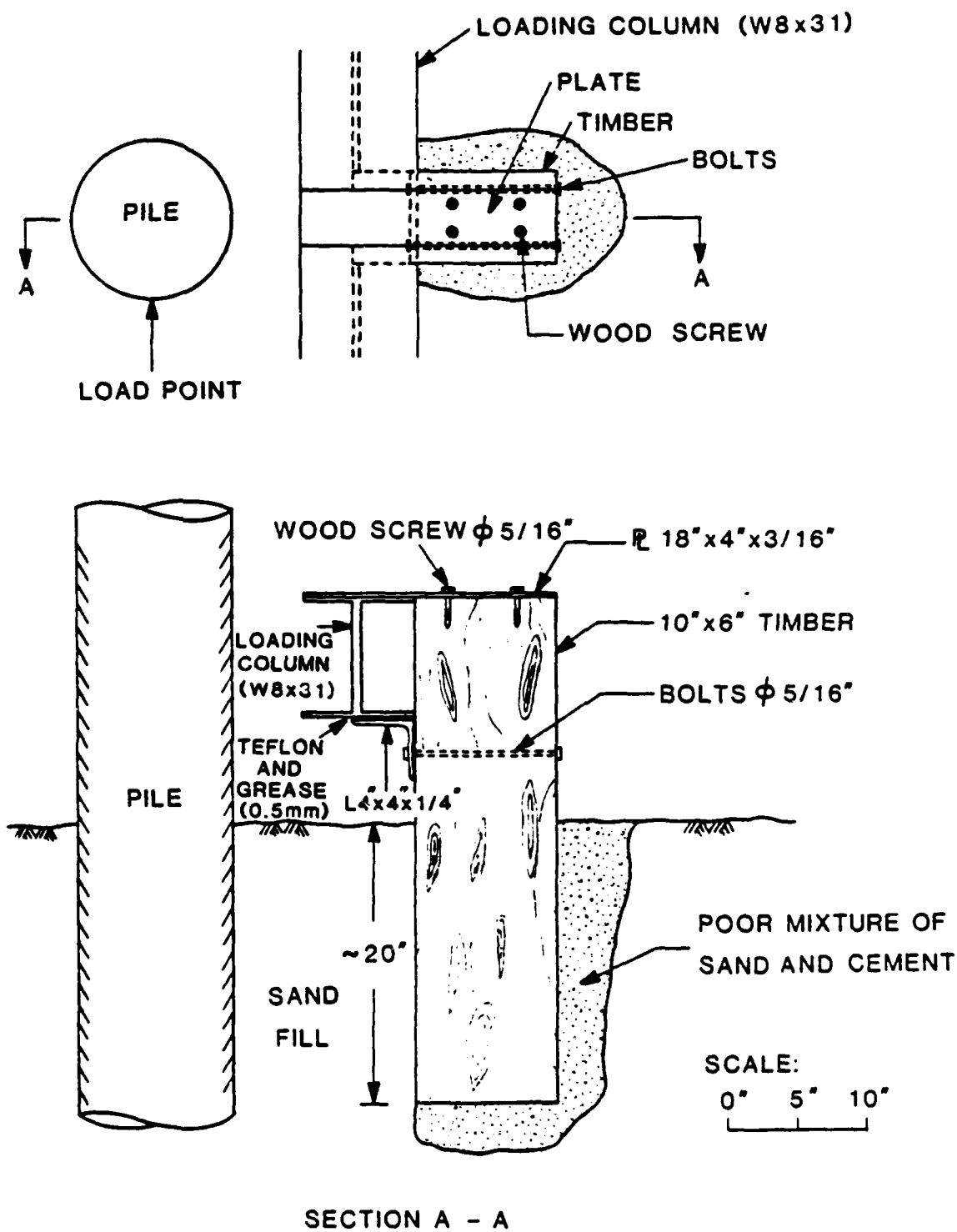
Fig. 3.9. Loading Frame Support.

45

PILE MOUNTING
PLATE

PIN LEADS

CHANNEL CROSS MEMBERS
C6 x 8.2

ROD
CLEVIS

NUTS

PILE

LOAD CELL

LOAD CELL
MOUNTING
PLATE

HINGE BRACKET
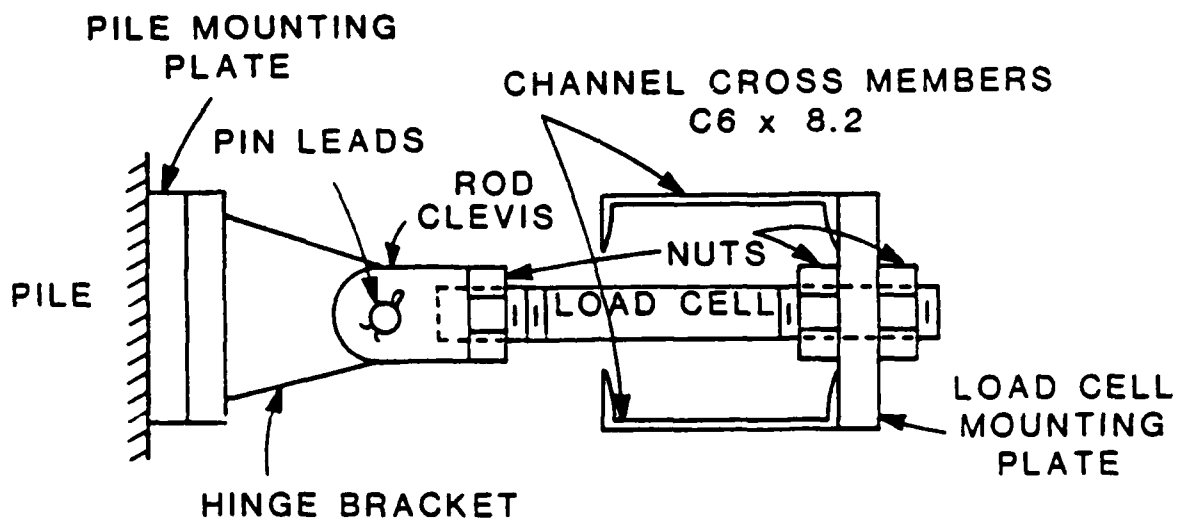
Fig. 3.10. Load-Cell Assembly (After Brown
and Reese, 1985).

equipment consisting of a panel board to which leads from electronic instruments (strain gages, load cells and linear potentiometers) were connected, a single regulated direct current 10-volt AC power supply (operated at 5 volts), two Hewlett-Packard 3497 A data acquisition/control units (which received voltages from the panel board, amplified and converted voltages to digital signals, and transmitted the signals to the microcomputer), and a single Hewlett-Packard 85 microcomputer used to control the digital data acquisition units, convert the readings to engineering units, and record all data on casette tapes.

A description of instruments used to measure deflections, bending moments, and load is presented below.

3.3.1. Deflection Instruments

Pile-head deflections and rotations were measured on each pile in the system by using linear potentiometers of the conductive-plastic type. One linear potentiometer was used to measure deflections approximately at the loading level; the other linear potentiometer was used to measure deflections at a level about 4 ft above the loading point. Rotations were determined from differences in potentiometer readings over a known spacing between potentiometers. The accuracy of this type of linear potentiometer has been estimated at about $\pm$ 0.005 in. (O'Neill and Dunnavant, 1984).

A total of 20 linear potentiometers was used to monitor the 9 piles in the group and the "far field" pile (Pile Q).

All linear potentiometers for the group piles were mounted on a reference frame that was supported by two 60-ft-deep, 48-in.-diameter steel casings located on either side of the pit (Fig. 3.1). [Those casings had been used to isolate reaction rods from deep anchors when the pile group was tested axially in clay (O'Neill and Hawkins, 1982).]

3.3.2. Bending Moment Instruments

The bending moment measurements were made on instrumented pipes, 6.625-in. outside diameter, 0.310-in. wall thickness (Schedule 40), grouted into each of the 9 piles in the group. The grout mix consisted of 2 parts of fine sand to 1 part of cement with a water-to-cement ratio of 0.5 (Brown and Reese, 1985).

Strain gages (Micro-Measurements, Type CEA-06-500UW-120) were affixed to the outside of the insert pipes at different levels. Each level consisted of 4 gages, configured as two vertical gages on each side of a north-south direction wired in a full bridge configuration at the panel board (located in an instrumentation trailer). Lead wires were encased in a PVC pipe and a flexible sheathing made of foam from the end of the PVC pipe to the top of the grout-filled pipe. Calibrations between bridge output and moment obtained by Brown and Reese (1985), described earlier, were used in this study.

3.3.3. Load Measurements

Each load cell depicted in Fig. 3.10 consisted of a pipe

48

section instrumented with a full-bridge, epoxy-bonded strain gage system. These load cells were calibrated prior to the tests so that relationships between output voltage and load were known. Hence, data from the load cells were acquired and processed in a manner similar to the bending moment data on the piles.

A large tent was placed over the site in order to provide protection against possible rain and thermal effects. The weather during the three days of testing was cool and dry.

CHAPTER IV

EVALUATION OF INTERACTION FACTORS BETWEEN TWO PILES

When a pile group is subjected to a horizontal load and/or moment, the flexibility of each pile in the group is influenced by the presence of neighboring piles. Such loads induce reactions in the soil and, consequently, deformations in the soil mass surrounding the other piles These deformations in turn reduce the load required to produce a given deformation in the pile being affected. Such an influence is customarily quantified in terms of pile-head behavior by the use of an α factor. The purpose of this chapter is to define and evaluate α factors for groups of two free-head piles, simultaneously loaded and embedded in a non-elastic sand mass using the principle of relative flexibilities.

4.1. Simple 2-Pile Interaction Model (Free-Head)

For the system composed of two identical piles loaded as shown in Fig. 4.1 (Piles V and Y), the general flexibility matrix is expressed as:

$$
\begin{bmatrix} F_{11} & F_{12} \\ F_{21} & F_{22} \end{bmatrix}
\begin{bmatrix} P_v \\ P_y \\ M_v \\ M_y \end{bmatrix}
=
\begin{bmatrix} \delta_v{}^g \\ \delta_y{}^g \\ \theta_v{}^g \\ \theta_y{}^g \end{bmatrix}
, \qquad (4.1)
$$

50
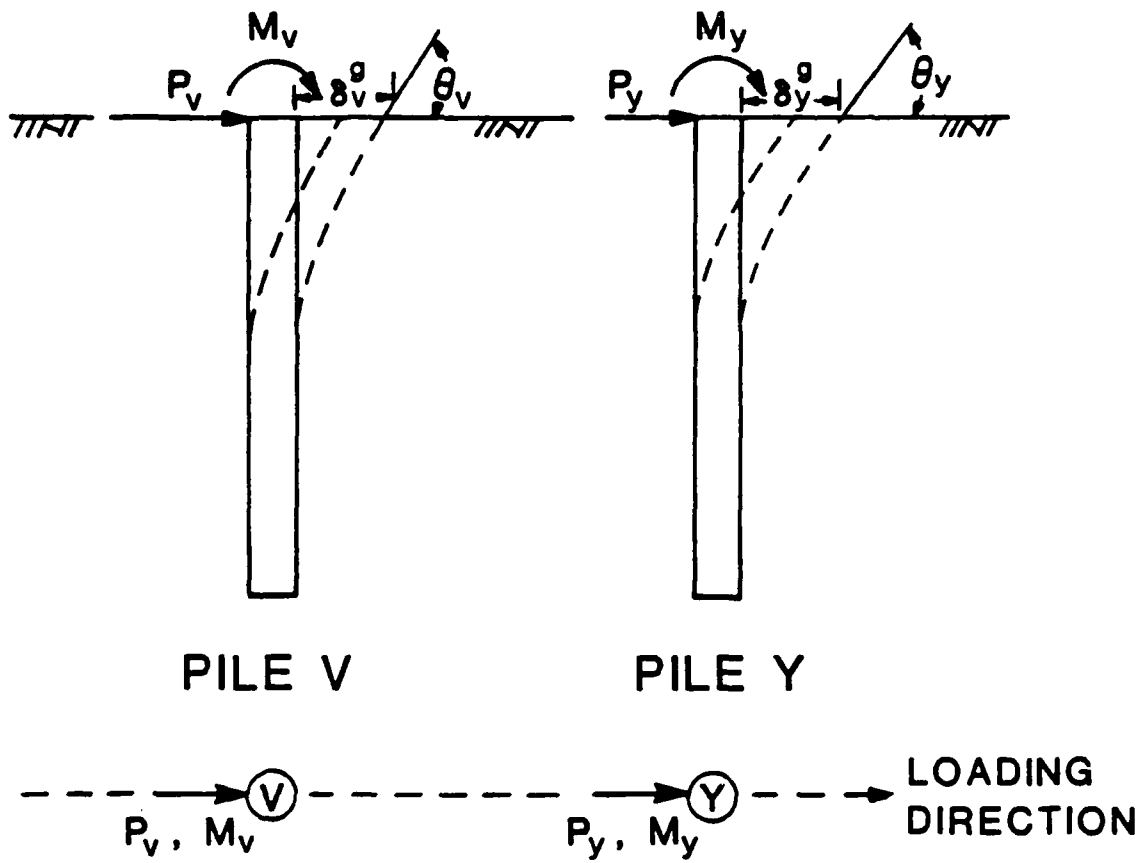
Fig. 4.1.   Two-Pile Group Model (Free-Headed).

51

or,

$$\left[F \right] \left[L \right] = \begin{bmatrix} \delta^g \\ \theta^g \end{bmatrix} ,$$

where

F = Final flexibility matrix,

L = Load matrix (P = horizontal load, M = moment),

δ^g = Pile-head deflection in the group,

θ^g = Pile-head rotation in the group.

Partitioning the flexibility matrix of Eq. 4.1,

$$\left[F_{11} \right] \begin{bmatrix} P_v \\ P_y \end{bmatrix} + \left[F_{12} \right] \begin{bmatrix} M_v \\ M_y \end{bmatrix} = \begin{bmatrix} \delta_v{}^g \\ \delta_y{}^g \end{bmatrix} , \qquad (4.2)$$

and

$$\left[F_{21} \right] \begin{bmatrix} P_v \\ P_y \end{bmatrix} + \left[F_{22} \right] \begin{bmatrix} M_v \\ M_y \end{bmatrix} = \begin{bmatrix} \theta_v{}^g \\ \theta_y{}^g \end{bmatrix} . \qquad (4.3)$$

For a free-(pinned-)head pile system, with no applied moment, $M_v = M_y = 0$, Eqs. 4.2 and 4.3 become:

$$\left[F_{11} \right] \begin{bmatrix} P_v \\ P_y \end{bmatrix} = \begin{bmatrix} \delta_v{}^g \\ \delta_y{}^g \end{bmatrix} \qquad (4.4)$$

and

$$\left[F_{21} \right] \begin{bmatrix} P_v \\ P_y \end{bmatrix} = \begin{bmatrix} \theta_v{}^g \\ \theta_y{}^g \end{bmatrix} . \qquad (4.5)$$

Expanding Eq.(4.4) gives

$$\begin{bmatrix} f_{vv} & f_{vy} \\ f_{yv} & f_{yy} \end{bmatrix} \begin{bmatrix} P_v \\ P_y \end{bmatrix} = \begin{bmatrix} \delta_v{}^g \\ \delta_y{}^g \end{bmatrix} , \qquad (4.6)$$

where

f_{vv} = single Pile V flexibility,

f_{yy} = single Pile Y flexibility,

f_{vy} = additional flexibility in Pile V due to loading of Pile Y,

f_{yv} = additional flexibility in Pile Y due to loading of Pile V,

P_v = load on Pile V,

P_y = load on Pile Y,

$\delta_v{}^g$ = deflection of Pile V in group, and

$\delta_y{}^g$ = deflection of Pile Y in group.

Cross-coupling factors between deflection and rotation can be developed from Eq.(4.5), following the procedure described subsequently. However, such factors are not needed in the analysis of pinned-headed groups and will not be evaluated here.

Displacement flexibility factors can be obtained as follows:

f_{vv} = secant to single-Pile V load-deflection curve;

f_{yy} = secant to single-Pile Y load-deflection curve.

f_{vy} and f_{yv} can be obtained from Eq.(4.6),

$$f_{vv} P_v + f_{vy} P_y = \delta_v{}^g ;$$

53

then

$$f_{vy} = (\delta_v{}^g - f_{vv} P_v) / P_y = (\delta_v{}^g - \delta_v{}^s) / P_y \qquad (4.7)$$

$$= \underline{\frac{\text{defl. of Pile V in group} - \text{defl. of single Pile V.}}{\text{load on Pile Y}}}$$

Furthermore,

$$f_{yv} P_v + f_{yy} P_y = \delta_y{}^g ;$$

so that

$$f_{yv} = (\delta_y{}^g - f_{yy} P_y) / P_v = (\delta_y{}^g - \delta_y{}^s) / P_v \qquad (4.8)$$

$$= \underline{\frac{\text{defl. of Pile Y in group} - \text{defl. of single Pile Y.}}{\text{load on Pile V}}}$$

α factors can be defined by rewriting Eq. 4.6 as follows:

$$f_{vv} \begin{bmatrix} 1 & f_{vy}/f_{vv} \\ f_{yv}/f_{vv} & f_{yy}/f_{vv} \end{bmatrix} \begin{bmatrix} P_v \\ P_y \end{bmatrix} = \begin{bmatrix} \delta_v{}^g \\ \delta_y{}^g \end{bmatrix} .$$

Assuming that $f_{vv} = f_{yy}$, the special flexibility matrix can finally be written as:

$$f_{vv} \begin{bmatrix} 1 & \alpha_{vy} \\ \alpha_{yv} & 1 \end{bmatrix} \begin{bmatrix} P_v \\ P_y \end{bmatrix} = \begin{bmatrix} \delta_v{}^g \\ \delta_y{}^g \end{bmatrix} ,$$

in which

$$\alpha_{vy} = f_{vy}/f_{vv} \quad (4.9); \qquad \alpha_{yv} = f_{yv}/f_{vv} . \quad (4.10)$$

α_{vy} is presumably a function of the load on Pile Y, number of cycles of load, spacing between Piles V and Y, and direction of loading expressed by the departure angle, ξ, defined previously. Likewise, α_{yv} is a function of the

54

load on Pile V, number of cycles of load, spacing between Piles V and Y, and direction of loading. In an ideal elastic soil, α_{vy} and α_{yv} are the same. In a real soil, particularly a sand, α_{yv} is not necessarily equal to α_{vy} because of the tendency for a leading pile to react more load than a trailing pile ("shadowing").

The single-pile flexibility (f_{vv}, f_{yy}) may be affected by the pile structural flexibility, the nonlinear-soil flexibility and the pile location in the group (outer or inner pile), because of different installation-induced stress states in the soil surrounding the various group piles.

The next section explains the experimental procedure that was followed in order to evaluate α factors from the general sequence of pile group testing (Conf. 1 through Conf. 5) using the mathematical context just described.

4.2. Evaluation of Data

4.2.1. Single Pile V and Pile Y flexibilities (Confs. 1,2)

Values obtained from testing Pile V (Conf. 1) and Pile Y (Conf. 2) were plotted as shown on Figs. A.2 - A.7 in the Appendix. Due to a malfunction of the load cell on Pile V for the load level of $\pm$ 4 kips, deflections only for higher loads ($\pm$ 12, $\pm$ 20 kips) are presented. It is believed that the two plotted points for Pile V are not sufficient for confident curve fitting; consequently, the fitting process for the single pile was performed based entirely on data from Conf. 2 (Pile Y).

Six load-deflection curves (Figs. A.2 - A.7) were fitted by a second-order least-squares equation and plotted for 1, 20 and 100 cycles of load and for each direction of loading (north and south). Zeroes for load levels $\pm$ 12 and $\pm$ 20 kips, Cycles 1, 20 and 100, correspond to the zero measured before applying the load $\pm$ 4 kips, Cycle 1. It is observed that deflections for higher loads on Pile V are in general close to the fitted curves obtained with data from Pile Y. Therefore, it is assumed that single Pile-V and Pile-Y flexibilities are equivalent ($f_{vv} = f_{yy}$). Based on those graphs, deflections corresponding to loads of 3, 7, 10, 13, and 16 kips, for cycles 1, 20, and 100 and for each loading direction were determined and stored (a total of 30 values). Values of single pile flexibilities (f_{vv}) were then computed and substituted into Eqs. 4.9 and 4.10. The resulting values of deflections also represent the values for the single pile deflections in Eqs. 4.7 and 4.8. Single pile flexibility computations for a load of 10 kips are illustrated in Figs. A.2 and A.5.

4.2.2. Two-Pile Group Flexibilities (Conf.3, S/D = 3)

4.2.2.1. Loading North, $\xi = 0°$ (Toward V)

Figs. A.8 - A.10 were developed in a manner similar to Figs. A.2 - A.7, except that they represent data from the test on the 2-pile group (Piles V and Y loaded together). Deflections of Pile V (leading pile) and loads on Pile Y (trailing pile) for loads of 3, 7, 10, 13 and 16 kips on

Pile V, for Cycles 1, 20, and 100, were determined and stored (30 values; 10 values from each graph). Such values represent deflections of Pile V as one of a 2-pile group and loads on Pile Y that are input into Eq. 4.7. Based on the stored values, additional flexibilities of Pile V due to loads on Pile Y (Eq. 4.7) and interaction factors α_{vy} (Eq. 4.9) were computed. A graphical illustration of the calculation of f_{vy} and α_{vy} from these data for a load of 10 kips on Pile V is shown on Fig. A.8. Values of α_{vy} (loading north) as a function of number of cycles of load (1, 20, 100) and load magnitude on Pile Y are plotted on Fig. 4.2. Linear fits to the discrete data so obtained are also shown.

4.2.2.2. Loading South, $\xi = 0°$ (Toward Y)

Figs. A.11 - A.13 represent conditions similar to those in Figs. A.8 - A.10, except that loading is toward Pile Y. Deflections of Pile Y (leading pile) and loads on Pile V (trailing pile) for loads 3, 7, 10, 13, and 16 kips on Pile Y, for Cycles 1, 20, 100, were determined and stored as before (30 values; 10 values from each graph). Such values represent deflections of Pile Y and loads on Pile V for use in Eq. 4.8. From the stored values, additional flexibilities of Pile Y due to loads on Pile V (Eq. 4.8) and interaction factors α_{yv} (Eq. 4.10) were computed. Values of α_{yv} (loading south) as a function of number of cycles of load, and load magnitude on Pile V, are shown on Fig. 4.3.

Physically, Figs. 4.2 and 4.3 represent the effect of a trailing pile on a leading pile ($\xi = 0°$). Ideally, these

57
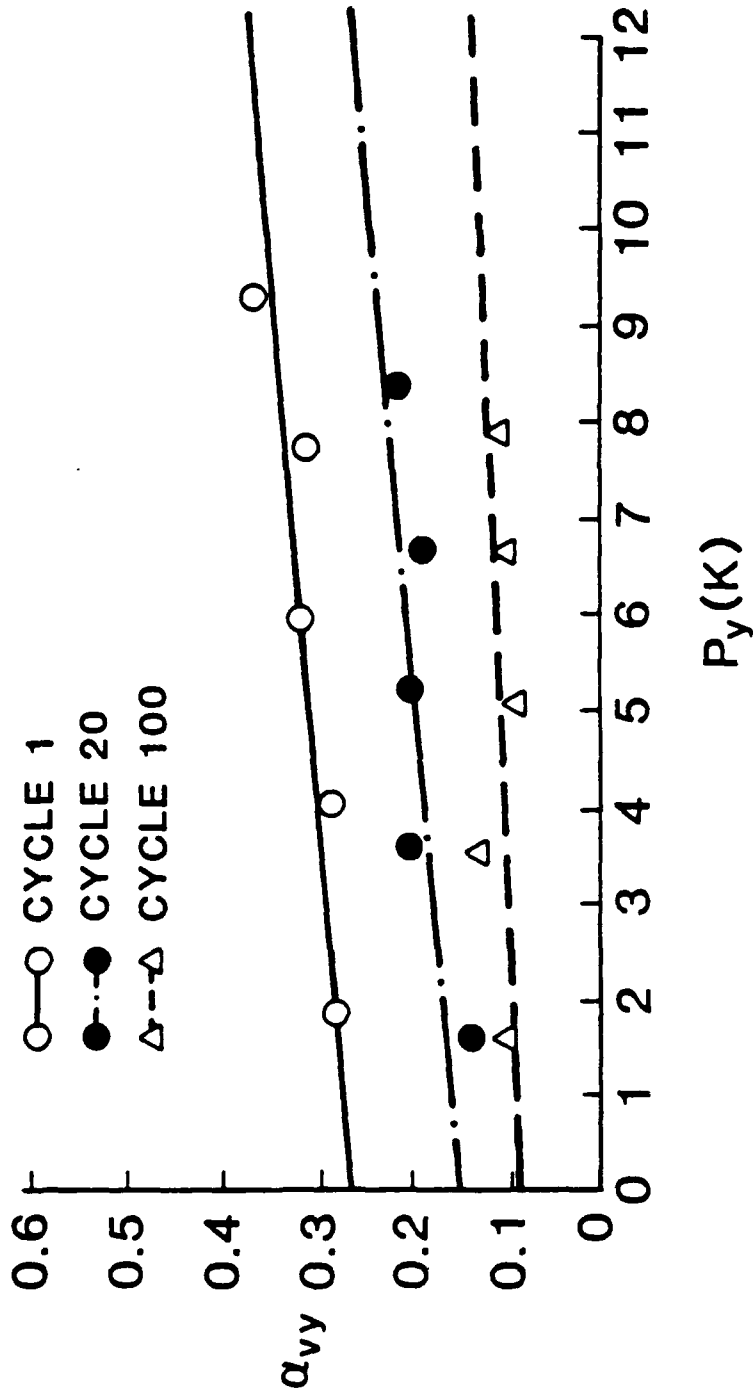
Fig. 4.2. α_{vy} vs. P_y, $\xi = 0°$, Loading North (Toward V), S/D = 3.
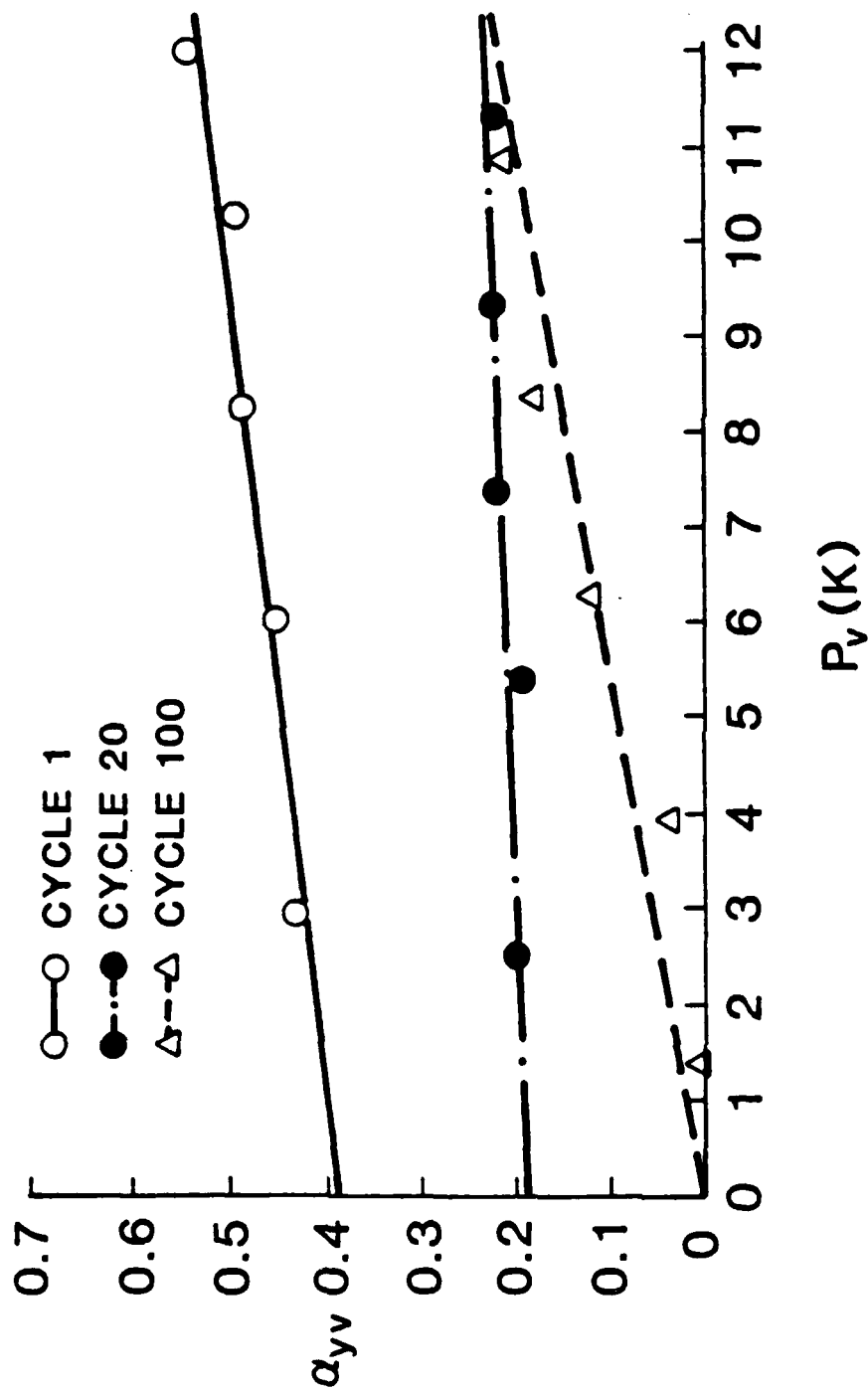
Fig. 4.3. α_{yv} vs. P_v, $\xi = 0°$, Loading South (Toward Y), $S/D = 3$.

59

figures should be identical. Some differences are evident because of normal experimental errors in load and deflection measurements and possibly because of asymmetric soil stiffening effects produced by the presence of unloaded surrounding piles and loading history. In order to minimize such effects, averages of the data presented in Figs. 4.2 and 4.3 were obtained and plotted in Fig. 4.4, which represents α_{ij} factors for effect of the trailing pile (j) on the leading pile (i) in a 2-pile group with 3 diameter spacing, and loaded parallel to the pile alignment. It is observed that this α factor increases with increasing load magnitude but decreases as the number of load cycles increases. Errors in measurements of both load and deflection affect the calculations of the final values of α. An estimate of the effects of errors in displacement measurements on α is given in Appendix B.

4.2.2.3. Loading South, $\xi = 180°$ (Toward Y)

Figs. A.14 – A.16 were also generated for Configuration 3. From these graphs, deflections of Pile V (trailing pile) and loads on Pile Y (leading pile) for values of load on Pile V were determined and stored (26 values; 10 from Fig. A-13, 8 from Fig. A-14 and 8 from Fig. A-15). Additional flexibilities of Pile V due to loads on Pile Y (Eq. 4.7) and interaction factors α_{vy} (Eq. 4.9) were computed. A graphical illustration of the computations of f_{vy} and α_{vy} from these data for a load of 10 kips on Pile V is shown on Fig. A.14. Fig. 4.5 shows values of α_{vy} as a function of number

60

Fig. 4.4. α_{ij} vs. P_j, $\xi = 0°$, $S/D = 3$.

61
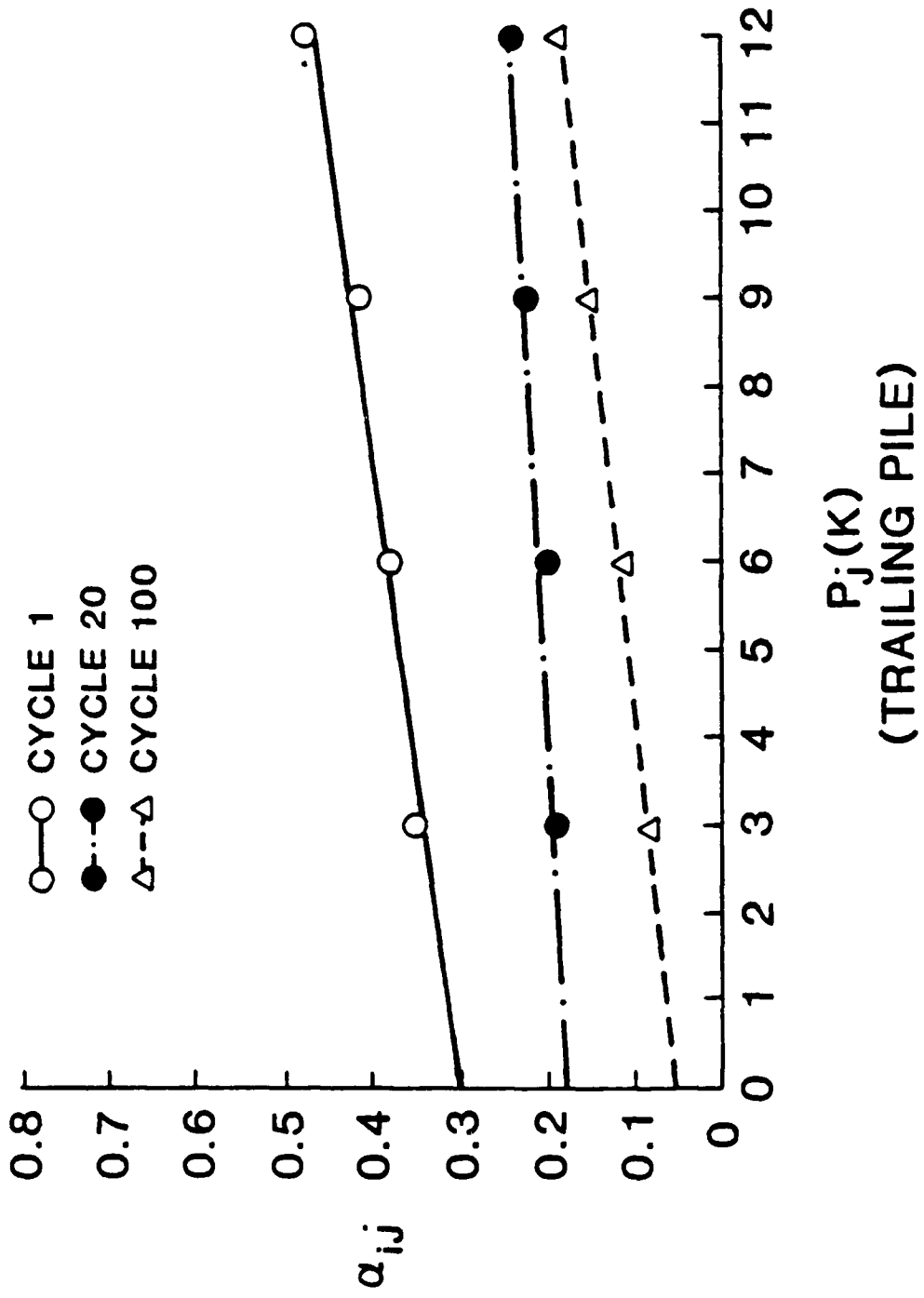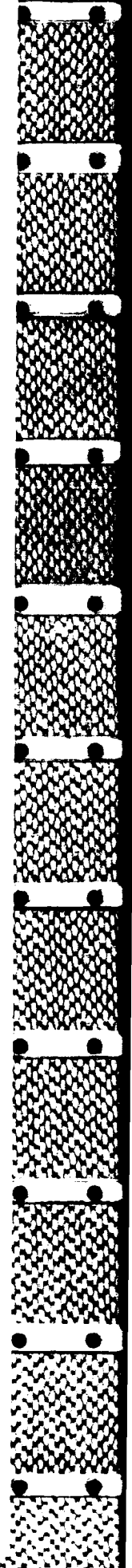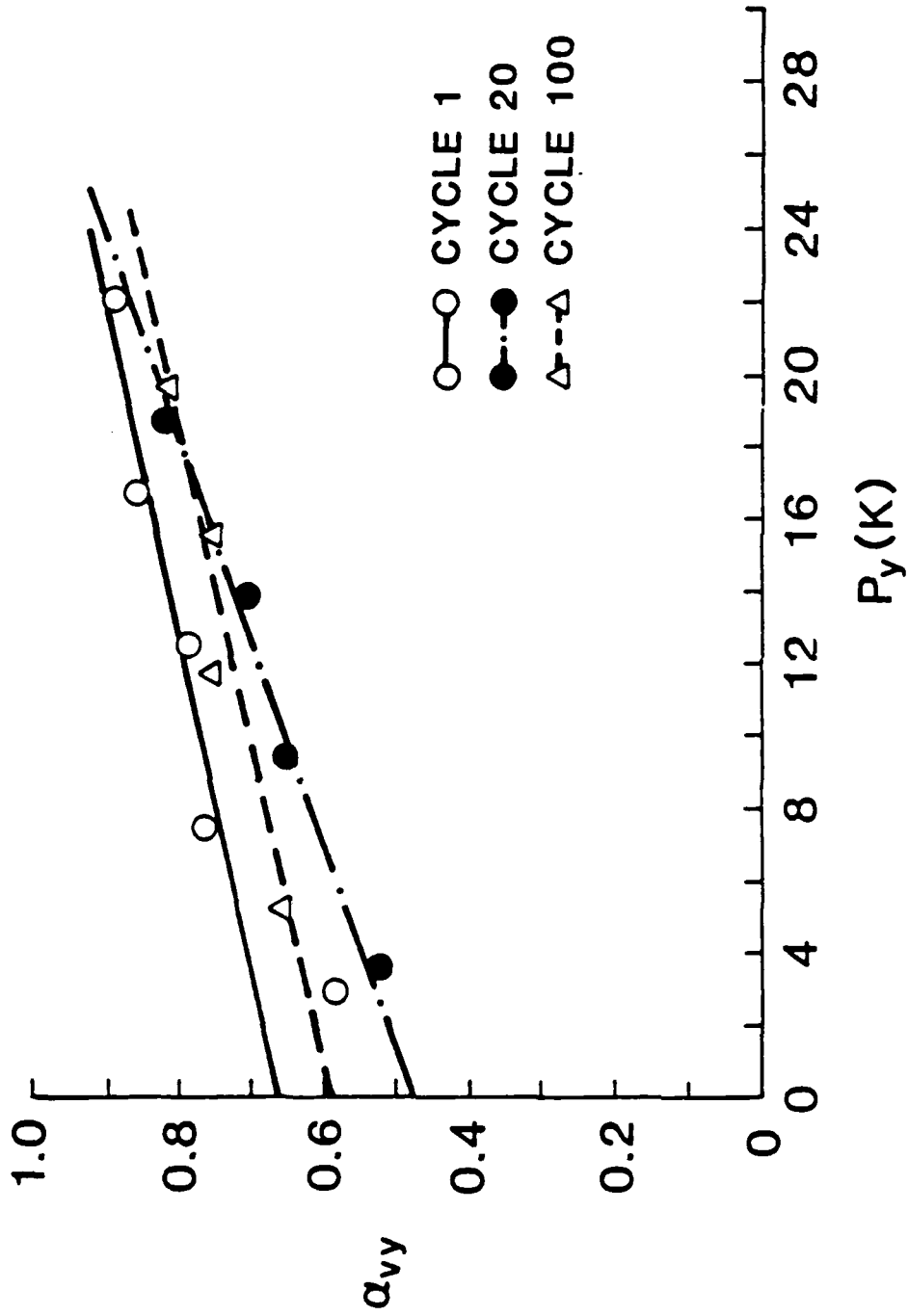
Fig. 4.5. α_{vy} vs. P_y, $\xi = 180°$, Loading South (Toward Y), $S/D = 3$.

62

of cycles of load and load magnitude on Pile Y.

4.2.2.4. Loading North, $\xi = 180°$ (Toward V)

Figs. A.17 - A.19 show data similar to Figs. A.14 - A.16 but for loading toward Pile V. From these graphs, deflections of Pile Y (trailing pile) and loads on Pile V (leading pile) for loads on Pile Y were determined and stored (22 values; 8 from Fig. A-16, 8 from Fig. A-17, 6 from Fig. A-18). Additional flexibilities of Pile Y due to loads on Pile V (Eq. 4.8) and interaction factors α_{yv} (Eq. 4.10) were computed. Fig. 4.6 shows values of α_{yv} as a function of number of cycles of load and load magnitude on Pile V. Again, the results were averaged. Fig 4.7 is the result of averaging Figs. 4.5 and 4.6 and represents α_{ij} factors vs. load magnitude for effect of the leading pile (j) on the trailing pile (i) ($\xi = 180°$) and a spacing of 3 diameters.

Fig. 4.7 can be compared directly with Fig 4.4. It is evident that the effect of the leading pile on the trailing pile (Fig.4.7) is much more significant than the effect of the trailing pile on the leading pile (Fig. 4.4). This effect can be explain physically by the fact that the lateral motion of the leading pile reduces the lateral confining stress on the soil in front of the trailing pile, which has a very significant softening effect on the flexibility of the trailing pile, whereas lateral motion of the trailing pile produces relatively little net strain increase around the leading pile.

There is also less dependence on the cycle number in

63
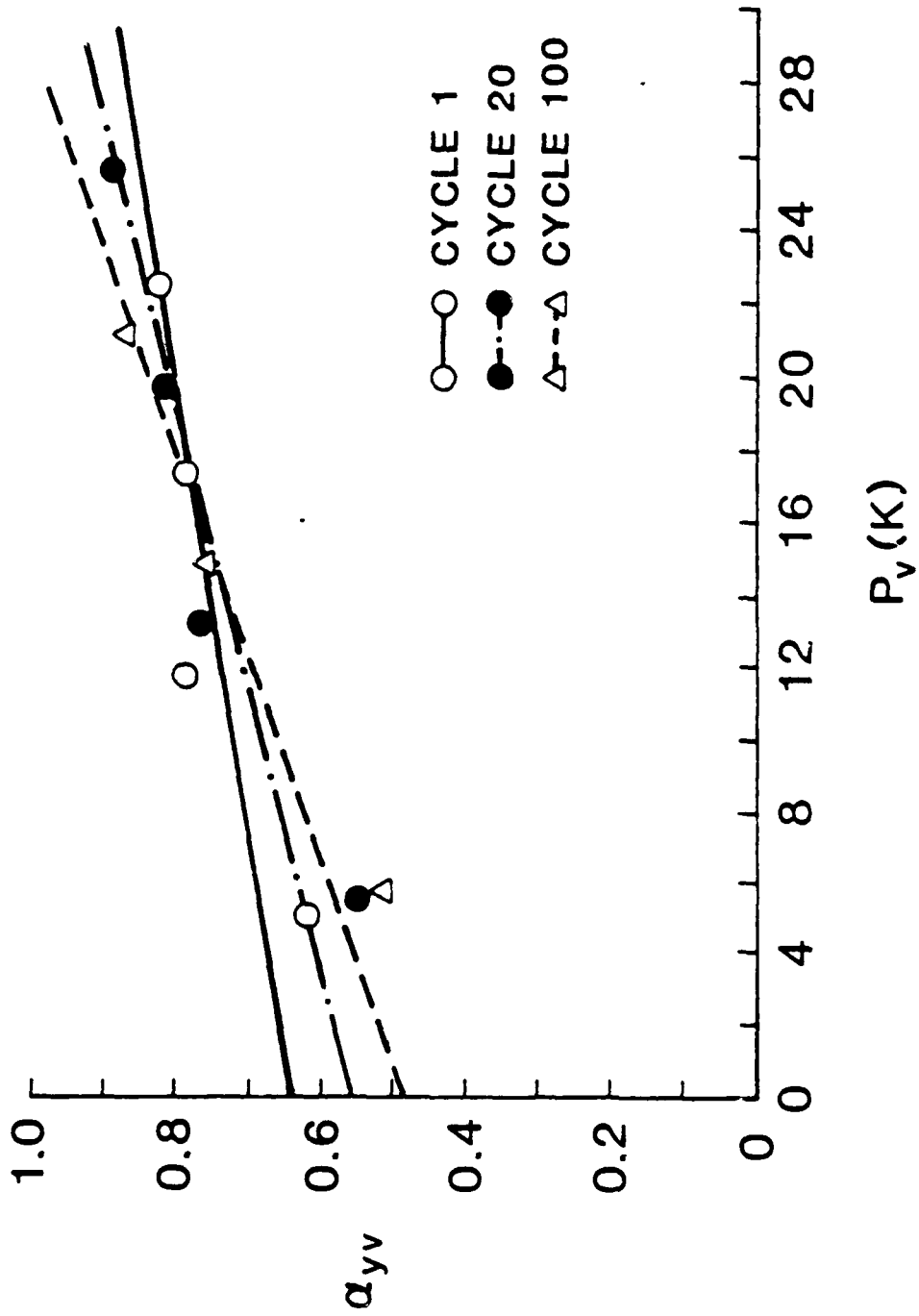
Fig. 4.6. α_{yv} vs. P_v, $\xi = 180°$, Loading North (Toward V), S/D = 3.

64
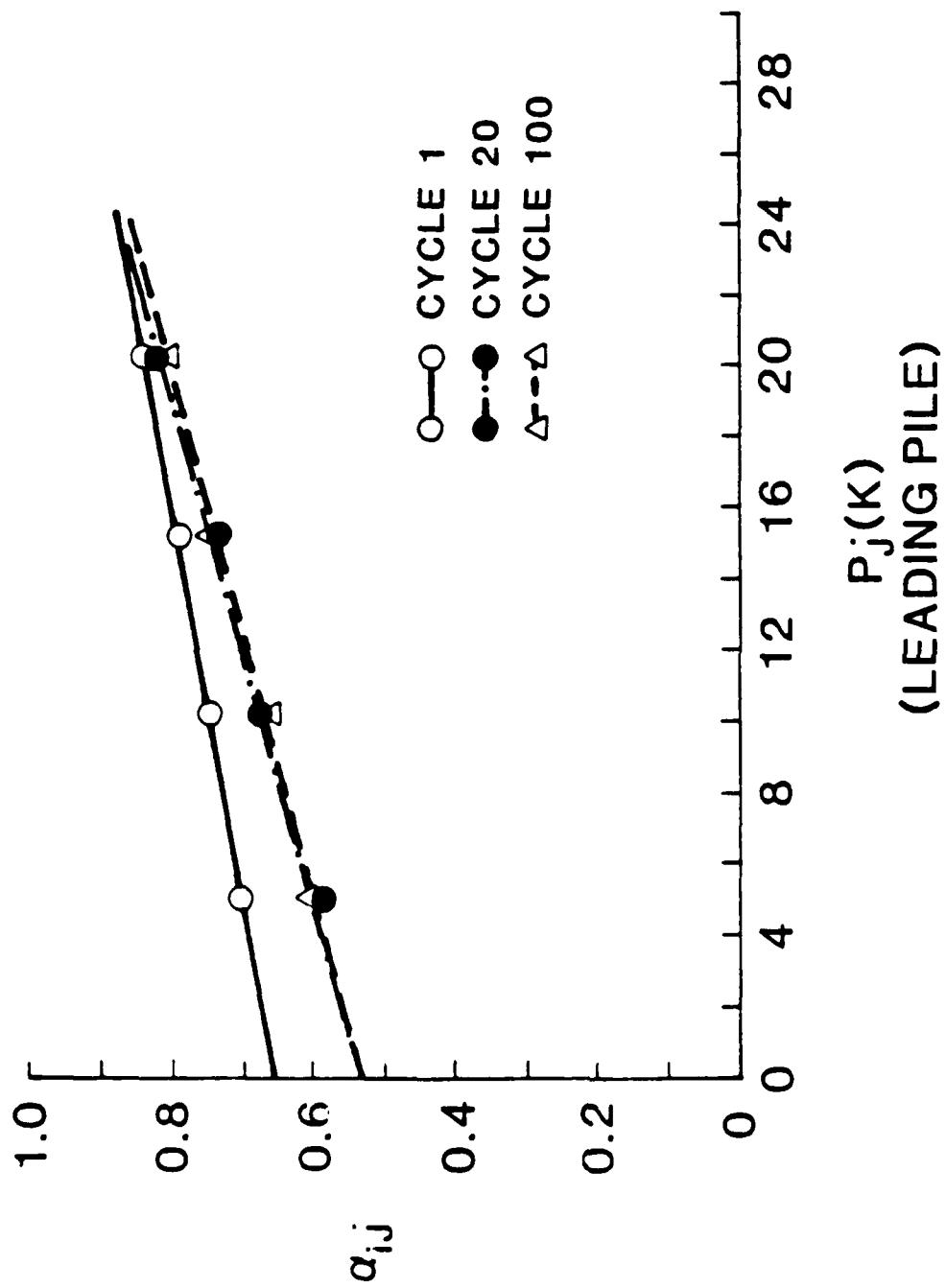
Fig. 4.7. α_{ij} vs. P_j, $\xi = 180°$, $S/D = 3$.

the effect described in Fig. 4.7 than in the effect described in Fig. 4.4.

4.2.3. Two-Pile Group Flexibilities (Conf.4, S/D = 6)

By analogy with the 2-pile group interaction model, but for a system composed of three identical piles (Piles S, V, and Y) subjected to a pile-head horizontal load only, the general flexibility matrix for free-headed piles can be reduced to the following expression:

$$
\begin{bmatrix}
f_{ss} & f_{sv} & f_{sy} \\
f_{vs} & f_{vv} & f_{vy} \\
f_{ys} & f_{yv} & f_{yy}
\end{bmatrix}
\begin{bmatrix}
P_s \\
P_v \\
P_y
\end{bmatrix}
=
\begin{bmatrix}
\delta_s^{\,g} \\
\delta_v^{\,g} \\
\delta_y^{\,g}
\end{bmatrix}
\quad , \quad (4.11)
$$

where

f_{ss}, f_{vv}, f_{yy} = Single pile (S, V, Y) flexibilities,

f_{sv}, f_{vs} = Additional flexibility in Pile S due to loading on Pile V, and vice versa,

f_{sy}, f_{ys} = Additional flexibility in Pile S due to loading on Pile Y, and vice versa,

f_{vy}, f_{yv} = Additional flexibility in Pile V due to loading on Pile Y, and vice versa,

P_s, P_v, P_y = Horizontal loads on Piles S, V and Y, and

$\delta_s^{\,g}, \delta_v^{\,g}, \delta_y^{\,g}$ = Deflections of Piles S, V and Y in the group.

66

From Eq. 4.11,

$$f_{ss} \; P_s + f_{sv} \; P_v + f_{sy} \; P_y \; = \; \delta_s{}^g;$$

$$f_{ys} \; P_s + f_{yv} \; P_v + f_{yy} \; P_y \; = \; \delta_y{}^g.$$

Then, flexibility coupling between Piles S and Y (6-diam. spacing) is given by:

$$f_{sy} = (\delta_s{}^g - f_{ss} \; P_s - f_{sv} \; P_v) \; / \; P_y$$

$$= (\delta_s{}^g - \delta_s{}^s - f_{sv} \; P_v) \; / \; P_y \; , \qquad (4.12)$$

$$f_{ys} = (\delta_y{}^g - f_{yy} \; P_y - f_{yv} \; P_v) \; / \; P_s$$

$$= (\delta_s{}^g - \delta_y{}^s - f_{yv} \; P_v) \; / \; P_s \; . \qquad (4.13)$$

Values of f_{sv} and f_{yv} from the 2-pile group flexibilities computed in previous sections are assummed to be valid for Eqs. 4.12 and 4.13. Loads P_s, P_v and P_y are obtained from the test where Piles S, V, and Y were loaded simultaneously (Conf. 4).

Assuming that $f_{ss} = f_{vv} = f_{yy}$, the general flexibility equation can be written as:

$$f_{ss} \begin{bmatrix} 1 & \alpha_{sv} & \alpha_{sy} \\ \alpha_{vs} & 1 & \alpha_{vy} \\ \alpha_{ys} & \alpha_{yv} & 1 \end{bmatrix} \begin{bmatrix} P_s \\ P_v \\ P_y \end{bmatrix} = \begin{bmatrix} \delta_s{}^g \\ \delta_v{}^g \\ \delta_y{}^g \end{bmatrix} \; ,$$

in which

$$\alpha_{sy} = f_{sy} \; / \; f_{ss} \qquad (4.14); \qquad \alpha_{ys} = f_{ys} \; / \; f_{ss} \; . \qquad (4.15)$$

Based on Eq. 4.11, but replacing deflections (δ) by rotations (θ), deflection-rotation cross-coupling α factors could also be obtained if they are required.

67

4.2.3.1. Loading North, $\xi = 0°$ (Toward S)

Figs. A.20 - A.22 are plots of data from the test on the 3-pile in-line group (Piles S, V and Y loaded simultaneously) loaded toward the north. Deflections of Pile S (leading pile) and loads on Pile V and Y (trailing piles) for loads of 3, 7, 10, 13 and 16 kips on Pile S were determined from these plots and stored (45 values; 15 values from each graph). Such values represent deflections of Pile S in the group and loads on Pile V and Pile Y for use in Eq. 4.12. Values of f_{sv} are taken to be identical to those of f_{vy} obtained from the 2-pile group analysis for a spacing of 3 diameters for loading to the north (Section 4.2.2.1). Based on the stored values, additional flexibilities of Pile S due to loads on Pile Y (Eq. 4.12) and interaction factors α_{sy} (Eq. 4.14) were computed. A graphical illustration of the determination of f_{sy} and α_{sy} from these data for a load of 10 kips on Pile S is shown on Fig. A.20. Values of α_{sy} (loading north) as a function of number of cycles of load (1, 20, 100) and load magnitude on Pile Y, are plotted on Fig. 4.8.

4.2.3.2. Loading South, $\xi = 0°$ (Toward Y)

Data and fitted relationships are shown in Figs. A.23 - A.25 in terms of deflections on Pile Y (leading pile) and loads on Piles V and S (trailing piles) for loads of 3, 7, 10, 13 and 16 kips on Pile Y. 45 values, 15 values from each graph, were stored. Such values represent the deflections of Pile Y in the group and load on Piles V and S for use in Eq.
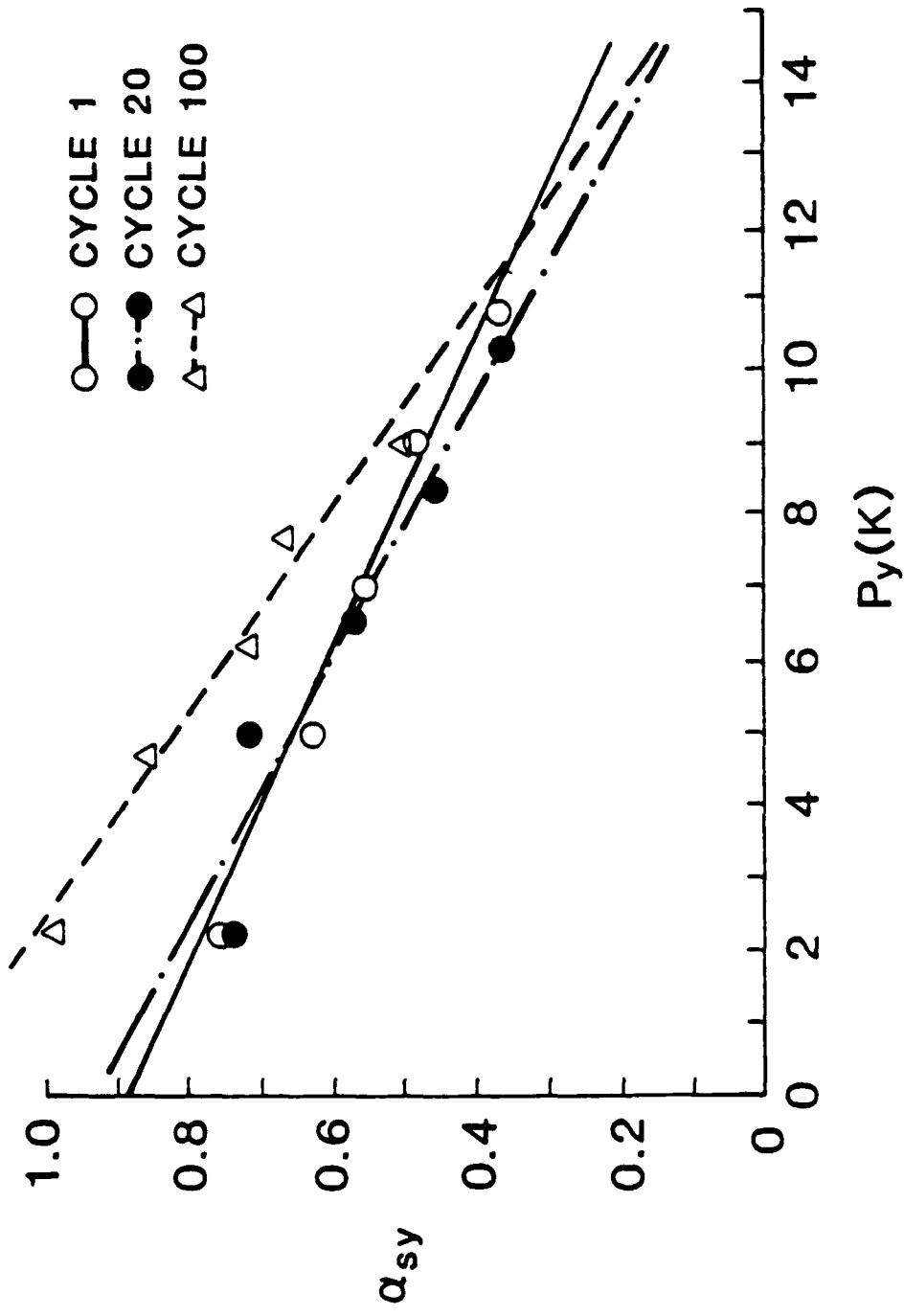
Fig. 4.8. α_{sy} vs. P_y, $\xi = 0°$, Loading North (Toward S), S/D = 6.

4.13. Values of f_{yv} for loading to the south were calculated previously in Section 4.2.2.2. Based on the stored values, additional flexibilities of Pile Y due to loads on Pile S (Eq. 4.13) and interaction factors α_{ys} (Eq. 4.15) were computed. The resulting values of α_{ys} (loading south) as a function of number of cycles of load (1, 20, 100) and load magnitude on Pile S are plotted on Fig. 4.9.

Fig 4.10 is the result of averaging Figs. 4.8 and 4.9 and represents the best estimate of α_{ij} factors vs. load magnitude on the trailing pile (P_j) for $\xi = 0°$ and a spacing of 6 diameters. Unfortunately, the results shown in Fig. 4.10 appear to be unreasonable. First, α-factors at most load levels and cycle numbers exceed those in Fig. 4.4 ($S/D = 3$). Furthermore, α-factors decrease markedly with increasing magnitude of load, which is inconsistent with observations from other configurations. Computed α-factors for this case are more subject to errors in measurements and to assumptions concerning flexibility than for other configurations. For example, it was assumed that $f_{ss} = f_{yy}$ and that the flexibility of the 2-pile group Y-V was identical to the flexibility of the Y-V subgroup in the tests on piles Y-V-S in order to apply the mathematical procedure for computing α factors. Also, the α factor for effect of a trailing pile on a leading pile involves division by the measured load on the trailing pile, which is much smaller than that on a leading pile, so that small absolute errors in reading load lead to relatively large errors in α. The cumulative
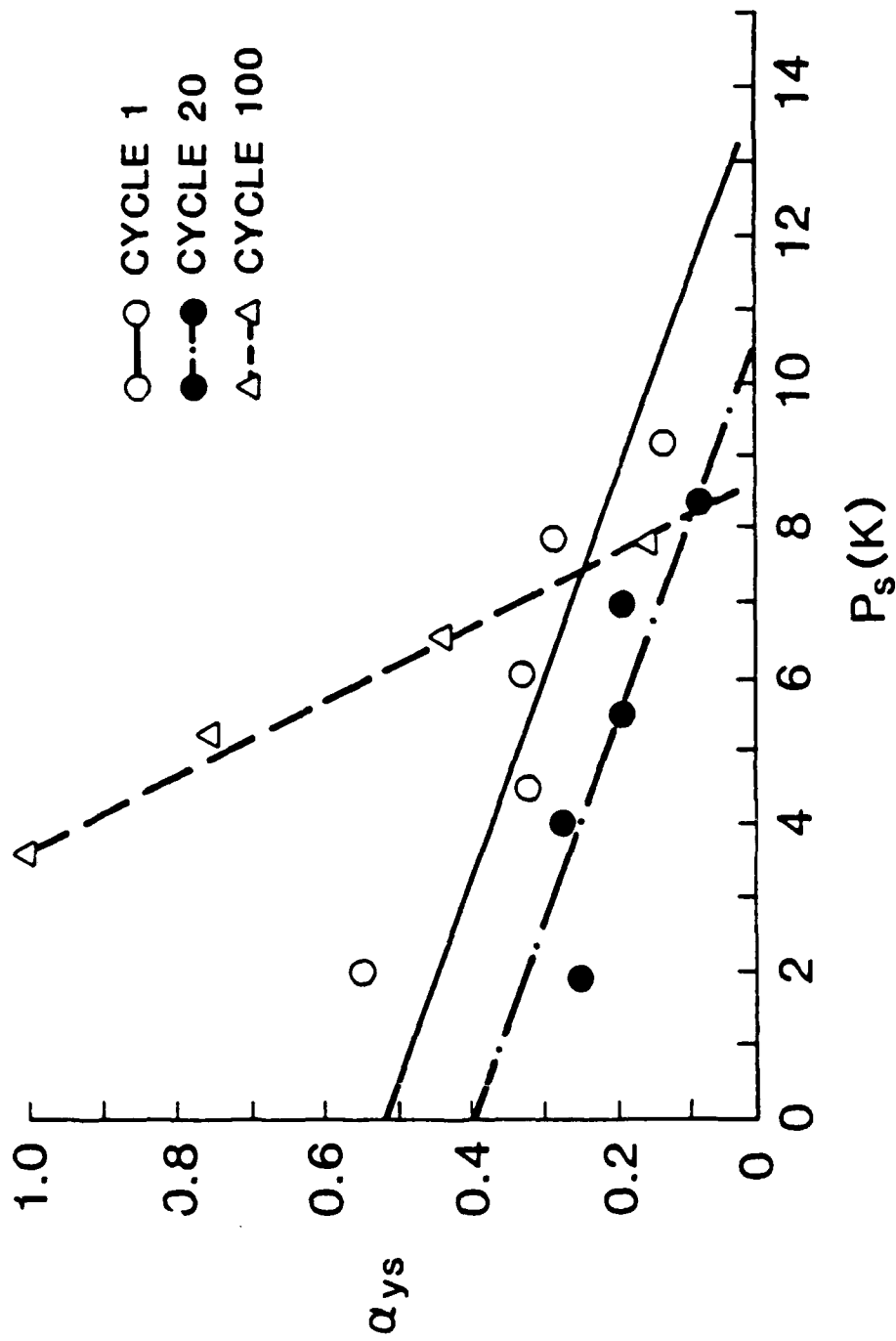
Fig. 4.9. α_{ys} vs. P_s, $\xi = 0°$, Loading South (Toward Y), S/D = 6.
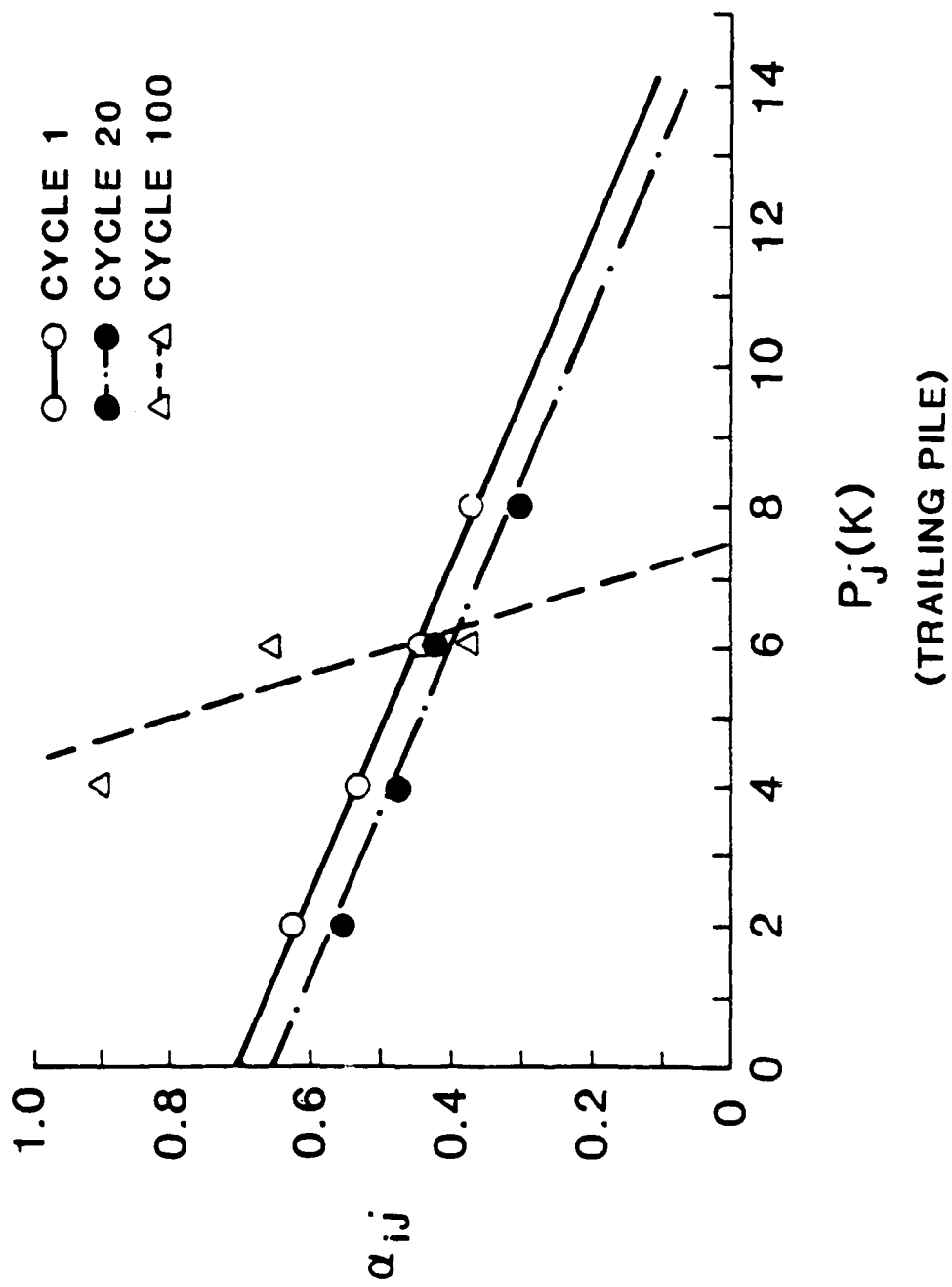
Fig. 4.10. α_{ij} vs. P_j, $\xi = 0°$, $S/D = 6$ (Questionable Validity).

72

effect of these phenomena are believed to have produced the unreasonably high α-values in Fig. 4.10. An evaluation of the cumulative effects of errors in displacement measurements for this configuration is offered in Appendix B. In order to resolve this problem, an "approximate" alternative based on Eq. 1.1 and data from Configuration 2 was then considerated. α_{sy} was recomputed from loading Pile Y and measuring the deflection on the unloaded Pile S (Loading north, $\xi = 0°$) for different load levels and number of cycles. It is believed the physical presence of the unloaded Pile V in Configuration 2 may have affected values of α_{sy} by stiffening the soil between the subscripted piles. Calculations of α_{sy} are presented in Table 4.1 and displayed graphically on Fig. 4.10.a. The results appear more consistent with the results for S/D = 3 than those in Fig. 4.10.

4.2.3.3. Loading South, $\xi = 180°$ (Toward Y)

From Figs. A.26 to A.28, deflections of Pile S (trailing pile) and loads on Pile V and Pile Y (leading pile) for Configuration 4 for loads of 3, 7, 10, and 13 kips on Pile S were determined and stored (36 values; 12 values from each graph). Values of f_{sv} are assumed equivalent to those of f_{vy} obtained from the 2-pile group analysis for loading to the south (Section 4.2.2.3). Additional flexibilities of Pile S due to loads on Pile Y (Eq. 4.12) and interaction factors α_{sy} (Eq. 4.14) were thus computed. A graphical illustration of the determination of f_{sy} and α_{sy} from these data for a load of 10 kips on Pile S is shown in Fig. A.26. Fig. 4.11

73

Table 4.1. α_{sy} from Conf. 2, Loading North, $\xi = 0°$, S/D = 6

CYCLE	P_y (kips)	δ_y (in.)	δ_s* (in.)	α_{sy}**
1	3.93	0.075	0.018	0.24
20	3.08	0.065	0.011	0.17
100	4.38	0.078	0.0046	0.06
1	12.12	0.276	0.118	0.43
20	11.89	0.302	0.066	0.22
100	12.10	0.325	0.039	0.12
1	19.74	0.499	0.214	0.43
20	18.26	0.553	0.188	0.34
100	19.38	0.615	0.147	0.24

* Pile S unloaded in Conf. 2

** $\alpha_{sy} = \delta_s / \delta_y$
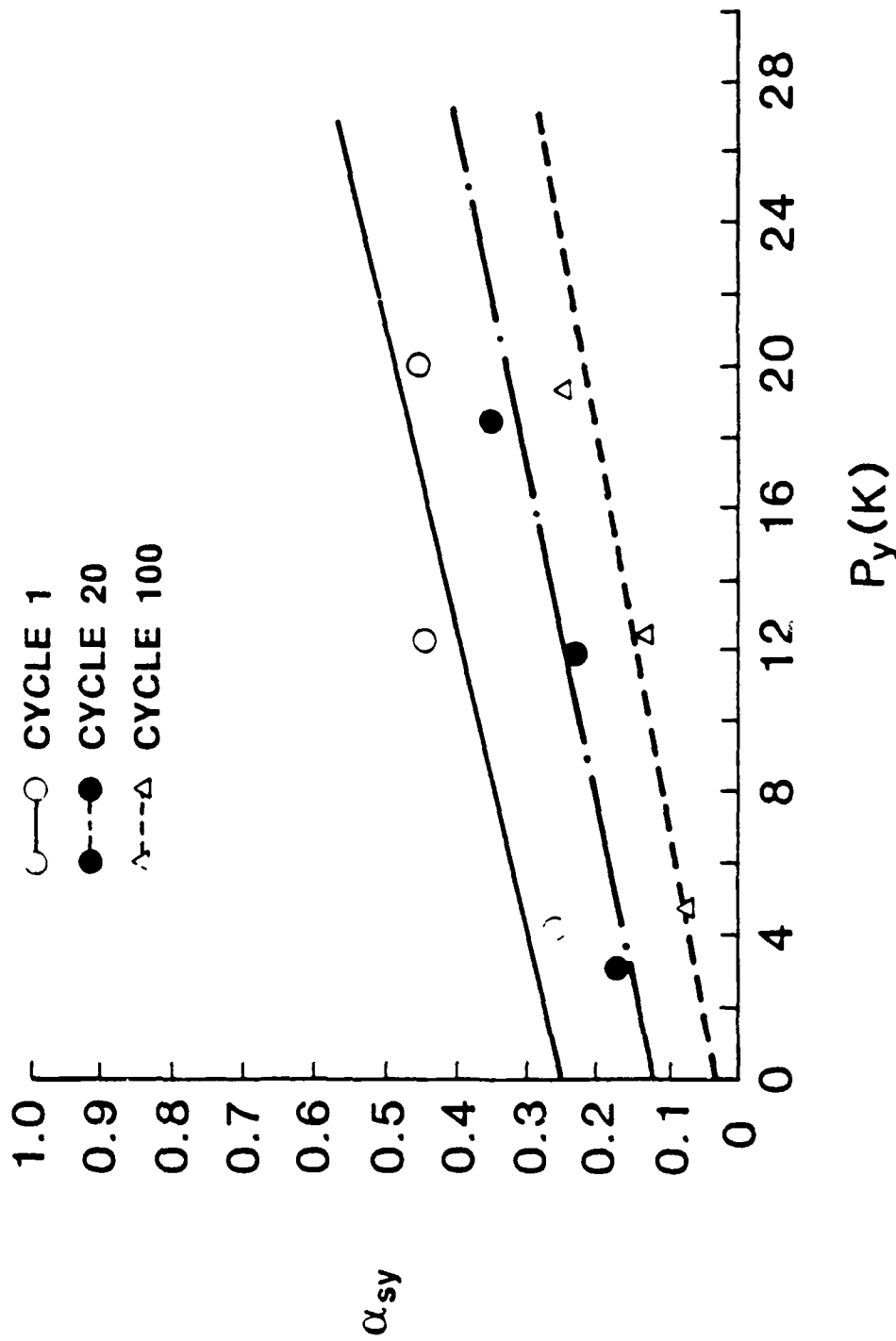
Fig. 4.10.a. α_{sy} vs. P_y, $\xi = 0°$, Loading North (Toward S), S/D = 6 (Alternative).
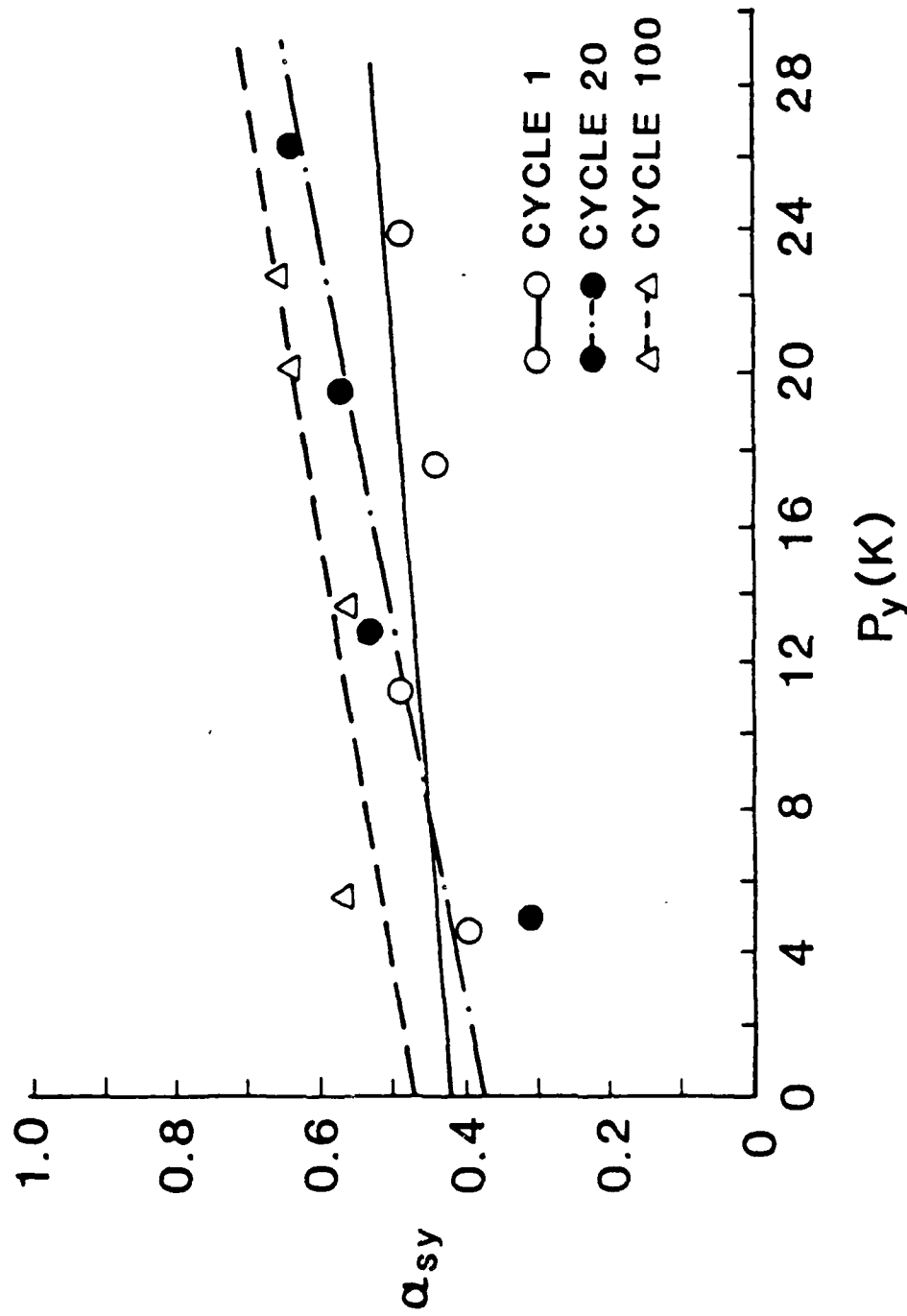
Fig. 4.11. α_{sy} vs. P_y, $\xi = 180°$, Loading South (Toward Y), $S/D = 6$.

shows values of α_{sy} as a function of number of cycles of load and load magnitude on Pile Y.

4.2.3.4. Loading North, $\xi = 180°$ (Toward S)

From Figs. A.29 to A.31, deflections on Pile Y (trailing pile) and loads on Pile V and Pile Y (leading pile) for loads of 3, 7, 10, 13 and 16 kips on Pile Y were determined and stored (39 values; 15 values from Fig. A-28, 12 values from Fig. A-29, 12 values from Fig. A-30). Values of f_{yv} for loading to the north (spacing of 3 diameters) were calculated previously in Section 4.2.2.4. Additional flexibilities of Pile Y due to loads on Pile S (Eq. 4.13) and interaction factors α_{ys} (Eq. 4.14) were calculated. Fig. 4.12 shows values of α_{ys} as a function of number of cycles of load and load magnitude on Pile S.

Fig 4.13 is the result of averaging Figs. 4.11 and 4.12 and represents α_{ij} vs. load magnitude on the leading pile (P_j) for $\xi = 180°$ and a spacing of 6 diameters. The resulting pattern of α factors appears reasonable in Fig. 4.13.

4.2.4. Two-Pile Group Flexibilities (Conf. 5, S/D = 3)

Based on Eq. 4.11, but for a system of three identical piles (Piles X, Y, and Z) subjected only to a pile-head shear, the general flexibility matrix can be written as:

$$
\begin{bmatrix}
f_{xx} & f_{xy} & f_{xz} \\
f_{yx} & f_{yy} & f_{yz} \\
f_{zx} & f_{zy} & f_{zz}
\end{bmatrix}
\begin{bmatrix}
P_x \\
P_y \\
P_z
\end{bmatrix}
=
\begin{bmatrix}
\delta_x{}^g \\
\delta_y{}^g \\
\delta_z{}^g
\end{bmatrix}
, \qquad (4.16)
$$

77
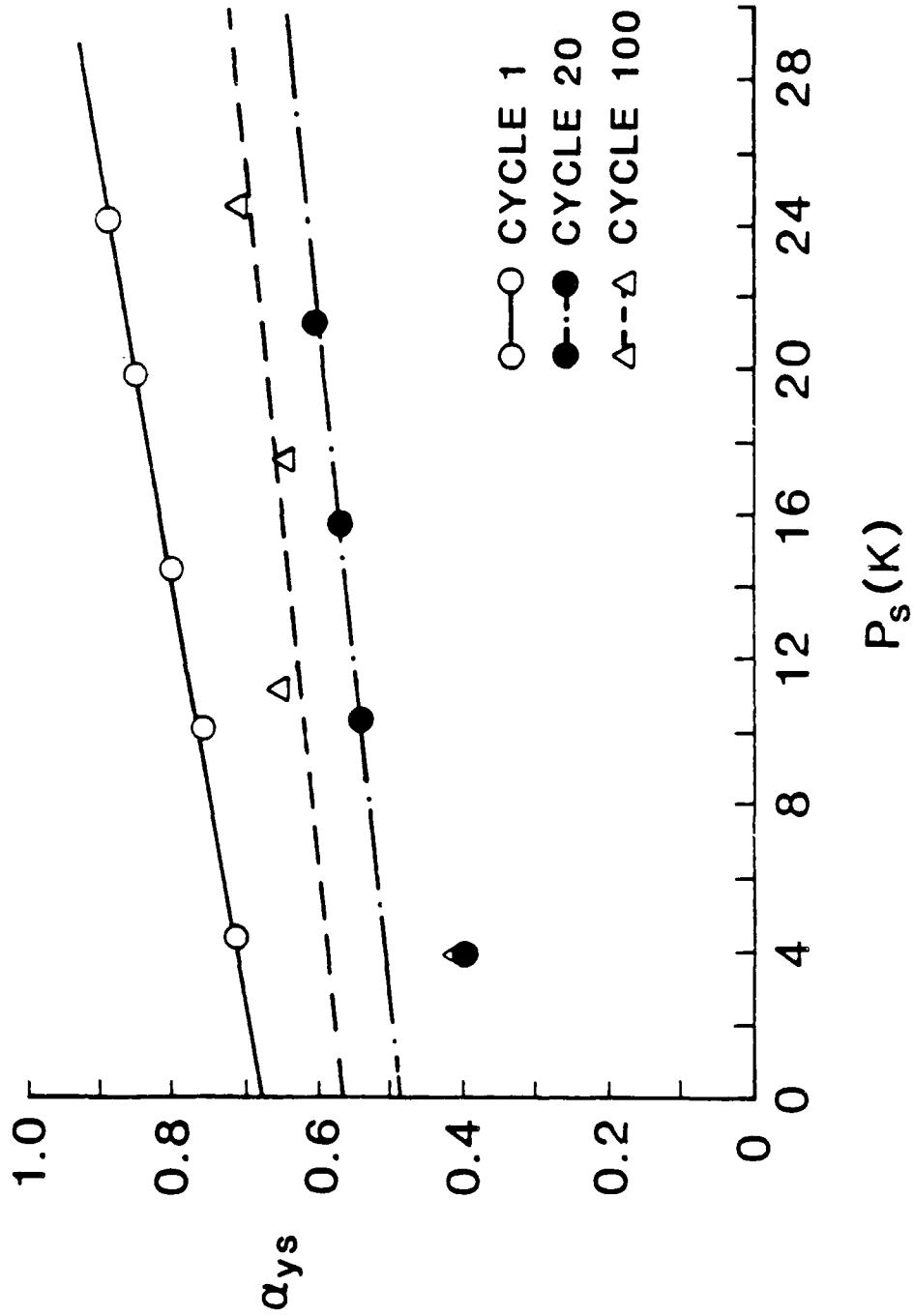
Fig. 4.12. α_{ys} vs. P_s, $\xi = 180°$, Loading North (Toward S), S/D = 6.

Fig. 4.13. α_{ij} vs. P_j, $\xi = 180°$, $S/D = 6$.

79
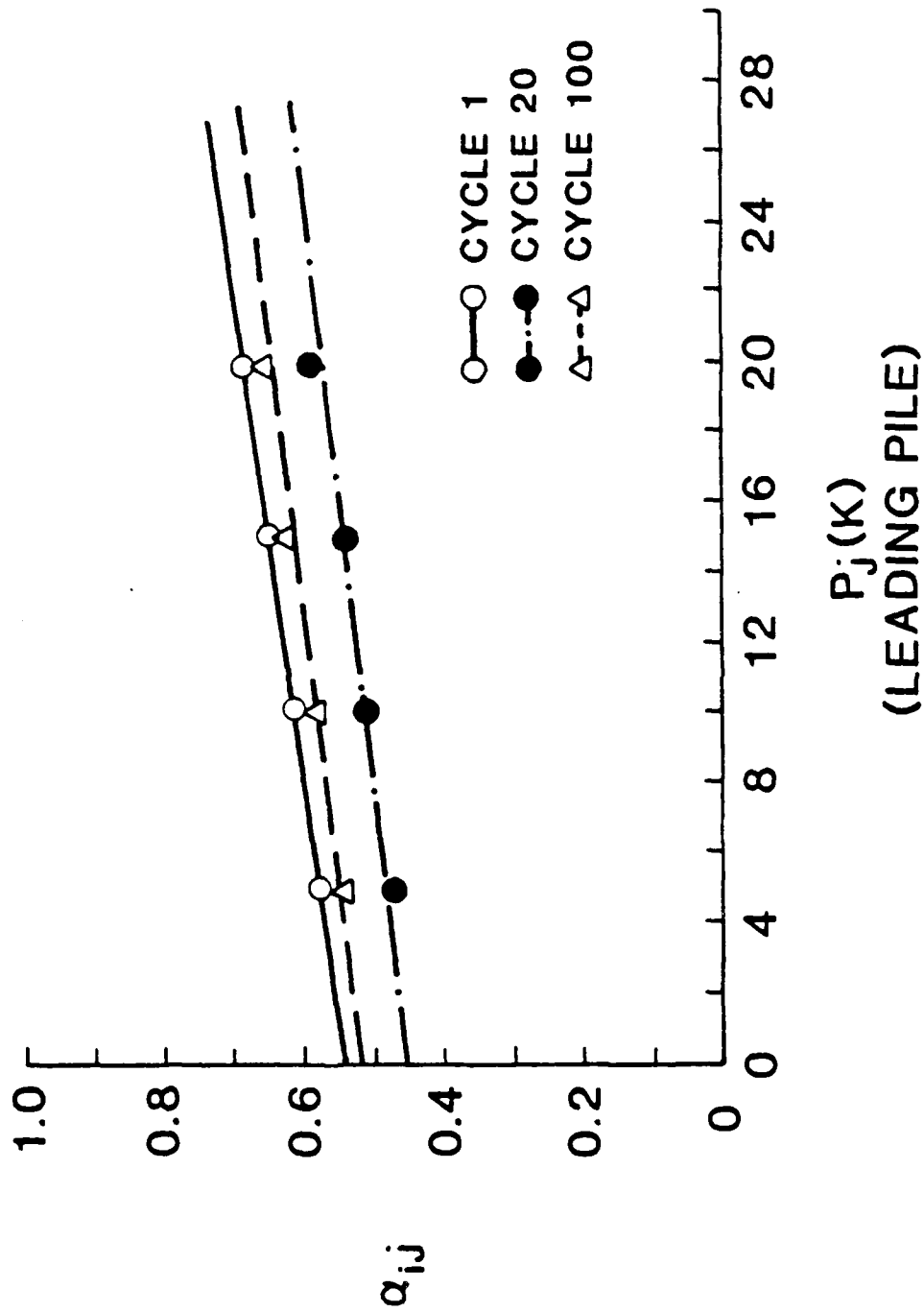
in which

f_{xx}, f_{yy}, f_{zz} = Single pile (X, Y, Z) flexibilities,

f_{xy}, f_{yx} = Additional flexibility in Pile X due to loading on Pile Y, and vice versa,

f_{xz}, f_{zx} = Additional flexibility in Pile X due to loading on Pile Z, and vice versa,

f_{yz}, f_{zy} = Additional flexibility in Pile Y due to loading on Pile Z, and vice versa,

P_x, P_y, P_z = Horizontal loads on Piles X, Y, and Z, and

$\delta_x{}^g$, $\delta_y{}^g$, $\delta_z{}^g$ = Deflections of Piles X, Y and Z in the group.

The flexibility terms in Eq. 4.16 can be evaluated by loading three piles (X, Y and Z) side by side (ξ = 90°, Fig. 3.4).

From Eq. 4.16

$$f_{yx}\ P_x + f_{yy}\ P_y + f_{yz}\ P_z = \delta_y{}^g. \qquad (4.17)$$

Since no test for a 2-pile group, loaded side by side, was possible with the available test arrangement, it is assumed that the influence (additional flexibility) on Pile Y due to loads on Pile X (f_{yx}) and the influence on Pile Y due to loads on Pile Z (f_{yz}) are the same. Therefore, Eq. 4.17 becomes:

$$f_{yz}\ P_z + f_{yy}\ P_y + f_{yz}\ P_z = \delta_y{}^g .$$

Then,

$$f_{yz} = f_{yx} = (\delta_y{}^g - f_{yy}\ P_y)/2\ P_z = (\delta_y{}^g - \delta_{\bar{y}}{}^s)/2\ P_z \qquad (4.18)$$

It is also assumed that $f_{xx} = f_{zz} = f_{yy}$, where f_{yy} is as measured in Config. 2. The general flexibility matrix can then be written as:

$$f_{yy} \begin{bmatrix} 1 & \alpha_{xy} & \alpha_{xz} & P_x \\ \alpha_{yx} & 1 & \alpha_{yz} & P_y \\ \alpha_{zx} & \alpha_{zy} & 1 & P_z \end{bmatrix} = \begin{bmatrix} \delta_x{}^g \\ \delta_y{}^g \\ \delta_z{}^g \end{bmatrix} ,$$

where

$$\alpha_{yz} = \alpha_{yx} = f_{yz} / f_{yy} . \tag{4.19}$$

Based on Eq. 4.16, but replacing deflections (δ) by rotations (θ), rotation-deflection cross-coupling α factors could be determined if necessary.

4.2.4.1. Loading North, $\xi = 90°$

From the test data on Figs. A.32 – A.34, deflections on Pile Y and loads on Pile Z (or X) for loads of 3, 7, 10, 13 and 16 kips on Pile Y were determined and stored (30 values; 10 from each graph). Such values represent the deflections of Pile Y in the group and loads on Pile Z for use in Eq. 4.18. Flexibility values (f_{yz}) and influence factors α_{yz} (Eq. 4.19) were thus computed. A graphical illustration of the determination of f_{yz} and α_{yz} from these data for a load of 10 kips on Pile Y is shown on Fig. A.32. Values of α_{yz} (loading north) as a function of number of cycles of load (1, 20, 100) and load magnitude on Pile Z are shown in Fig. 4.14.
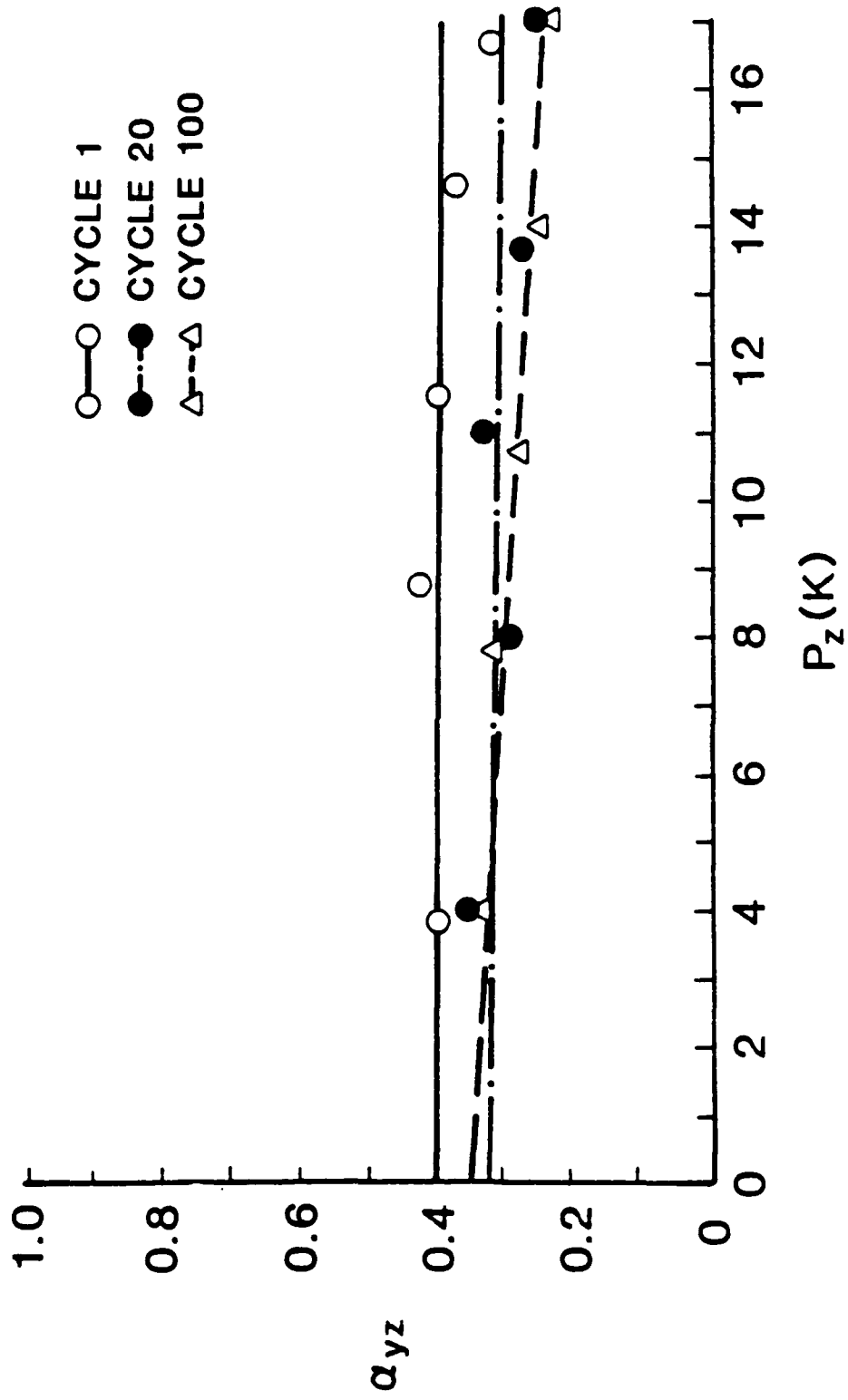
Fig. 4.14. α_{yz} vs. P_z, $\xi = 90°$, Loading North, S/D = 3.

82

4.2.4.2. Loading South, $\xi = 90°$

Figs. A.35 - A.37 present data and fitted curves simi-
lar to those in Figs. A.32 - A.34, except for the case of
loading to the south. Using a procedure identical to that
described in the previous section, flexibility values f_{yz}
(Eq. 4.18) and influence factors α_{yz} (Eq. 4.19) were compu-
ted. Values of α_{yz} (loading south) as a function of number
of cycles of load and load magnitude on Pile Z are plotted
in Fig. 4.15.

Fig. 4.16 is the result of averaging Figs. 4.14 and
4.15 and represents α_{ij} factors vs. load magnitude on an ad-
jacent pile (P_j) when $\xi = 90°$ at a spacing of 3 diameters.
Note that these factors are much less dependent on load mag-
nitude than the factors for in-line piles. An evaluation of
the cumulative effects of errors in displacement measure-
ments for this configuration is offered in Appendix B.

4.2.5. α Factors For Spacing Greater Than 6 Diam.

Approximate α factors for in-line piles at a distance
exceeding the distance between the loaded piles in the group
(> 6 diameters) were also obtained following the philosophy
expressed in Eq. 1.1. This was done by dividing deflections
of the unloaded "far-field" pile (Pile Q) in Conf. 4 by de-
flections of the same pile loaded as an isolated pile for
the average load of the 3 piles in the group (Conf. 4) times
3 (the number of loaded piles in Conf. 4). The latter de-
flections were obtained from free-head testing of the iso-

83
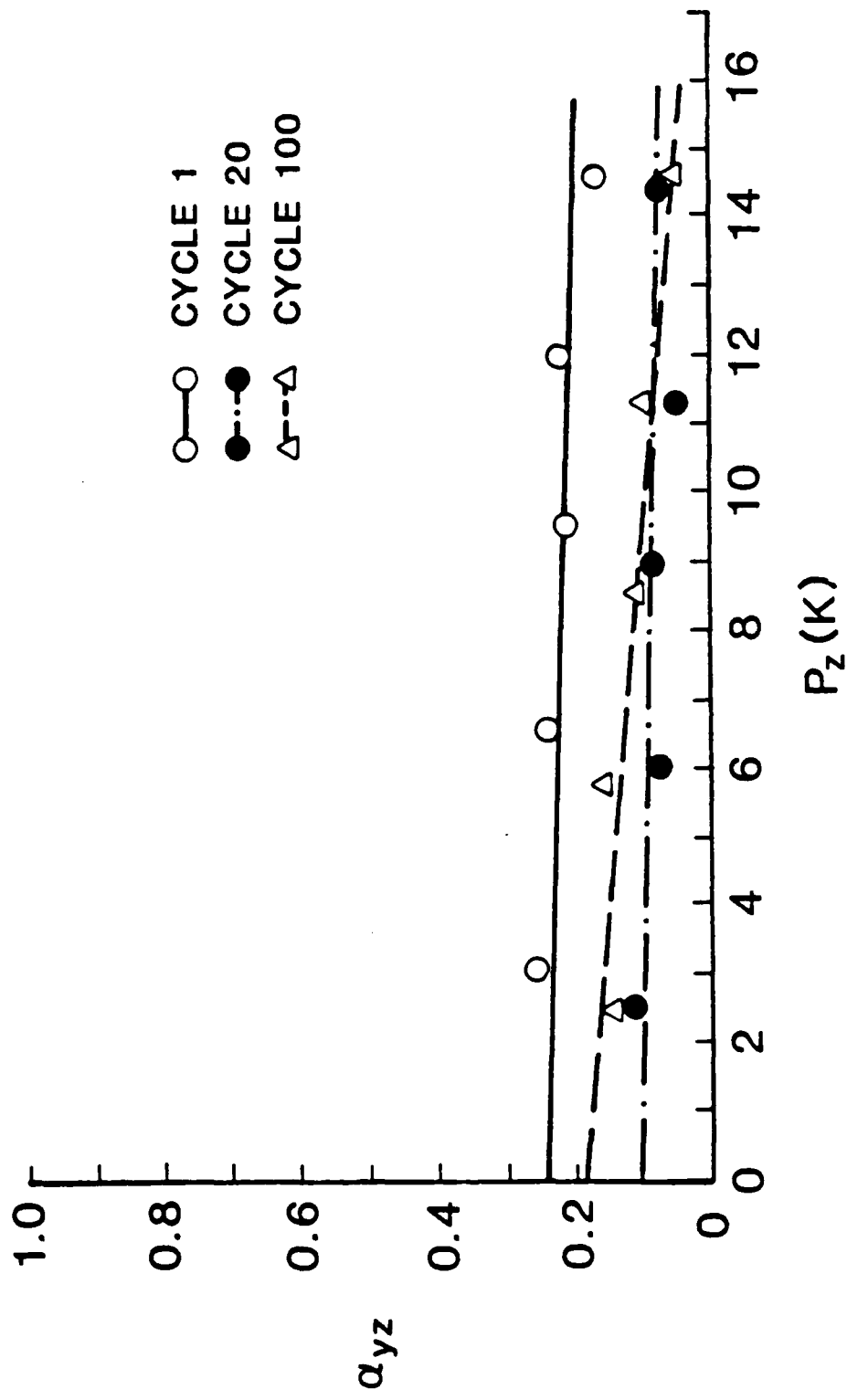
Fig. 4.15. α_{yz} vs. P_z, $\xi = 90°$, Loading South, S/D = 3.

84
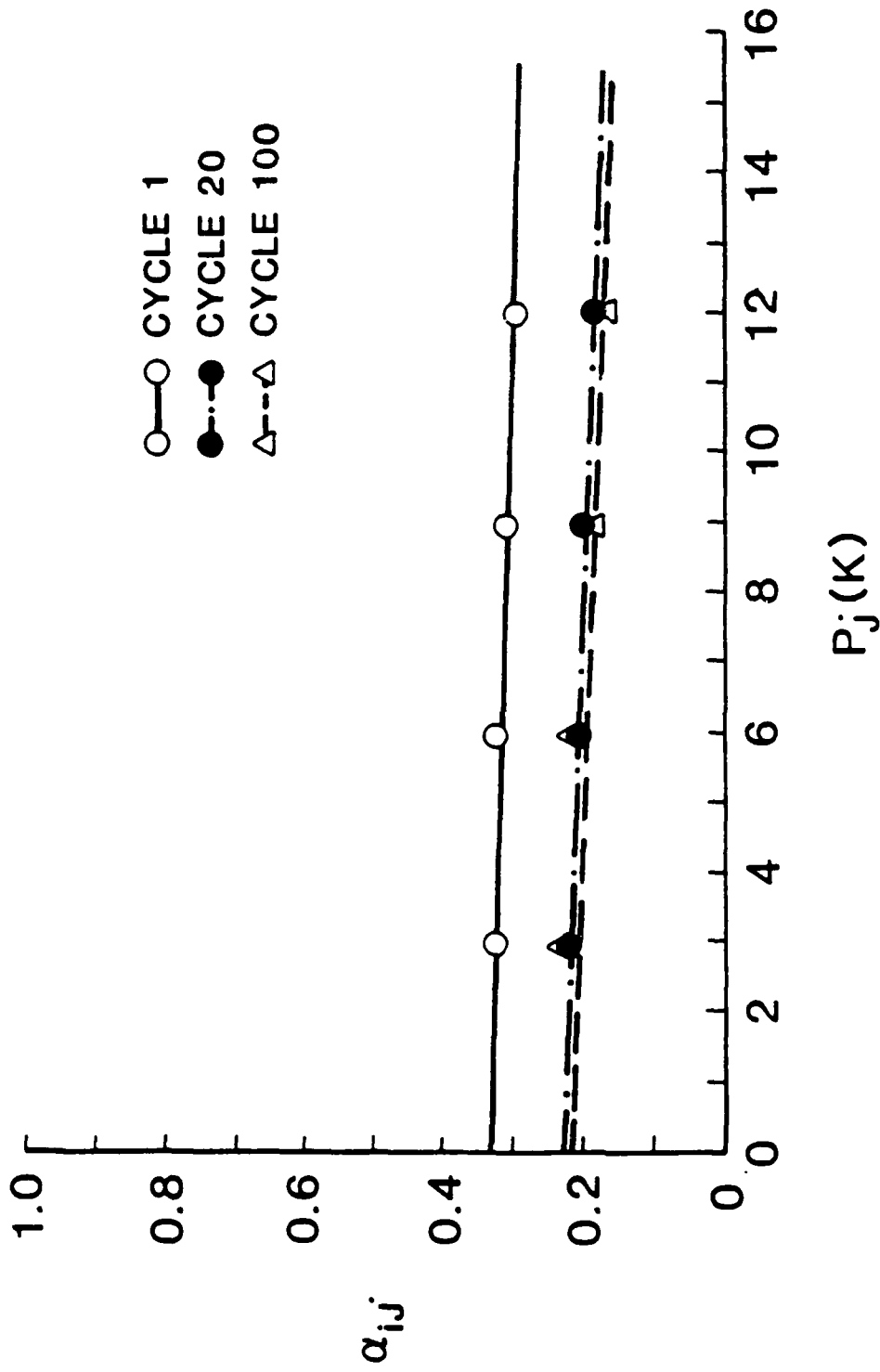
Fig. 4.16. α_{ij} vs. P_j, $\xi = 90°$, $S/D = 3$.

lated pile by Morrison (1986). The computed values are representative of α factors for an equivalent spacing between piles of 11.2 diameters [distance between the middle pile (Pile V) in Conf. 4 and the far-field pile (Pile Q)]. Only α factors for loading to the north were obtained; however, due to the large distance between the piles, it is assumed that these factors are also valid for $\xi = 180°$. Table 4.2 summaries the values of the average load levels, deflections of Pile Q when unloaded (Conf. 4) and loaded by itself (Morrison, 1986), and the computed α factors for different numbers of cycles of load. Such α factors are displayed graphically on Fig. 4.17 in the generic form α_{ij} vs. P_j.

4.3. Design Charts

Pile-supported structures subjected to horizontal loads are generally designed to undergo limited displacements. The current design practice usually limits the foundation displacements to values in the order of 5 per cent of the diameter of a single pile or less. Load values in Figs. 4.4, 4.7, 4.10.a, 4.13, 4.16 and 4.17 have therefore been normalized by a load on the single pile that corresponds to a displacement of 5% of a single pile diameter (10.75 in.) and denoted as $^S P_{5\%}$. Figs. 4.18, 4.19, 4.20, 4.21, 4.22, 4.23 are plots of the former figures in which α is graphed versus normalized load and in which some smoothing of the data from the former set of curves has been done. They represent preliminary design charts that may be used in design practice for similar situations in the absence of more specific

86

Table 4.2. $\alpha_{q,svy/3}$ from Conf. 4, Loading North, $\xi = 0°$ (Assumed = $180°$), S/D = 11.2

CYCLE	P (k) [*]	δ_q (in.) [**] loaded by itself	δ_q (in.) unloaded	$\alpha_{q,svy/3}$ [***]
1	4.24	0.150	0.036	0.080
20	4.51	0.190	0.033	0.058
100	4.25	0.160	0.008	0.017
1	12.81	0.540	0.173	0.107
20	11.74	0.540	0.107	0.066
100	11.73	0.500	0.035	0.023
1	20.76	1.060	0.382	0.120
20	18.68	0.940	0.197	0.070
100	17.72	0.880	0.053	0.020

[*]   Average load of Piles S, V, Y together (Conf. 4), loading north.

[**]   From Morrison (1986)

[***]
$$\alpha_{q,svy/3} = \frac{\delta_q \text{ (unloaded)} / 3}{\delta_q \text{ (loaded by itself)}}$$
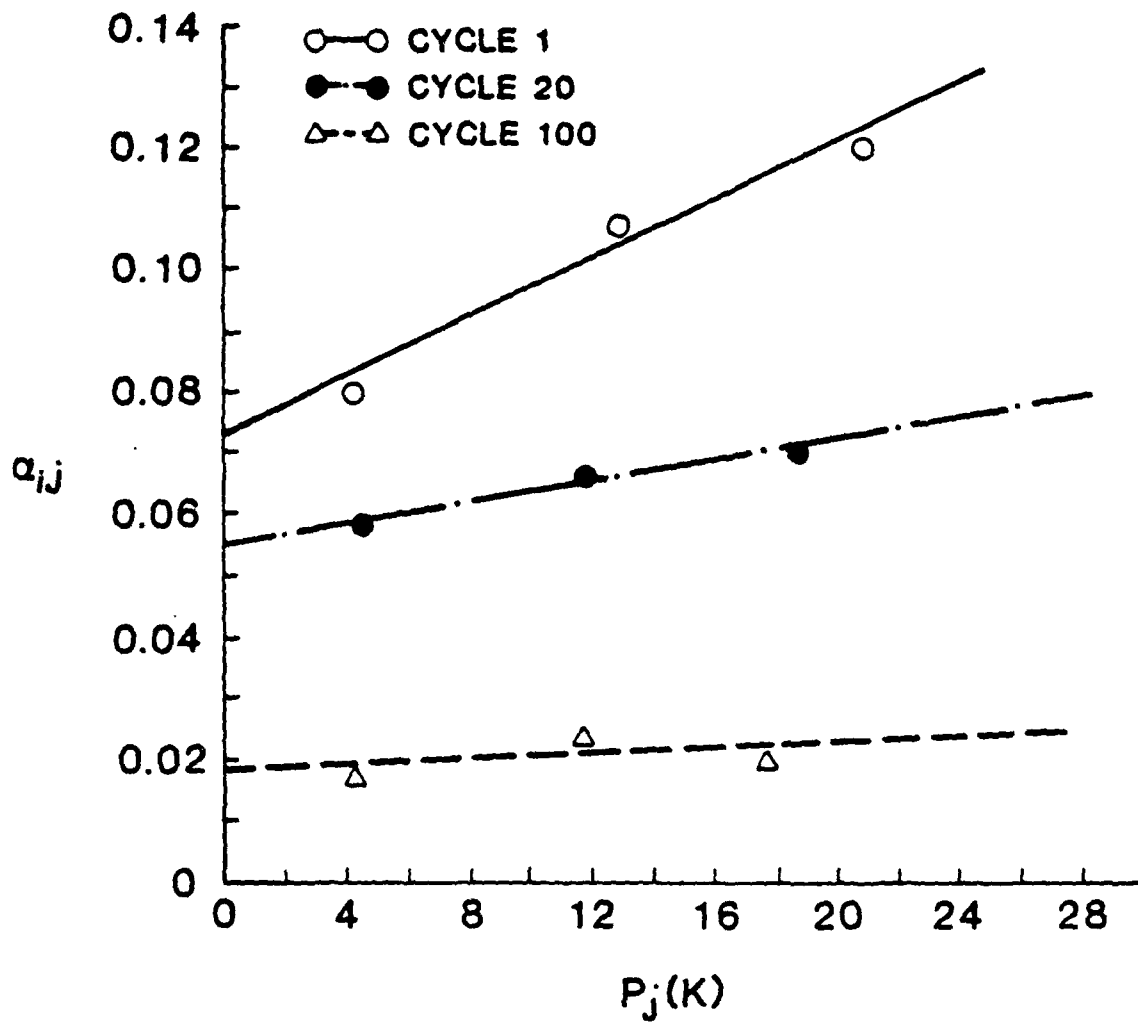
Fig. 4.17. α_{ij} vs. P_j, $\xi = 0°$ (Assumed = 180°), Loading North, S/D = 11.2.

88
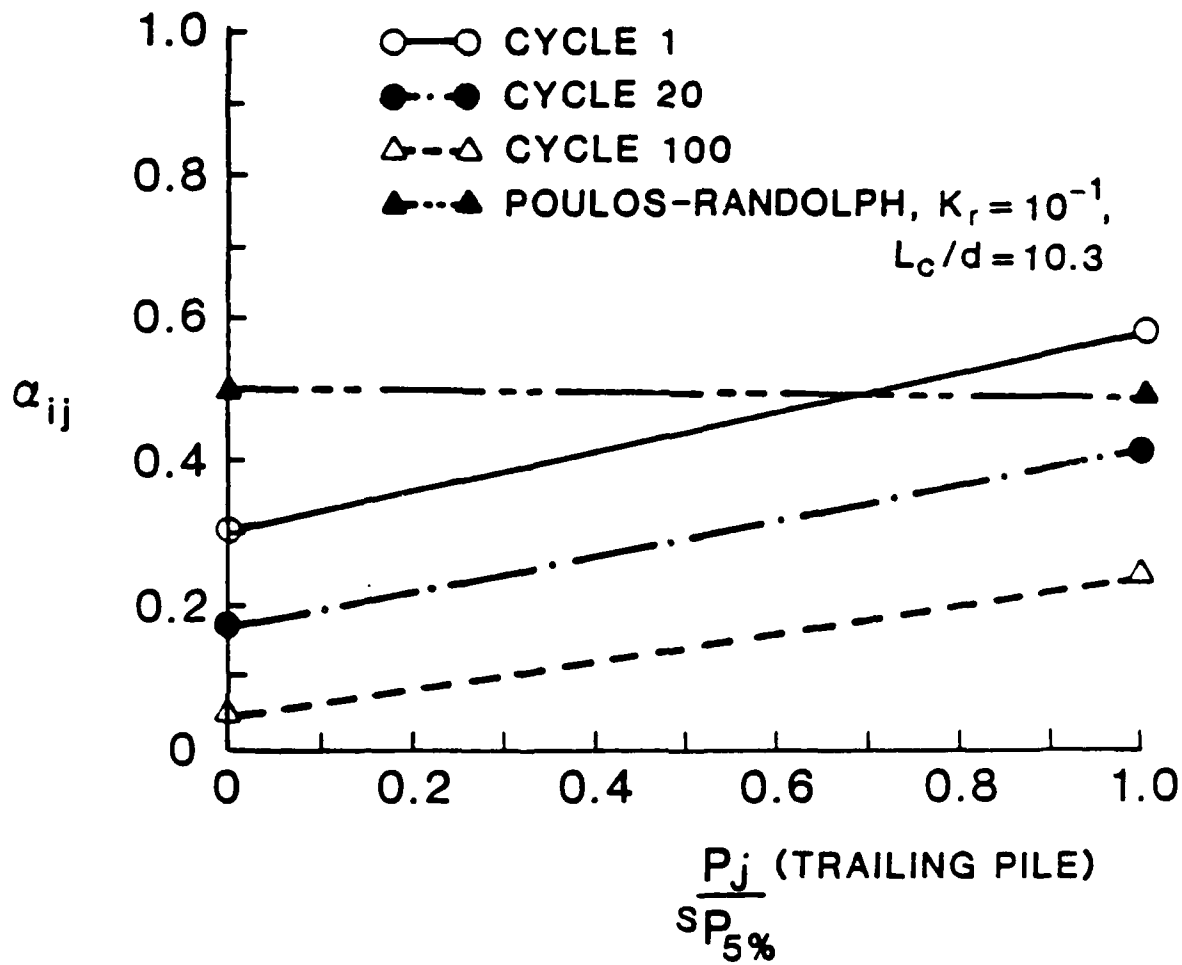
Fig. 4.18. Design Chart: α_{ij} vs. $P_j/{}^S P_{5\%}$ for $\xi = 0°$, $S/D = 3$.
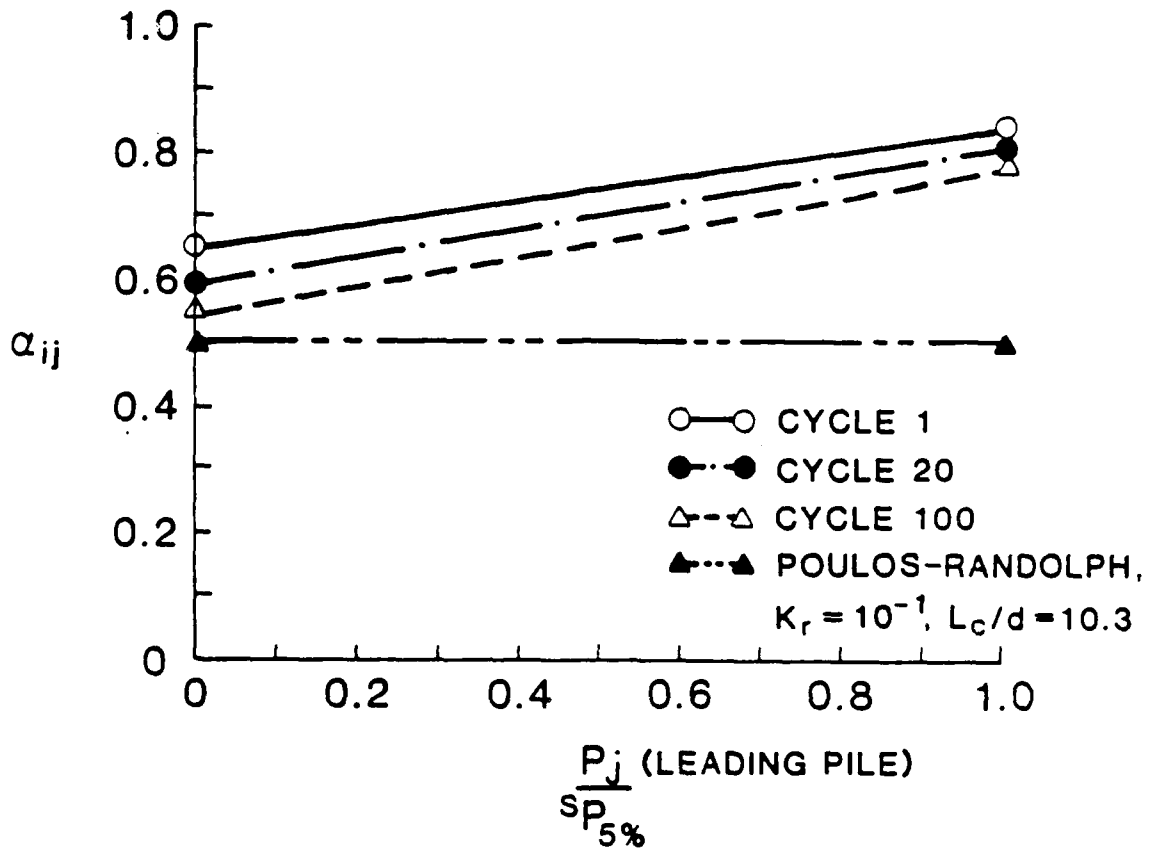
Fig. 4.19. Design Chart: α_{ij} vs. $P_j/{}^SP_{5\%}$ for $\xi = 180°$, S/D = 3.
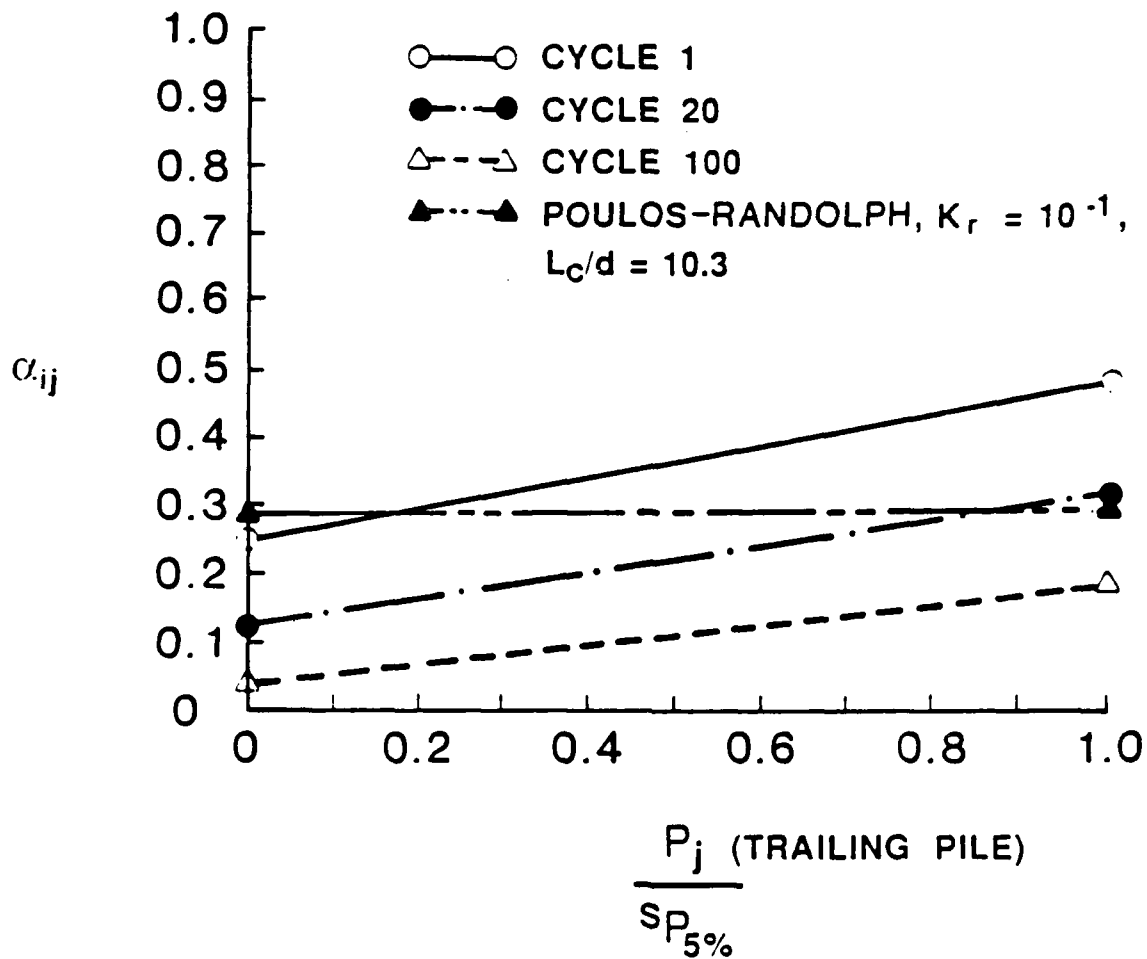
Fig. 4.20. Design Chart: α_{ij} vs. $P_j/^S P_{5\%}$ for $\xi = 0°$, $S/D = 6$.

91
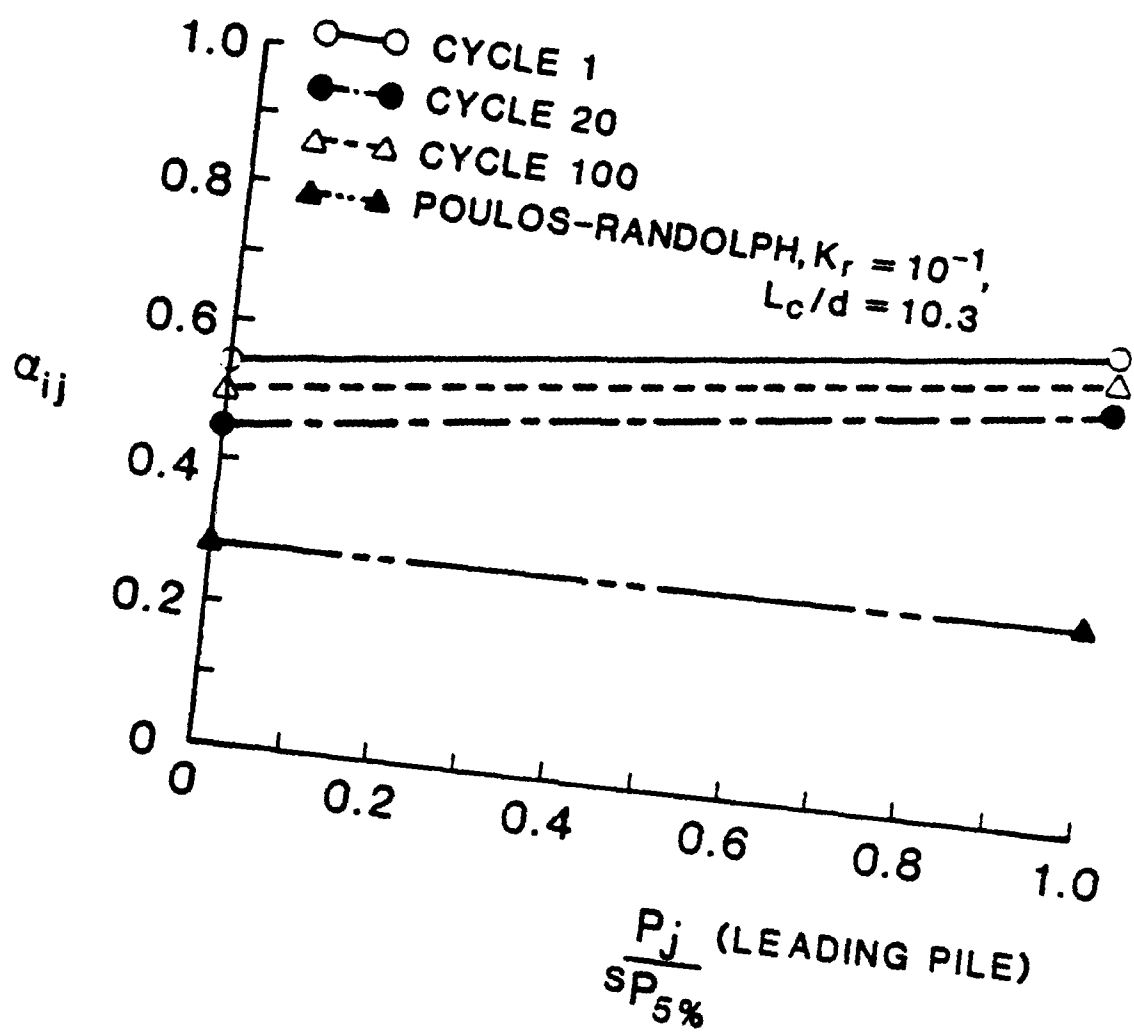
Fig. 4.21. Design Chart: α_{ij} vs. $P_j/{}^sP_{5\%}$ for $\xi = 180°$, $S/D = 6$.

92
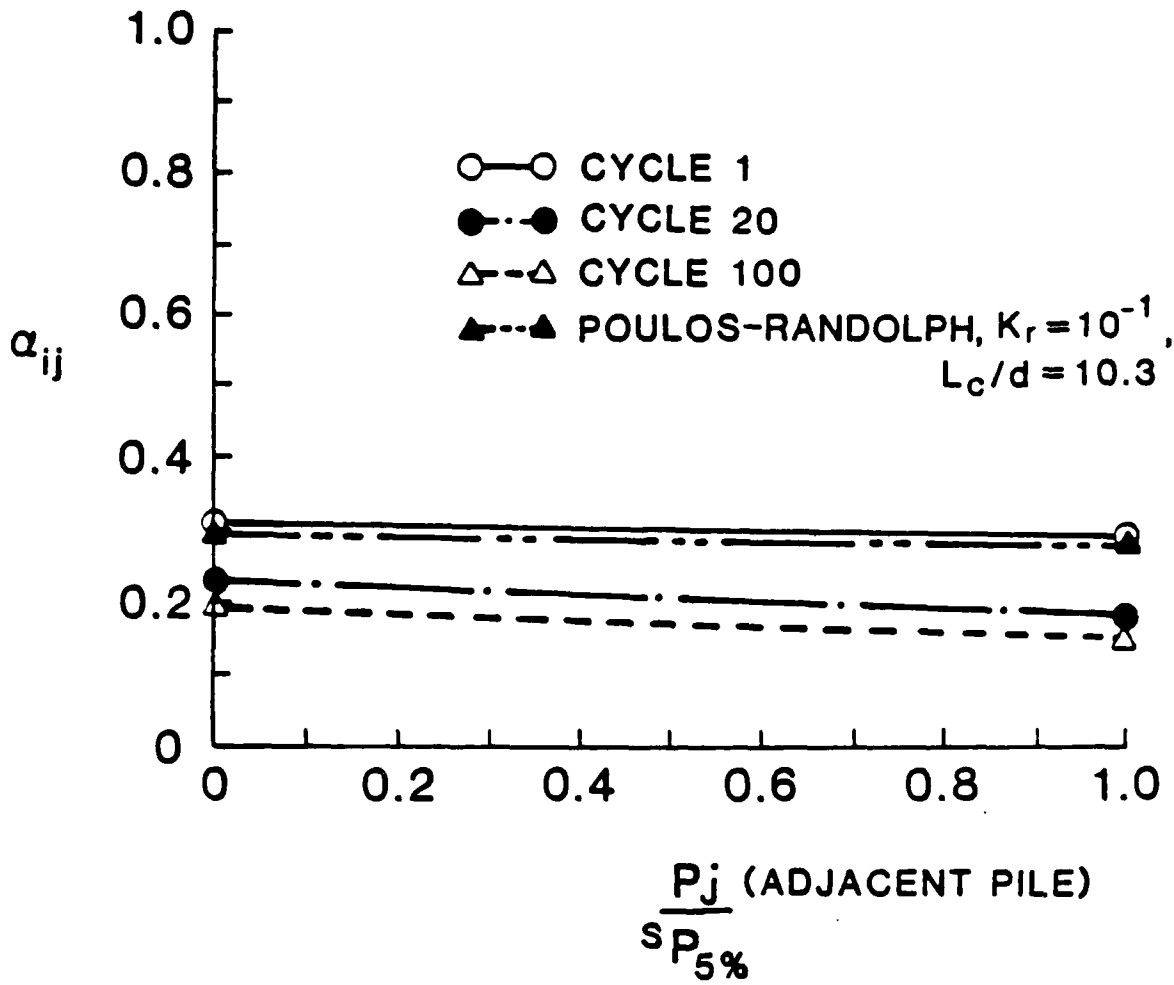
Fig. 4.22. Design Chart: α_{ij} vs. $P_j/^SP_{5\%}$ for $\xi = 90°$, S/D = 3.
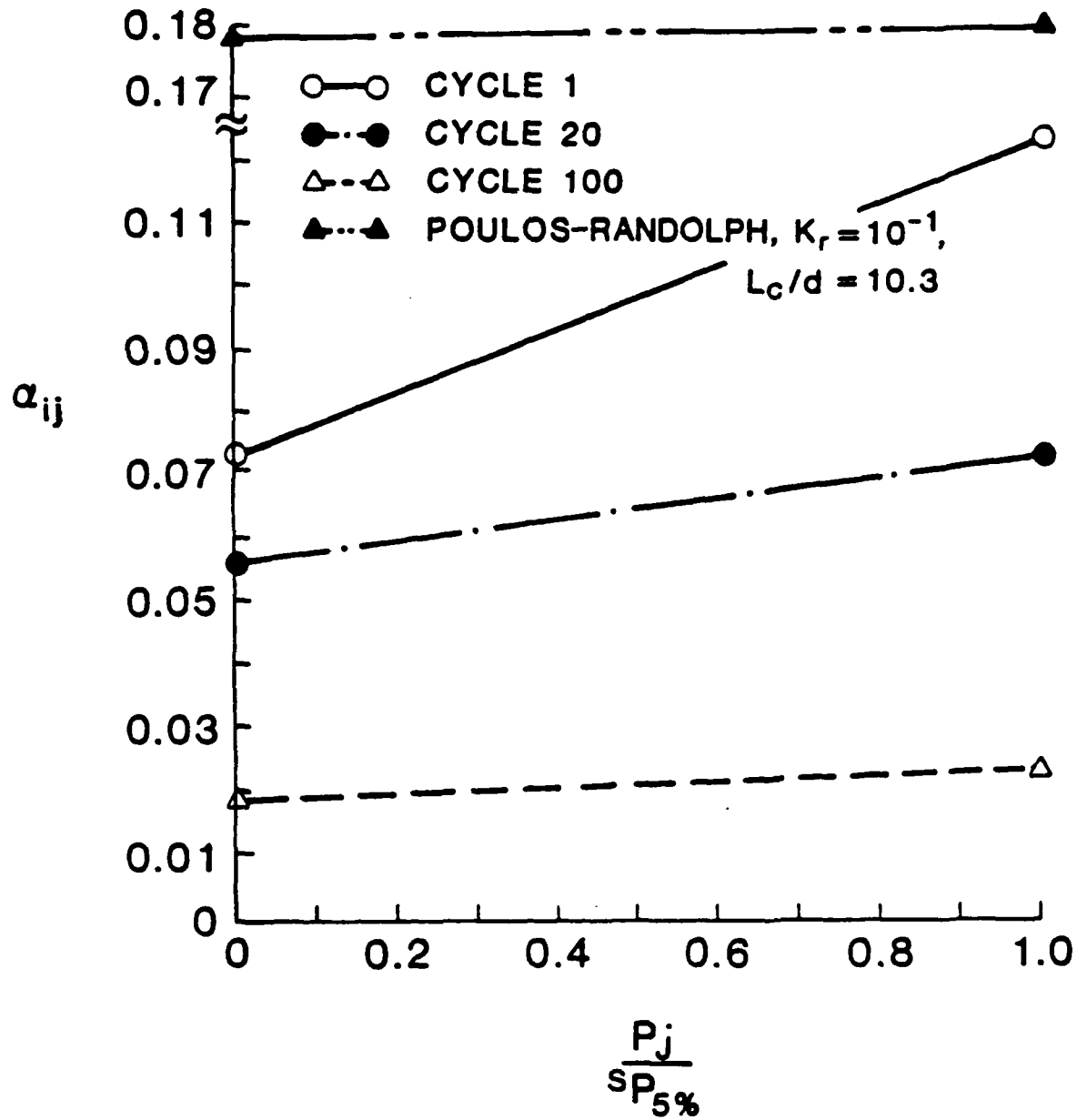
Fig. 4.23.   Design Chart: α_{ij} vs. $P_j/{}^sP_{5\%}$ for $\xi = 0°$
(Assumed = 180°), S/D = 11.2.

94

information. For comparison, also displayed are the values obtained from Poulos-Randolph α factors ($\alpha_{\rho H}$ from Fig. 1.2, with $L = L_c$ defined from Fig. 1.3) for K_r (dimensionless pile flexibility factor) of 10^{-1} and the ratio L_c/d of 10.3 (L_c = that part of the pile that deforms appreciably under lateral loading, d = pile diameter), which are appropriate parameters for the test conditions. These factors are reasonable representations of relative pile-soil stiffness for this test.

Elastic and experimental interaction factors may differ primarily because of the following reasons: 1) Elastic α factors assume that the soil is elastic with a constant Young's modulus while experimental α factors consider the soil to be highly nonlinear; 2) Elastic α factors were developed based on the assumption of a plate embedded in an elastic medium, whereas the experimental α factors were developed for circular piles in granular soils; 3) The state of stress in the soil located in front and back of the piles for elastic and experimental interaction factors are substantially different; elastic α's reflect the presence of compression (front) and tensile (back) stresses of equal magnitude which are unlikely to happen, especially in granular soils. Experimental interaction factors do not consider tensile stresses behind the pile.

Figs. 4.24 - 4.28 display the design α values shown on Figs. 4.18 - 4.23 in a slightly different, but more useful,
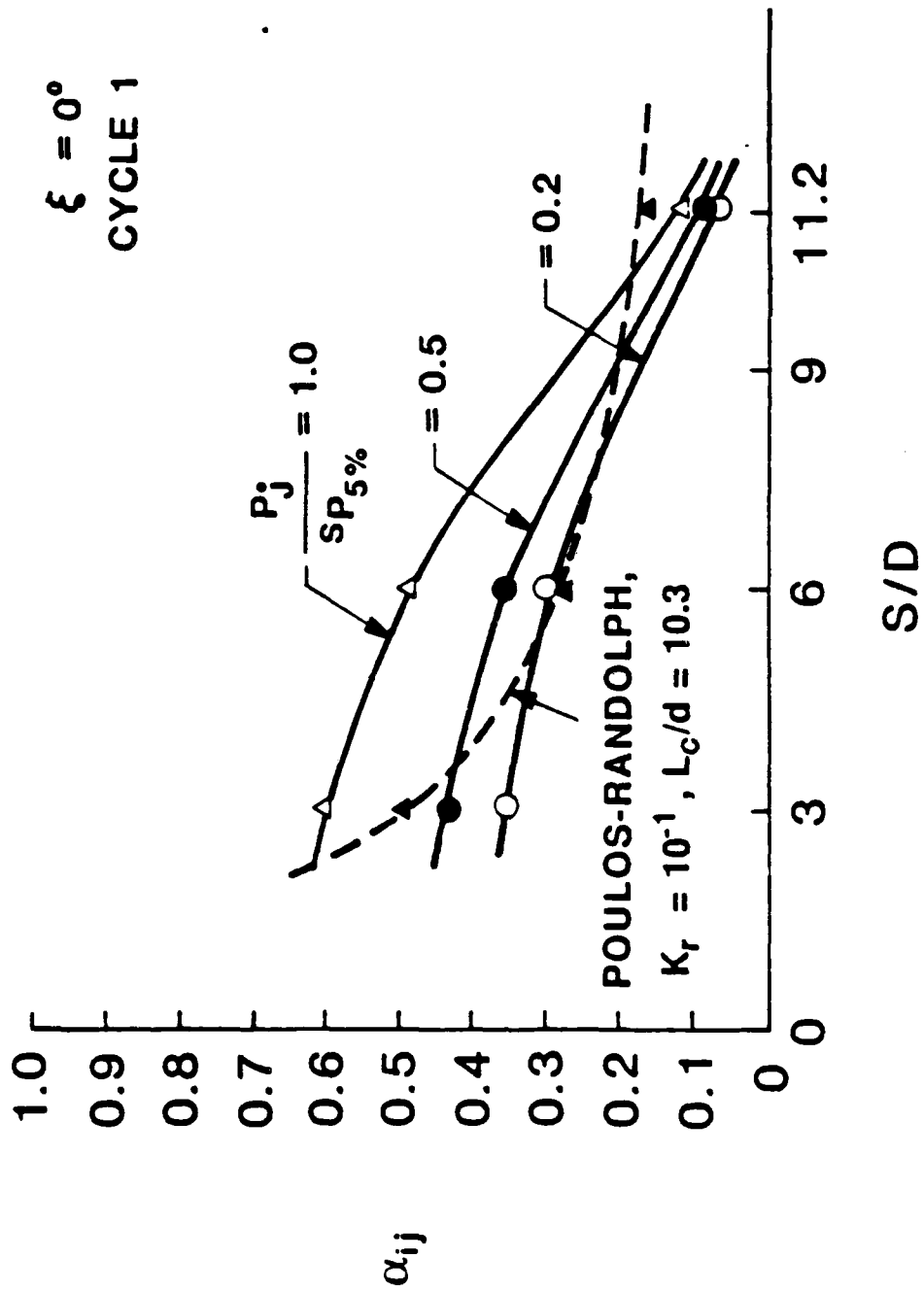
Fig. 4.24. Design Chart: α_{ij} vs. S/D for $\xi = 0°$, Cycle 1.
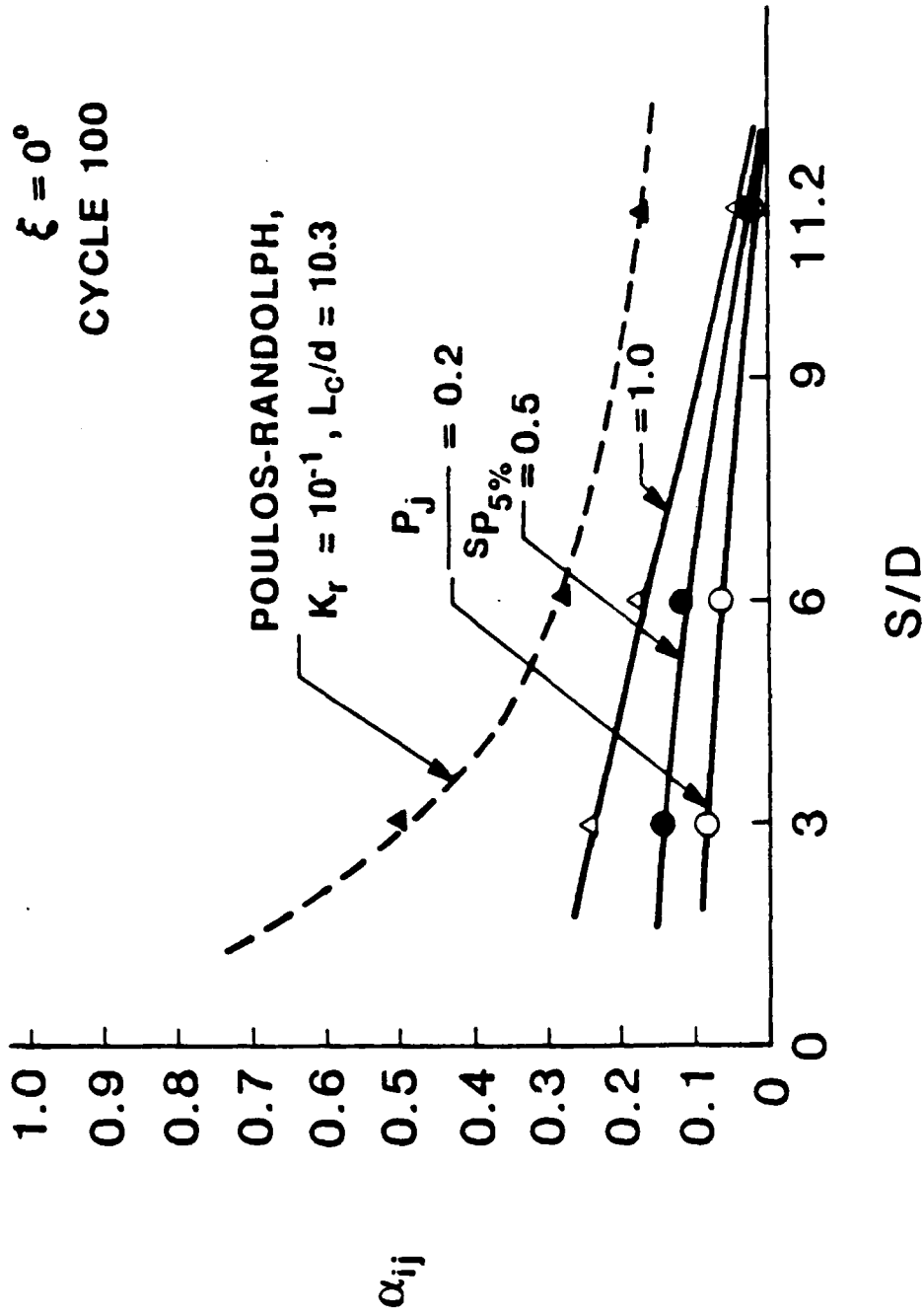
Fig. 4.25. Design Chart: α_{ij} vs. S/D for $\xi = 0°$, Cycle 100.
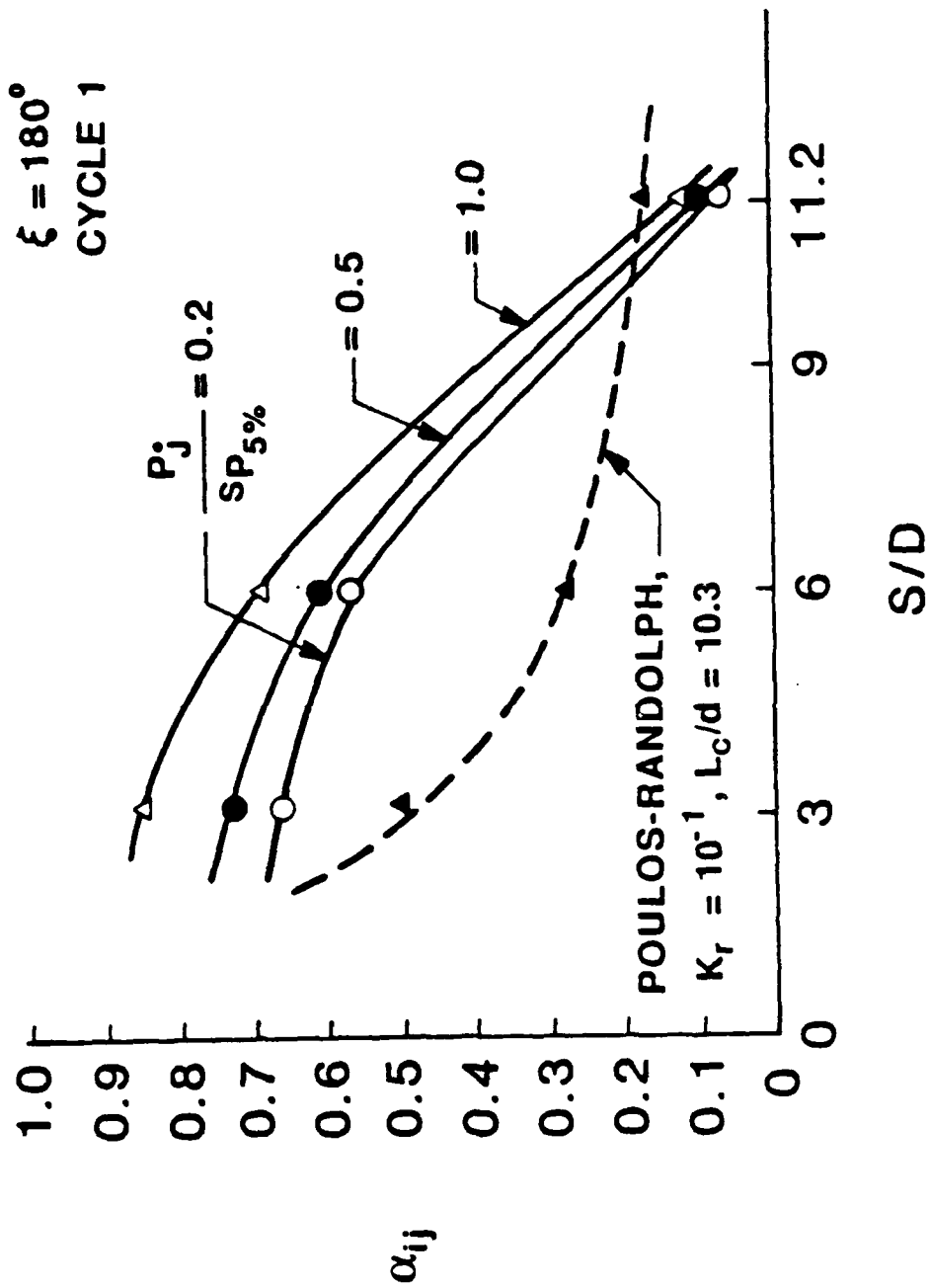
Fig. 4.26. Design Chart: α_{ij} vs. S/D for ξ = 180°, Cycle 1.

98
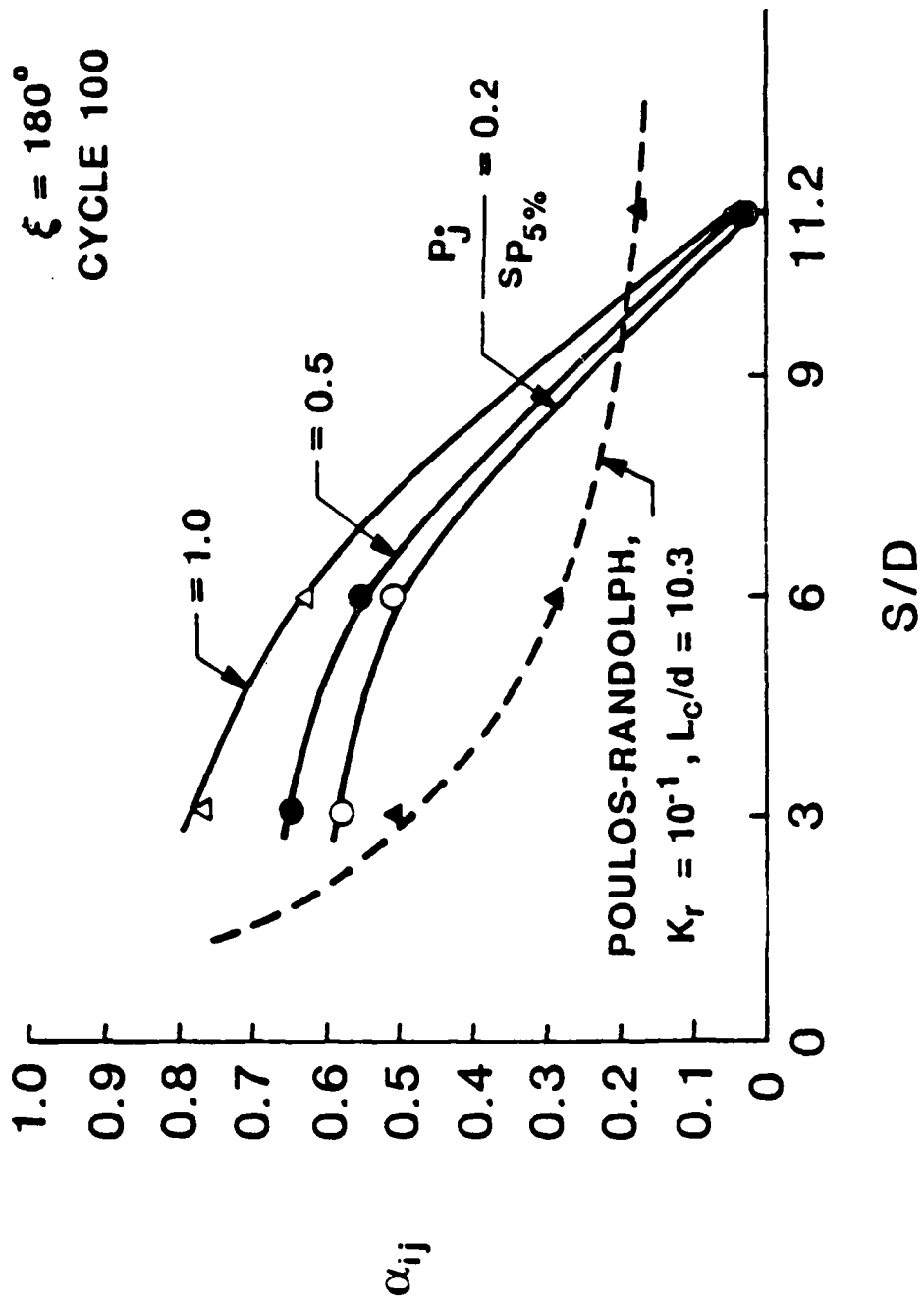
Fig. 4.27. Design Chart: α_{ij} vs. S/D for $\xi = 180°$, Cycle 100.
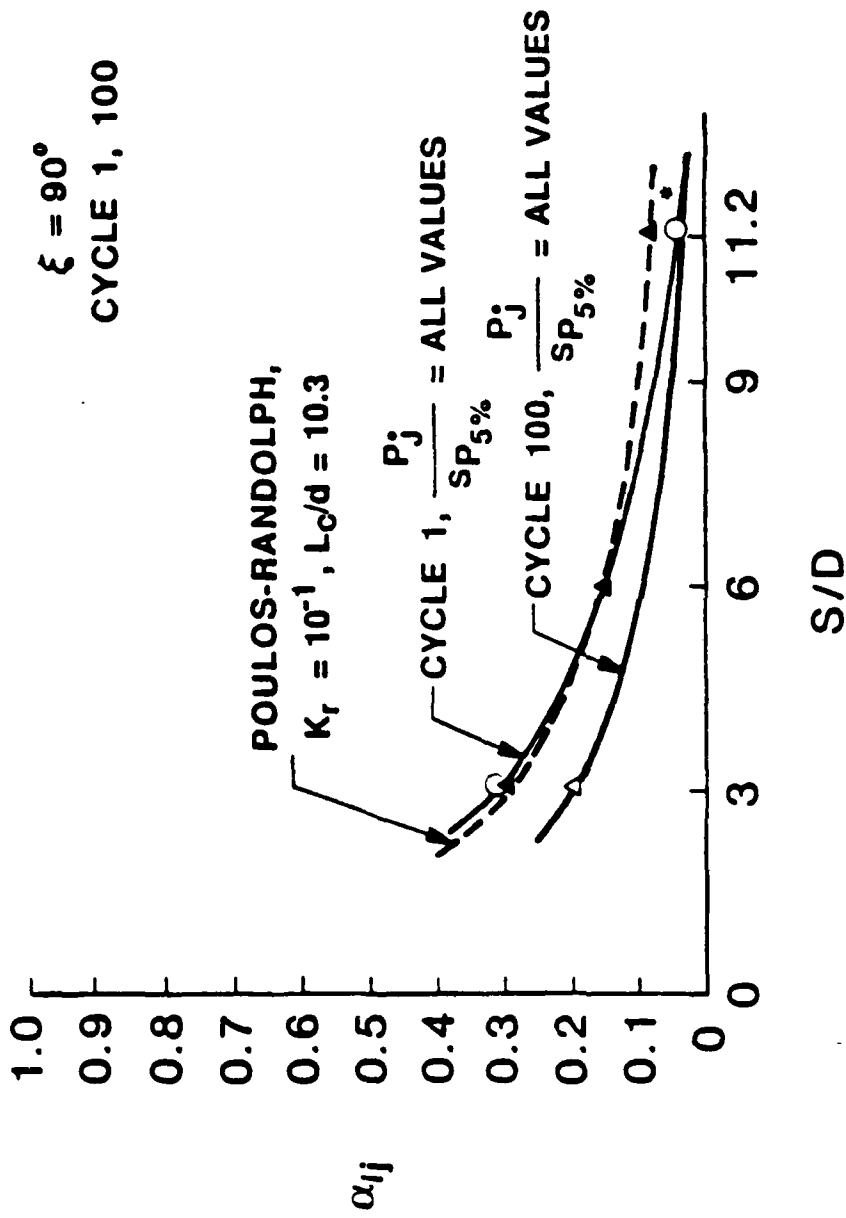
99

Fig. 4.28. Design Chart: α_{ij} vs. S/D for $\xi = 90°$, Cycles 1 and 100.

100

way. It is recommended that, for conditions similar to the test conditions, free- or pinned-headed pile groups be designed using α factors from Figs. 4.24 - 4.27 for in-line piles ($\xi = 0°$ or $180°$), taking the "Cycle 1" values for monotonic loading and the "Cycle 100" values for sustained cyclic loading. Fig 4.28 should be used for side-by-side piles ($\xi = 90°$). Note that spacing dependence for side-by-side piles was established by assuming that at a spacing of 11.2 diameters behavior was identical to the average value measured for all loads and cycle numbers for in-line far-field loading.

Several features are evident in Figs. 4.24 - 4.28. First, the α-factor is lower for $\xi = 0°$ (effect of trailing pile on leading pile) than for $\xi = 180°$ (effect of leading pile on trailing pile). Second, the α-factor increases with increasing magnitude of load and, generally, decreases with increasing numbers of cycles of applied load for in-line piles. For side-by-side piles, load magnitude had a minimal effect on α, while α also decreased with increasing numbers of load cycles. The influence of in-line piles at an S/D of 11.2 diameters was evident, although less than is predicted by elastic (Poulos-Randolph) theory. Finally, the α-factors obtained in this experiment in sand were generally larger than those predicted by elastic theory for S/D < 9 except for $\xi = 0°$ Cycle 1, low loads, and $\xi = 0°$ Cycle 100, all loads.

A pinned-headed group of laterally loaded vertical piles can be analyzed using the principles described in Chater I and the design charts presented in Figs. 4.24 - 4.28. Such an analysis presumes that the 2-pile α factors are in fact valid for a larger group. For example, the assumption must be made that the effect of a leading pile on a trailing pile is the same whether the leading pile is itself trailing another pile or whether it is the frontmost pile in the group. This assumption is intuitively only approximate. In the Chapter V, therefore, the interaction factors developed in this chapter will be used to model the lateral load test on the entire group of nine piles that was conducted just prior to the interaction tests described herein in order to investigate the validity of their application.

CHAPTER V

CALIBRATION OF EXPERIMENTAL INTERACTION FACTORS

The purpose of this chapter is to model the load-deformation behavior of the full nine-pile group under study subjected to a horizontal load, at Cycles 1 and 100, using the experimental interaction factors from Figs. 4.24 to 4.28, and the flexibility matrix scheme described in Fig. 1.4. The distribution of load among the piles in the group and group deflection are compared with those obtained by Morrison (1986) from a lateral loaded test on the complete nine-pile group and those from an elastic (Poulos-Randolph) analysis.

5.1. Horizontal Interaction of a Nine-Pile Group (Free-Headed) in the Direction of Load

For a system composed of nine free-headed piles, subjected to a horizontal load, the general flexibility matrix (deflections only) can be expressed as shown on Fig. 5.1. Such a system of simultaneous equations can be easily solved by the method of Gaussian elimination. The following sections analyze that particular pile group subjected to a load level of ± 7 k per pile (which is a reasonable design load for the pile group considered here), for Cycles 1 and 100,

The matrix equation shown:

$$
\begin{bmatrix}
1 & \alpha_{12} & \alpha_{13} & \alpha_{14} & \alpha_{15} & \alpha_{16} & \alpha_{17} & \alpha_{18} & \alpha_{19} & -1 \\
\alpha_{21} & 1 & \alpha_{23} & \alpha_{24} & \alpha_{25} & \alpha_{26} & \alpha_{27} & \alpha_{28} & \alpha_{29} & -1 \\
\alpha_{31} & \alpha_{32} & 1 & \alpha_{34} & \alpha_{35} & \alpha_{36} & \alpha_{37} & \alpha_{38} & \alpha_{39} & -1 \\
\alpha_{41} & \alpha_{42} & \alpha_{43} & 1 & \alpha_{45} & \alpha_{46} & \alpha_{47} & \alpha_{48} & \alpha_{49} & -1 \\
\alpha_{51} & \alpha_{52} & \alpha_{53} & \alpha_{54} & 1 & \alpha_{56} & \alpha_{57} & \alpha_{58} & \alpha_{59} & -1 \\
\alpha_{61} & \alpha_{62} & \alpha_{63} & \alpha_{64} & \alpha_{65} & 1 & \alpha_{67} & \alpha_{68} & \alpha_{69} & -1 \\
\alpha_{71} & \alpha_{72} & \alpha_{73} & \alpha_{74} & \alpha_{75} & \alpha_{76} & 1 & \alpha_{78} & \alpha_{79} & -1 \\
\alpha_{81} & \alpha_{82} & \alpha_{83} & \alpha_{84} & \alpha_{85} & \alpha_{86} & \alpha_{87} & 1 & \alpha_{89} & -1 \\
\alpha_{91} & \alpha_{92} & \alpha_{93} & \alpha_{94} & \alpha_{95} & \alpha_{96} & \alpha_{97} & \alpha_{98} & 1 & -1 \\
1 & 1 & 1 & 1 & 1 & 1 & 1 & 1 & 1 & 0
\end{bmatrix}
\begin{bmatrix}
P_1 \\ P_2 \\ P_3 \\ P_4 \\ P_5 \\ P_6 \\ P_7 \\ P_8 \\ P_9 \\ \delta^g / I'_H
\end{bmatrix}
=
\begin{bmatrix}
0 \\ 0 \\ 0 \\ 0 \\ 0 \\ 0 \\ 0 \\ 0 \\ 0 \\ P^g
\end{bmatrix}
$$
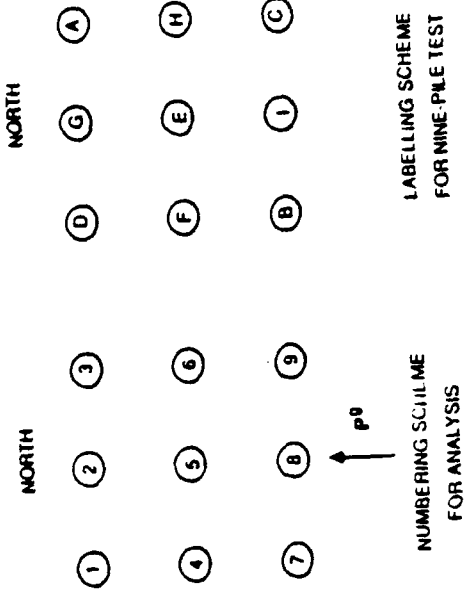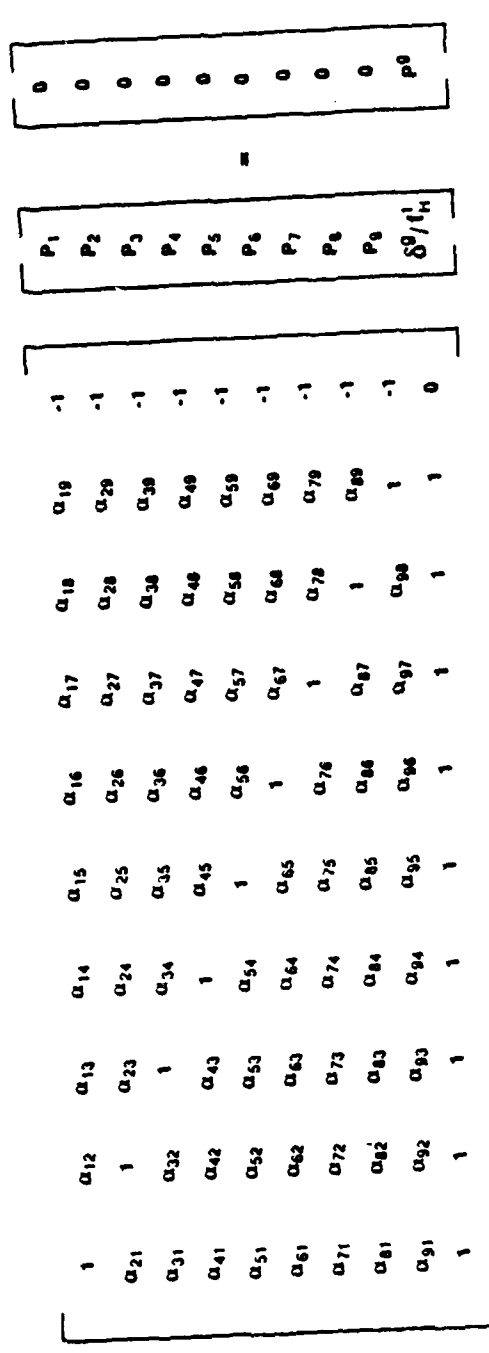
$\alpha_{12}, \alpha_{13}, \ldots, \alpha_{98}$ = INTERACTION FACTOR BETWEEN SUBSCRIPTED PILES (FREE-HEADED)

$P_1, P_2, \ldots, P_9$ = PILE LOAD

P^g = GROUP LOAD

δ^g = GROUP DEFLECTION

I'_H = HORIZONTAL DEFLECTION OF SINGLE PILE UNDER UNIT LOAD (SINGLE PILE FLEXIBILITY)

NORTH

```
(A)   (D)   (G)
(H)   (F)   (E)
(C)   (B)   (I)
```

LABELLING SCHEME FOR NINE-PILE TEST

NORTH

```
(1)   (2)   (3)
(4)   (5)   (6)
(7)   (8)   (9)
```

P^g

NUMBERING SCHEME FOR ANALYSIS

Fig. 5.1. Flexibility Matrix for a Nine-Pile Group (Free-Headed).

loading north and south, as a means of calibrating the derived interaction factors. Correspondence between the spacing between any two piles in the group and ξ is given below:

SPACING OF:	ξ
3 diam.	0°, 90°, 180°
6 diam.	0°, 90°, 180°
4.20 diam.	45°, 135°
6.71 diam.	26.6°, 63.4°,116.6°, 153.4°
8.49 diam.	45°, 135°

5.1.1. Load Distribution and Group Deflection for Cycle 1, Loading North

Group load $P^g = 66.08$ k

Average load per pile $P_j = 66.08/9 = 7.34$ k

Single pile flexibility f_H^1 (From Fig. A.2) $= 0.14/7.34$

$$= 0.019 \text{ in./k}$$

$^sP_{5\%} = 21$ k (Fig. A.2); then $P_j/^sP_{5\%} = 7.34/21 = 0.35$.

Interaction factors for departure angles of 0°, 90° and 180° are obtained from Figs. 4.24, 4.26, 4.28. Interaction factors for ξ different from 0°, 90° and 180° are obtained from Fig. 5.2 (solid line), which has been plotted based on a graphical procedure displayed in Fig. 5.2.a. Such a procedure specifies a large rate of change in α as ξ approaches 180° to express the effect of a pile on a second pile in its direct shadow. Each "leading" pile is treated as a leading pile regardless of whether it is in the front row of the
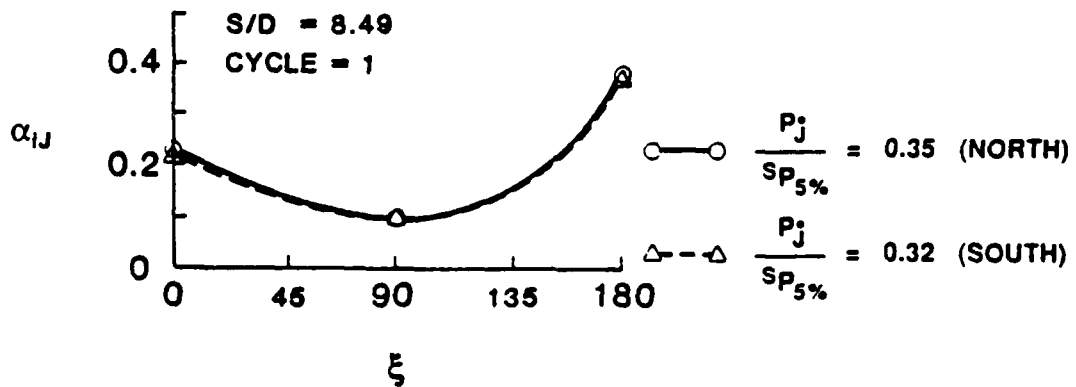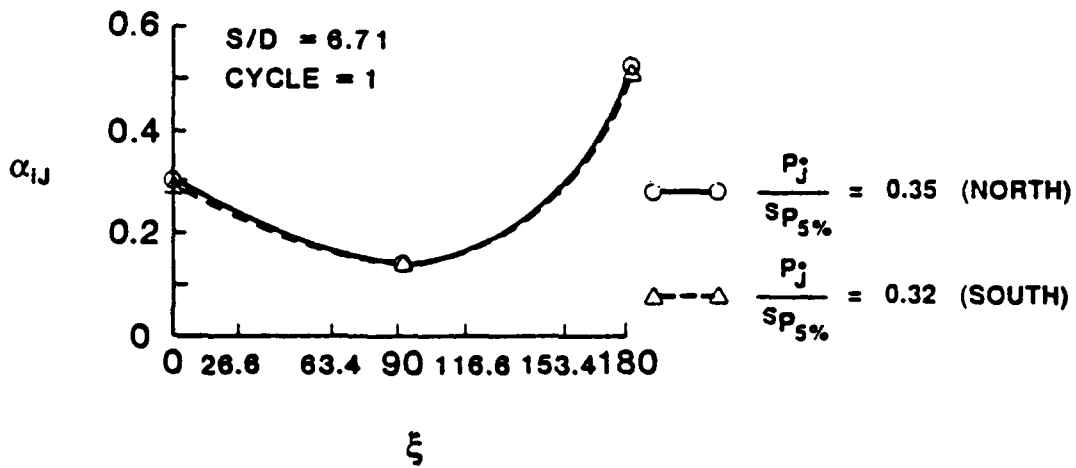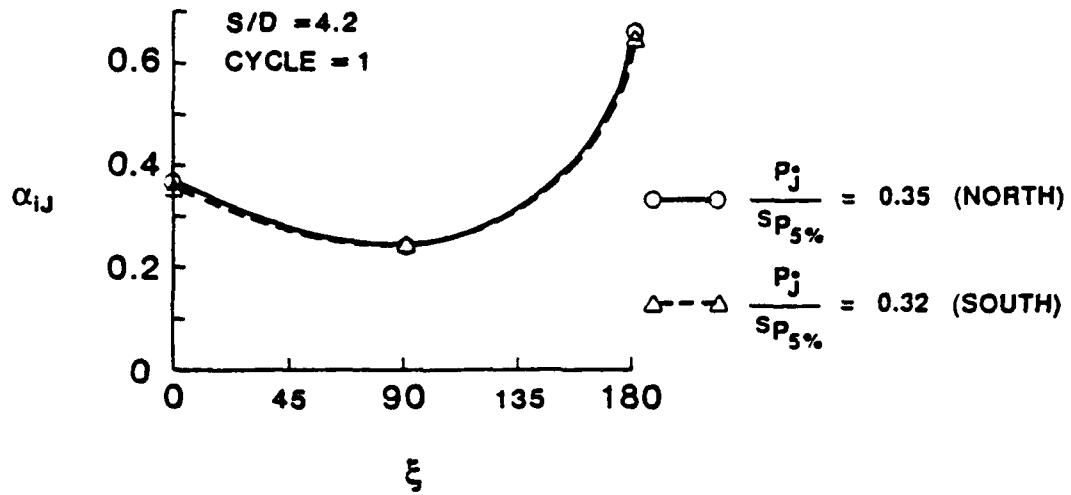
Fig. 5.2. α_{ij} vs. ξ for S/D = 4.2, 6.71 and 8.49,
Cycle 1, Loading North and South.
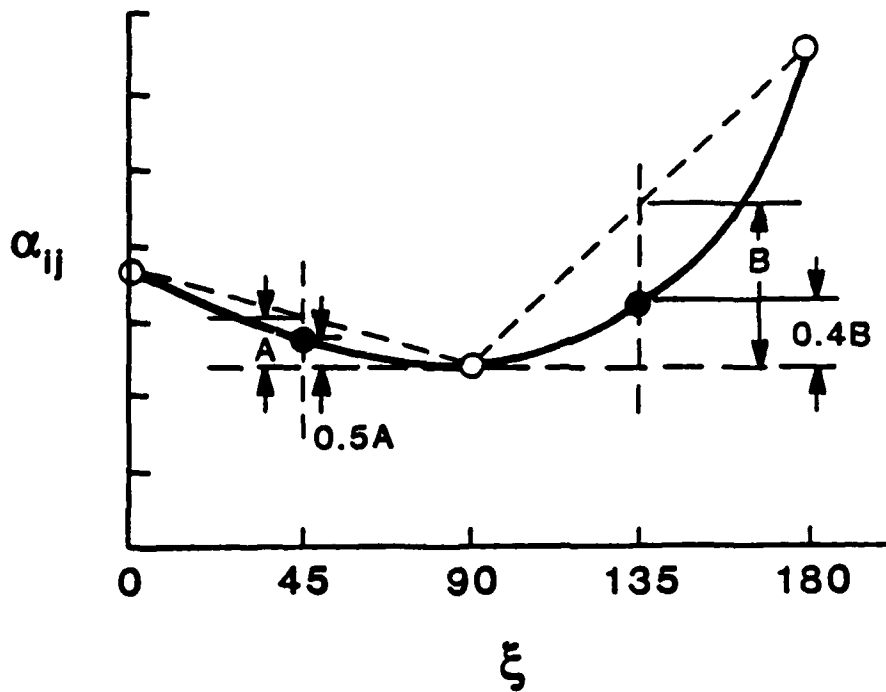
O α_{ij} FOR $\xi = 0°$, $90°$, $180°$ BASED ON
    INTERPOLATIONS FROM FIGS. 4.24 - 4.28.

● α_{ij} ESTIMATED GRAPHICALLY FOR
    INTERMEDIATE VALUES OF ξ (45°, 135°).

Fig. 5.2.a.   Graphical Estimation of α_{ij} for Values of
              ξ Different from 0°, 90° and 180°.

107

group or is merely in front of another pile. The flexibility matrix for these conditions is presented in tabular form as follows:

Element	$\xi(°)$	S/D	Figure	α_{ij}
1,1	–	–	–	1.0
1,2	90	3	4.28	0.30
1,3	90	6	4.28	0.16
1,4	0	3	4.24	0.39
1,5	45	4.2	5.2	0.29
1,6	63.4	6.71	5.2	0.18
1,7	0	6	4.24	1.33
1,8	26.6	6.71	5.2	0.24
1,9	45	8.49	5.2	0.14
1,10	–	–	–	-1.0
C(1)	–	–	–	0.0
2,1	90	3	4.28	0.30
2,2	–	–	–	1.0
2,3	90	3	4.28	0.30
2,4	45	4.2	5.2	0.29
2,5	0	3	4.24	0.39
2,6	45	4.2	5.2	0.29
2,7	26.6	6.71	5.2	0.24
2,8	0	6	4.24	0.33
2,9	26.6	6.71	5.2	0.24
2,10	–	–	–	-1.0
C(2)	–	–	–	0.0
3,1	90	6	4.28	0.16
3,2	90	3	4.28	0.30
3,3	–	–	–	1.0
3,4	63.4	6.71	5.2	0.18
3,5	45	4.2	5.2	0.29
3,6	0	3	4.24	0.39
3,7	45	8.49	5.2	0.14
3,8	26.6	6.71	5.2	0.24
3,9	0	6	4.24	0.33
3,10	–	–	–	-1.0
C(3)	–	–	–	0.0
4,1	180	3	4.26	0.69
4,2	135	4.2	5.2	0.32
4,3	116.6	6.71	5.2	0.17
4,4	–	–	–	1.0
4,5	90	3	4.28	0.30
4,6	90	6	4.28	0.16
4,7	0	3	4.24	0.39

4,8	45	4.2	5.2	0.29
4,9	63.4	6.71	5.2	0.18
4,10	–	–	–	-1.0
C(4)	–	–	–	0.0
5,1	135	4.2	5.2	0.32
5,2	180	3	4.26	0.69
5,3	135	4.2	5.2	0.32
5,4	90	3	4.28	0.30
5,5	–	–	–	1.0
5,6	90	3	4.28	0.30
5,7	45	4.2	5.2	0.29
5,8	0	3	4.24	0.39
5,9	45	4.2	5.2	0.29
5,10	–	–	–	-1.0
C(5)	–	–	–	0.0
6,1	116.6	6.71	5.2	0.17
6,2	135	4.2	5.2	0.32
6,3	180	3	4.26	0.69
6,4	90	6	4.28	0.16
6,5	90	3	4.28	0.30
6,6	–	–	–	1.0
6,7	63.4	6.71	5.2	0.18
6,8	45	4.2	5.2	0.29
6,9	0	3	4.24	0.39
6,10	–	–	–	-1.0
C(6)	–	–	–	0.0
7,1	180	6	4.26	0.59
7,2	153.4	6.71	5.2	0.32
7,3	135	8.49	5.2	0.16
7,4	180	3	4.26	0.69
7,5	135	4.2	5.2	0.32
7,6	116.6	6.71	5.2	0.17
7,7	–	–	–	1.0
7,8	90	3	4.28	0.30
7,9	90	6	4.28	0.16
7,10	–	–	–	-1.0
C(7)	–	–	–	0.0
8,1	153.4	6.71	5.2	0.32
8,2	180	6	4.26	0.59
8,3	153.4	6.71	5.2	0.32
8,4	135	4.2	5.2	0.32
8,5	180	3	4.26	0.69
8,6	135	4.2	5.2	0.32
8,7	90	3	4.28	0.30
8,8	–	–	–	1.0
8,9	90	3	4.28	0.30
8,10	–	–	–	-1.0
C(8)	–	–	–	0.0

9,1	135	8.49	5.2	0.16
9,2	153.4	6.71	5.2	0.32
9,3	180	6	4.26	0.59
9,4	116.6	6.71	5.2	0.17
9,5	135	4.2	5.2	0.32
9,6	180	3	4.26	0.69
9,7	90	6	4.28	0.16
9,8	90	3	4.28	0.30
9,9	–	–	–	1.0
9,10	–	–	–	-1.0
C(9)	–	–	–	0.0
10,1	–	–	–	1.0
10,2	–	–	–	1.0
10,3	–	–	–	1.0
10,4	–	–	–	1.0
10,5	–	–	–	1.0
10,6	–	–	–	1.0
10,7	–	–	–	1.0
10,8	–	–	–	1.0
10,9	–	–	–	1.0
10,10	–	–	–	0.0
C(10)	–	–	–	66.08

The C terms in the above table represent terms in the load vector.

Fig 5.3 summarizes the results obtained after solving the flexibility matrix equation (Fig. 5.1) using the experimental interaction factors developed in this report. Such results are also compared with those obtained by Morrison (1986), annexed as Table C.1. in Appendix C, as well as with results obtained using elastic interaction factors (Poulos-Randolph).

5.1.2. Load Distribution and Group Deflection for Cycle 1, Loading South

Group load $P^g = 63.47$ k

Average load per pile $P_j = 63.47/9 = 7.05$ k

CYCLE : 1
LOADING : NORTH
GROUP LOAD : 66.08K

AVERAGE LOAD PER PILE : 7.34K

$$\frac{P_j}{^sP_{5\%}} = 0.35$$

NORTH

①	②	③
14.07K	10.33K	14.07K → EXPERIMENTAL α's
8.53K	9.16K	9.24K → MORRISON'S TEST
10.71K	7.82K	10.71K → POULOS-RANDOLPH α's

④	⑤	⑥
5.62K	3.00K	5.62K
8.05K	8.86K	6.12K
3.59K	0.38K	3.59K

⑦	⑧	⑨
5.33K	2.67K	5.33K
7.40K	3.90K	4.82K
10.71K	7.82K	10.71K

AVERAGE LOAD PER ROW

(1 2 3)

12.82K
8.97K
9.74K

(4 5 6)

4.74K
7.67K
2.52K

(7 8 9)

4.44K
5.37K
9.74K

GROUP DEFLECTION

EXPERIMENTAL α's : 0.50 in.

MORRISON'S TEST : 0.35 in.

POULOS-RANDOLPH α's : 0.46 in.

Fig. 5.3. Load Distribution and Group Deflection for Cycle 1, Loading North, Group Load = 66.08 k.

111
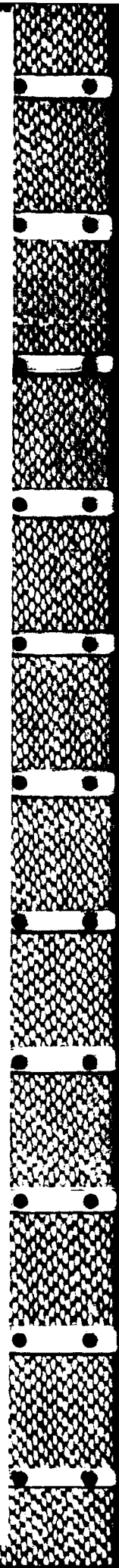
Single pile flexibility $f_H{}^1$ (From Fig. A.5) $=$ 0.14/7.05

$$= 0.020 \text{ in./k}$$

${}^S P_{5\%} =$ 22 k (Fig. A.5); then $P_j/{}^S P_{5\%} =$ 7.05/22 $=$ 0.32 .

Following the same logic as before, values of α for $\xi =$ 0°, 90°, and 180° are obtained from Figs. 4.24, 4.26 and 4.28, and values of α for ξ different from 0°, 90°, 180° are obtained from the dashed line in Fig. 5.2 for loading to the south. The flexibility matrix for this case is as follows:

Element	$\xi(°)$	S/D	Figure	α_{ij}
1,1	–	–	–	1.0
1,2	90	3	4.28	0.30
1,3	90	6	4.28	0.16
1,4	180	3	4.26	0.68
1,5	135	4.2	5.2	0.31
1,6	116.6	6.71	5.2	0.16
1,7	180	6	4.26	0.57
1,8	153.4	6.71	5.2	0.31
1,9	135	8.49	5.2	0.15
1,10	–	–	–	-1.0
C(1)	–	–	–	0.0
2,1	90	3	4.28	0.30
2,2	–	–	–	1.0
2,3	90	3	4.28	0.30
2,4	135	4.2	5.2	0.31
2,5	180	3	4.26	0.68
2,6	135	4.2	5.2	0.31
2,7	153.4	6.71	5.2	0.31
2,8	180	6	4.26	0.57
2,9	153.4	6.71	5.2	0.31
2,10	–	–	–	-1.0
C(2)	–	–	–	0.0
3,1	90	6	4.28	0.16
3,2	90	3	4.28	0.30
3,3	–	–	–	1.0
3,4	116.6	6.71	5.2	0.16
3,5	135	4.2	5.2	0.31
3,6	180	3	4.26	0.68
3,7	135	8.49	5.2	0.15
3,8	153.4	6.71	5.2	0.31

112

3,9	180	6	4.26	0.57
3,10	–	–	–	-1.0
C(3)	–	–	–	0.0
4,1	0	3	4.24	0.38
4,2	45	4.2	5.2	0.28
4,3	63.4	6.71	5.2	0.17
4,4	–	–	–	1.0
4,5	90	3	4.28	0.30
4,6	90	6	4.28	0.16
4,7	180	3	4.26	0.68
4,8	135	4.2	5.2	0.31
4,9	116.6	6.71	5.2	0.16
4,10	–	–	–	-1.0
C(4)	–	–	–	0.0
5,1	45	4.2	5.2	0.28
5,2	0	3	4.24	0.38
5,3	45	4.2	5.2	0.28
5,4	90	3	4.28	0.30
5,5	–	–	–	1.0
5,6	90	3	4.28	0.30
5,7	135	4.2	5.2	0.31
5,8	180	3	4.26	0.68
5,9	135	4.2	5.2	0.31
5,10	–	–	–	-1.0
C(5)	–	–	–	0.0
6,1	63.4	6.71	5.2	0.17
6,2	45	4.2	5.2	0.28
6,3	0	3	4.24	0.38
6,4	90	6	4.28	0.16
6,5	90	3	4.28	0.30
6,6	–	–	–	1.0
6,7	116.6	6.71	5.2	0.16
6,8	135	4.2	5.2	0.31
6,9	180	3	4.26	0.68
6,10	–	–	–	-1.0
C(6)	–	–	–	0.0
7,1	0	6	4.24	0.32
7,2	26.6	6.71	5.2	0.23
7,3	45	8.49	5.2	0.13
7,4	0	3	4.24	0.38
7,5	45	4.2	5.2	0.28
7,6	63.4	6.71	5.2	0.17
7,7	–	–	–	1.0
7,8	90	3	4.28	0.30
7,9	90	6	4.28	0.16
7,10	–	–	–	-1.0
C(7)	–	–	–	0.0

8,1	26.6	6.71	5.2	0.23
8,2	0	6	4.24	0.32
8,3	26.6	6.71	5.2	0.23
8,4	45	4,2	5.2	0.28
8,5	0	3	4.24	0.38
8,6	45	4,2	5.2	0.28
8,7	90	3	4.28	0.30
8,8	–	–	–	1.0
8,9	90	3	4.28	0.30
8,10	–	–	–	-1.0
C(8)	–	–	–	0.0
9,1	45	8.49	5.2	0.13
9,2	26.6	6.71	5.2	0.23
9,3	0	6	4.24	0.32
9,4	63.4	6.71	5.2	0.17
9,5	45	4.2	5.2	0.28
9,6	0	3	4.24	0.38
9,7	90	6	4.28	0.16
9,8	90	3	4.28	0.30
9,9	–	–	–	1.0
9,10	–	–	–	-1.0
C(9)	–	–	–	0.0
10,1	–	–	–	1.0
10,2	–	–	–	1.0
10,3	–	–	–	1.0
10,4	–	–	–	1.0
10,5	–	–	–	1.0
10,6	–	–	–	1.0
10,7	–	–	–	1.0
10,8	–	–	–	1.0
10,9	–	–	–	1.0
10,10	–	–	–	0.0
C(10)	–	–	–	63.47

Similarly, the load distribution and group deflection obtained after solving the flexibility matrix equation for the nine-pile group, using experimental α factors, are compared with the results obtained by Morrison (Table C.2) and by those from an elastic analysis of the pile group in Fig. 5.4.

CYCLE : 1
LOADING : SOUTH
GROUP LOAD : 63.47K

AVERAGE LOAD PER PILE : 7.05K

$$\frac{P_J^s}{{}^sP_{5\%}} = 0.32$$

NORTH

①	②	③	
5.35K	2.74K	5.35K	→ EXPERIMENTAL α's
5.26K	4.56K	5.69K	→ MORRISON'S TEST
10.29K	7.51K	10.29K	→ POULOS-RANDOLPH α's

④	⑤	⑥
5.54K	3.03K	5.54K
6.25K	4.70K	5.99K
3.45K	0.36K	3.45K

⑦	⑧	⑨
13.15K	9.58K	13.15K
9.24K	10.82K	10.97K
10.29K	7.51K	10.29K

AVERAGE LOAD PER ROW

GROUP DEFLECTION

①②③

4.48K
5.17K
9.36K

EXPERIMENTAL α's : 0.50 in.

MORRISON'S TEST : 0.45 in.

POULOS-RANDOLPH α's : 0.46 in.

④⑤⑥

4.70K
5.64K
2.42K

⑦⑧⑨

11.96K
10.34K
9.36K

Fig. 5.4. Load Distribution and Group Deflection for
Cycle 1, Loading South, Group Load = 63.47 k.

5.1.3. Load Distribution and Group Deflection for Cycle 100, Loading North

Group load $P^g = 64.83$ k

Average load per pile $P_j = 64.83/9 = 7.20$ k

Single pile flexibility f_H^1 (From Fig. A.4)$= 0.16/7.20$

$$= 0.022 \text{ in./k}$$

$^SP_{5\%} = 18$ k (Fig. A.4); then $P_j/^SP_{5\%} = 7.20/18 = 0.40$.

Values of α for $\xi = 0°$, 90°, and 180° are obtained from Figs. 4.25, 4.27 and 4.28; values of α for ξ different from 0°, 90°, and 180° are taken from Fig. 5.5 (solid line). The general flexibility matrix for this case is given by:

Element	$\xi(°)$	S/D	Figure	α_{ij}
1,1	–	–	–	1.0
1,2	90	3	4.28	0.20
1,3	90	6	4.28	0.10
1,4	0	3	4.25	0.13
1,5	45	4.2	5.5	0.13
1,6	63.4	6.71	5.5	0.09
1,7	0	6	4.25	0.07
1,8	26.6	6.71	5.5	0.09
1,9	45	8.49	5.5	0.05
1,10	–	–	–	-1.0
C(1)	–	–	–	0.0
2,1	90	3	4.28	0.20
2,2	–	–	–	1.0
2,3	90	3	4.28	0.20
2,4	45	4.2	5.5	0.13
2,5	0	3	4.25	0.13
2,6	45	4.2	5.5	0.13
2,7	26.6	6.71	5.5	0.09
2,8	0	6	4.25	0.07
2,9	26.6	6.71	5.5	0.09
2,10	–	–	–	-1.0
C(2)	–	–	–	0.0
3,1	90	6	4.28	0.10
3,2	90	3	4.28	0.20
3,3	–	–	–	1.0
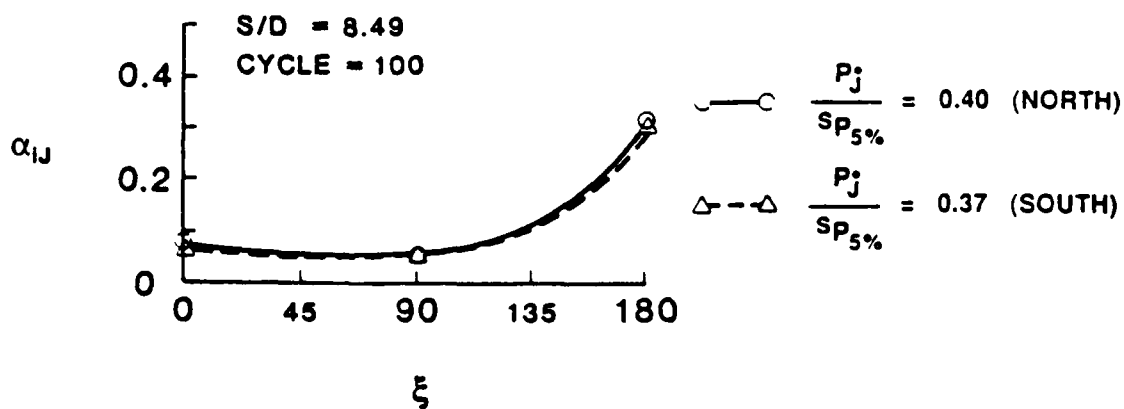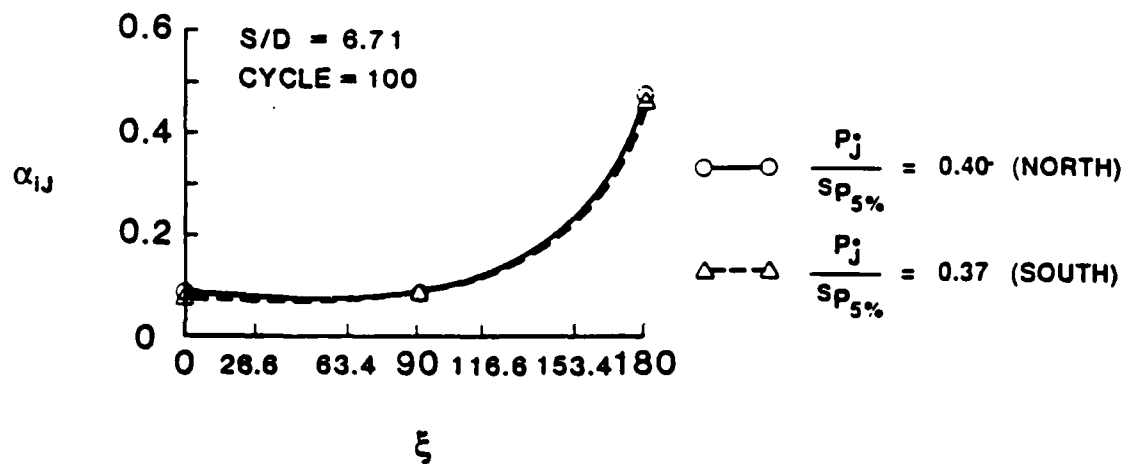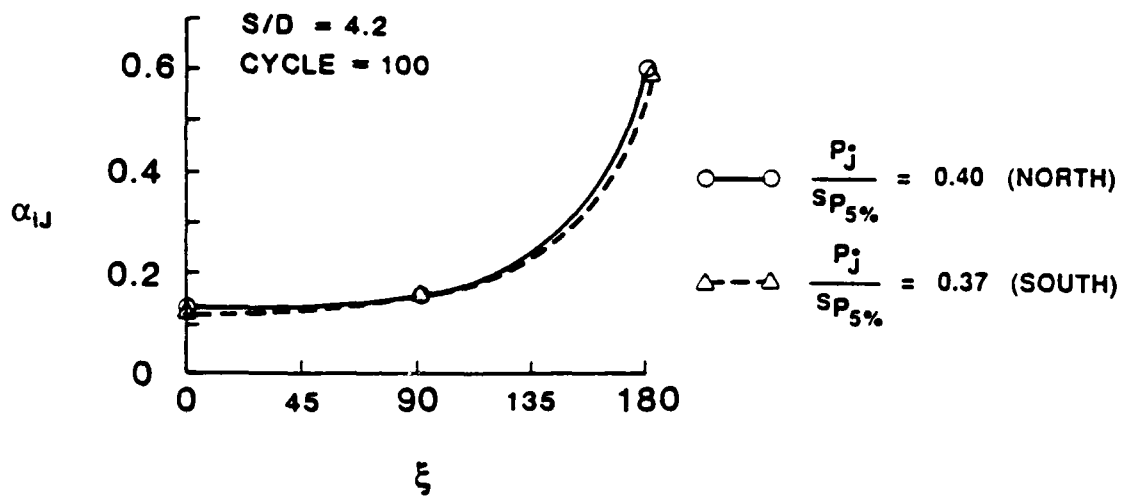
Fig. 5.5. α_{ij} vs. ξ for S/D = 4.2, 6.71 and 8.49, Cycle 100, Loading North and South.

3,4	63.4	6.71	5.5	0.09
3,5	45	4.2	5.5	0.13
3,6	0	3	4.25	0.13
3,7	45	8.49	5.5	0.05
3,8	26.6	6.71	5.5	0.09
3,9	0	6	4.25	0.07
3,10	-	-	-	-1.0
C(3)	-	-	-	0.0
4,1	180	3	4.27	0.62
4,2	135	4.2	5.5	0.22
4,3	116.6	6.71	5.5	0.11
4,4	-	-	-	1.0
4,5	90	3	4.28	0.20
4,6	90	6	4.28	0.10
4,7	0	3	4.25	0.13
4,8	45	4.2	5.5	0.13
4,9	63.4	6.71	5.5	0.09
4,10	-	-	-	-1.0
C(4)	-	-	-	0.0
5,1	135	4.2	5.5	0.22
5,2	180	3	4.27	0.62
5,3	135	4.2	5.5	0.22
5,4	90	3	4.28	0.20
5,5	-	-	-	1.0
5,6	90	3	4.28	0.20
5,7	45	4.2	5.5	0.13
5,8	0	3	4.25	0.13
5,9	45	4.2	5.5	0.13
5,10	-	-	-	-1.0
C(5)	-	-	-	0.0
6,1	116.6	6.71	5.5	0.11
6,2	135	4.2	5.5	0.22
6,3	180	3	4.27	0.62
6,4	90	6	4.28	0.10
6,5	90	3	4.28	0.20
6,6	-	-	-	1.0
6,7	63.4	6.71	5.5	0.09
6,8	45	4.2	5.5	0.13
6,9	0	3	4.25	0.13
6,10	-	-	-	-1.0
C(6)	-	-	-	0.0
7,1	180	6	4.27	0.53
7,2	153.4	6.71	5.5	0.23
7,3	135	8.49	5.5	0.11
7,4	180	3	4.27	0.62
7,5	135	4.2	5.5	0.22
7,6	116.6	6.71	5.5	0.11
7,7	-	-	-	1.0

7,8	90	3	4.28	0.20
7,9	90	6	4.28	0.10
7,10	–	–	–	-1.0
C(7)	–	–	–	0.0
8,1	153.4	6.71	5.5	0.23
8,2	180	6	4.27	0.53
8,3	153.4	6.71	5.5	0.23
8,4	135	4.2	5.5	0.22
8,5	180	3	4.27	0.62
8,6	135	4.2	5.5	0.22
8,7	90	3	4.28	0.20
8,8	–	–	–	1.0
8,9	90	3	4.28	0.20
8,10	–	–	–	-1.0
C(8)	–	–	–	0.0
9,1	135	8.49	5.5	0.11
9,2	153.4	6.71	5.5	0.23
9,3	180	6	4.27	0.53
9,4	116.6	6.71	5.5	0.11
9,5	135	4.2	5.5	0.22
9,6	180	3	4.27	0.62
9,7	90	6	4.28	0.10
9,8	90	3	4.28	0.20
9,9	–	–	–	1.0
9,10	–	–	–	-1.0
C(9)	–	–	–	0.0
10,1	–	–	–	1.0
10,2	–	–	–	1.0
10,3	–	–	–	1.0
10,4	–	–	–	1.0
10,5	–	–	–	1.0
10,6	–	–	–	1.0
10,7	–	–	–	1.0
10,8	–	–	–	1.0
10,9	–	–	–	1.0
10,10	–	–	–	0.0
C(10)	–	–	–	64.83

Load distribution and group deflection obtained after solving the matrix equation are shown in Fig. 5.6, as well as comparisons with results obtained by Morrison (1986) from Table C.3 and with results from an elatic analysis of the pile group (Poulos-Randolph).

CYCLE : 100   AVERAGE LOAD PER PILE : 7.20K
LOADING : NORTH
GROUP LOAD : 64.83K $\dfrac{P_J^\bullet}{^sP_{5\%}} = 0.40$

NORTH

①	②	③
14.90K	12.56K	14.90K ➤ EXPERIMENTAL α's
8.45K	9.24K	9.62K ➤ MORRISON'S TEST
10.51K	7.67K	10.51K ➤ POULOS-RANDOLPH α's

④	⑤	⑥
5.23K	3.53K	5.23K
7.77K	8.76K	5.83K
3.52K	0.37K	3.52K

⑦	⑧	⑨
3.36K	1.71K	3.36K
7.19K	3.48K	4.47K
10.51K	7.67K	10.51K

AVERAGE LOAD PER ROW   GROUP DEFLECTION

①②③

14.12K   EXPERIMENTAL α's : 0.46 in.
9.10K   MORRISON'S TEST : 0.34 in.
9.56K   POULOS-RANDOLPH α's : 0.52 in.

④⑤⑥

4.66K
7.45K
2.47K

⑦⑧⑨

2.81K
5.04K
9.56K

Fig. 5.6. Load Distribution and Group Deflection for
Cycle 100, Loading North, Group Load = 64.83 k.

120

5.1.4. Load Distribution and Group Deflection for Cycle 100, Loading South

Group Load $P^g = 58.48$ k

Average load per pile $P_j = 6.49$ k

Single pile flexibility f_H^1 (From Fig. A.7) $= 0.13/6.49$

$$= 0.020 \text{ in./k}$$

$^SP_{5\%} = 17.5$ k (Fig. A.7); then $P_j/^SP_{5\%} = 6.49/17.5 = 0.37$.

Values of α for $\xi = 0°$, $90°$, and $180°$ are obtained from Figs. 4.25, 4.27 and 4.28; values of α for ξ different from $0°$, $90°$, and $180°$ are obtained from the dashed line in Fig. 5.5 (loading south). The flexibility matrix for this case is presented in tabular form as follows:

Element	$\xi(°)$	S/D	Figure	α_{ij}
1,1	–	–	–	–
1,2	90	3	4.28	0.20
1,3	90	6	4.8	0.10
1,4	180	3	4.2	0.61
1,5	135	4.2	5.5	0.21
1,6	116.6	6.71	5.5	0.10
1,7	180	6	4.27	0.52
1,8	153.4	6.71	5.5	0.22
1,9	135	8.49	5.5	0.10
1,10	–	–	–	-1.0
C(10)	–	–	–	0.0
2,1	90	3	4.28	0.20
2,2	–	–	–	1.0
2,3	90	3	4.28	0.20
2,4	135	4.2	5.5	0.21
2,5	180	3	4.27	0.61
2,6	135	4.2	5.5	0.21
2,7	153.4	6.71	5.5	0.22
2,8	180	6	4.27	0.52
2,9	153.4	6.71	5.5	0.22
2,10	–	–	–	-1.0
C(2)	–	–	–	0.0
3,1	90	6	4.28	0.10

3,2	90	3	4.28	0.20
3,3	–	–	–	1.0
3,4	116.6	6.71	5.5	0.10
3,5	135	4.2	5.5	0.21
3,6	180	3	4.27	0.61
3,7	135	8.49	5.5	0.10
3,8	153.4	6.71	5.5	0.22
3,9	180	6	4.27	0.52
3,10	–	–	–	-1.0
C(3)	–	–	–	0.0
4,1	0	3	4.25	0.12
4,2	45	4.2	5.5	0.12
4,3	63.4	6.71	5.5	0.08
4,4	–	–	–	1.0
4,5	90	3	4.28	0.20
4,6	90	6	4.28	0.10
4,7	180	3	4.27	0.61
4,8	135	4.2	5.5	0.21
4,9	116.6	6.71	5.5	0.10
4,10	–	–	–	-1.0
C(10)	–	–	–	0.0
5,1	45	4.2	5.5	0.12
5,2	0	3	4.25	0.12
5,3	45	4.2	5.5	0.12
5,4	90	3	4.28	0.20
5,5	–	–	–	1.0
5,6	90	3	4.28	0.20
5,7	135	4.2	5.5	0.21
5,8	180	3	4.27	0.61
5,9	135	4.2	5.5	0.21
5,10	–	–	–	-1.0
C(5)	–	–	–	0.0
6,1	63.4	6.71	5.5	0.08
6,2	45	4.2	5.5	0.12
6,3	0	3	4.25	0.12
6,4	90	6	4.28	0.10
6,5	90	3	4.28	0.20
6,6	–	–	–	1.0
6,7	116.6	6.71	5.5	0.10
6,8	135	4.2	5.5	0.21
6,9	180	3	4.27	0.61
6,10	–	–	–	-1.0
C(6)	–	–	–	0.0
7,1	0	6	4.25	0.06
7,2	26.6	6.71	5.5	0.08
7,3	45	8.49	5.5	0.04
7,4	0	3	4.25	0.12
7,5	45	4.2	5.5	0.12

7,6	63.4	6.71	5.5	0.08
7,7	–	–	–	1.0
7,8	90	3	4.28	0.20
7,9	90	6	4.28	–1.0
7,10	–	–	–	–1.0
C(7)	–	–	–	0.0
8,1	26.6	6.71	5.5	0.08
8,2	0	6	4.25	0.06
8,3	26.6	6.71	5.5	0.08
8,4	45	4.2	5.5	0.12
8,5	0	3	4.25	0.12
8,6	45	4.2	5.5	0.12
8,7	90	3	4.28	0.20
8,8	–	–	–	1.0
8,9	90	3	4.28	0.20
8,10	–	–	–	–1.0
C(8)	–	–	–	0.0
9,1	45	8.49	5.5	0.04
9,2	26.6	6.71	5.5	0.08
9,3	0	6	4.25	0.06
9,4	63.4	6.71	5.5	0.08
9,5	45	4.2	5.5	0.12
9,6	0	3	4.25	0.12
9,7	90	6	4.28	0.10
9,8	90	3	4.28	0.20
9,9	–	–	–	1.0
9,10	–	–	–	–1.0
C(9)	–	–	–	0.0
10,1	–	–	–	1.0
10,2	–	–	–	1.0
10,3	–	–	–	1.0
10,4	–	–	–	1.0
10,5	–	–	–	1.0
10,6	–	–	–	1.0
10,7	–	–	–	1.0
10,8	–	–	–	1.0
10,9	–	–	–	1.0
10,10	–	–	–	0.0
C(10)	–	–	–	58.48

Once again, Fig. 5.7 presents the results using experimental interaction factors, which are compared with those measured by Morrison (Table C.4) and those from an elastic analysis (Poulos-Randolph), for the same load and cyclic conditions.

123

CYCLE : 100
LOADING : SOUTH
GROUP LOAD : 58.48K

AVERAGE LOAD PER PILE : 6.49K

$$\frac{P_j}{{}^{s}P_{5\%}} = 0.37$$

NORTH

(1)	(2)	(3)
3.12K	1.63K	3.12K → EXPERIMENTAL α's
4.55K	4.22K	5.81K → MORRISON'S TEST
9.48K	6.92K	9.48K → POULOS-RANDOLPH α's

(4)	(5)	(6)
4.87K	3.34K	4.87K
5.29K	4.20K	5.85K
3.18K	0.33K	3.18K

(7)	(8)	(9)
13.19K	11.10K	13.89K
7.96K	10.02K	10.57K
9.48K	6.92K	9.48K

AVERAGE LOAD PER ROW

GROUP DEFLECTION

(1 2 3)

2.62K
4.86K
8.63K

EXPERIMENTAL α's : 0.37 in.

MORRISON'S TEST : 0.44 in.

POULOS-RANDOLPH   α's : 0.42 in.

(4 5 6)

4.36K
5.11K
2.23K

(7 8 9)

12.73K
9.51K
8.63K

Fig. 5.7.   Load Distribution and Group Deflection for
Cycle 100, Loading South, Group Load = 58.48 k.

The load distribution among the piles in the group from Figs. 5.3, 5.4, 5.6 and 5.7 shows that the shadowing effect can be evaluated reasonably accurately using experimental interaction factors developed in this report. Leading, or front, piles developed loads larger than the loads developed by the row of trailing, or rear, piles. Better agreement for load distribution among the piles in the group and group deflection was obtained when the pile group was loaded to the south rather than to the north. There are two reasons why loading to the north may have been less representative of modelled behavior than was loading to the south. First, substantial rotation of the loading frame about a vertical axis occurred during Morrison's load test when loading was to the north. This may have reduced, in some proportion, the shadowing effect, such that use of the α factors developed here overpredicted shear load differences among the piles. The frame rotation may have reduced the reacting load in front piles, increasing the load on rear piles and reducing the group deflection. The details of the pile alignment may have also contributed to unrepresentative behavior during loading to the north. Pile R was driven about one-half diameter to the east of its intended alignment (O'Neill and Hawkins, 1982), so that Pile U did not fully shadow it during loading to the north. Moreover, Pile S was slightly out of line with Pile V, and Pile T was battered inadvertently to the northeast, so that its immediate trailing pile (W) was actually farther from Pile T below

125

the ground surface than was assumed in the calculations. The X-U, Y-V, and Z-W alignment (leading and second row piles for loading to the south) was much closer to the ideal alignment considered in the calculations summarized in this chapter. For these reasons loading to the south is considered to represent the conditions modelled much better than loading to the north. As a summary comparison, distributions of the group load based on the average load per row and deflections, loading south, is given in Table 5.1.

Holloway, Moriwaki, Finno and Green (1982) reported a similar behavior of front and rear piles in a laterally loaded pile group test performed for the U.S. Army Corps of Engineers (St. Louis District); front piles encounter a stiffer and stronger soil resistance than rear piles, as the inner soil mass tracks the deformation of the front piles. Results of lateral load tests on small-scale piles, 1-in. in diameter (Cox, Dixon and Murphy, 1984), in very soft clay, confirm the same phenomenon and serve to suggest that shadowing effects occur in all soils.

Some commentary concerning Table 5.1 is in order. First, the α factors based on elasticity theory provided very good estimates of deflection. However, they underestimated loads on the leading and second row and overestimated loads on the piles in the rear row. The experimental α factors provided a better prediction of the pattern of load distribution than did the elasticity-based factors for Cycle

Table 5.1. Load by Row, as Per Cent of Total, and Deflection for Nine-Pile Group Test, Loading South

Row	Experimental α's	Morrison's Load Test	Poulos-Randolph α's
	CYCLE 1		
Front	56 % (0.50)	48 % (0.45)	44 % (0.46)
Second	22 % (0.50)	26 % (0.45)	11 % (0.46)
Third	21 % (0.50)	24 % (0.45)	44 % (0.46)
	CYCLE 100		
Front	65 % (0.37)	48 % (0.44)	44 % (0.42)
Second	22 % (0.37)	26 % (0.44)	11 % (0.42)
Third	13 % (0.37)	24 % (0.44)	44 % (0.42)

Note: Deflections shown in parentheses in inches

1 (static loading). In Cycle 100 the pattern was predicted well, but the shear loads on the leading row of piles were predicted to be larger than those measured. While this feature suggests that use of the experimental α factors in design will produce conservative results with respect to the estimation of shear load in the most heavily loaded piles, it also suggests that the two-pile interaction factors developed here are not strictly representative of behavior of piles in a much larger group. Cycling loading of the larger group produced higher stiffnesses in the trailing piles than those predicted, probably due to increased sand densification around trailing piles not produced in the two-pile tests.

5.2. Design Procedure

The purpose of this section is to provide a step-by-step design procedure for the evaluation of the behavior of a free-head pile group embedded in medium to dense sand, using the experimental interaction factors developed in this report. Such steps are as follows:

A. Compute the average load per pile, P_j.
$$P_j = \frac{\text{Group load, } P^g}{\text{Number of piles in group, } n}$$

B. Compute the single pile flexibility, f_H^1 (secant to single-pile load-deflection curve for the average load per pile obtained in A) from a single pile theoretical solution or load test.

C. Normalize the average load per pile, $(P_j/{}^S P_{5\%})$, by a

128

load on the single pile that corresponds to a displacement of 5% of a single pile diameter.

D. Formulate the flexibility matrix equation (free-head) for the pile group based on Fig. 1.4.

E. Evaluate every element (α_{ij}) in the formulated matrix from D, for a particular direction of load, number of cycles of load, loading level $(P_j/{}^SP_{5\%})$, spacing and departure angle (ξ) between subscripted piles. For departure angles $0°$, $90°$, and $180°$, use Figs. 4.24 – 4.28 directly; for departure angles different from $0°$, $90°$, and $180°$, follow the graphical procedure given in Fig. 5.2.a.

F. Compute load distribution $(P_1,...,P_n)$ and group deflection, δ^g, by solving the flexibility matrix equation from E.

5.3. Induced Bending Moments due to Group Action

It is intended in this section to provide general information about the effect of group action on bending moments, for in-line $(\xi = 0°, 180°)$ and side-by-side $(\xi = 90°)$ alignments. Observations are presented for the loading level of ± 12 kips and static conditions (Cycle 1).

5.3.1. In-Line Alignment

The induced bending moments due to group action for in-line piles, for S/D =3, can be obtained from plots of bending moments vs. depth when (1) Pile V (Fig. 3.4) was loaded as a single pile (Conf. 1), (2) Piles V and Y were loaded

129

together (Conf. 3), and (3) Piles S, V, and Y were loaded as a group (Conf. 4). Such plots, in which the bending moment has been normalized by the pile-head shear, are shown in Figs. 5.8.a and 5.8.b. A minor effect of the trailing pile on bending moments in the leading pile ($\xi = 0°$), for S/D =3, can be observed from the plots for Pile V in Conf. 1, and Piles V and Y in Conf. 3, loading north (Fig. 5.8.a). The magnitude of the effect may have been reduced by the physical presence of the unloaded Pile S, stiffening the soil between Piles S and V. The effect of the leading pile on bending moments in the trailing pile ($\xi = 180°$), for S/D =3, can be observed from similar graphs but for loading to the south (Fig. 5.8.b). In this case the magnitude of moment in the trailing pile is increased by about 10 per cent. Additional induced bending moment occurred in Pile V in Conf. 4 for both loading directions, particularly when Pile V became a trailing pile (Fig. 5.8.a).

5.3.2. Side-by-Side Alignment

The induced bending moments generated by the group action for a side-by-side alignment ($\xi = 90°$) can be observed in Figs. 5.9.a and 5.9.b. Those figures represent normalized bending moments in Pile Y vs. depth when Pile Y was loaded as a single pile (Conf. 2), and loaded with Piles X and Z as a group (Conf. 5), loading north and south. The substantial difference in the induced bending moment on Pile Y, loading north, compared to the induced moment load-

130

PILE : V
CYCLE : 1
LOADING : NORTH

MOMENT/LATERAL LOAD, IN.
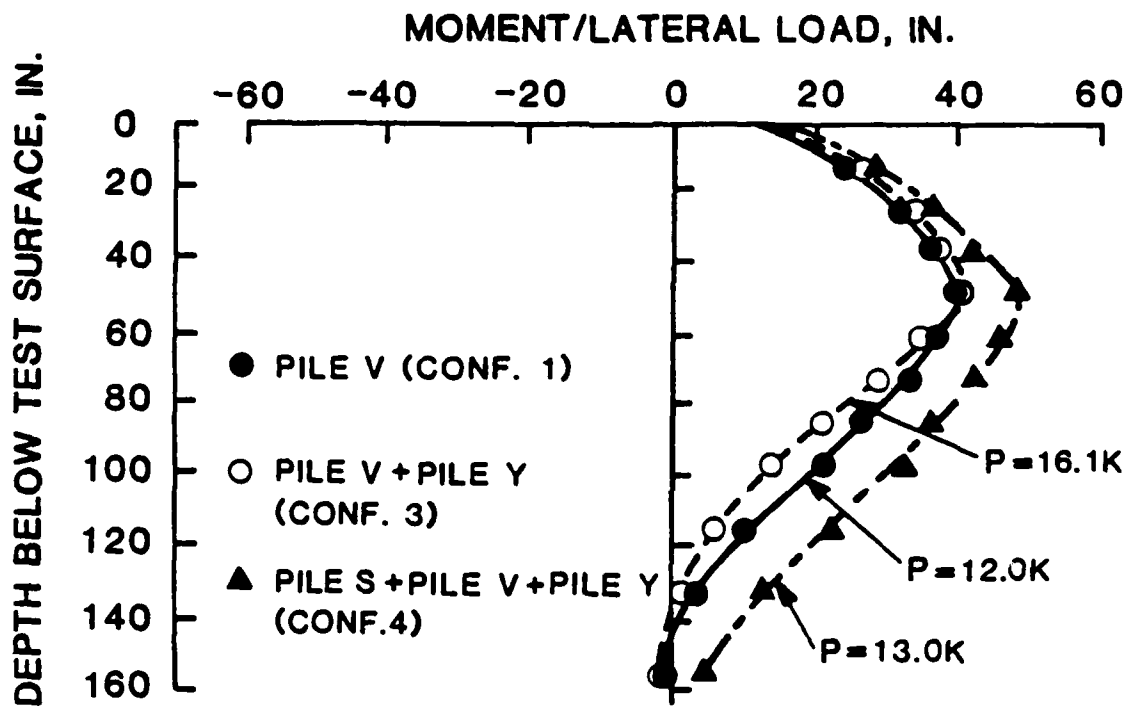
Fig. 5.8.a.   Normalized Bending Moments vs. Depth: Pile V,
Cycle 1, Loading North, Confs. 1, 3 and 4.

131

PILE : V
CYCLE : 1
LOADING : SOUTH
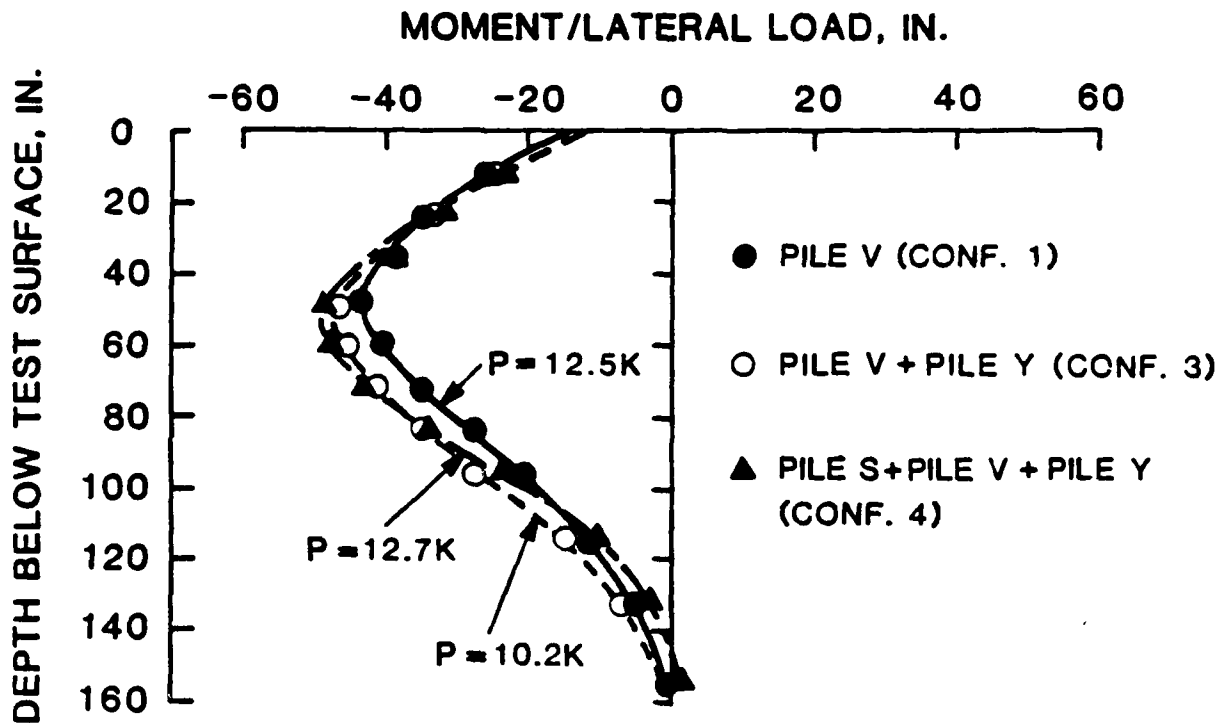
Fig. 5.8.b.   Normalized Bending Moments vs. Depth: Pile V,
Cycle 1, Loading South, Confs. 1, 3 and 4.

132
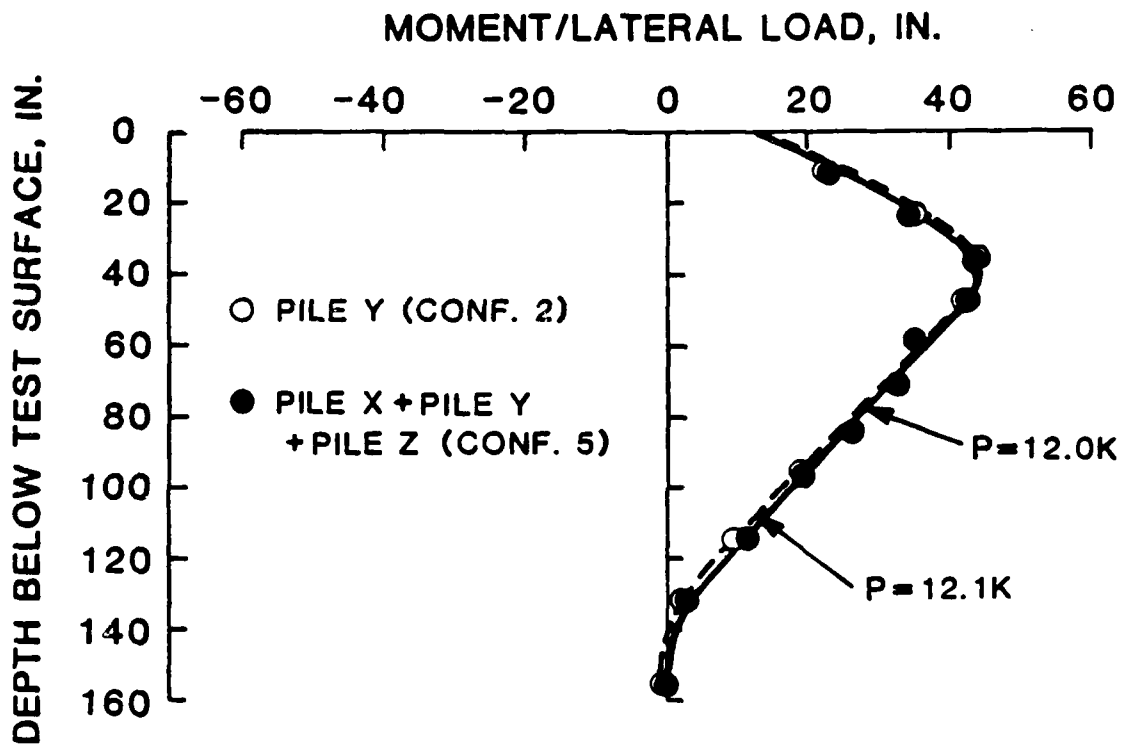
Fig. 5.9.a.   Normalized Bending Moments vs. Depth: Pile Y,
              Cycle 1, Loading North, Confs. 2 and 5.

133

PILE : Y
CYCLE : 1
LOADING : SOUTH
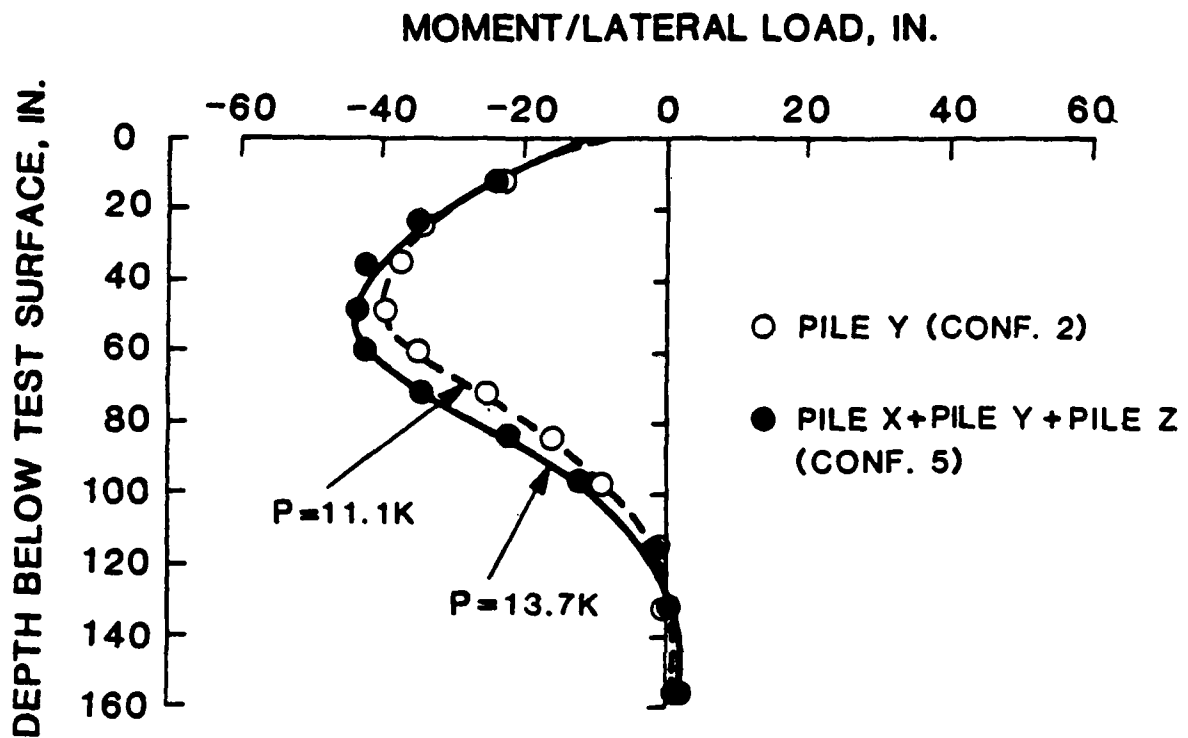
Fig. 5.9.b. Normalized Bending Moments vs. Depth: Pile Y, Cycle 1, Loading South, Confs. 2 and 5.

134

ing south, may have been caused by the confining of the soil mass to the north of the X-Y-Z subgroup due to the presence of the unloaded Piles U, V and W in Conf. 5. However, in either direction the effect of side-by-side loading at $S/D = 3$ is much less than that for in-line loading at $S/D = 3$. This observation is consistent with the relative magnitude of the α factors for side-by-side and in-line modes.

It is also noteworthy that moments were generally unaffected below a depth of 120 in. for side-by-side loading, which indicates that all significant pile-soil-pile interaction occured in the sand, whereas induced moments can be observed below 120 in. for the in-line configuration (Figs. 5.8.a, 5.8.b), indicating the possibility that the clay present below 120 in. may have affected interaction somewhat for in-line loading.

135

CHAPTER VI

SUMMARY AND CONCLUSIONS

6.1. Summary and Conclusions

A series of large-scale lateral load tests was conducted on single piles and groups of two and three vertical (free-head) piles in order to evaluate free-head lateral pile-soil-pile interaction in terms of a pile-head interaction factor known as α. The piles consisted of instrumented 10.75-in. diameter steel pipes, which were initially driven into stiff clay, the upper 10 ft of which was later removed, forming a pit. Poorly graded fine sand was placed in the pit and compacted to a relative density of about 50%. Geotechnical test results obtained from CPT and SPT tests indicated the presence of a dense to very dense sand at the time of the testing for this study, which followed a cyclic lateral load test on the piles as part of a coherent nine-pile group. Densification of the sand was believed due to the cycling effect of the earlier test. Readings for all piles, consisting of pile-head shears, pile-head deflections and bending moments, were taken at load levels of $\pm$ 4, $\pm$ 12 and $\pm$ 20 kips, for Cycles 1, 5, 10, 20, 100, loading north and south; the load was applied one foot above the test surface; the sequence for the pile testing consisted of five

different configurations of loading, providing data for spacings of 3 diam., 6 diam., and greater than 6 diam., for departure angles of 0°, 90°, and 180°. Interaction factors were computed and displayed graphically, using relative flexibilities computed from load-deflection curves generated for each of the loading configurations. Interaction factors between two piles were determined as a function of: (1) pile-head load, (2) number of cycles of load, (3) departure angle (0°, 90°, 180°), and (4) spacing between the two piles (3D, 6D, and 11.2D). Load values were normalized by a load on a single pile that corresponded to a displacement of 5% of a single-pile diameter. Design charts were then developed and presented in two different ways: (1) experimental α's vs. normalized load $(P_j/^S P_{5\%})$, and (2) experimental α's vs. spacing between any two piles in the group. Elastic α's were also included in the former charts for comparison. The nine-pile group behavior (load distribution and group deflection) was then evaluated using the experimental α's developed in this document, for an average load of ± 7 kips per pile, loading in both directions. In order to check the validity of the experimental interaction factors, comparisons were made with results from a lateral load test performed by Morrison (1986) for the same pile group, and with results obtained from an elastic analysis. Comparisons of measured results and behavior predicted by the experimental α factors indicated good or conservative correlations, for Cycles 1 and 100, loading to the south. Rotations

137

in the loading frame during the nine-pile group test and imperfect positioning of piles in the leading row when the group was loaded to the north may have caused the higher differences in predicted and measured behavior. Elastic solutions showed a different pattern of behavior, in which the group deflections were predicted relatively accurately but in which equal loads were taken by the front and third rows, and much lower loads were taken by the middle row, a pattern dissimilar to the observations in the nine-pile test.

A preliminary step-by-step design procedure for evaluation of free-head pile groups was suggested. A prelimary study of induced bending moments was performed, indicating that, similar to the effect on α factors, the effect of group action on bending moments was different when a pile in a group was acting as a leading or trailing pile or was side-by-side with adjacent loaded piles.

It is concluded that the experimentally determined α factors and the related preliminary design method can provide reasonable predictions of displacement and distribution of shear loads among pinned- or free-head vertical piles arranged in pile groups in medium to very dense submerged sand. These factors appear appropriate for piles with elastic relative stiffness (K_r, defined in Fig. 1.2, with $L = L_c$ defined in Fig. 1.3) values of about 0.1 (the values for the test piles). With regard to shear in the most heavily loaded piles, the design method was found to be accurate to conservative.

6.2. Recommendations for Further Study

The experimental interaction factors for lateral displacement under horizontal load vectors were evaluated for one particular case: free-(pinned-)head vertical piles embedded in medium to dense submerged sand. In order to develop a better understanding of lateral group action in general, it will be desirable to develop similar experimental interaction factors for other conditions of loading (e.g., applied rotation only), fixity (fixed-head piles), soil types (loose sand, soft and stiff clays), and pile types (other relative stiffness values and pile cross sections). It is advisable that such experimentally developed factors be calibrated by conducting parallel tests on larger groups, as was done in this study. Since such comprehensive experiments would be expensive to conduct at full scale, it is suggested that they be conducted either in a centrifuge or in a soil pressure chamber that can replicate in-situ stress conditions, with a few field-scale verifications. It is also recommended that further study of the effects of group action on bending moments be conducted for the conditions different from those considered here.

REFERENCES

1. Blaney, G. W., "Lateral Response of a Single Pile in Overconsolidated Clay to Relatively Low Frequency Harmonic Pile-Head Loads and Harmonic Ground Surface Loads," Unpublished dissertation presented to The University of Houston - University Park in partial fulfillment of the requirements for the degree of Doctor of Philosophy, December 1983.

2. Brooker, E. W., and Ireland, H. O., "Earth Pressures at Rest Related to Stress History," Canadian Geotechnical Journal, Vol. 2, No. 1, February 1965, p. 14.

3. Brown, D. A., and Reese, L. C., "Behavior of a Large-Scale Pile Group Subjected to Cyclic Lateral Loading," Geothecnical Engineering Report GR85-12, The University of Texas at Austin, Austin, Texas, May 1985.

4. Butterfield, R., and Douglas, R. A., "Flexibility Coefficients for the Design of Piles and Pile Groups," Construction Industry Research and Information Association Technical Note 108, London, 1981.

5. Cox, W. R., Dixon, D. A., and Murphy, B. S., "Lateral-Load Tests on 25.4-mm (1-in.) Diameter Piles in Very Soft Clay in Side-by-Side and In-Line Groups," ASTM STP 835, American Society for Testing and Materials, Philadelphia, Pa, 1984, pp. 122-139.

6. Holloway, D. M., Moriwaki, Y., Finno, R. J., and Green, R. K., "Lateral Load Response of a Pile Group in Sand," Proceedings, Second International Conference on Numerical Methods in Offshore Piling, I.C.E., 1982.

7. Mahar, L. J., and O'Neill, M. W., "Geotechnical Characterization of Desiccated Clay," Journal of Geotechnical Engineering, ASCE, Vol. 108, No. GT11, January 1983, pp. 56-71.

8. Morrison, C., "A Lateral Load Test of a Full-Scale Pile Group in Sand," M.S.C.E. Thesis, Deparment of Civil Engineering, The University of Texas at Austin, December 1986.

9. O'Neill, M.W., "Group Action in Offshore Piles," Proceedings, Geothecnical Practice in Offshore Engineering, ASCE, 1983, pp. 25-64.

10. O'Neill, M. W., Hawkins, R. A., and Audibert, J. M. E., "Installation of Pile Group in Overconsolidated Clay," Journal of the Geotechnical Engineering Division, ASCE, Vol. 108, No. GT11, November 1982, pp. 1369-1386.

11. O'Neill, M. W., and Hawkins, R. A., "Pile-head Behavior of Rigidly Capped Pile Group," Transportation Research Record 884, Transportation Research Board, Washington, D.C., 1982, pp. 1-7.

12. O'Neill, M. W., and Dunnavant, T. W., "A Study of the Effects of Scale, Velocity, and Cyclic Degradability on Laterally Loaded Single Piles in Overconsolidated Clay," Report No. UHCE 84-7, Department of Civil Engineering, University of Houston - University Park, October 1984.

13. Peck, R. B., Hanson, W. E., and Thornburn, T. H., Foundation Engineering, 2nd Edition, John Wiley and Sons, New York, 1974, p. 310.

14. Poulos, H. G., "Behavior of Laterally Loaded Piles: II- Pile Groups," Journal of the Soil Mechanics and Foundations Division, ASCE, Vol. 97, No. SM5, May 1971, pp. 733-751.

15. Poulos, H. G., and Davis, E. H., Pile Foundation Analysis and Design, John Wiley and Sons, New York, 1980.

16. Prakash, S., Soil Dynamics, McGraw-Hill Book Company, New York, 1981, p. 129.

17. Randolph, M. F., and Poulos, H. G., "Estimating the Flexibility of Offshore Pile Groups," Proceedings, Second International Conference on Numerical Methods in Offshore Piling, I.C.E., 1982, pp. 313-328.

18. Schmertmann, J. H., "Measurements of In-Situ Shear Strength," Proceedings, Specialty Conference on In-Situ Measurements of Soil Properties, A.S.C.E., Raleigh, N.C., Vol. 2, June 1975, pp. 79-99.

APPENDIX A

PILE-HEAD LOAD-DEFLECTION RELATIONSHIPS

Table A.1. Configurations

CONFIGURATION	LOAD
1	Pile V
2	Pile Y
3	Piles V and Y
4	Piles S, V, and Y
5	Piles X, Y, and Z

Table A.2. Load Points with Respect to Ground Level

PILE	DISTANCE ABOVE GROUND LEVEL (in.)
S	12.3
V	12.8
X	12.0
Y	12.2
Z	12.4

A3

EFFECT OF j
ON i, $\xi = 0°$

EFFECT OF i
ON j, $\xi = 180°$

EFFECT OF i
ON j, $\xi = 90°$
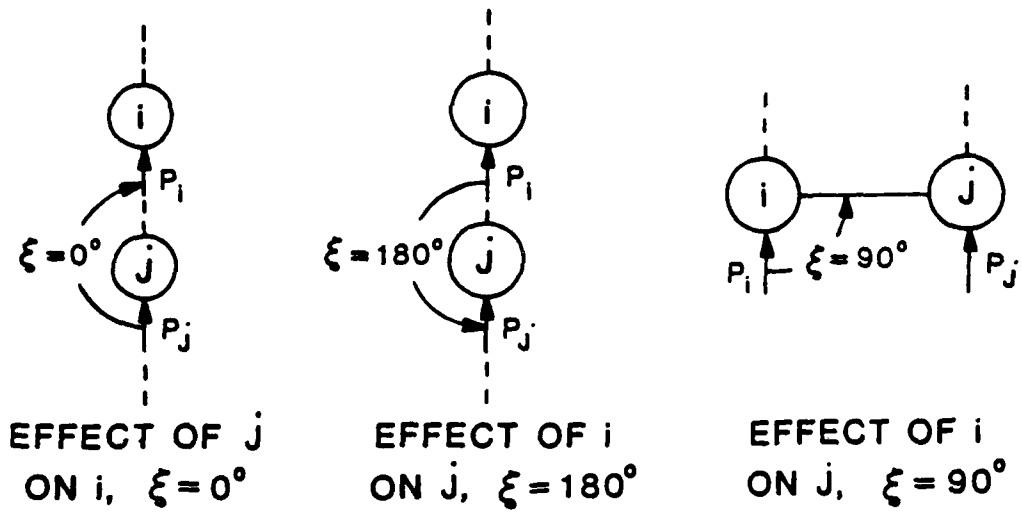
Fig. A.1.a. Definition of ξ.

2-WAY
CYCLING

N
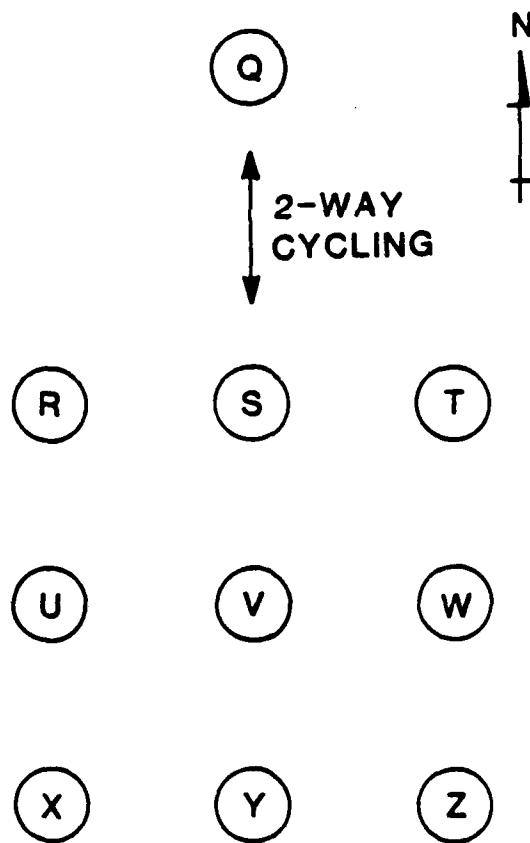
Fig. A.1.b. Group Layout Notation.

A4

CONFIGURATION: 1 or 2   PILE V ▲
PILE: V or Y   PILE Y +
CYCLE: 1
LOADING: NORTH

$$f_{yy} = f_{vv} = \frac{0.22}{10} = 0.022 \text{ in./k}$$
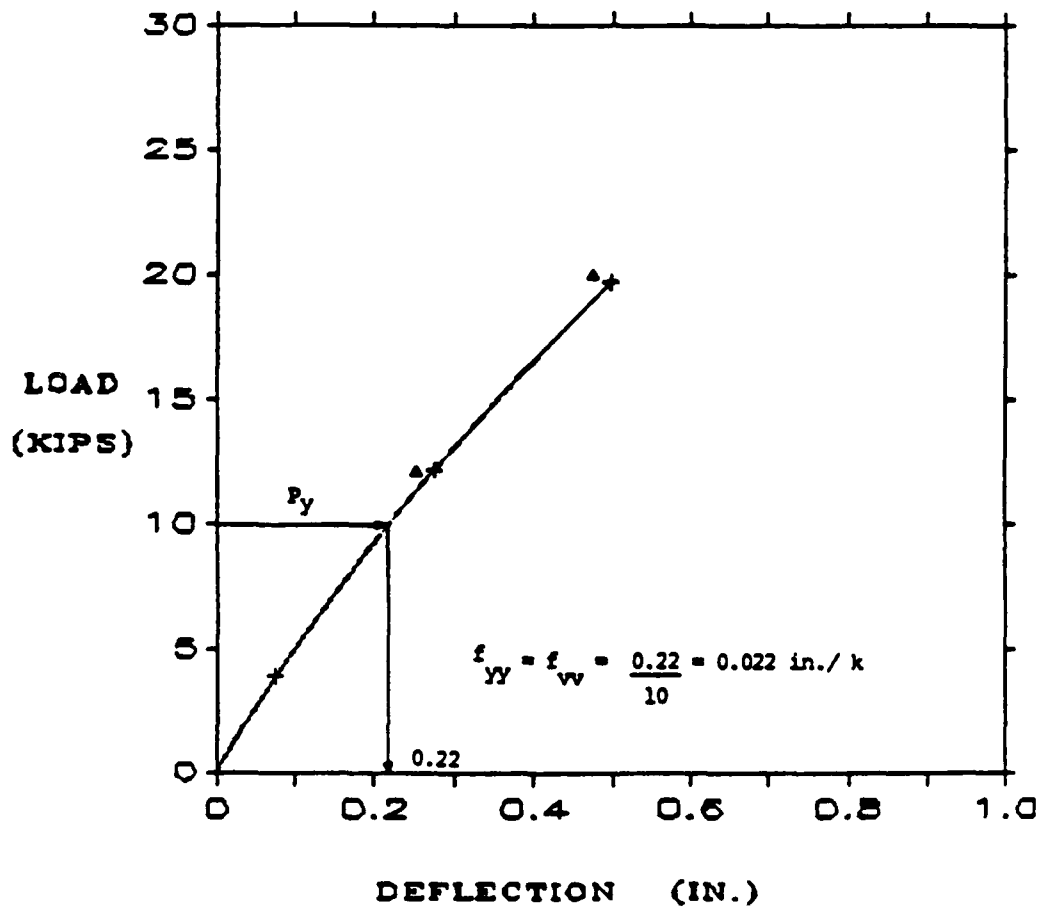
Fig. A.2. Pile-Head Load vs. Deflection, Conf. 1 and 2,
           Cycle 1, Loading North.

A5

CONFIGURATION: 1 or 2   PILE V △
PILE: V or Y   PILE Y +
CYCLE: 20
LOADING: NORTH
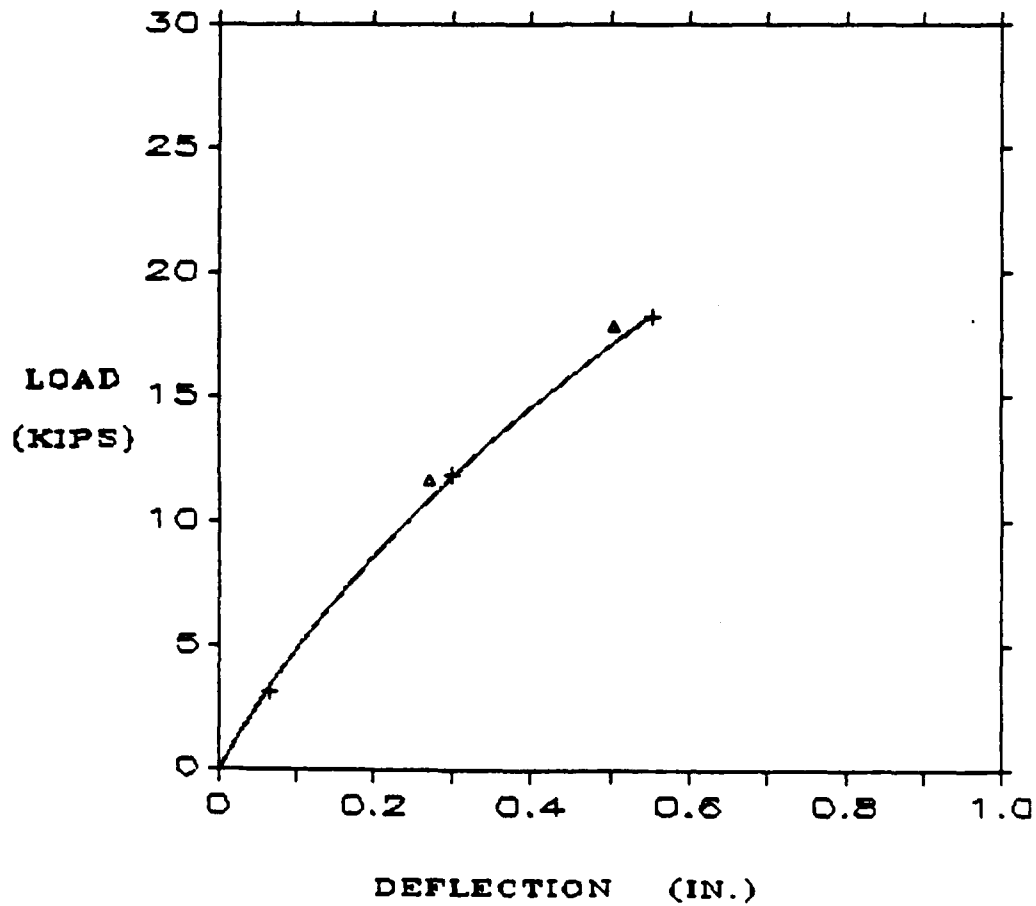
Fig. A.3.   Pile-Head Load vs. Deflection, Conf. 1 and 2,
Cycle 20, Loading North.

CONFIGURATION: 1 or 2   PILE V △
PILE: V or Y   PILE Y +
CYCLE: 100
LOADING: NORTH

Fig. A.4.   Pile-Head Load vs. Deflection, Conf. 1 and 2,
            Cycle 100, Loading North.

A7

CONFIGURATION: 1 or 2   PILE V △
PILE: V or Y   PILE Y +
CYCLE: 1
LOADING: SOUTH

$f_{yy} = f_{vv} = \dfrac{0.215}{10} = 0.0215$ in./ k
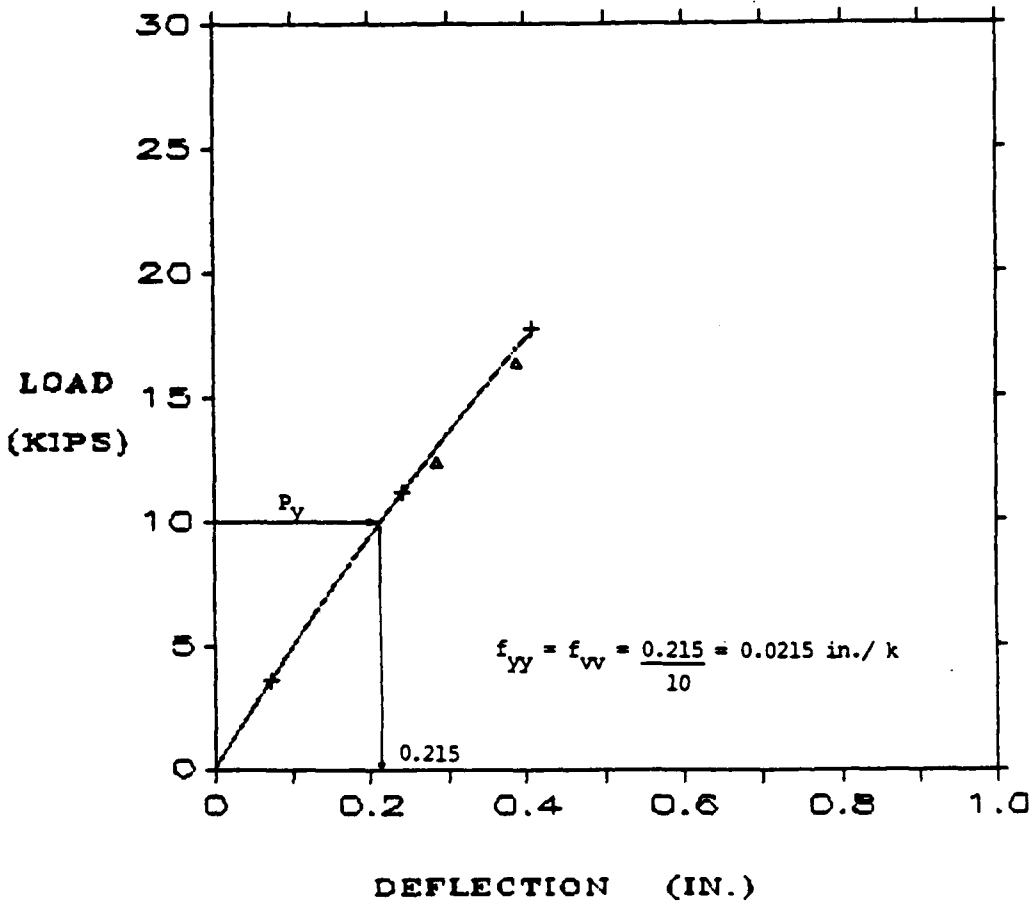
Fig. A.5.   Pile-Head Load vs. Deflection, Conf. 1 and 2,
            Cycle 1, Loading South.

A8

CONFIGURATION: 1 or 2   PILE V △
PILE: V or Y   PILE Y +
CYCLE: 20
LOADING: SOUTH
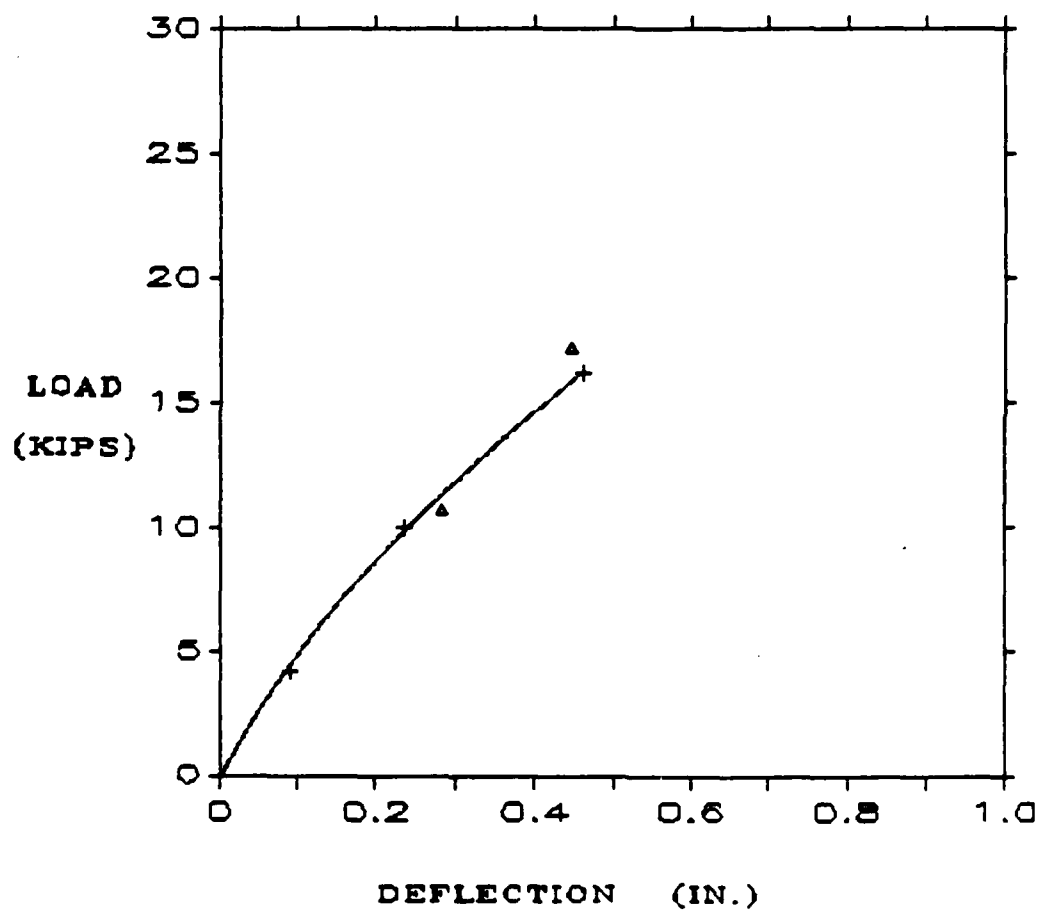
Fig. A.6. Pile-Head Load vs. Deflection, Conf. 1 and 2,
          Cycle 20, Loading South.
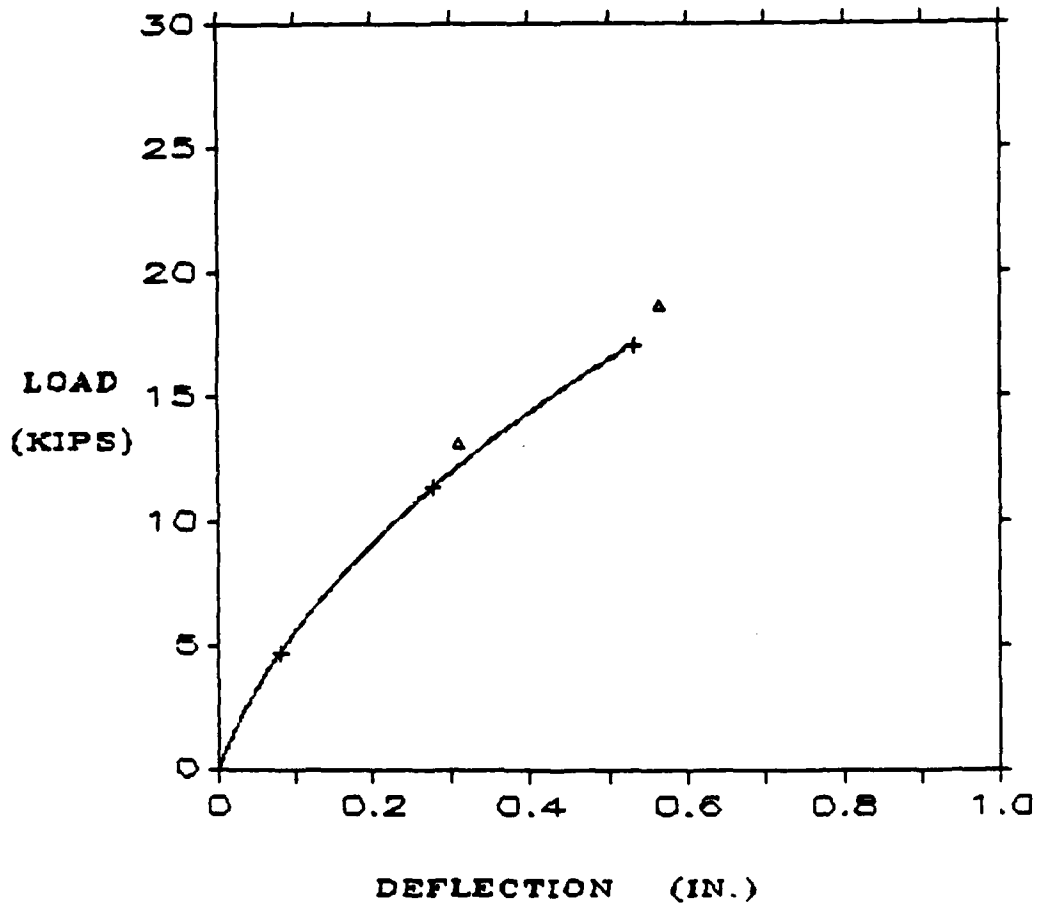
A9

CONFIGURATION: 1 or 2   PILE V △
PILE: V or Y   PILE Y +
CYCLE: 100
LOADING: SOUTH

Fig. A.7. Pile-Head Load vs. Deflection, Conf. 1 and 2,
Cycle 100, Loading South.

A10

CONFIGURATION: 3   Pv vs. Dv   +
PILES: V,Y   Py vs. Dv   O
CYCLE: 1
LOADING: NORTH, ξ= 0

P_y

$P_y = 6.0^k$

$f_{vy} = \dfrac{0.26 - 0.22}{6.0} = 0.0067$ in. / k

$\alpha_{vy} = \dfrac{0.0067}{0.022} = 0.30$

0.26

LOAD (KIPS)
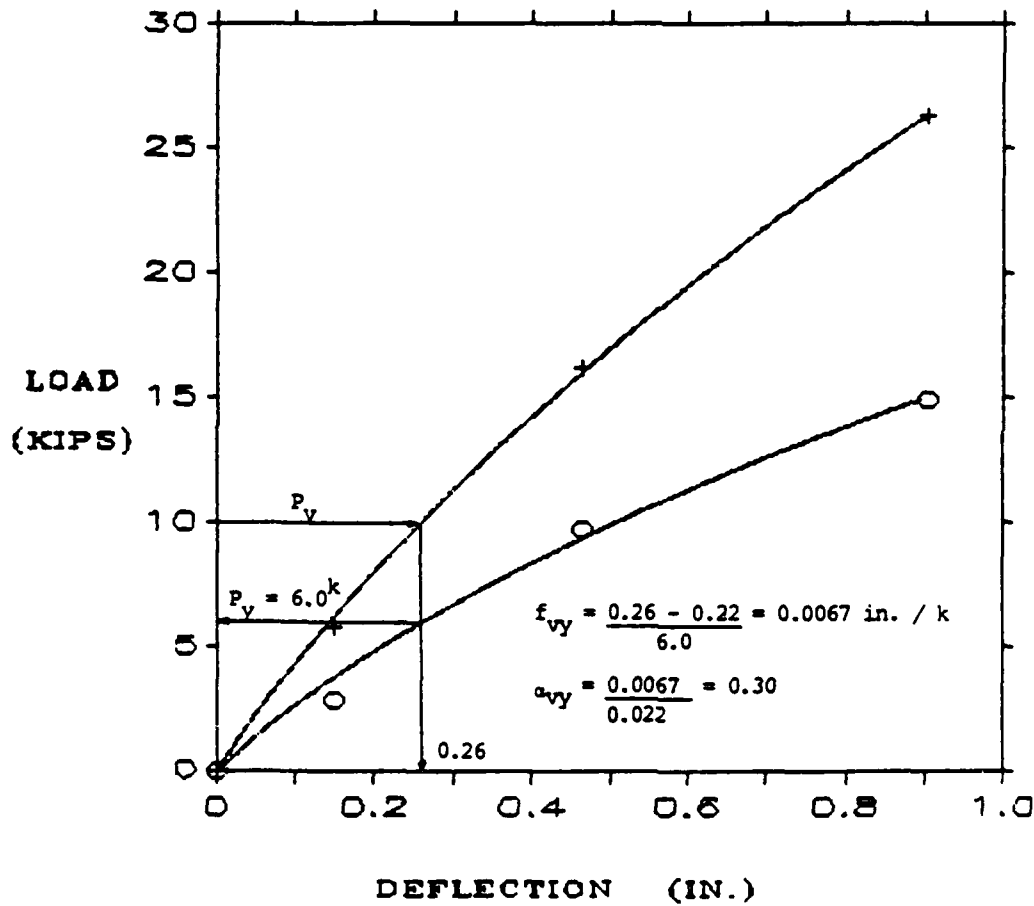
DEFLECTION   (IN.)

Fig. A.8.   Pile-Head Load vs. Deflection, Conf. 3,
            Cycle 1, Loading North, ξ = 0°.

A11

CONFIGURATION: 3   Fv vs. Dv   +
PILES: V,Y   Fy vs. Dv   O
CYCLE: 20
LOADING: NORTH.   ɟ= 0
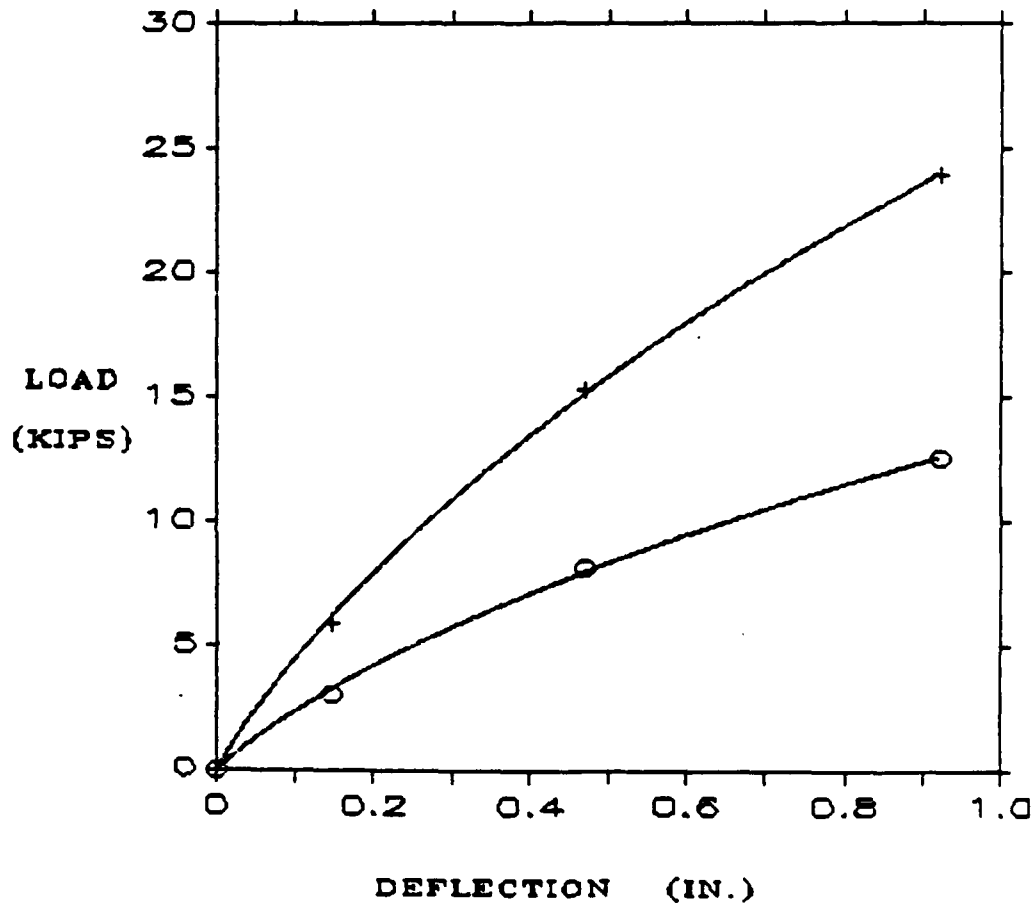
Fig. A.9.   Pile-Head Load vs. Deflection, Conf. 3,
            Cycle 20, Loading North, ξ = 0°.

A12

CONFIGURATION: 3   Pv vs. Dv +
PILES: V,Y   Py vs. Dv ○
CYCLE: 100
LOADING: NORTH, ξ=0
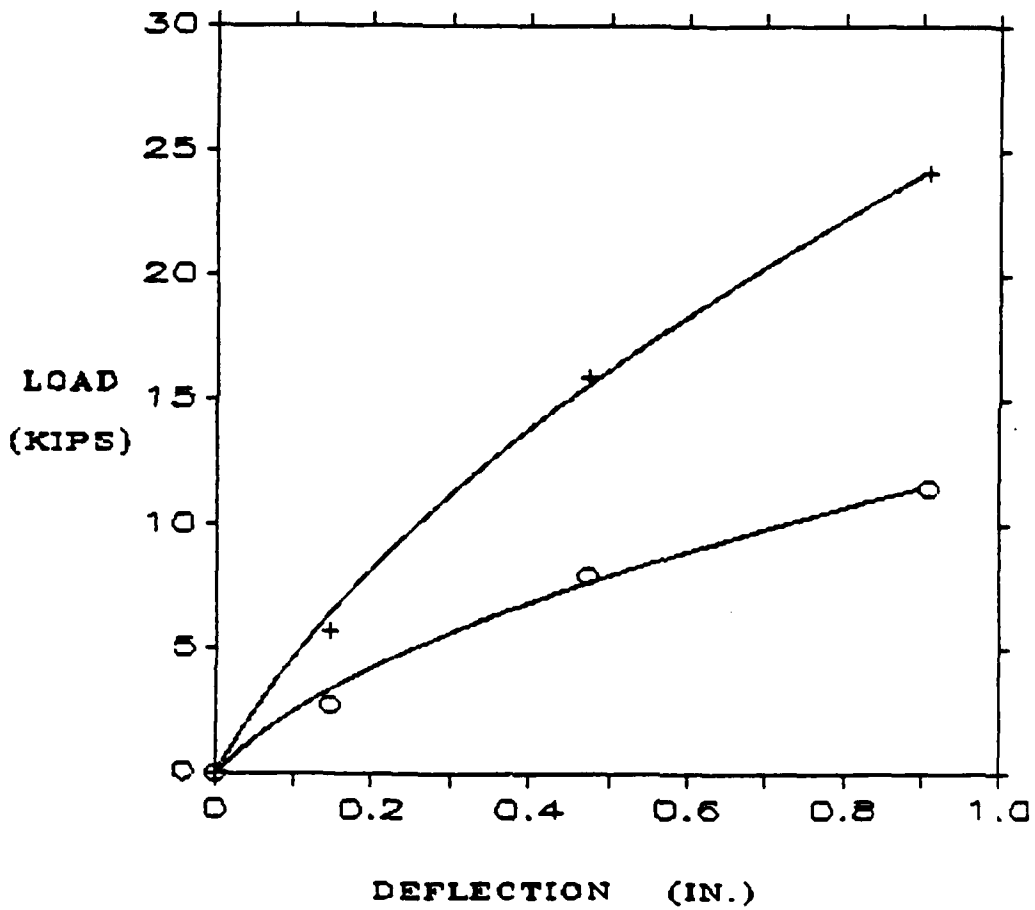
Fig. A.10.   Pile-Head Load vs. Deflection, Conf. 3,
             Cycle 100, Loading North, ξ = 0°.

A13

CONFIGURATION: 3   Py vs. Dy +
PILES: V,Y   Pv vs. Dy O
CYCLE: 1
LOADING: SOUTH. ξ=0
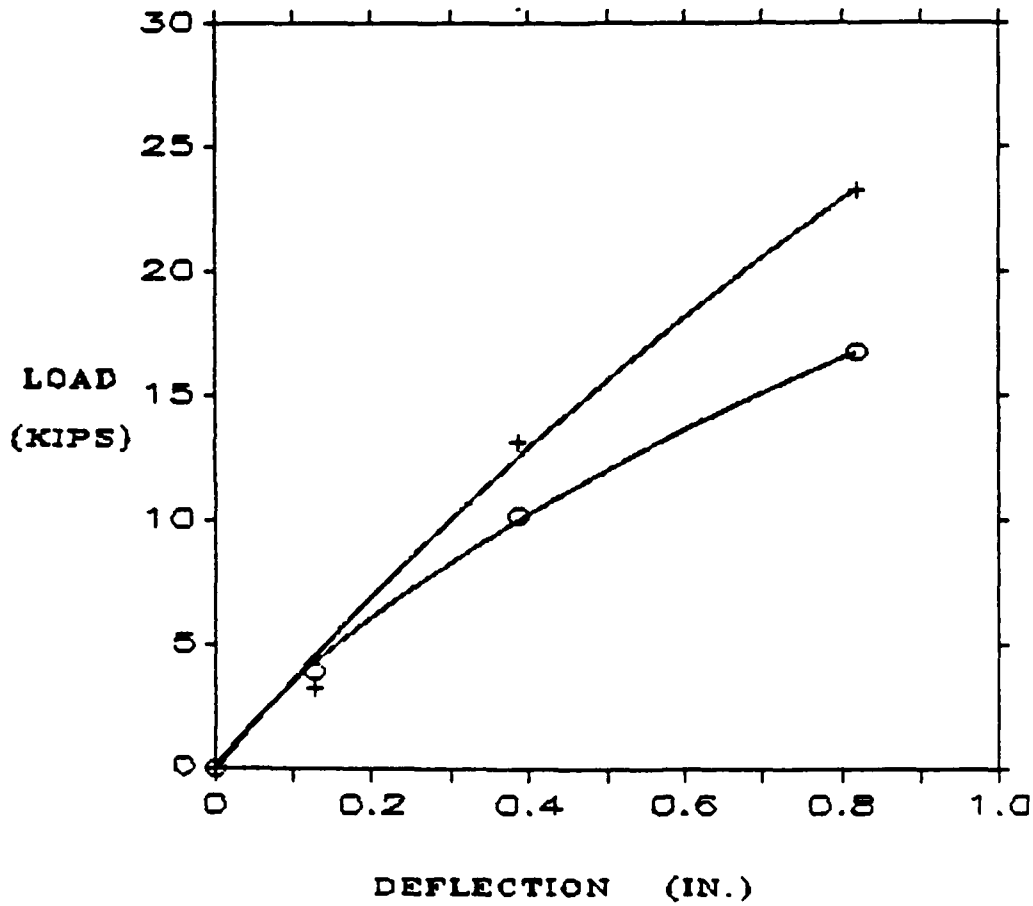
Fig. A.11.   Pile-Head Load vs. Deflection, Conf. 3,
             Cycle 1, Loading South, ξ = 0°.

A14

CONFIGURATION: 3   Py vs. Dy +
PILES: V,Y   Pv vs. Dy O
CYCLE: 20
LOADING: SOUTH, ƒ=0
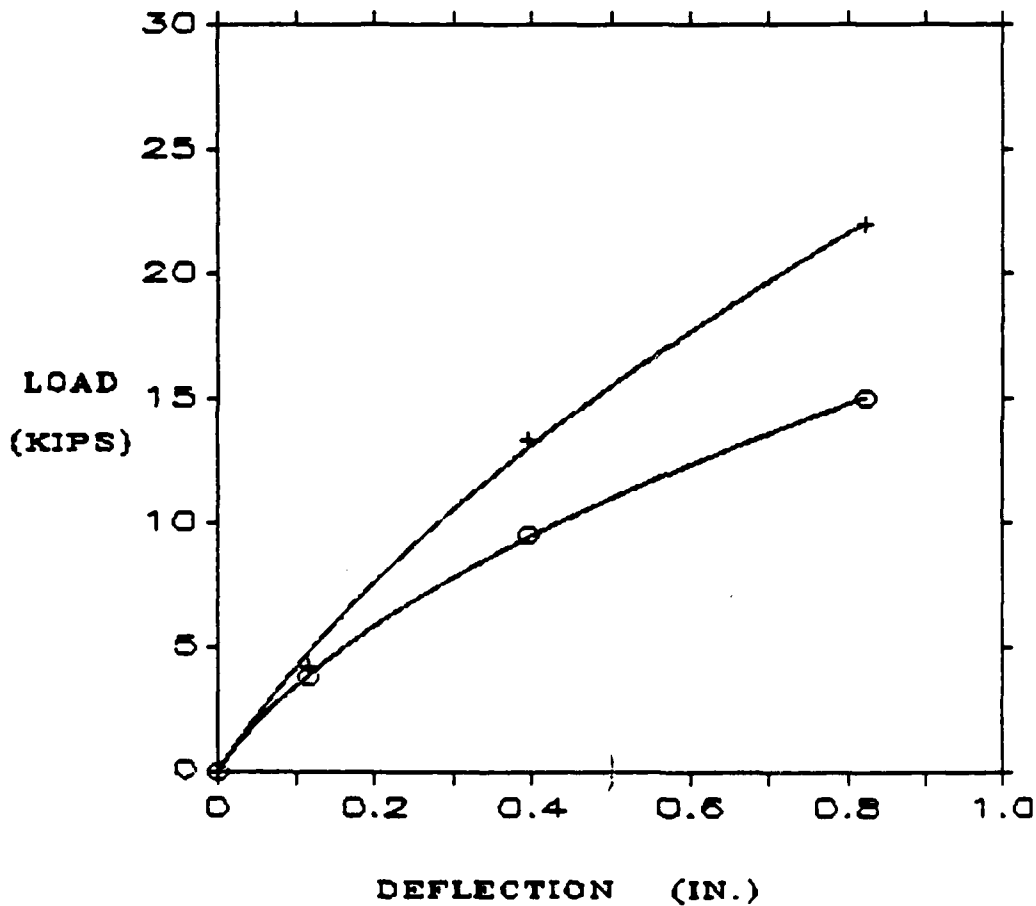
Fig. A.12.   Pile-Head Load vs. Deflection, Conf. 3,
             Cycle 20, Loading South, x = 0°.

CONFIGURATION: 3   Py vs. Dy +
PILES: V,Y   Pv vs. Dy O
CYCLE: 100
LOADING: SOUTH. ↑=0
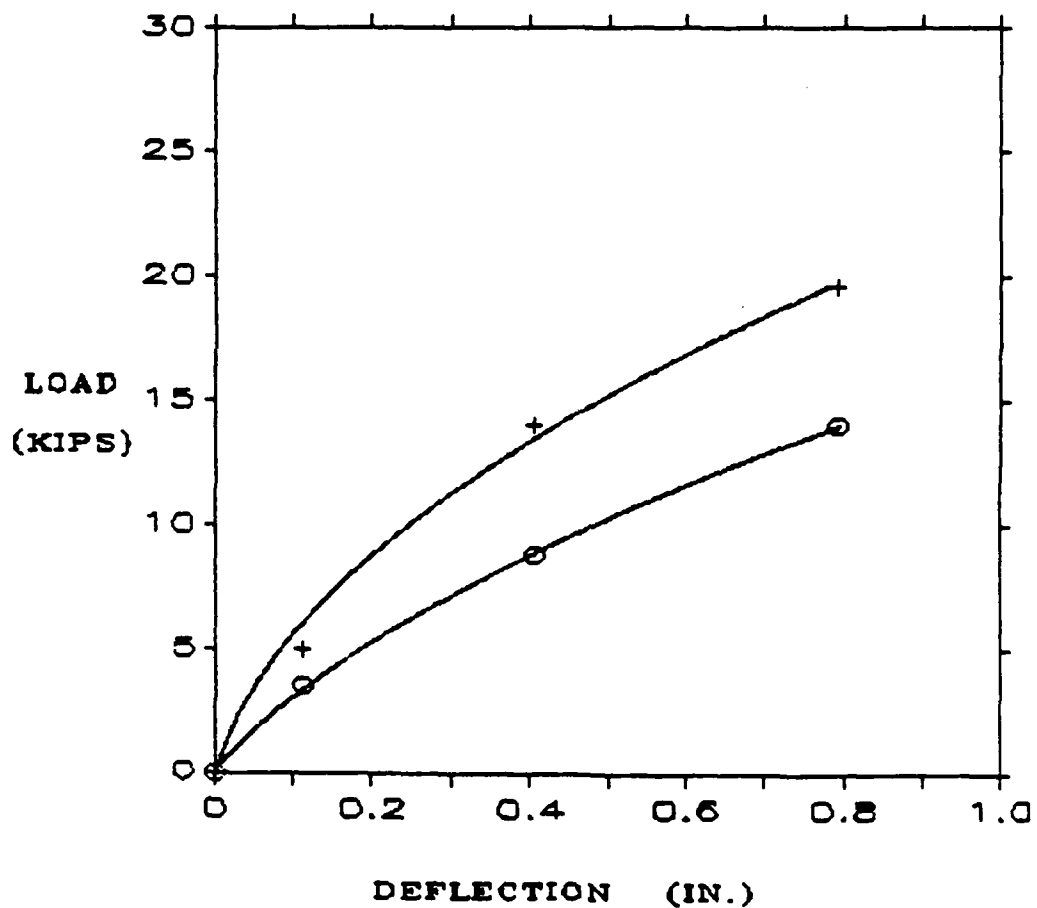
Fig. A.13.   Pile-Head Load vs. Deflection, Conf. 3,
             Cycle 100, Loading South, ξ = 0°.

A16

CONFIGURATION: 3   Pv vs. Dv +
PILES: V,Y   Py vs. Dv O
CYCLE: 1
LOADING: SOUTH. ξ= 180

Fig. A.14. Pile-Head Load vs. Deflection, Conf. 3,
            Cycle 1, Loading South, ξ = 180°.

A17

CONFIGURATION: 3   Pv vs. Dv +
PILES: V,Y   Py vs. Dv O
CYCLE: 20
LOADING: SOUTH. ξ=180

Fig. A.15.   Pile-Head Load vs. Deflection, Conf. 3,
             Cycle 20, Loading South, ξ = 180°.

A18

CONFIGURATION: 3   Pv vs. Dv +
PILES: V,Y   Py vs. Dv O
CYCLE: 100
LOADING: SOUTH.   ξ=180
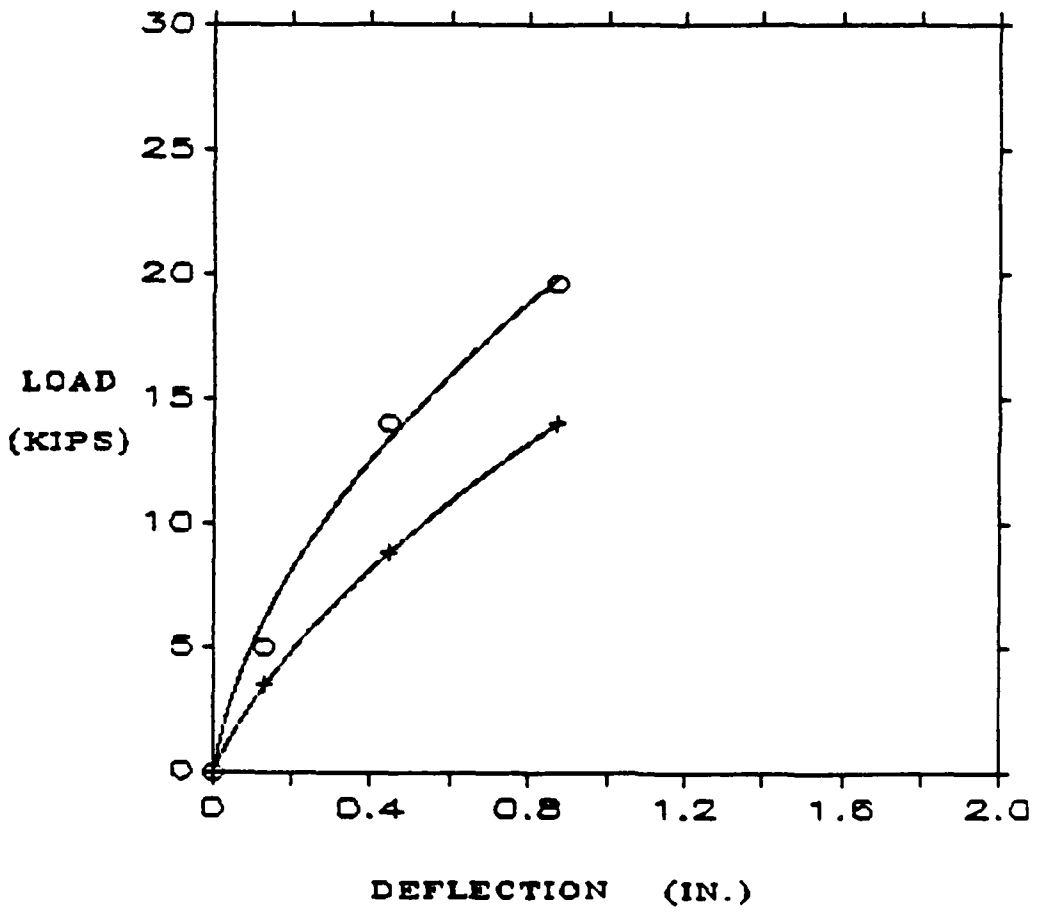
Fig. A.16. Pile-Head Load vs. Deflection, Conf. 3,
            Cycle 100, Loading South, ξ = 180°.

A19

CONFIGURATION: 3   Py vs. Dy   +
PILES: V,Y   Pv vs. Dy   O
CYCLE: 1
LOADING: NORTH.   φ=180
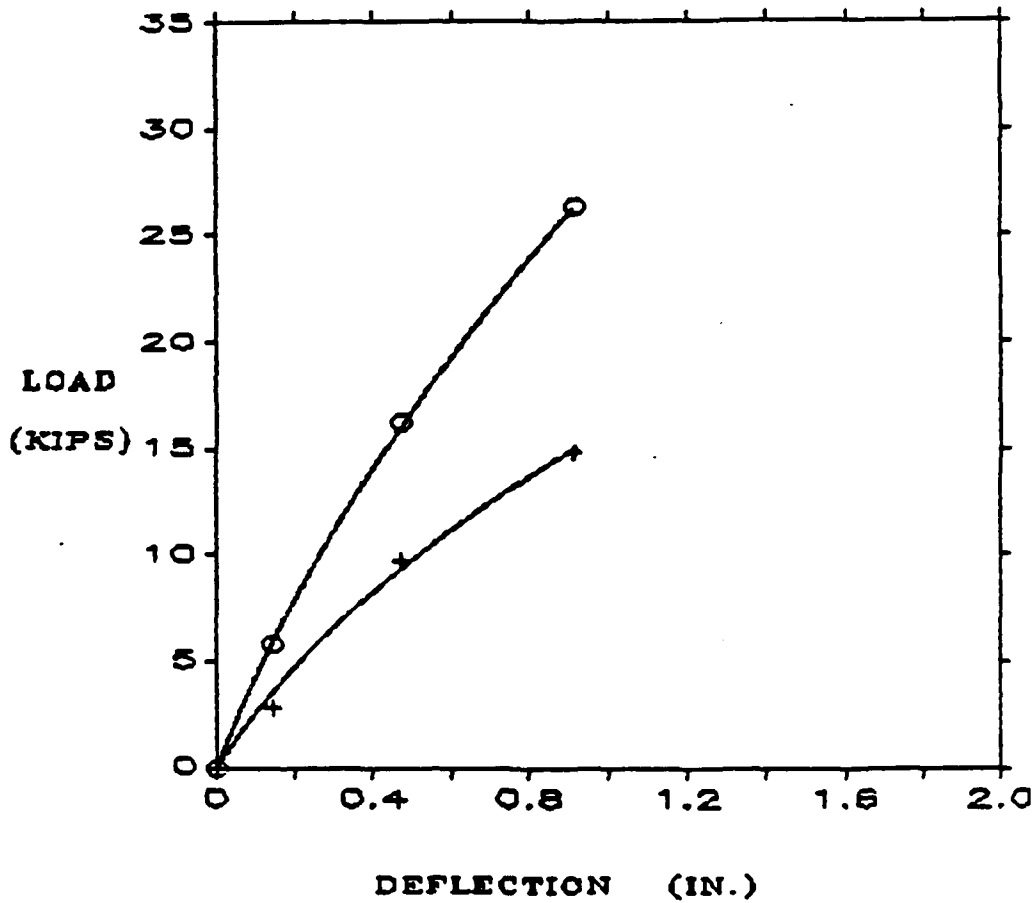
Fig. A.17.   Pile-Head Load vs. Deflection, Conf. 3,
              Cycle 1, Loading North, ξ = 180°.

A20

CONFIGURATION: 3   Py vs. Dy   +
PILES: V,Y   Pv vs. Dy   O
CYCLE: 20
LOADING: NORTH.   ƒ=180
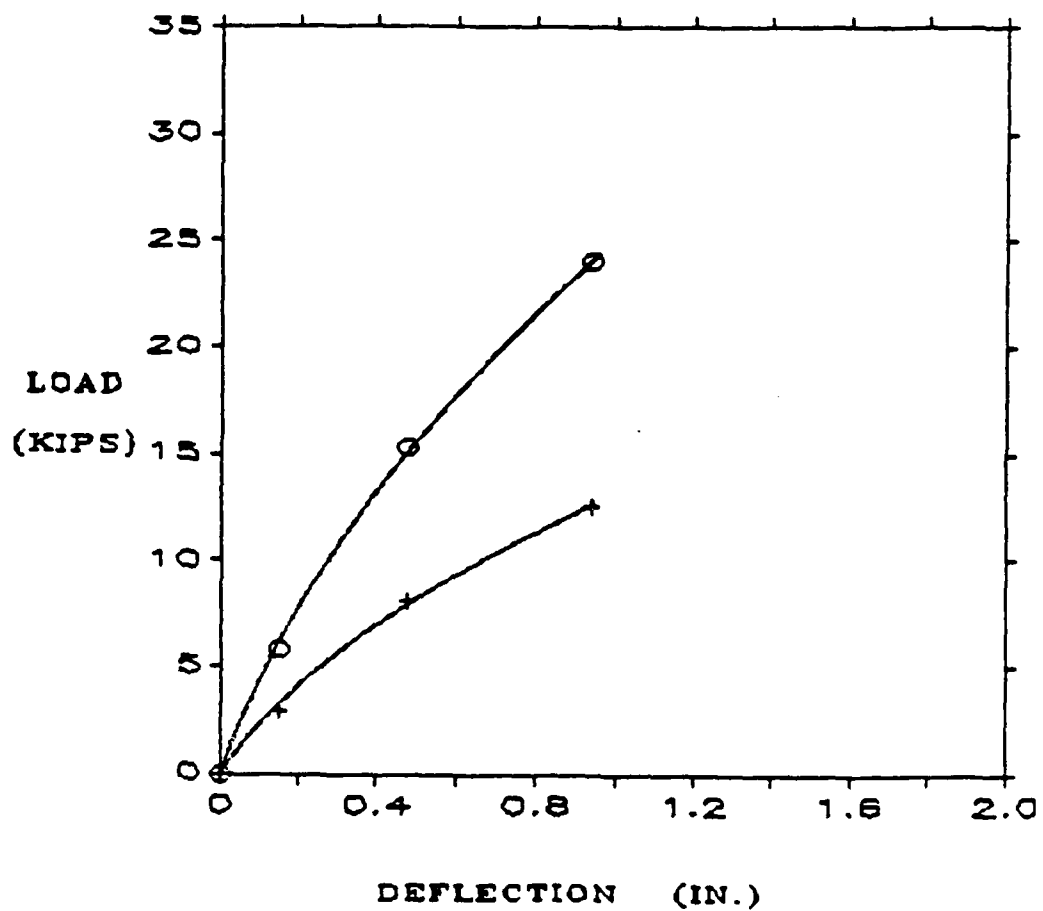
Fig. A.18. Pile-Head Load vs. Deflection, Conf. 3,
            Cycle 20, Loading North, ξ = 180°.

A21

CONFIGURATION: 3 **Py vs. Dy** +
PILES: V,Y **Pv vs. Dy** O
CYCLE: 100
LOADING: NORTH. **ξ=180**

Fig. A.19. Pile-Head Load vs. Deflection, Conf. 3,
     Cycle 100, Loading North, ξ = 180°.

A22

CONFIGURATION: 4   Ps vs. Ds +
PILES: S,V,Y   Pv vs. Ds ×
CYCLE: 1   Py vs. Ds ○
LOADING: NORTH. ξ= 0

$f_{sy} = \dfrac{0.38 - 0.22 - 9.0 \times 0.0084^{*}}{7.0} = 0.012$ in./k

$a_{sy} = \dfrac{0.012}{0.022} = 0.54$

* from 2-pile group analysis (S/D = 3)

Fig. A.20.   Pile-Head Load vs. Deflection, Conf. 4,
             Cycle 1, Loading North, ξ = 0°.

A23

CONFIGURATION: 4   Ps vs. Ds +
PILES: S,V,Y   Pv vs. Ds ✕
CYCLE: 20   Py vs. Ds ◯
LOADING: NORTH, *= 0

Fig. A.21.   Pile-Head Load vs. Deflection, Conf. 4,
             Cycle 20, Loading North, ξ = 0°.

A24
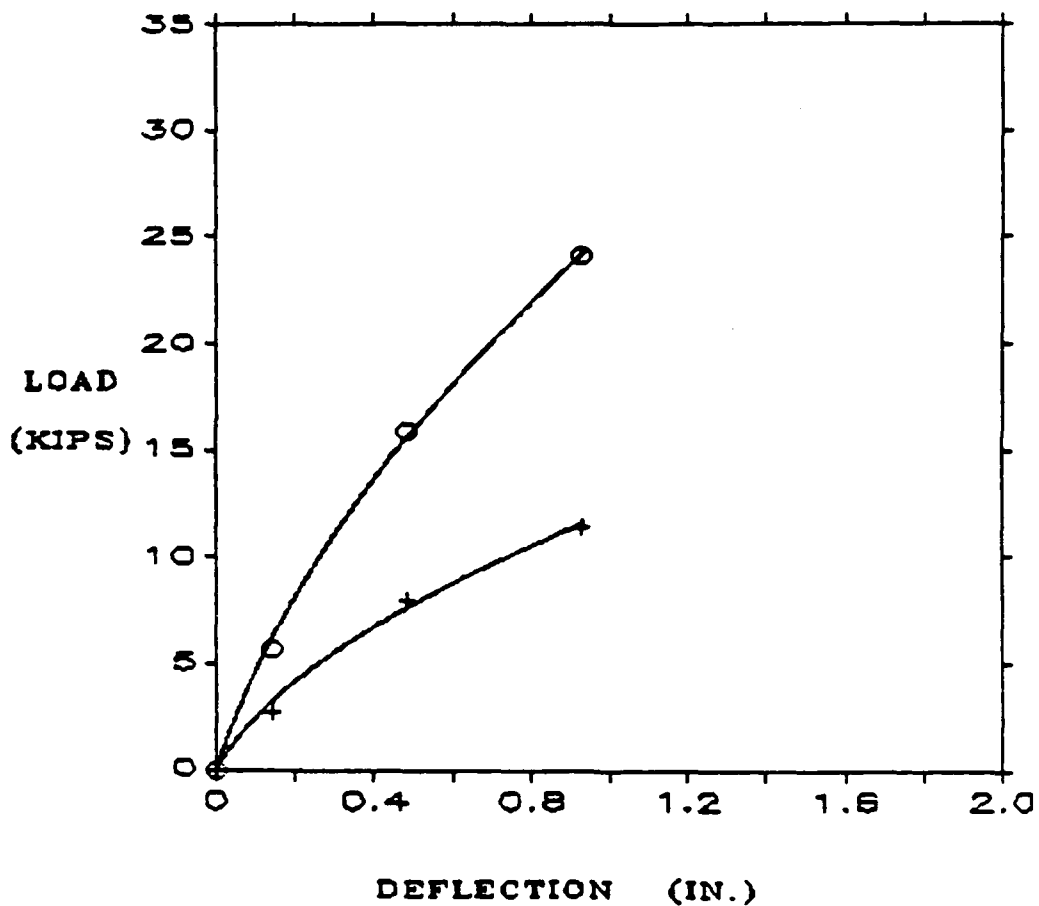
CONFIGURATION: 4

PILES: S,V,Y

CYCLE: 100

LOADING: NORTH, *ξ* = 0

Ps vs. Ds +

Pv vs. Ds X

Py vs. Ds O
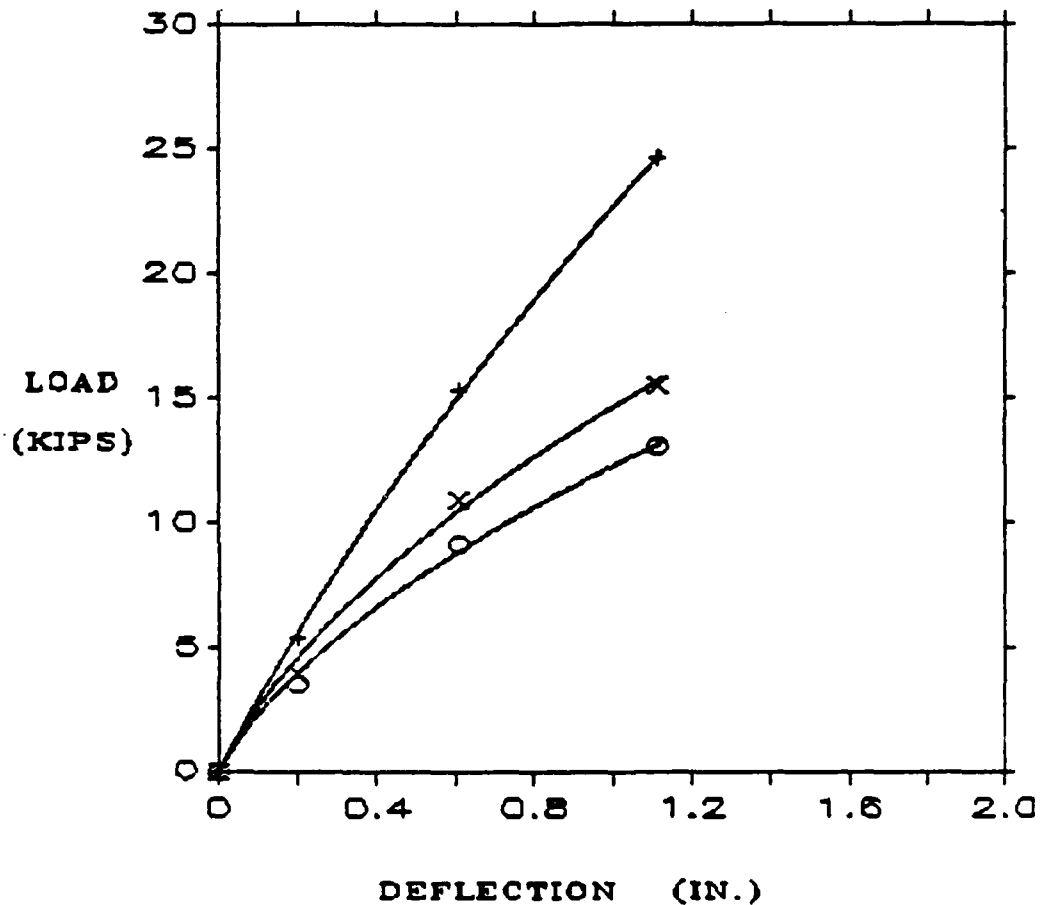
Fig. A.22. Pile-Head Load vs. Deflection, Conf. 4,
            Cycle 100, Loading North, ξ = 0°.

A25

CONFIGURATION: 4   Py vs. Dy   +
PILES: S,V,Y   Pv vs. Dy   X
CYCLE: 1   Ps vs. Dy   O
LOADING: SOUTH, ξ= 0

Fig. A.23.   Pile-Head Load vs. Deflection, Conf. 4,
   Cycle 1, Loading South, ξ = 0°.

A26
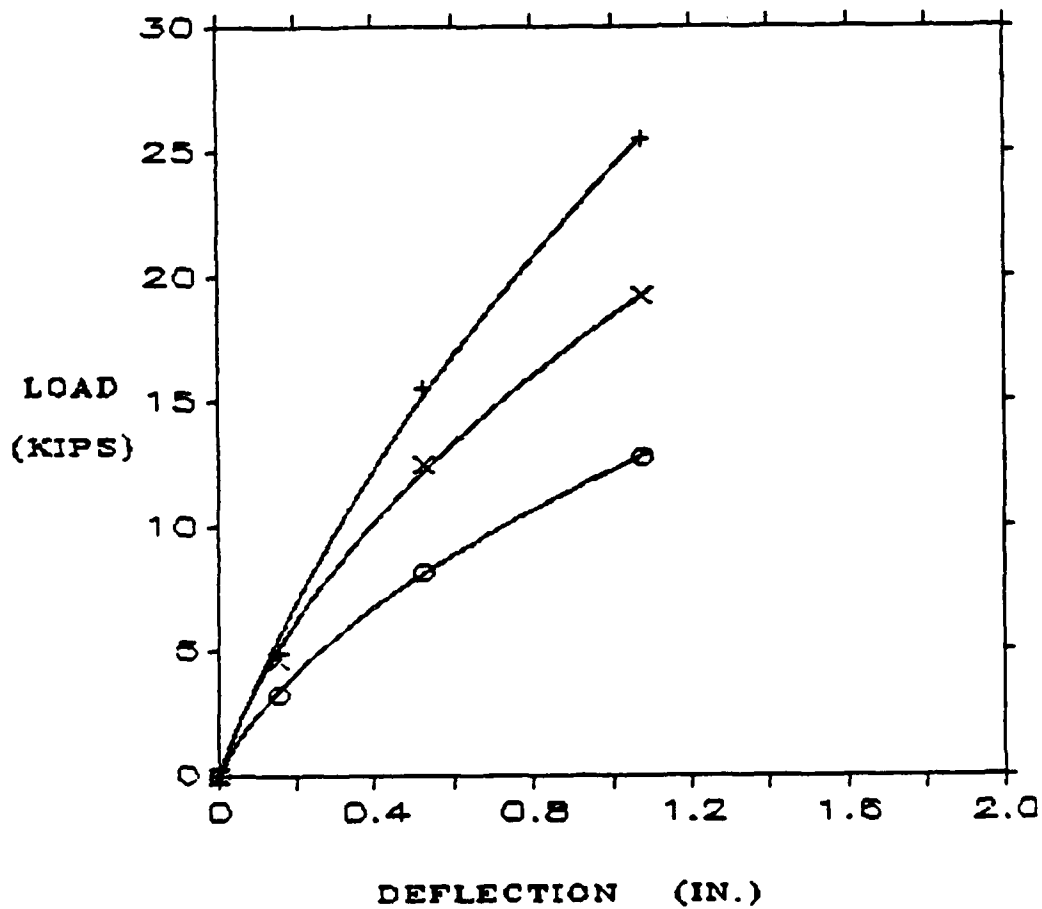
Fig. A.24. Pile-Head Load vs. Deflection, Conf. 4,
            Cycle 20, Loading South, ξ = 0°.

A27

CONFIGURATION: 4   Py vs. Dy +
PILES: S,V,Y   Pv vs. Dy ✕
CYCLE: 100   Ps vs. Dy ○
LOADING: SOUTH, ξ= 0

Fig. A.25. Pile-Head Load vs. Deflection, Conf. 4,
Cycle 100, Loading South, ξ = 0°.

A28

CONFIGURATION: 4   Ps vs. Ds +
PILES: S,V,Y   Pv vs. Ds X
CYCLE: 1   Py vs. Ds O
LOADING: SOUTH. ξ= 180

$P_y = 17.3^k$

$P_v = 13.8^k$

P_s

$f_{sy} = \dfrac{0.63 - 0.215 - 13.8 \times 0.018^*}{17.3} = 0.0096 \ in./k$

$\alpha_{sy} = \dfrac{0.0096}{0.0215} = 0.44$

0.63

* from 2-pile group analysis (S/D = 3)

LOAD (KIPS)
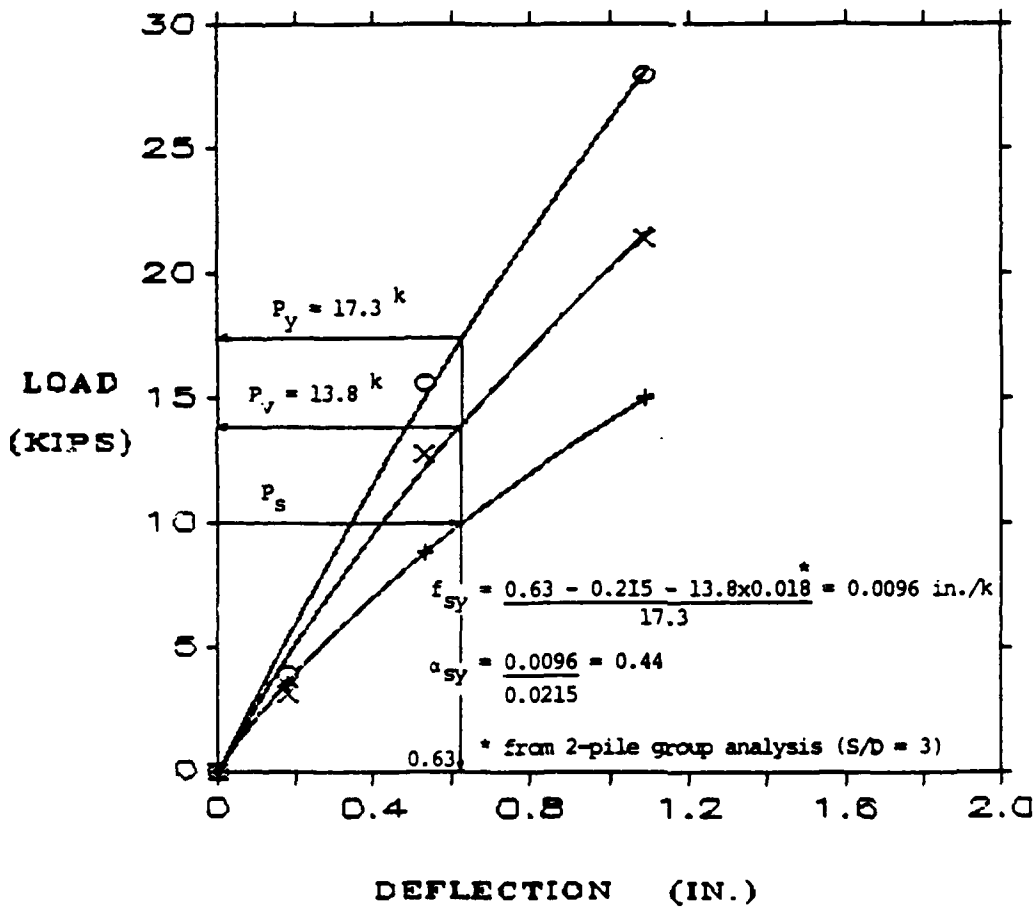
DEFLECTION (IN.)

Fig. A.26. Pile-Head Load vs. Deflection, Conf. 4,
            Cycle 1, Loading South, ξ = 180°.

A29

CONFIGURATION: 4   Ps vs. Ds +

PILES: S,V,Y   Pv vs. Ds X

CYCLE: 20   Py vs. Ds O

LOADING: SOUTH. ξ= 180

Fig. A.27. Pile-Head Load vs. Deflection, Conf. 4,
Cycle 20, Loading South, ξ = 180°.

Fig. A.28.   Pile-Head Load vs. Deflection, C nf. 4,
            Cycle 100, Loading South, ξ = 18 °.

A31

CONFIGURATION: 4   Py vs. Dy   +
PILES: S,V,Y   Pv vs. Dy   ╳
CYCLE: 1   Ps vs. Dy   ○
LOADING: NORTH. ξ= 180

Fig. A.29.   Pile-Head Load vs. Deflection, Conf. 4,
             Cycle 1, Loading North, ξ = 180°.

A32

CONFIGURATION: 4   Py vs. Dy +
PILES: S,V,Y   Pv vs. Dy X
CYCLE: 20   Pa vs. Dy O
LOADING: NORTH.   ξ = 180
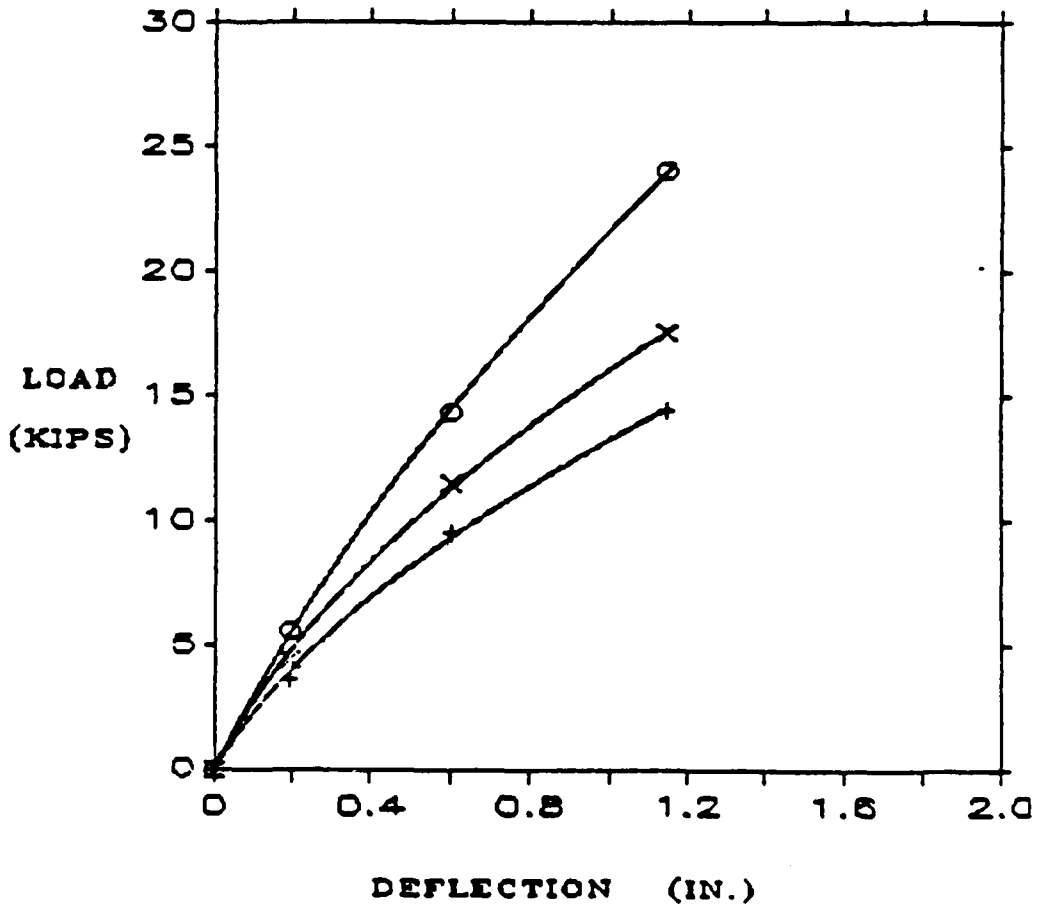
Fig. A.30. Pile-Head Load vs. Deflection, Conf. 4,
            Cycle 20, Loading North, ξ = 180°.

A33

CONFIGURATION: 4   Py vs. Dy   +
PILES: S,V,Y   Pv vs. Dy   X
CYCLE: 100   Ps vs. Dy   O
LOADING: NORTH, f= 180
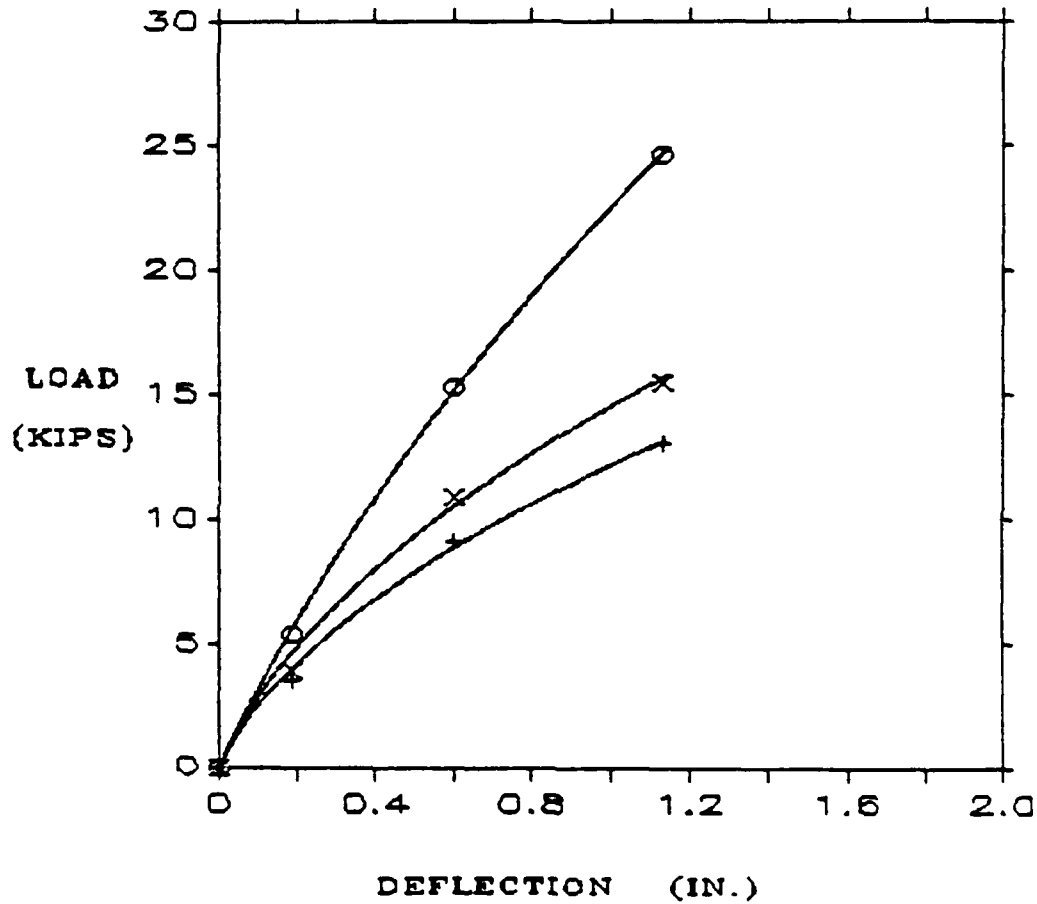
Fig. A.31.   Pile-Head Load vs. Deflection, Conf. 4,
             Cycle 100, Loading North, ξ = 180°.

A34

CONFIGURATION: 5   Py vs. Dy $+$
PILES: X,Y,Z   Pz vs. Dy $\bigcirc$
CYCLE: 1
LOADING: NORTH, ξ= 90

$P_z = 11.4^{\,k}$

P_y

$$f_{yz} = \frac{0.42 - 0.22}{2 \times 11.4} = 0.0088 \text{ in./k}$$

$$\alpha_{yz} = \frac{0.0088}{0.022} = 0.40$$

0.42

LOAD (KIPS)
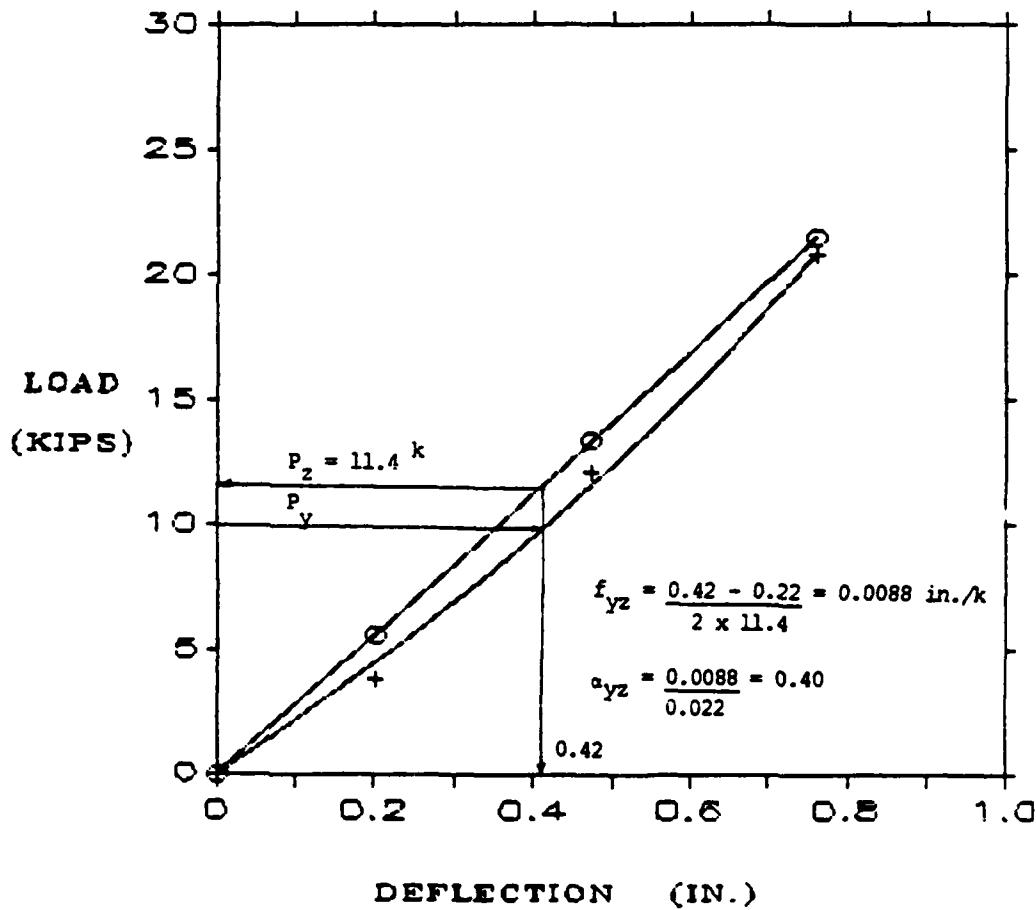
DEFLECTION (IN.)

Fig. A.32.   Pile-Head Load vs. Deflection, Conf. 5,
Cycle 1, Loading North, ξ = 90°.

A35

CONFIGURATION: 5   Py vs. Dy   +
PILES: X,Y,Z   Pz vs. Dy   O
CYCLE: 20
LOADING: NORTH. ξ= 90
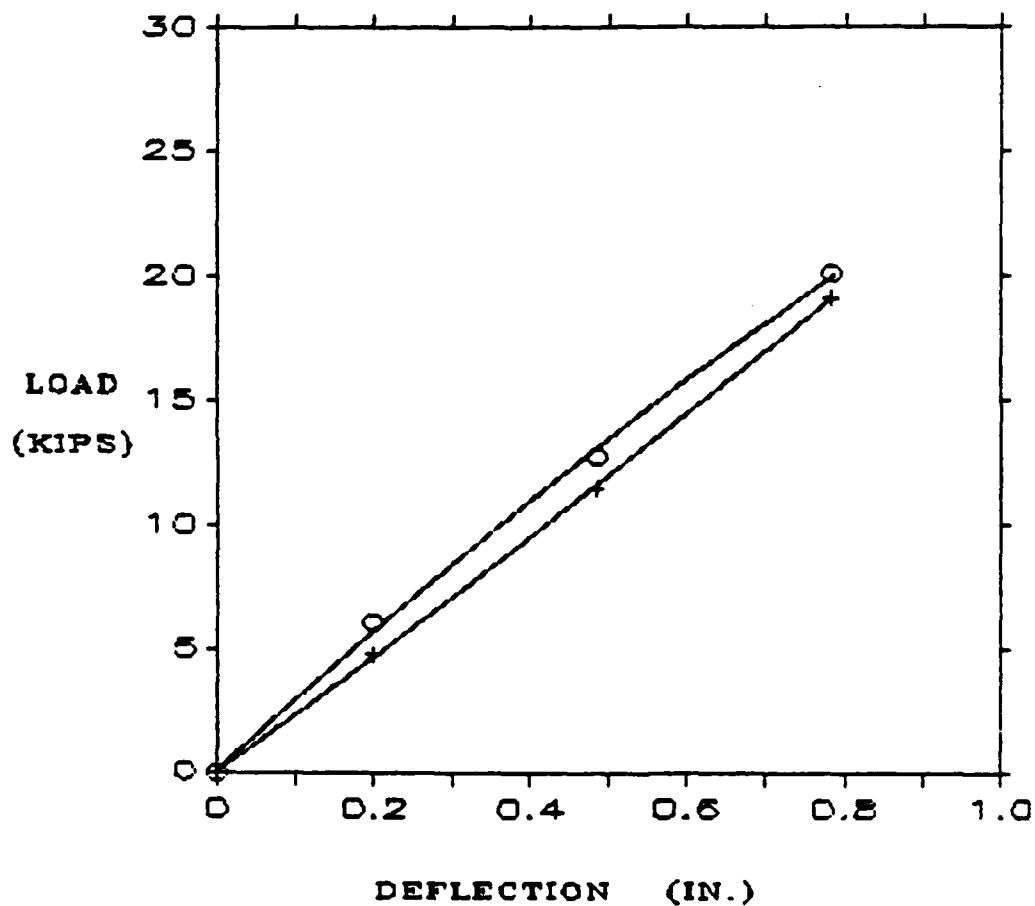
Fig. A.33.   Pile-Head Load vs. Deflection, Conf. 5,
              Cycle 20, Loading North, ξ = 90°.

A36

CONFIGURATION: 5   Py vs. Dy   +
PILES: X,Y,Z   Pz vs. Dy   O
CYCLE: 100
LOADING: NORTH. ξ= 90
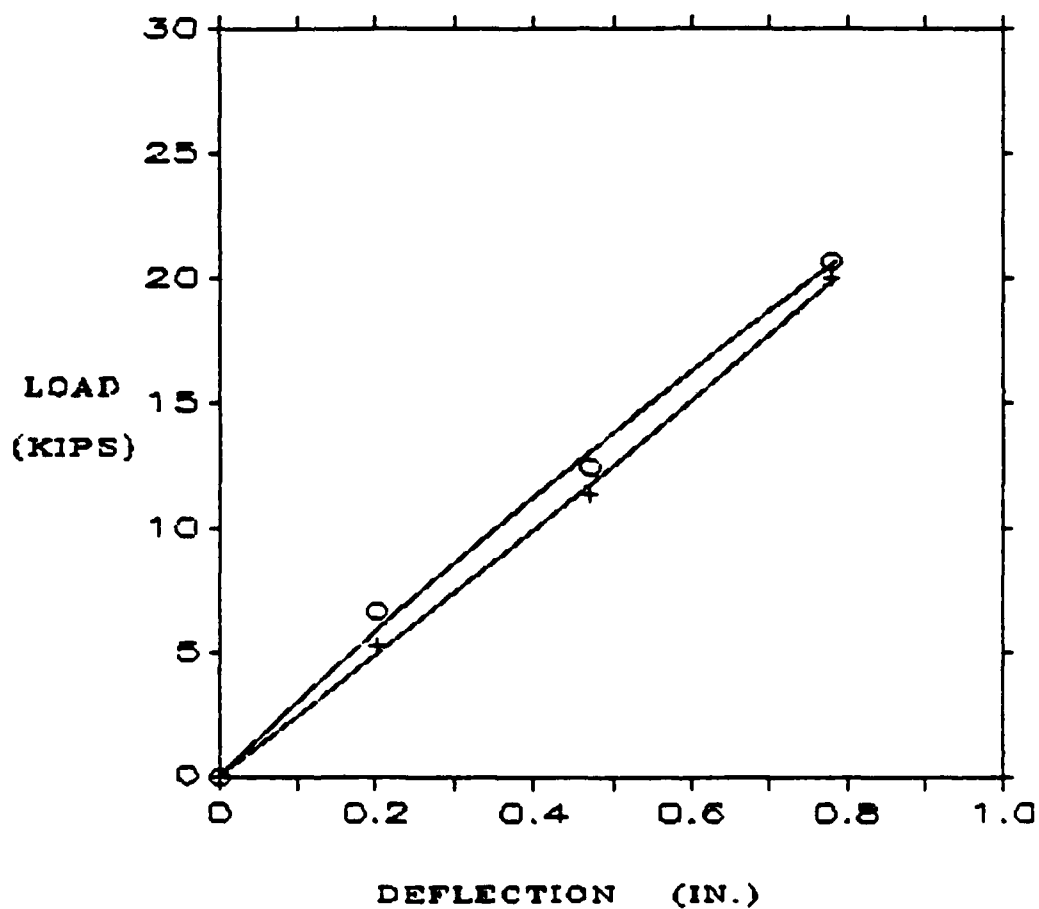
Fig. A.34.   Pile-Head Load vs. Deflection, Conf. 5,
             Cycle 100, Loading North, ξ = 90°.

A37

CONFIGURATION: 5   Py vs. Dy   +
PILES: X,Y,Z   Pz vs. Dy   O
CYCLE: 1
LOADING: SOUTH, ξ= 90
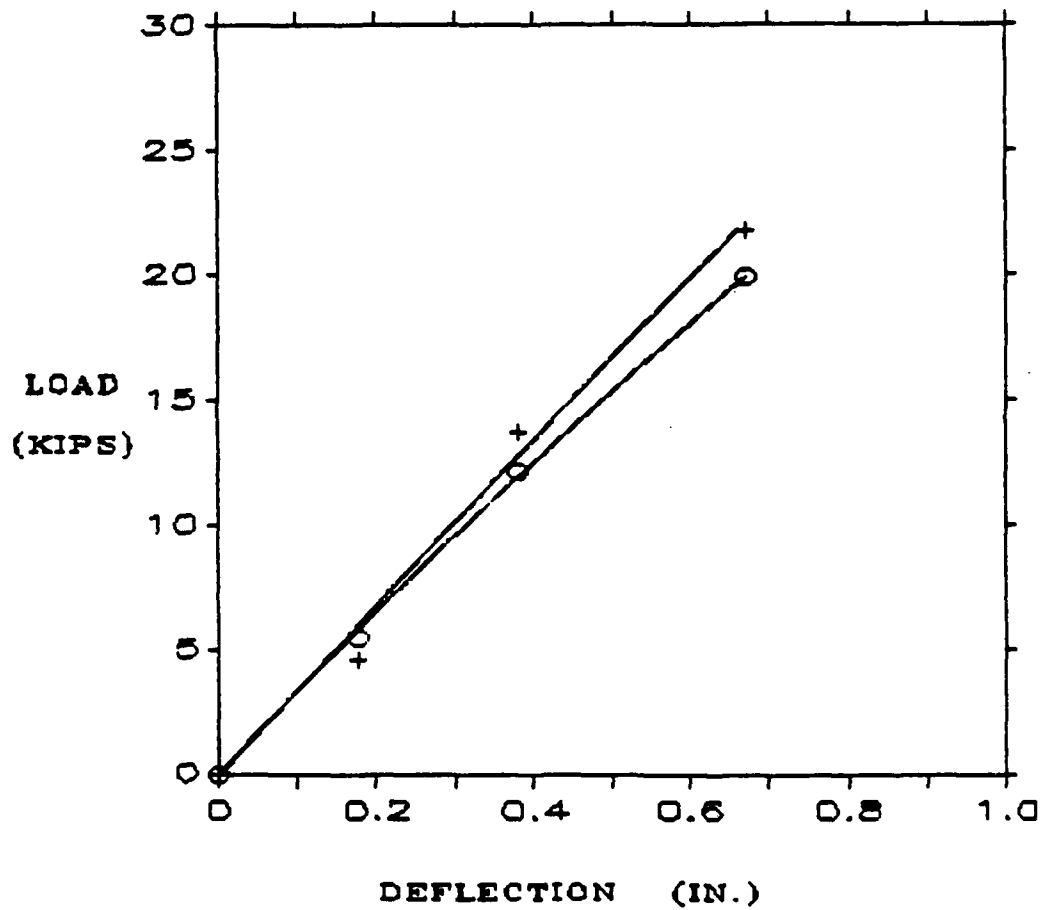
Fig. A.35.   Pile-Head Load vs. Deflection, Conf. 5,
             Cycle 1, Loading South, ξ = 90°.

A38

CONFIGURATION: 5   Py vs. Dy +
PILES: X,Y,Z   Pz vs. Dy O
CYCLE: 20
LOADING: SOUTH, ξ= 90
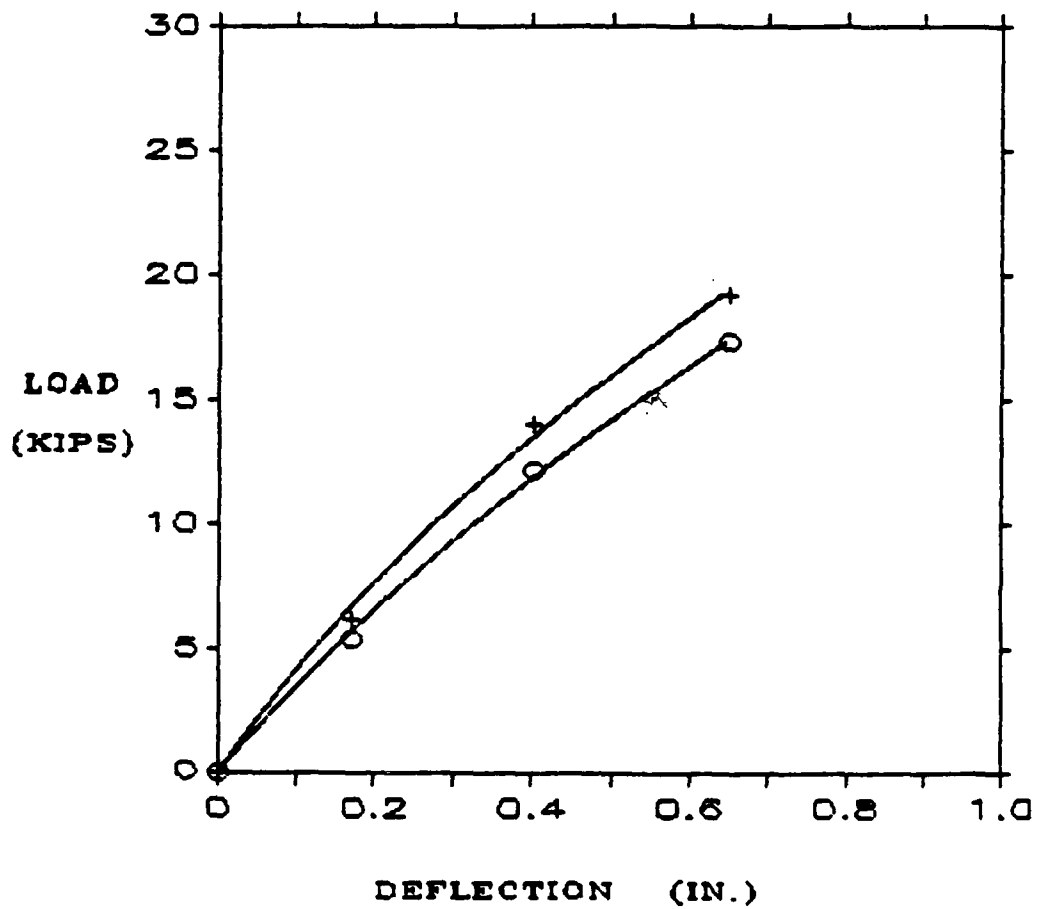
Fig. A.36.   Pile-Head Load vs. Deflection, Conf. 5,
              Cycle 20, Loading South, ξ = 90°.

A39

CONFIGURATION: 5   Py vs. Dy +
PILES: X,Y,Z   Pz vs. Dy O
CYCLE: 100
LOADING: SOUTH. ξ= 90
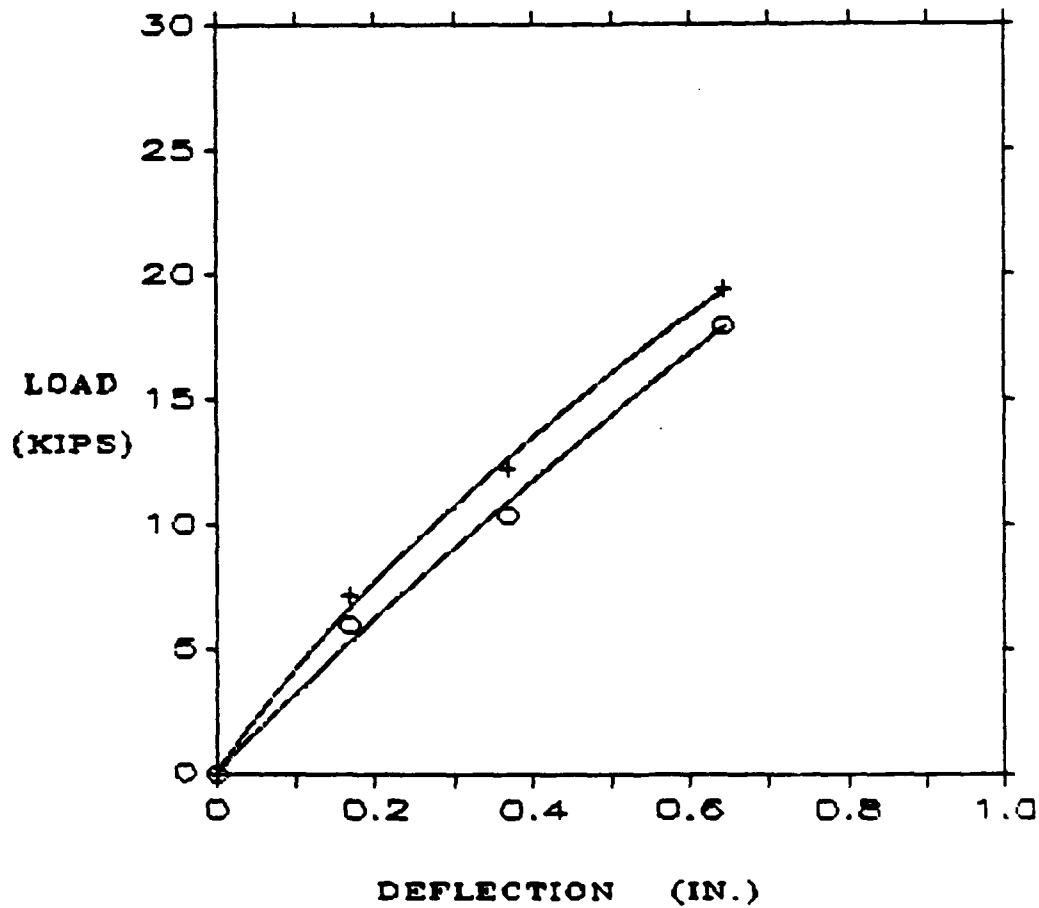
Fig. A.37.   Pile-Head Load vs. Deflection, Conf. 5,
             Cycle 100, Loading South, ξ = 90°.

A40

APPENDIX B

SENSITIVITY OF ALPHA FACTORS DUE TO
ERRORS IN DISPLACEMENT MEASUREMENTS

The purpose of this Appendix is to determine the sensitivity of α factors to possible error in the displacement measurements during testing. This is done by adding and substracting 0.005 in. (estimated accuracy of the linear potentiometers) to the deflections obtained from the fitted curves for monotonic load levels of 3 and 10 kips, for cases when $\xi = 0°$ and $180°$ (S/D = 3), $\xi = 0°$ and $180°$ (S/D = 6), and $\xi = 90°$ (S/D = 3). Numerical computations of such errors are presented in the following sections.

B.1. $\xi = 0°$, S/D = 3, Cycle 1, North, (Figs. A.2, A.8)

B.1.1. Load of 3 kips on Pile V

Deflections + 0.005 in.

$$f_{vv} = f_{yy} = \frac{0.06 + 0.005}{3.0} = 0.0217 \text{ in./k}$$

$$f_{vy} = \frac{(0.07 + 0.005) - (0.06 + 0.005)}{1.8} = 0.0056 \text{ in./k}$$

$$\alpha_{vy} = \frac{0.0056}{0.0217} = 0.25$$

Deflections - 0.005 in.

$$f_{vv} = f_{yy} = \frac{0.06 - 0.005}{3.0} = 0.0183 \text{ in./k}$$

$$f_{vy} = \frac{(0.07 - 0.005) - (0.06 - 0.005)}{1.8} = 0.0056 \text{ in./k}$$

$$\alpha_{vy} = \frac{0.0056}{0.0183} = 0.30$$

The actual value of α_{vy} for loads of 3 k on Pile V and 1.8 k on Pile Y is 0.28 (Fig.4.2).

B.1.2. Load of 10 kips on Pile V

Deflections + 0.005 in.

$$f_{vv} = f_{yy} = \frac{0.22 + 0.005}{10.0} = 0.0225 \text{ in./k}$$

$$f_{vy} = \frac{(0.26 + 0.005) - (0.22 + 0.005)}{6.0} = 0.0067 \text{ in./k}$$

$$\alpha_{vy} = \frac{0.0067}{0.0225} = 0.29$$

Deflections − 0.005 in.

$$f_{vv} = f_{yy} = \frac{0.22 - 0.005}{10.0} = 0.0215 \text{ in./k}$$

$$f_{vy} = \frac{(0.26 - 0.005) - (0.22 - 0.005)}{6.0} = 0.0067 \text{ in./k}$$

$$\alpha vy = \frac{0.0067}{0.0215} = 0.31$$

The actual value of α_{vy} for loads of 10 k on Pile V and 6 k on Pile Y is 0.30 (Fig. 4.2).

B.2. $\xi = 180°$, S/D = 3, Cycle 1, South, (Figs. A.5, A.14)

B.2.1. Load of 3 kips on Pile V

Deflections + 0.005 in.

$$f_{vv} = f_{yy} = \frac{0.06 + 0.005}{3.0} = 0.0217 \text{ in./k}$$

$$f_{vy} = \frac{(0.095 + 0.005) - (0.06 + 0.005)}{3.0} = 0.0117 \text{ in./k}$$

$$\alpha_{vy} = \frac{0.0117}{0.0217} = 0.53$$

B4

Deflections – 0.005 in.

$$f_{vv} = f_{yy} = \frac{0.06 - 0.005}{3.0} = 0.0183 \text{ in./k}$$

$$f_{vy} = \frac{(0.095 - 0.005) - (0.06 - 0.005)}{3.0} = 0.0117 \text{ in./k}$$

$$\alpha_{vy} = \frac{0.0117}{0.0183} = 0.63$$

The actual value of α_{vy} for loads of 3 k on Pile V and 3 k on Pile Y is 0.58 (Fig. 4.5).

B.2.2. Load of 10 kips on Pile V

Deflections + 0.005 in.

$$f_{vv} = f_{yy} = \frac{0.215 + 0.005}{10.0} = 0.022 \text{ in./k}$$

$$fvy = \frac{(0.42 + 0.005) - (0.215 + 0.005)}{12.2} = 0.017 \text{ in./k}$$

$$\alpha_{vy} = \frac{0.017}{0.022} = 0.77$$

Deflections – 0.005 in.

$$f_{vv} = f_{yy} = \frac{0.215 - 0.005}{10.0} = 0.021 \text{ in./k}$$

$$f_{vy} = \frac{(0.42 - 0.005) - (0.215 - 0.005)}{12.2} = 0.017 \text{ in./k}$$

$$\alpha_{vy} = \frac{0.017}{0.021} = 0.81$$

The actual value of α_{vy} for loads of 10 k on Pile V and 12.2 k on Pile Y is 0.79 (Fig. 4.5).

B.3. $\xi = 0°$, $S/D = 6$, Cycle 1, North, (Figs. A.2, A.20)

B.3.1. Load of 3 kips on Pile S

Deflections + 0.005 in.

$$f_{ss} = f_{yy} = \frac{0.06 + 0.005}{3.0} = 0.0217 \text{ in./k}$$

$$f_{sy} = \frac{(0.11+0.005) - (0.06+0.005) - ((3\times0.0055)+0.005)^*}{2.2}$$

* From 2-pile group analysis (S/D = 3)

$$= 0.013 \text{ in./k}$$

$$\alpha_{sy} = \frac{0.0130}{0.0217} = 0.59$$

Deflections − 0.005 in.

$$f_{ss} = f_{yy} = \frac{0.06 - 0.005}{3.0} = 0.0183 \text{ in./k}$$

$$f_{sy} = \frac{(0.11-0.005) - (0.06-0.005) - ((3\times0.0055)-0.005)}{2.2}$$

$$= 0.0175 \text{ in./k}$$

$$\alpha_{sy} = \frac{0.0175}{0.0183} = 0.95$$

The actual value of α_{sy} for loads of 3 k on Pile S and 2.2 k on Pile Y is 0.76 (Fig. 4.8).

B.3.2. Load of 10 kips on Pile S

Deflections + 0.005 in.

$$f_{ss} = f_{yy} = \frac{0.22 + 0.005}{10.0} = 0.0225 \text{ in./k}$$

$$f_{sy} = \frac{(0.38+0.005) - (0.22+0.005) - ((9\times0.0084)+0.005)^*}{7.0}$$

* From 2-pile group analysis (S/D = 3)

B6

$$= 0.0113 \text{ in./k}$$

$$\alpha_{sy} = \frac{0.0113}{0.0225} = 0.50$$

<u>Deflections - 0.005 in.</u>

$$f_{ss} = f_{yy} = \frac{0.22 - 0.005}{10.0} = 0.0215 \text{ in./k}$$

$$f_{sy} = \frac{(0.38-0.005) - (0.22-0.005) - ((9 \times 0.0084)-0.005)}{7.0}$$

$$= 0.0128 \text{ in./k}$$

$$\alpha_{sy} = \frac{0.0128}{0.0215} = 0.59$$

The actual value of α_{sy} for loads of 10 k on Pile S and 7 k on Pile Y is 0.54 (Fig. 4.8).

B.4. $\xi = 180°$, S/D = 6, Cycle 1, South, (Figs. A.5, A.26)

B.4.1. Load of 3 kips on Pile S

<u>Deflections + 0.005 in.</u>

$$f_{ss} = f_{yy} = \frac{0.06 + 0.005}{3.0} = 0.0217 \text{ in./k}$$

$$f_{sy} = \frac{(0.15+0.005) - (0.06+0.005) - ((4 \times 0.014)+0.005)^{*}}{4.5}$$

* From 2-pile group analysis

$$= 0.0064 \text{ in./k}$$

$$\alpha_{sy} = \frac{0.0064}{0.0217} = 0.29$$

<u>Deflections - 0.005 in.</u>

$$f_{ss} = f_{yy} = \frac{0.06 - 0.005}{3.0} = 0.0183 \text{ in./k}$$

$$f_{sy} = \frac{(0.15-0.005) - (0.06-0.005) - ((4 \times 0.014)-0.005)}{4.5}$$

$= 0.0087$ in./k

$$\alpha_{sy} = \frac{0.0087}{0.0183} = 0.47$$

The actual value of α_{sy} for loads of 3 k on Pile S and 4.5 k on Pile Y is 0.38 (Fig.4.11).

B.4.2. Load of 10 kips on Pile S

<u>Deflections + 0.005 in.</u>

$$fss = fyy = \frac{0.215 + 0.005}{10.0} = 0.022 \text{ in./k}$$

$$f_{sy} = \frac{(0.63+0.005) - (0.215+0.005) - ((13.8 \times 0.018)+0.005)^{*}}{17.3}$$

* From 2-pile group analysis (S/D = 3)

$= 0.0093$ in./k

$$\alpha_{sy} = \frac{0.0093}{0.0220} = 0.42$$

<u>Deflections - 0.005 in.</u>

$$f_{ss} = f_{yy} = \frac{0.215 - 0.005}{10.0} = 0.021 \text{ in./k}$$

$$f_{sy} = \frac{(0.63-0.005) - (0.215-0.005) - ((13.8 \times 0.018)-0.005)}{17.3}$$

$= 0.0099$ in./k

$$\alpha_{sy} = \frac{0.0099}{0.0210} = 0.47$$

The actual value of α_{sy} for loads of 10 k on Pile S and 17.3 k on Pile Y is 0.44 (Fig.4.11).

B.5. $\xi = 90°$, S/D = 3, Cycle 1, North, (Figs. A.2, A.32)

B.5.1. Load of 3 kips on Pile Y

Deflections + 0.005 in.

$$f_{yy} = \frac{0.06 + 0.005}{3.0} = 0.0217 \text{ in./k}$$

$$f_{yz} = \frac{(0.12 + 0.005) - (0.06 + 0.005)}{2 \times 3.85} = 0.0078 \text{ in./k}$$

$$\alpha_{yz} = \frac{0.0078}{0.0217} = 0.36$$

Deflections - 0.005 in.

$$f_{yy} = \frac{0.06 - 0.005}{3.0} = 0.0183 \text{ in./k}$$

$$f_{yz} = \frac{(0.12 - 0.005) - (0.06 - 0.005)}{2 \times 3.85} = 0.0078 \text{ in./k}$$

$$\alpha_{yz} = \frac{0.0078}{0.0183} = 0.42$$

The actual value of α_{yz} for loads of 3 k on Pile Y and 3.85 k on Pile Z is 0.39 (Fig.4.14).

B.5.2. Load of 10 kips on Pile Y

Deflections + 0.005 in.

$$f_{yy} = \frac{0.22 + 0.005}{10.0} = 0.0225 \text{ in./k}$$

$$f_{yz} = \frac{(0.42 + 0.005) - (0.22 + 0.005)}{2 \times 11.4} = 0.0088 \text{ in./k}$$

$$\alpha_{yz} = \frac{0.0088}{0.0225} = 0.39$$

Deflections - 0.005 in.

$$f_{yy} = \frac{0.22 - 0.005}{10.0} = 0.0215 \text{ in./k}$$

$$f_{yz} = \frac{(0.42 - 0.005) - (0.22 - 0.005)}{2 \times 11.4} = 0.0088 \text{ in./k}$$

$$\alpha_{yz} = \frac{0.0088}{0.0215} = 0.41$$

The actual value of α_{yz} for loads of 10 k on Pile Y and 11.4 k on Pile Z is 0.40 (Fig. 4.14).

APPENDIX C

MORRISON'S LOAD TEST DATA

HOUSTON PILE GROUP STUDY

FIELD DATA FROM LATERAL LOAD TEST OF DEC 13, 1984

CYCLE NO.   1

LOADING NORTH

LOAD ON GROUP   =   66.08 FROM SUM OF PILE LOAD CELLS

EAST CAP DEFL.   =   .28326 INCHES

WEST CAP DEFL.   =   .47461 INCHES

NORTH

```
D   G   A

F   E   H

B   I   C
```

PILE LEGEND

AT LOAD
POINT :

DEFL.	.29	.40	.31	.38	.36	.39	.35	.30	.40	.35
LOAD	9.24	7.40	4.82	8.53	8.86	8.05	9.16	6.12	3.90	7.34

Table C.1.   Morrison's Load Test: Cycle 1, Loading North, Group Load = 66.08 k   (Morrison, 1986).

HOUSTON PILE GROUP STUDY

FIELD DATA FROM LATERAL LOAD TEST OF DEC 13, 1984

CYCLE NO.   1

LOADING SOUTH

LOAD ON GROUP   =   - 63.47 FROM SUM OF PILE LOAD CELLS

EAST CAP DEFL.   =   - .41985 INCHES

WEST CAP DEFL.   =   - .34048 INCHES

NORTH

```
      D    G    A

      F    E    H

      B    I    C
```

PILE LEGEND

AT LOAD
POINT :

DEFL.	- .48	- .40	- .48	- .41	- .46	- .41	- .46	- .50	- .43	- .45
LOAD	- 5.69	- 9.24	- 10.97	- 5.26	- 4.70	- 6.25	- 4.56	- 5.99	- 10.82	- 7.05

Table C.2.   Morrison's Load Test: Cycle 1, Loading South,
Group Load = 63.47 k   (Morrison, 1986).

HOUSTON PILE GROUP STUDY

FIELD DATA FROM LATERAL LOAD TEST OF DEC 13, 1984

CYCLE NO. 100

LOADING NORTH

LOAD ON GROUP = 64.83 FROM SUM OF PILE LOAD CELLS

EAST CAP DEFL. = .16384 INCHES

WEST CAP DEFL. = .54212 INCHES

NORTH

D	G	A
F	E	H
B	I	C

PILE LEGEND

AT LOAD
POINT :

DEFL.	.21	.46	.22	.44	.35	.46	.34	.22	.38	.34
LOAD	9.62	7.19	4.47	8.45	8.76	7.77	9.24	5.83	3.48	7.20

Table C.3. Morrison's Load Test: Cycle 100, Loading North,
Group Load = 64.83 k (Morrison, 1986).

HOUSTON PILE GROUP STUDY

FIELD DATA FROM LATERAL LOAD TEST OF DEC 13, 1984

CYCLE NO.   100

LOADING SOUTH

LOAD ON GROUP = - 58.48 FROM SUM OF PILE LOAD CELLS

EAST CAP DEFL. = - .48906 INCHES

WEST CAP DEFL. = - .24902 INCHES

NORTH

```
        D   G   A

        F   E   H

        B   I   C
```

PILE LEGEND

AT LOAD
POINT :

DEFL.	- .56	- .30	- .56	- .31	- .45	- .45	- .31	- .58	- .41	- .44
LOAD	- 5.81	- 7.96	- 10.57	- 4.55	- 4.20	- 5.29	- 4.22	- 5.85	- 10.02	- 6.50

Table C.4. Morrison's Load Test: Cycle 100, Loading South, Group Load = 58.48 k (Morrison, 1986).

APPENDIX D

NOTATION

The following symbols are used in this report:

CPT = Cone penetration test;

D = Pile diameter;

E = Pile Young's modulus;

f_H^1 = Horizontal deflection of single pile under a unit load (Single pile flexibility);

f_{ii} = Single Pile i flexibility;

f_{ij} = Additional flexibility in Pile i due to a load on Pile j;

I = Pile moment of inertia;

K_o = Coefficient of earth pressure at rest;

K_r = Pile relative stiffness;

L = Pile length;

L_c = Critical length;

M_i = Pile-head moment on Pile i;

N = Number of blows per foot;

n = Number of piles in the group;

OCR = Overconsolidation ratio;

P^g = Group load;

P_i = Horizontal pile-head load on Pile i;

q_c = Cone tip resistance;

S = Spacing between piles;

SPT = Standard penetration test;

$r_{5\%}$ = Load on single pile that corresponds to a displacement of 5% of the single pile diameter;

S_u = Undrained shear strength;

$UP_{\alpha_{ij}}$ = Experimental free-head interaction factor between Piles i and j for lateral displacement (U) under a horizontal load vector (P);

ΘM_{α} = Interaction factor for head rotations;

ΘP_{α} = Interaction factor for cross-coupling between head rotations and shears;

UM_{α} = Interaction factor for cross-coupling between head deflections and moments;

UF_{α} = Interaction factor for lateral deflection (Fixed-head conditions);

v_{α} = Free-head interaction factor for vertical loads;

$\alpha_{\rho H}$ = Elastic free-head interaction factor for displacement;

β = Departure angle (Elastic approach);

δ^g = Group deflection in the direction of loading;

δ_i = Pile-head deflection of Pile i in the direction of loading;

δ_i^g = Pile-head deflection of Pile i in group;

ε_{50} = Axial strain in UU triaxial test at which one-half of the maximum principal stress difference is developed;

ϕ = Angle on the internal friction of the soil;

γ' = Effective unit weight of the soil;

v_s = Poisson's ratio;

ξ = Departure angle for experimental interaction factors.